

MAX-PLANCK-INSTITUT FÜR POLYMERFORSCHUNG IN MAINZ

# **Novel Organic Semiconductors and Their Applications in Electronics**

Dissertation

zur Erlangung des Grades

“Doktor der Naturwissenschaften”

am Fachbereich Chemie, Pharmazie und Geowissenschaften der

Johannes Gutenberg-Universität in Mainz

**Debin Xia**

Geboren in Heilongjiang Province, China

Mainz, 2015

Dekan: Prof. Dr.

1. Berichterstatter: Prof. Dr.

2. Berichterstatter: Prof. Dr.

Tag der mündlichen Prüfung:

Die vorliegende Arbeit wurde in der Zeit von Juli 2012 bis Dezember 2015 im Max-Planck-Institut für Polymerforschung in Mainz unter der Betreuung von ..... und ..... durchgeführt.

**Dedicated to My Family**



***“It is strange that only extraordinary men make the discoveries,  
which later appear so easy and simple.”***

**Georg C. Lichtenberg**



# Table of Contents

Abbreviations.....	iv
Chapter I. Introduction .....	1
I.1 General Background.....	1
I.2 Specific devices.....	3
I.2.1 Organic field effect transistors .....	3
I.2.2 Organic Photovoltaics .....	4
I.2.3 Organic light emitting diodes.....	6
I.3 Organic semiconductors .....	8
I.3.1 N-type OFET materials .....	8
I.3.2 Non-fullerene acceptors.....	12
I.3.3 Blue-emitting materials.....	16
I.4 Motivation and objectives.....	20
I.5 References .....	23
Chapter II. Solution-Processable n-Type Angular-Shaped Organic Semiconductors .....	30
II.1 Introduction .....	30
II.2 Synthesis.....	33
II.3 Photophysical, electrochemical, and thermal properties .....	35
II.4 Crystal structure analysis.....	38
II.5 Density functional theory calculations.....	39
II.6 Self-organization .....	40
II.7 OFET properties.....	43
II.8 Conclusions.....	45
II.9 References.....	45
Chapter III. Fused Bis-Benzothiadiazoles as Electron Acceptors.....	49
III.1 Introduction .....	49
III.2 Synthesis.....	51
III.3 Crystal structure analysis.....	53
III.4 Photophysical and electrochemical properties.....	55
III.5 Density functional theory calculations.....	56
III.6 Conclusions .....	58
III.7 References.....	59

Chapter IV. Layered Electron Acceptors from Dimerized Acenes End-capped with 1,2,5-Thiadiazoles .....	63
IV.1 Introduction.....	64
IV.2 Synthesis .....	65
IV.3 Crystal structure analysis .....	71
IV.4 Photophysical and electrochemical properties .....	73
IV.5 Density functional theory calculations .....	79
IV.6 Conclusions.....	81
IV.7 References .....	82
Chapter V. A Cruciform Electron Acceptor for Solution Processed Non-fullerene Organic Solar Cells.....	85
V.1 Introduction.....	85
V.2 Synthesis and characterization .....	86
V.3 Photophysical, electrochemical, and thermal properties.....	90
V.4 Crystal structure analysis .....	92
V.5 OPV properties.....	93
V.7 Conclusions .....	97
V.8 References .....	98
Chapter VI. Novel Cruciform Electron-Deficient Molecule with Dicyanovinylene Substitution .....	103
VI.1 Introduction.....	103
VI.2 Synthesis and characterization .....	105
VI.3 Crystal structure analysis .....	109
V.4 Photophysical and electrochemical properties.....	113
VI.5 Density functional theory calculations .....	114
VI.6 Conclusions .....	115
VI.7 References .....	116
Chapter VII. Spiro-Fluorene Based Blue Fluorescent Emitters.....	120
VII.1 Introduction.....	120
VII.2 Blue emitter based on dihydroindenofluorene units.....	120
VII.2.1 Synthesis and characterization .....	120
VII.2.2 Crystal structure analysis.....	126
VII.2.3 Photophysical, electrochemical, and thermal properties .....	128
VII.2.4 Density functional theory calculations.....	131
VII.3 Cruciform blue emitter based on ladder-type tetra-p-phenylene units.....	132

VII.3.1 Synthesis and characterization .....	132
VII.3.2 Crystal structure analysis .....	136
VII.3.3 Photophysical, electrochemical, and thermal properties .....	137
VII.3.4 Density functional theory calculations .....	140
VII.4 Conclusions .....	141
VII.5 References .....	142
Chapter VIII. Experimental Section .....	145
VIII.1 Reagents and analytical techniques .....	145
VIII.2 Material Synthesis .....	149
VIII.3 Crystallographic data .....	185
List of Publications .....	201
Acknowledgments .....	203
Curriculum Vitae .....	207

# Abbreviations

Å	angstrom
AFM	atomic force microscopy
Alq <sub>3</sub>	tris(8-hydroxyquinolino)aluminium
AIE	aggregation induced emission
AcOH	acetic acid
B3LYP	Becke, three-parameter, Lee-Yang-Parr
BHJ	bulk heterojunction
BuLi	butyl lithium
CIE	Commission Internationale de l'Eclairage
COSY	correlation spectroscopy
CV	cyclic voltammetry
DCB	dichlorobenzene
DCM	dichloromethane
DFT	density functional theory
DMAC	dimethylacetamide
DMF	N,N-dimethylformamide
DSC	differential scanning calorimetry
EQE	external quantum efficiency
ESI+	electrospray positive ionization
EML	emissive layer
ETL	electron transport layer
Fc	ferrocene
FD-MS	field desorption mass spectrometry
HMBC	heteronuclear single quantum coherence
HRMS	high resolution mass spectrometry
HOMO	highest occupied molecular orbital
HTL	hole transport layer
$I_{on}/I_{off}$	current on/off ratio
ITO	indium tin oxide
$J_{sc}$	short circuit current

LUMO	lowest unoccupied molecular orbital
MALDI-MS	matrix-assisted laser desorption ionization mass spectrometry
MP	melting point
NBS	N-bromosuccinimide
NMP	nuclear magnetic resonance
NOESY	nuclear Overhauser enhancement and exchange spectroscopy
OFETs	organic field-effect transistors
OLEDs	organic light emitting diodes
OPVs	organic photovoltaics
OSCs	organic semiconductors
PCE	power conversion efficiency
PDI	perylene diimide
P3HT	poly(3-hexylthiophene)
PL	photoluminescence
PLQY	photoluminescence quantum yield
POM	polarized optical microscopy
PTB7	polythieno[3,4-b]-thiophene-co-benzodithiophene
RT	room temperature
S <sub>1</sub>	the lowest excited singlet state
T <sub>1</sub>	the lowest excited triplet state
TA	transient absorption
TCE	1,1,1,2-tetrachloroethane
TADF	thermally activated delayed fluorescence
TFA	trifluoroacetic acid
THF	tetrahydrofuran
TGA	thermogravimetric analysis
TOSCY	total correlation spectroscopy
μ <sub>e</sub>	electron mobility
UV-Vis	ultraviolet-visible
V <sub>oc</sub>	open circuit voltage
XRD	X-ray photoelectron spectroscopy



# Chapter I. Introduction

## I.1 General Background

Since the discovery of the conducting behavior of polyacetylene by Shirakawa, MacDiarmid, and Heeger in 1977,<sup>[1]</sup> great efforts have been focused on developing and synthesizing novel  $\pi$ -conjugated materials for the next generation of electronics, that is, organic electronics.<sup>[2-5]</sup> In comparison with the conventional inorganic solid state electronics, organic electronics present multiple advantages: (1) low fabrication costs and large area fabrications are achievable via solution processing techniques, such as slot-die coating or screen printing;<sup>[6]</sup> (2) low-temperature processing combined with mechanical flexibility of organic materials enable device integration with flexible substrate, such as fabrics or plastics,<sup>[7]</sup> leading to the possibility of electronic paper and roll-up displays.<sup>[8-9]</sup> These unique advantages lead to the major research and development in the field of organic electronic, which is focusing on three main types of applications: organic field-effect transistors (OFETs), organic photovoltaics (OPVs), and organic light emitting diodes (OLEDs).

Undoubtedly, organic semiconductors as key component of electronics play a pivotal role in device performance. Thus, the molecular design is very significant. The general design principles are listed as follows:

(1) Mobility:  $\pi$ -conjugated systems enable both intramolecular and intermolecular charge transport.

(2) Frontier molecular orbital (FMO) energy levels: a) energy levels of highest occupied molecular orbital (HOMO) and lowest unoccupied molecular orbital (LUMO) determine the electron donating and accepting properties of the material behavior (p-type, n-type, and ambipolar); b) for OLEDs and OFETs, suitable HOMO and LUMO energy levels allow efficient hole and electron injection from electrodes; c) in the case of OPVs, the energy difference between HOMO of donor and LUMO of acceptor influences the open circuit voltage of devices. Also, the effective exciton dissociation can be affected by the energy gap between LUMOs of donor and acceptor; and d) the emitting colors for OLEDs can be tuned by altering the energy gap between HOMO and LUMO.

(3) Crystallinity: crystalline materials normally show better mobilities than noncrystalline counterparts, since the former present better  $\pi$ -orbital overlap due to their self-assembly behavior in the solid state. Thus such crystalline materials are indeed potential semiconductors for achieving high-performance OFET devices, whereas crystallinity is detrimental to OPVs and OLEDs performance, due to the presence of huge grain boundaries and light scattering, respectively.

(4) Solubility: solubility issue can be easily brought about by the introduction of alkyl chains. However, the alkyl chain difference can dramatically influence the device performance especially for OFETs and OPVs, considering the intermolecular packing and morphology.

(5) Dimensionality: organic semiconductors with three dimensionality favors isotropic charge transfer.<sup>[10]</sup>

## I.2 Specific devices

### I.2.1 Organic field effect transistors

Since the first p-channel organic field-effect transistor based on polythiophene was fabricated in 1986 with a low mobility of  $10^{-5} \text{ cm}^2 \text{ V}^{-1} \text{ s}^{-1}$ ,<sup>[11]</sup> organic semiconductors have made a significant progress and currently surpass the performance of amorphous silicon. The state-of-the-art charge carrier mobilities are  $35.0 \text{ cm}^2 \text{ V}^{-1} \text{ s}^{-1}$  for vapor deposited thin films,<sup>[12]</sup>  $31.3 \text{ cm}^2 \text{ V}^{-1} \text{ s}^{-1}$  for solution-processed small molecules,<sup>[13]</sup> and  $36.3 \text{ cm}^2 \text{ V}^{-1} \text{ s}^{-1}$  for oriented thin polymeric films.<sup>[14]</sup> For single crystal devices, the mobility of  $15\text{-}40 \text{ cm}^2 \text{ V}^{-1} \text{ s}^{-1}$  was reported for rubrene.<sup>[15-17]</sup> Accordingly, OFETs are being considered for a variety of applications.

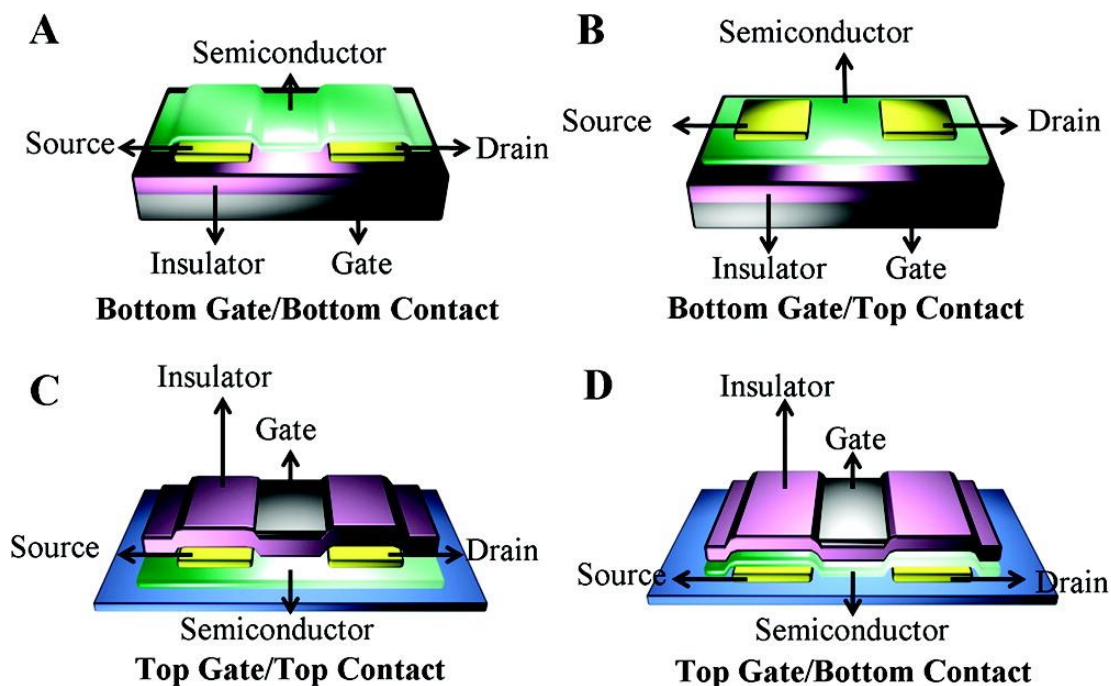


**Figure I-1.** Four types of OFETs. (A) Bottom gate/bottom contact, (B) Bottom gate/top contact, (C) Top gate/top contact, and (D) Top gate/bottom contact.<sup>[3]</sup>

A lot of literature is available on the fundamental physics of OFETs. In principle, an OFET can be regarded as a capacitor with a conducting channel between a source and a drain electrode.  $\text{SiO}_2$  or insulating polymers, such as polyimides or

polystyrene, act as dielectric layers. According to different device configurations, four types of OFETs can be identified (Figure I-1), namely, (A) the bottom gate bottom contact, (B) the bottom gate top contact, (C) the top gate top contact, and (D) the top gate bottom contact. The bottom gate bottom contact is the most prevalent device configuration, which is often used for routine screening and characterization due to its simplicity of fabrication. The OFET operation relies on the charge carrier accumulation in the semiconductor-insulator interface. When a gate voltage is applied, charges can be created in close vicinity to the semiconductor-insulator interface and then the source-drain current increases dramatically ("on" state) in response to the applied drain voltage. Without gate voltage, the intrinsic conductivity of most organic semiconductors is extremely low; the source-drain current through semiconductor thin film should be zero ("off" state) when no voltage is applied between the source and the drain.

## **I.2.2 Organic Photovoltaics**

In the 21<sup>st</sup> century, one of the most important issues is the energy. Nowadays, with the increasing energy demand, the consumption of fossil fuel (coal, oil and natural gas) results in a mass of environmental problems. To overcome this problem and look for alternative energies, photovoltaic cells have been used to generate electricity in a clean and renewable way. Organic photovoltaic (OPV) has unique benefits, such as solution processing, light weight and flexibility and thus attracts a great deal of attention.<sup>[18-22]</sup> Recently, the 9.2%<sup>[23]</sup> and 9.9%<sup>[24]</sup> power conversion efficiencies (PCEs) were reported on polymer- and small molecule-based single junction cells, respectively. The breakthrough of over 10% PCEs was also achieved in tandem solar cells.<sup>[25-27]</sup>

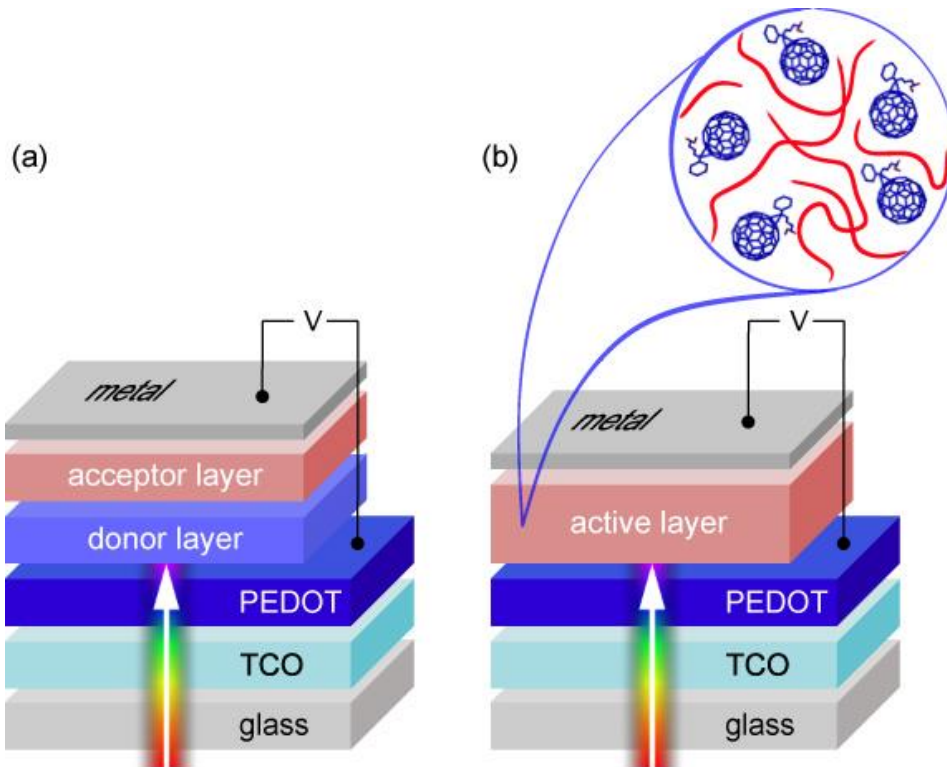


**Figure I-2.** Typical device configurations of organic solar cells: (a) bilayer device with planar heterojunction, (b) bulk heterojunction device.<sup>[28]</sup>

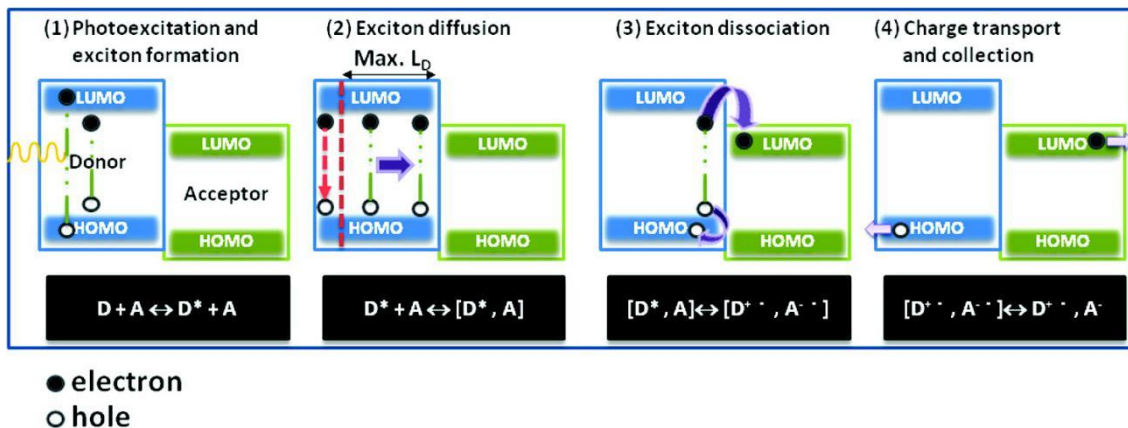


**Figure I-3.** Working mechanism for donor-acceptor heterojunction solar cells.<sup>[29]</sup>

Typical organic photovoltaic (OPV) incorporates a donor (p-type semiconductor) and an acceptor (n-type semiconductor) as active layer. According to the adopted device configuration, OPV can be divided into two principle types as shown in Figure I-2. Those are bilayer solar cells presented by Tang in the mid-1980s<sup>[30]</sup> and bulk heterojunction solar cell introduced by Alan Heeger in 1995,<sup>[31]</sup> respectively. In case of the bilayer heterojunction devices, charge generation is severely limited due to

small area of the donor-acceptor interface. The problem can be overcome by the bulk heterojunction configuration, which comprises only one single active layer with an interpenetrating donor-acceptor network. Figure I-3 illustrates the general working principle of BHJ solar cells. First, the singlet exciton (electron-hole pair) is generated when the donor material involves photoexcitation by the absorption of light energy. Second, the exciton diffuses to the donor-acceptor interface. Third, exciton dissociation occurs via electron transfer to the electronegative acceptor molecules. Lastly, free charge carriers transport and are collected at the respective electrodes, which generate photocurrent and photovoltage thereafter.

### **I.2.3 Organic light emitting diodes**

Organic light-emitting diodes (OLEDs) have been the driving force for the new generation of full color flat panel displays.<sup>[32]</sup> On the basis of electroluminescence, the first light emitting devices were reported by Pope et al. in 1963.<sup>[33]</sup> The considerable efficiency improvement was not achieved until 1987, when Tang and VanSlyke used tris(8-hydroxyquinolino)aluminium (Alq<sub>3</sub>) as emitter.<sup>[34]</sup> In 1990, the first polymer based OLED was reported by Friend and coworkers.<sup>[35]</sup> Almost a decade later, the principle was further extended by Forrest and Thompson by investigating the luminescence contribution from singlet and triplet excited states.<sup>[36]</sup> Recent advances in materials and engineering techniques have led to OLED applications in a variety of devices, such as mobile phones, digital cameras and televisions.

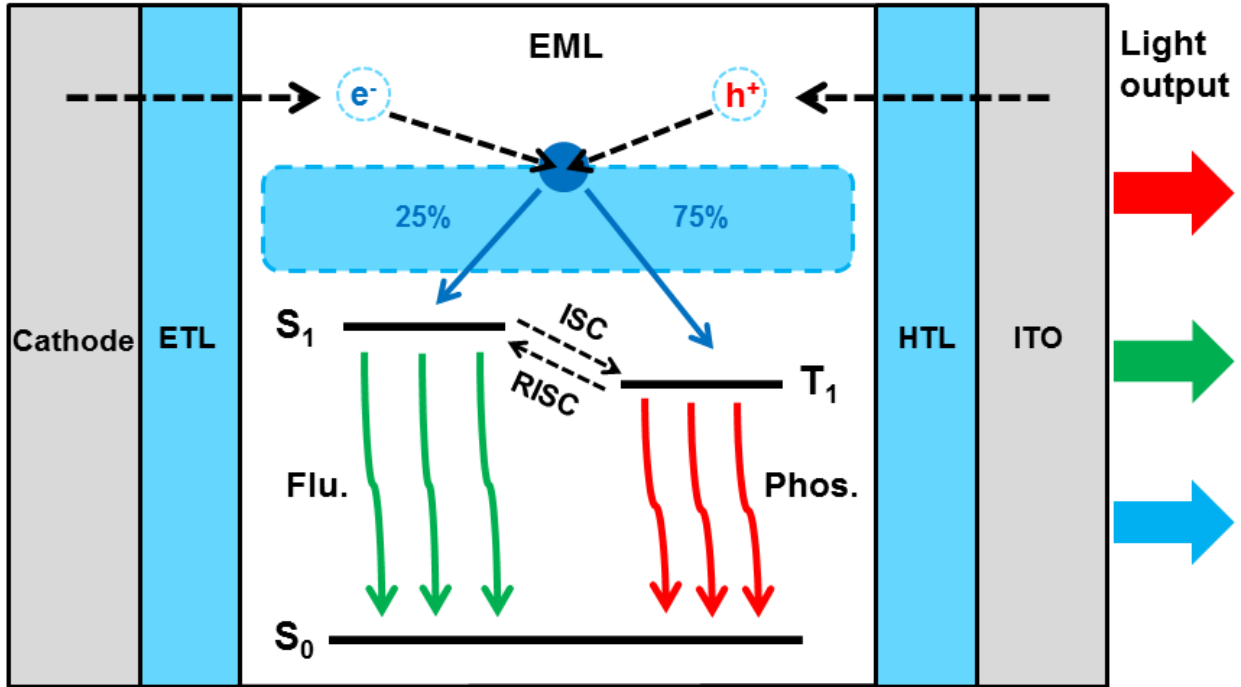


**Figure I-4.** Device structures of prototype sandwich-structure OLEDs and luminescence processes. ETL: Electron transport layer. EML: Emissive layer. HTL: Hole transport layer. ISC: intersystem crossing.

The typical device configuration and working principle of an OLED are illustrated in Figure I-4. The introduction of the hole transport layer (HTL) and the electron transport layer (ETL) is to minimize the energy barrier between the electrodes and the emissive materials, thereby enhancing the carrier injection. In terms of electrodes, normally, metals with a low work function, such as Mg, Ca, and Al are used as cathode to facilitate electron injection into the lowest unoccupied molecular orbital levels of the ETL material. A semi-transparent thin layer of indium-tin-oxide is common applied as anode enabling a light emission perpendicular to the substrate. When an external voltage is applied between the anode and the cathode, the injections of holes from the anode and electrons from the cathode occurs and the carriers migrate through the HTL and the ETL, respectively. The recombination of holes and electrons follows in the organic emissive layer, together with the formation of excitons (bound excited-state electron-hole pairs). Eventually, the relaxation of excitons to the ground state results in the light emission.

## I.3 Organic semiconductors

Classes of organic semiconductors (OSCs) can be divided into small molecules and conjugated polymers. In comparison with conjugated polymers, the main advantage of small molecules is that they are more amenable to scale-up while maintaining high purity and reproducibility. Another advantage is ease of processing. Small molecules can be processed into devices by two ways, namely, vacuum sublimation and solvent casting. Thus, we are particularly interested in semiconducting small molecules. This thesis focuses on n-type OSCs for OFETs, acceptors for OPVs, and blue-emitting materials for OLEDs, due to the following reasons, respectively. (1) N-type OSCs are essential for fabrication of circuits, whose performance is lagging behind that of p-type counterparts.<sup>[37-39]</sup> (2) Common electron acceptors for OPVs are fullerene derivatives, whose obvious drawbacks cannot be overcome, such as weak absorption in the visible region and restricted electronic tuning, causing the limited power conversion efficiencies.<sup>[40-44]</sup> (3) In comparison with red- and green-color luminescent materials, blue emitters generally show a noticeably inferior electroluminescence performance with regard to device efficiencies and color purity.<sup>[45-47]</sup>

### I.3.1 N-type OFET materials

Semiconducting materials as one indispensable part of OFET devices play a pivotal role. With the aim towards high-performance ambient-stable n-type OFETs, typical molecular-design strategies divided into three categories, namely, using fluorine, imide, and dicyanovinylene, to functionalize  $\pi$ -conjugated cores, respectively.

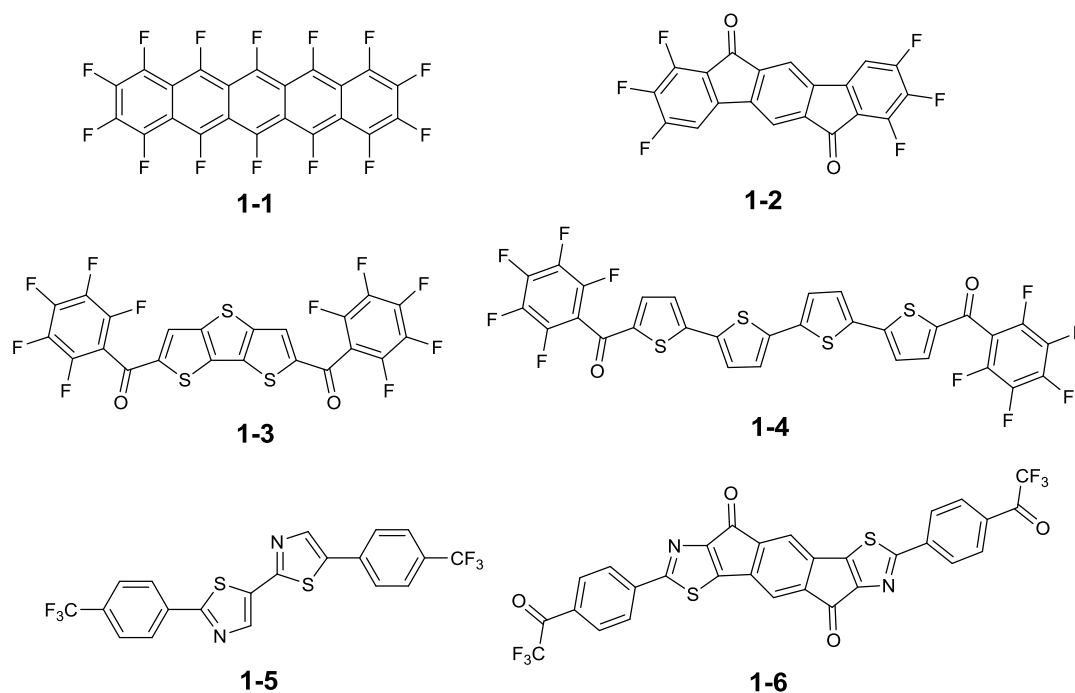


**Figure I-5.** Chemical structures of representative fluorine-containing semiconductors.

Fluorine is the strongest electron-withdrawing element in the periodic table. With the introduction of fluorine substituents into organic semiconductor molecules, n-type behavior can easily be realized (Figure I-5). For example, the benchmark molecule pentacene showed p-type transport behavior with a hole mobility of  $0.45 \text{ cm}^2/\text{Vs}$  based on evaporated thin films. Under the same condition, perfluoropentacene (**1-1**) possesses n-type characteristics and exhibited electron mobilities as high as  $0.11 \text{ cm}^2/\text{Vs}$ .<sup>[48]</sup> Also, the fluorine substituted indenofluorenedione (**1-2**) exhibited good device performances, with an electron mobility of  $0.16 \text{ cm}^2/\text{Vs}$  and an on/off current ratio of  $10^6$ .<sup>[49]</sup> Moreover, two novel n-type OSCs **1-3** and **1-4** were constructed via a combination of thiophene rings and pentafluorophenyl groups.<sup>[50-51]</sup> High electron mobilities of  $0.21 \text{ cm}^2/\text{Vs}$  and  $0.45 \text{ cm}^2/\text{Vs}$  were observed for compound **1-4** with solution-cast and vapor-deposited techniques, respectively. Another two representatives are trifluoromethyl endcapped molecules **1-5** and **1-6**. Molecule **1-5** adopts a two-dimensional columnar packing leading to high electron mobilities up to  $1.83 \text{ cm}^2/\text{Vs}$  on the OTS-treated substrate.<sup>[52]</sup> An electron mobility of  $0.39 \text{ cm}^2/\text{Vs}$  was also achieved based on **1-6**, whose performance is also good enough among pentacyclic dione-based materials.<sup>[53]</sup>

Imide is a functional group, which contributes a lot to forming high performance n-type molecules. That is mainly due to its strong electron-withdrawing capability, planarity, and solubilizing ability offered by N-imide substituents. The traditional imide based semiconductors are listed in Figure I-6. The introduction of the cyano groups into the cores can further increase the electron affinities, facilitating electron injections from electrodes.

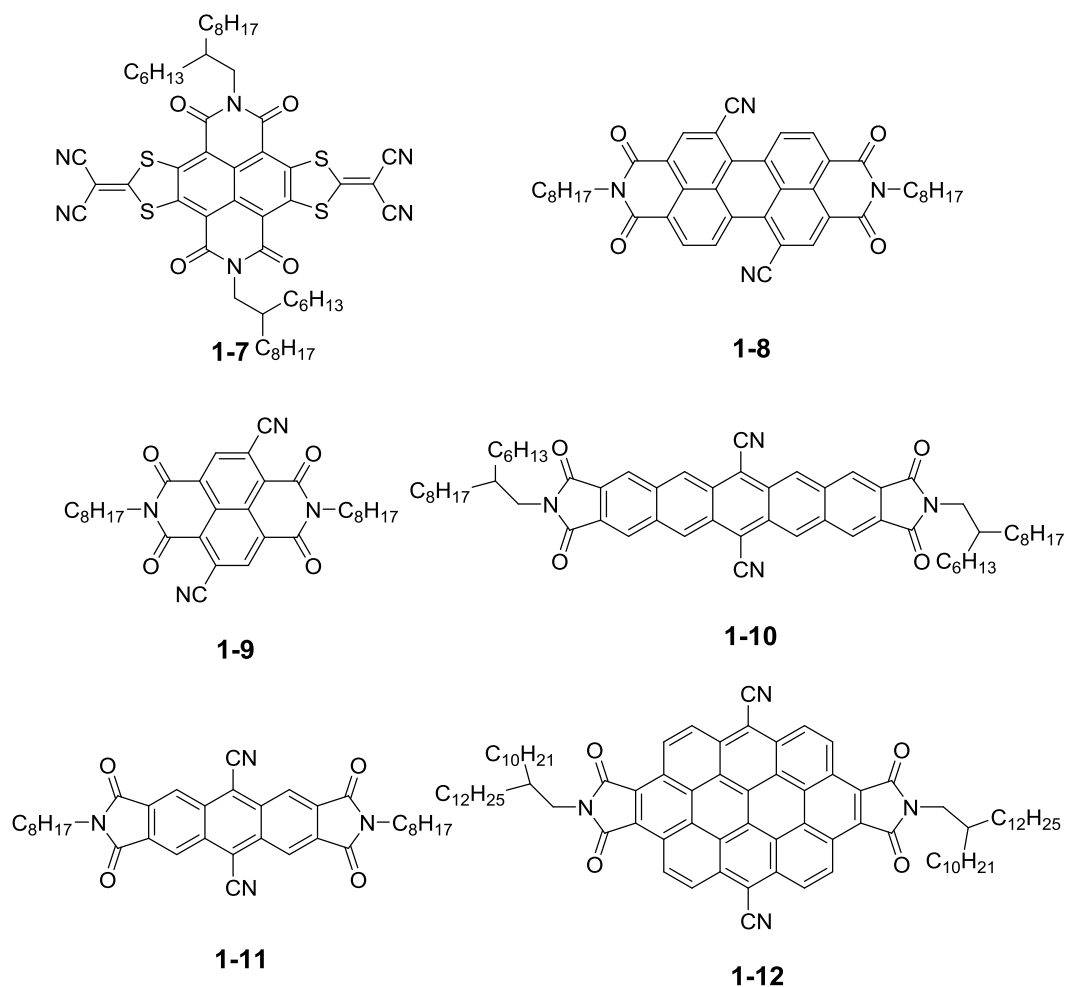


**Figure I-6.** Chemical structures of representative imide-based semiconductors.

Compounds **1-7**, **1-8**, and **1-9** have LUMO energy levels less than  $-4.3$  eV.<sup>[54-56]</sup> Ambient stable n-type solution-processed OFETs based on **1-7** show an unprecedented electron mobility of up to  $3.5$  cm<sup>2</sup>/Vs, which is ascribed to its dense in-plane molecular packing in the solid state.<sup>[54]</sup> However, **1-8** and **1-9** only show the electron mobilities around  $0.02$  cm<sup>2</sup>/Vs with  $I_{on/off}$  of  $10^3$  to  $10^5$  and  $0.10$  cm<sup>2</sup>/Vs with  $I_{on/off}$  of  $10^3$ , respectively. Furthermore, n-type OFET devices based on dicyano

substituted pentacene diimide (**1-10**),<sup>[57]</sup> anthracene diimide (**1-11**),<sup>[58]</sup> and ovalene diimide (**1-12**)<sup>[59]</sup> operate in air with mobilities of up to 0.07, 0.02 and 0.51 cm<sup>2</sup>/Vs, respectively.

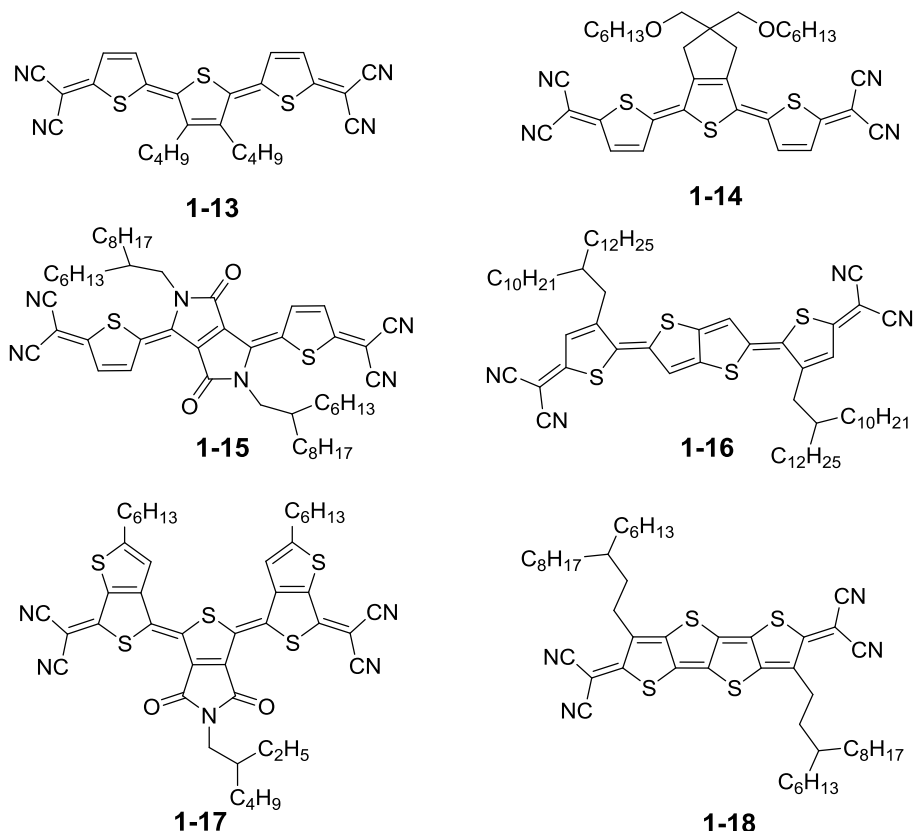


**Figure I-7.** Chemical structures of representative quinoidal thiophene-based semiconductors.

In Figure I-7, quinoidal thiophene derivatives endcapped with dicyanovinylene present a similar behavior to the well-known 7,7,8,8-tetracyanoquinodimethane (TCNQ), indicating their potentials as n-type organic semiconductors.<sup>[60]</sup> Mann's group firstly reported the application of the dicyano-methylene-terminated quinoidal terthiophene derivative **1-13** as semiconductor.<sup>[61]</sup> However, the electron mobilities were only about 10<sup>-3</sup> cm<sup>2</sup>/Vs for both vacuum-deposited and solution-processed devices. After that, a series of such analogues were developed and applied in n-type OFETs. Compound **1-14** has the same backbone as **1-13**, however, **1-14** displayed much better device performance with the electron mobility of up to 0.16 cm<sup>2</sup>/Vs.<sup>[62]</sup> By the introduction of the diketopyrrolopyrrole unit, Zhu's group constructed molecule **1-15**, whose solution-processed OFET devices showed ambient-stable n-type FET behavior with electron mobility of up to 0.35 cm<sup>2</sup>/Vs together with high *I*<sub>on/off</sub> ratios

( $10^5$  to  $10^6$ ).<sup>[63]</sup> Moreover, the varying alkyl chain positions on such quinoidal systems presented a significant impact on the device performance, which was revealed by Li's group.<sup>[64]</sup> Among such series of compounds, **1-16** displayed the best OFET performance ( $\mu_e = 0.22 \text{ cm}^2/\text{Vs}$ ). Thereafter, semiconductor **1-17** with two-dimensional  $\pi$ -expanded system was synthesized and exhibited outstanding semiconducting properties.<sup>[65]</sup> In ambient- and solution-processed OFETs, the mobilities and on/off ratios reached up to  $3.0 \text{ cm}^2/\text{Vs}$  and  $10^6$ , respectively. Another representative is **1-18**, which exhibited also a relatively high electron mobility of about  $0.9 \text{ cm}^2/\text{Vs}$  with good operating stability.<sup>[66]</sup>

### **I.3.2 Non-fullerene acceptors**

As we mentioned above, the inherent shortcomings of fullerenes for OPVs cannot be thoroughly overcome, thus developing novel alternative electron acceptors is essential and very meaningful. However, two years ago, it was a great challenge for non-fullerene bulk heterojunction (BHJ) solar cells to achieve power conversion efficiencies (PCEs) as high as that of fullerene-based solar cells.<sup>[67]</sup> During the past two years, through the cooperation between chemists, physics and engineers, the PCEs have been dramatically improved from less than 3% to 8.3%<sup>[44, 68-75]</sup> for solution-processed fullerene-free OPV devices. Although a wealth of novel non-fullerene electron acceptors have been developed in the field, the relationship between molecular structure and device performance remain unclear until now. To date, the successful non-fullerene electron acceptors can be divided into three types, namely, helical perylene diimide-, spatially extended perylene diimide-, and electron deficient endcapped acceptors.

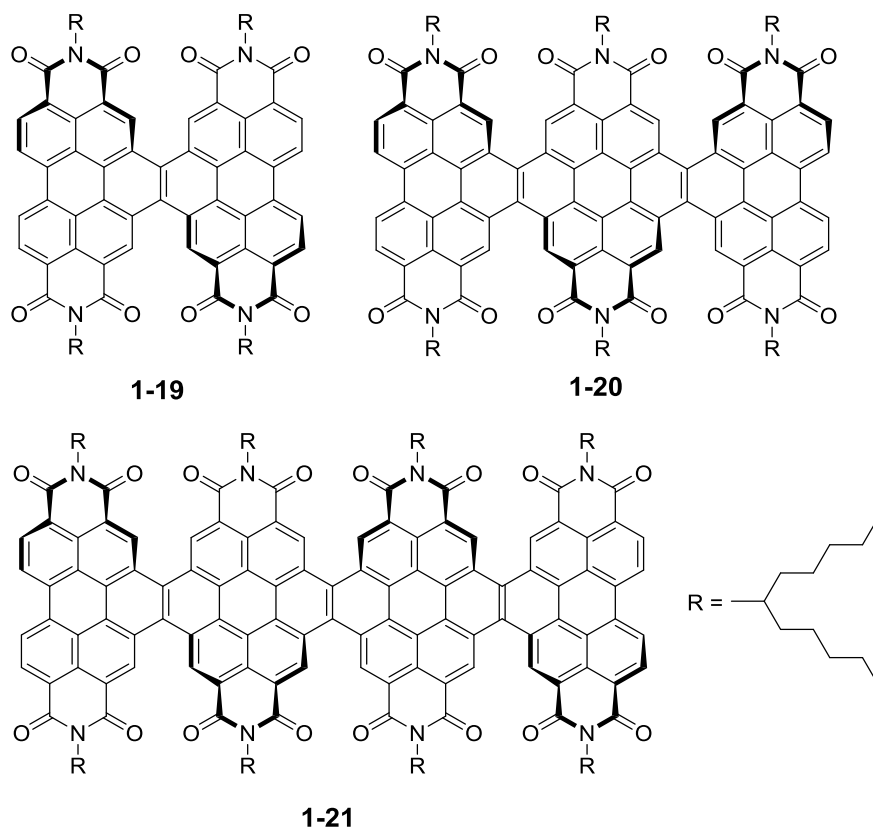


**Figure I-8.** Chemical structures of helical perylene diimide-based electron acceptors.

Until now, the highest PCE based on a non-fullerene solution-processed OPV device is 8.3%, which is due to the special properties of helical perylene diimide (PDI) derivatives (Figure I-8). These properties include: (1) relatively high electron mobilities in thin film transistors ( $0.04\text{-}0.05\text{ cm}^2/\text{Vs}$ ); (2) high molar extinction coefficient ( $10^5\text{ M}^{-1}\text{ cm}^{-1}$ ); (3) steric congestion in the cove areas leading to twisted structures, thus decreasing strong self-aggregation in the solid state. In 2014, the first helical perylene diimide-based electron acceptor (**1-19**) was reported by Nuckolls and coworkers.<sup>[76]</sup> Using traditional commercially available PTB7 as donor, an efficiency of 4.8% for a solution-processed non-fullerene solar cell was achieved. The PCE was enhanced to 6.1% when PBDTT-TT was used as donor, which was due to the increased short current arising from red-shifted absorption of PBDTT-TT relative to that of PTB7. In September 2015, the same group reported two more helices with different lengths, which were synthesized by fusing either three or four perylene diimide components together with a two-carbon bridge (**1-20** and **1-21**).<sup>[68]</sup> After optimization, the devices comprised of PTB7:**1-20** and PBDTT-TT:**1-20** exhibited a maximal PCE of 6.4% and 7.9%, respectively. Finally, the record PCE of 8.3% was

reached based on PBDTT-TT:**1-21** solar cells, which was ascribed to the efficient exciton generation, separation and carrier transport. These findings provide a new route to further improve the BHJ device performance.

Another concept is to construct spatially extended electron acceptors, since such network not only decreases the molecular aggregation in the solid state, but also facilitates isotropic charge transport. Considering the advantages of PDI mentioned above, several groups connected PDI units with varying cores, such as spirobifluorene,<sup>[77]</sup> thiophene,<sup>[78-79]</sup> tetraphenylethylene,<sup>[80]</sup> and triphenylamine,<sup>[81]</sup> to form several representative spatially extended electron acceptors (Figure I-9). Compounds **1-22** and **1-23** were constructed through a Suzuki coupling reaction and a Stille reaction protocol, respectively.<sup>[77]</sup> The low-lying LUMO energy levels of **1-22** and **1-23** were similar to each other (-3.7 eV), whereas the different bandgaps were observed (2.1 eV for **1-22** and 1.9 eV for **1-23**). After optimization, highest PCEs of

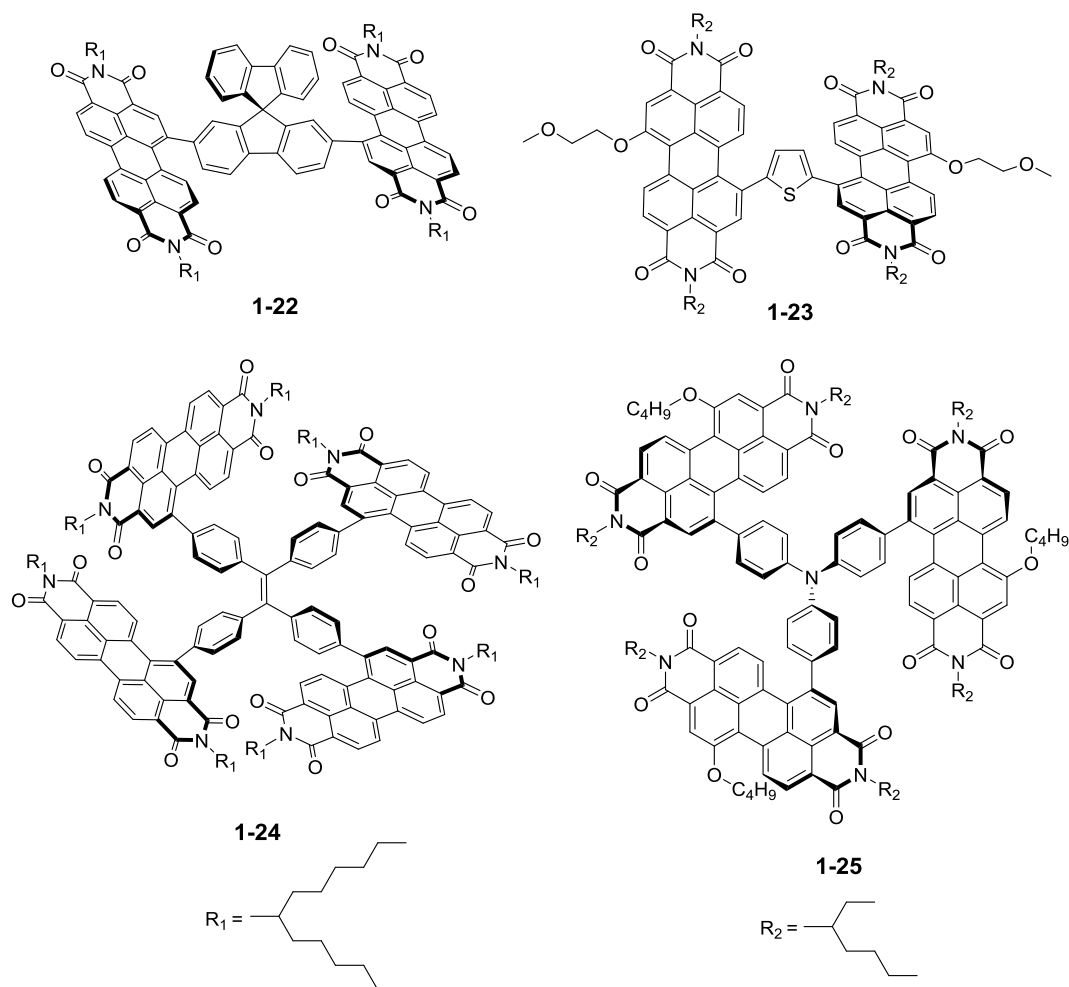
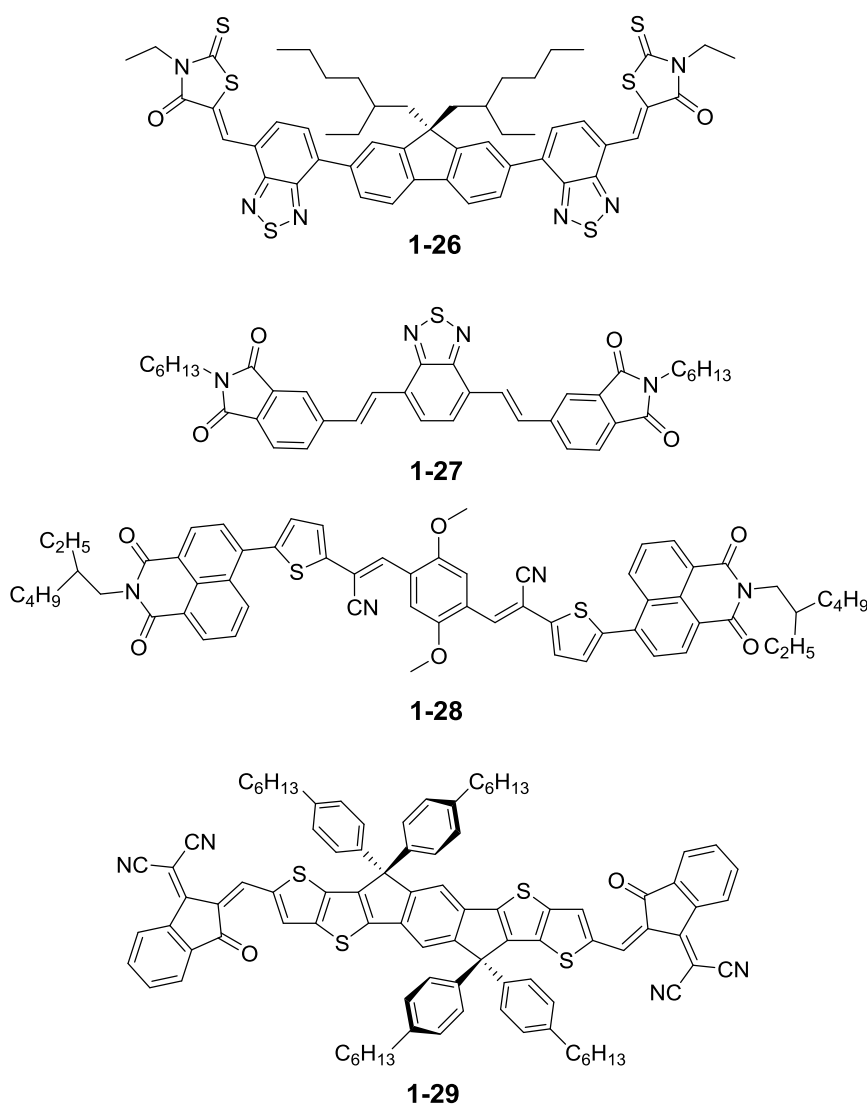


Figure I-9. Chemical structures of perylene diimide-based spatially extended electron acceptors.

6.3%<sup>[82]</sup> and 6.1%<sup>[78]</sup> were achieved from devices based on PBDTTT-C-T:**1-22** and PffBT4T-2DT:**1-23**, respectively. Yan and co-workers used “four-wing propeller-shape” **1-24** as electron acceptor PTB7-TH as donor, the device based on which yielded a PCE of 5.53%, with a  $V_{oc}$  of 0.91 V,  $J_{sc}$  of 11.7 mA cm<sup>-2</sup>, and FF of 0.52.<sup>[80]</sup> Star-shaped **1-25** was reported by Zhan and co-workers.<sup>[81]</sup> Using **1-25** as acceptor, OPV devices exhibited a PEC of up to 3.3% in conventional device architecture.



**Figure I-10.** Chemical structures of linear acceptors end-capped with electron deficient blocks.

Both the helical PDI materials and PDI-based molecules give a well-established performance when they are used as electron acceptors. Apart from that, linear small molecules have also demonstrated impressive OPV device performance. Four representative molecules are listed in Figure I-10. The molecular design strategy for

them is roughly the same. That is introducing terminal electron deficient units, such as rhodamine and imide. Holliday and coworkers reported novel electron acceptor **1-26** with a simple structure, which can be synthesized in high yields. The 4.1% PCE OPV device was realized when P3HT and **1-26** were employed as donor polymer and acceptor, respectively.<sup>[83]</sup> In comparison to **1-26**, compound **1-27** had a relatively high lying LUMO level (-3.5 eV), thus the  $V_{oc}$  of OPV device was as high as 1.11 V. Note that the PCE up to 3.7% was demonstrated, which might be relatively limited by the narrow absorption band of **1-27**.<sup>[84]</sup> The Park group employed **1-28** as electron acceptor and reported all-small molecule nonfullerene solar cell with a maximum PCE of 5.44%, a  $V_{oc}$  of 0.85 V, a  $J_{sc}$  of 9.68 mA cm<sup>-2</sup> and a FF of 0.66.<sup>[85]</sup> Very recently, Zhan and co-workers reported a novel electron acceptor **1-29**, exhibiting a strong and broad absorption in the visible and even NIR regions. Blend film consisted of PTB7-TH and **1-29** showed PCEs as high as 6.8%, which is even higher than that (6.05%) of PTB7-TH:PC<sub>61</sub>BM-based OPV devices.<sup>[86]</sup> This exciting result indeed indicates the performance of fullerene-free OPV devices can be further improved in the coming years.

### I.3.3 Blue-emitting materials

Nowadays, in the research field of OLEDs, more attention has been paid on blue-emitting materials. In comparison with blue-emitting phosphorescent materials, blue-emitting fluorescent materials have obvious advantages in terms of stability and lifetime, with respect to industrial application issue. Although phosphorescent materials can harvest both singlet and triplet excitons and endow OLEDs with the potential of reaching an internal efficiency of 100%, they still suffer from pure blue light. During the past decade, a wealth of outperforming fluorescent blue light-emitting materials have been developed, which are mainly based on fluorene, triphenylamine, carbazole, and anthracene.<sup>[87-91]</sup> Apart from that, employing thermally activated delayed fluorescence (TADF) materials<sup>[92-94]</sup> and aggregation induced emission (AIE) blue-color emitting materials<sup>[95-97]</sup> have also emerged as another high-performance OLEDs. In the following part, representative blue emitters have been chosen to illustrate their device performance.

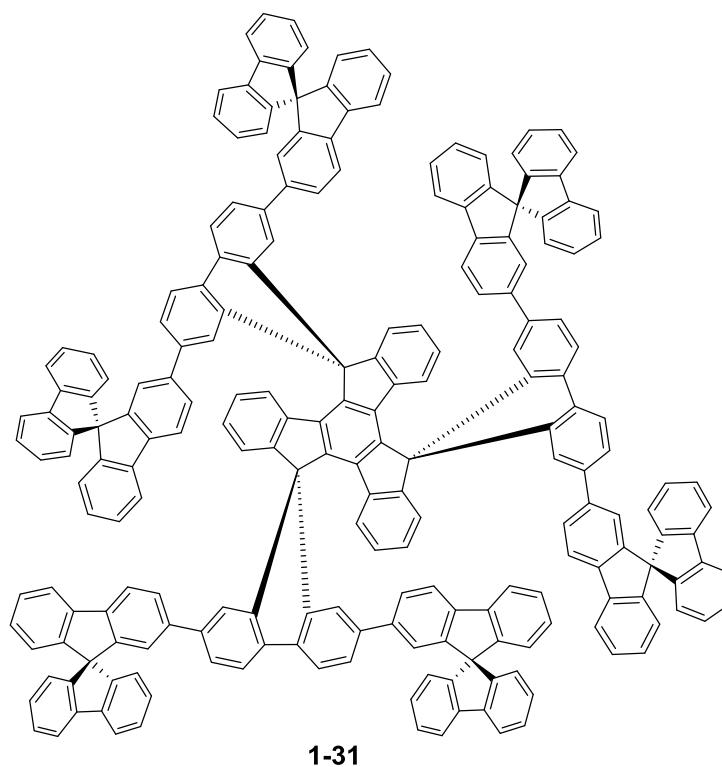
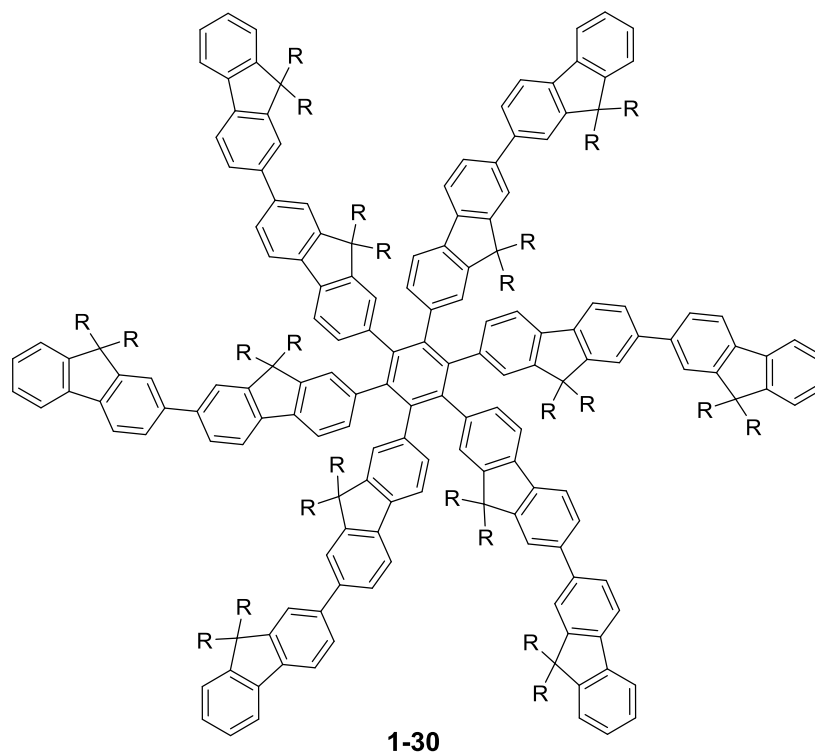
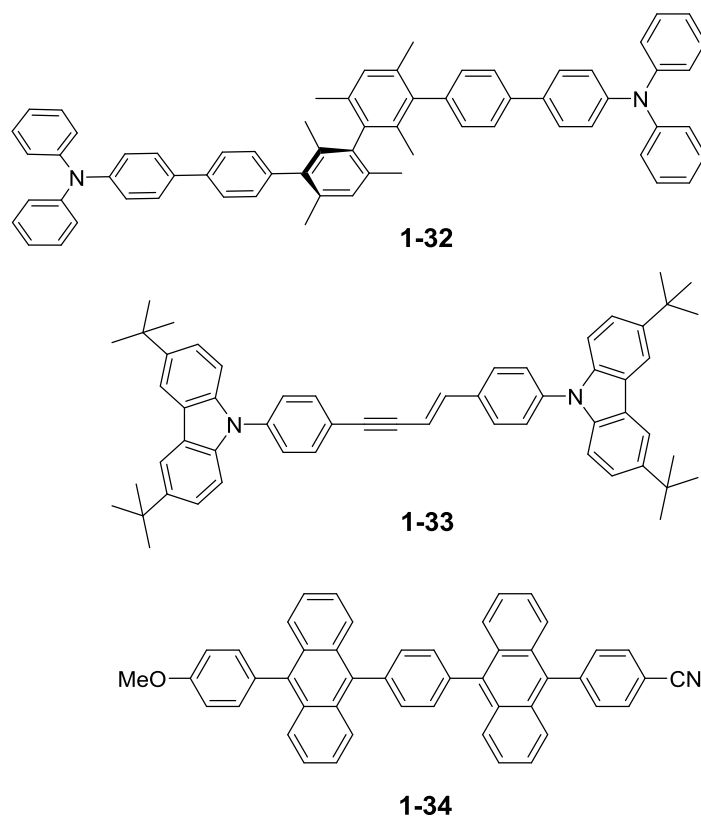


Figure I-11. Chemical structures of representative fluorene-based blue emitters.

Figure I-11 illustrates the typical fluorene-based blue emitters **1-30** and **1-31**, which were reported by Yang's and Pei's group, respectively. Star-burst molecule **1-30** exhibits a distinguished device performance, with EQE of 6.1%, current efficiency

of  $4.9 \text{ cd A}^{-1}$ , together with CIE of (0.17, 0.08). For molecule **1-30**, the introduction of alkyl chains on the C9 in the fluorene units can prevent the fluorene oxidation; however, the long alkyl chain act as insulator what can be relatively detrimental to the charge transfer. Construction of spiro-fluorene is another alternative way to prevent the C9 oxidation. The device based on molecule **1-31** with the configuration of ITO/PEDOT:PSS/PVK/**1-31**/TPBI/Ba/Al demonstrated stable blue emitting properties.



**Figure I-12.** Chemical structures of representative triphenylamine-, carbazole-, and anthracene-based blue emitters.

Triphenylamine, carbazole, and anthracene are also commonly used building blocks to construct novel blue emitters. Three representative compounds shown in Figure I-12 present good device performance. For example, the nondoped device based on **1-32** presented high deep blue-emitting efficiency with EQE up to 4.09% with CIE of (0.15, 0.09)<sup>[98]</sup> In the case of **1-33** and **1-34**, their doped devices also can achieve outstanding performances. The maximum EQEs (CE) for **1-33** and **1-34** are 7.1% ( $9.1 \text{ cd A}^{-1}$ ) and 12% ( $6.1 \text{ cd A}^{-1}$ ), respectively. <sup>[99-100]</sup>

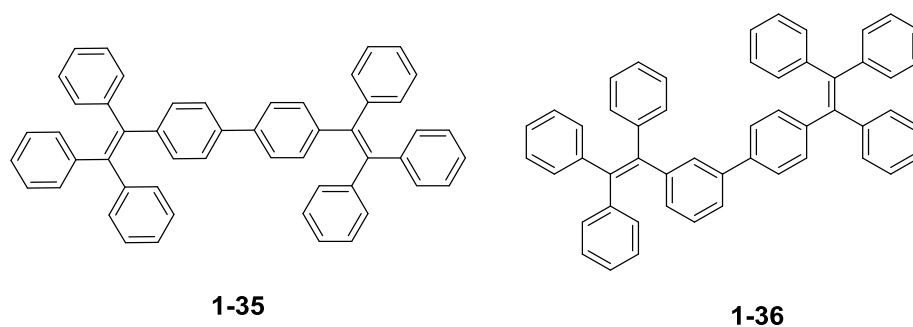


Figure I-13. Chemical structures of aggregation induced blue emitters.

In some cases, fluorophores suffer from the notorious aggregation, which can be detrimental to device performance. However, the compounds with aggregation-induced emission behavior used as device active layer can efficiently tackle the problem (Figure 1-13). Tang and co-workers employed tetraphenylethene (TPE) based compound **1-35** as emitter. The corresponding electroluminescence device showed a CE up to  $7.3 \text{ cd A}^{-1}$  with maximum emitting wavelength of 488 nm. To further investigate and explore the potential of TPE unit, Li and co-workers synthesized molecule **1-36** with a different linkage mode of two TPE moieties. Surprisingly, the EL peak of non-doped OLED device with **1-36** as active layer, was more blue-shifted, with EL peak at 459 nm, together with highest EQE of 1.9% and CE of  $2.8 \text{ cd A}^{-1}$ .<sup>[95]</sup>

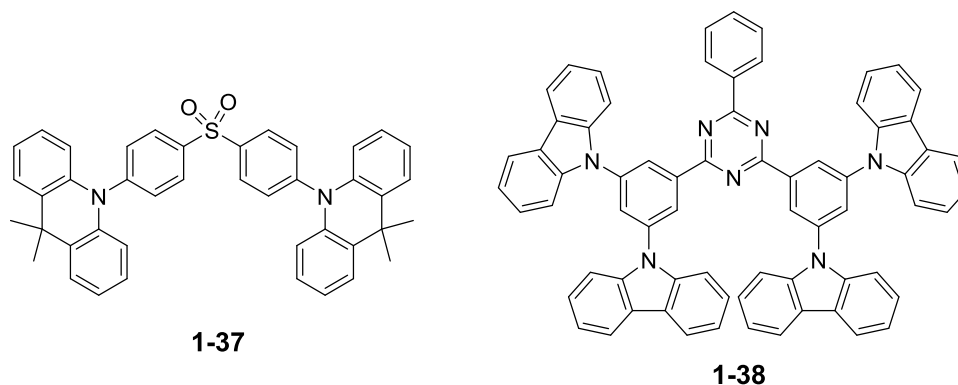


Figure I-14. Chemical structures of thermally activated delayed fluorescence blue emitters.

Recently, thermally activated delayed fluorescence (TADF) materials showed excellent device performance, since the 100% internal quantum efficiency could be reached theoretically. In order to achieve that, the energy gaps ( $\Delta E_{ST}$ ) between the lowest excited singlet state ( $S_1$ ) and the lowest excited triplet state ( $T_1$ ) should be  $<$

0.3 eV, which enable the thermally activated reverse intersystem crossing occur at room temperature. Adachi and co-workers proposed the TADF emitter design strategy, namely, constructing a highly distorted  $\pi$ -conjugated molecule with both bulky electron donor and acceptor moieties. According to this principle, emitter **1-37** and **1-38** shown in Figure I-14 were designed and synthesized by the groups of Adachi and Lee, respectively. For compound **1-37**, a maximum EQE of 19.5% was achieved with CIE of (0.16, 0.20), which is comparable to that of the best blue phosphorescent OLEDs reported to date.<sup>[101]</sup> Another representative blue TADF emitter is triazine-based compound **1-38**, which demonstrates not only high EQE of up to 18.9% with CIE of (0.16, 0.24), but also a long lifetime, over performing that of the blue phosphorescent OLEDs.<sup>[102]</sup>

## I.4 Motivation and objectives

As reviewed above, the performances of electronic devices strongly depended on one essential element, namely, the molecular structures. That also means, by manipulating molecular structures to alter their frontier orbital energy levels, geometries, solubility and so forth, novel functional materials can be developed for well-performing electronic devices. Undoubtedly, we can use synthetic tools to develop a wealth of materials with varying functionalities. However, our research interests specially lie in designing n-type semiconductors for OFETs, electron acceptors for OPVs, and blue-emitting materials for OLEDs.

From the molecular design and material application points of view, some interesting ideas came out:

- i) V-shaped p-type molecules used for OFET showed hole mobilities as high as  $9.5 \text{ cm}^2 \text{ V}^{-1} \text{ s}^{-1}$ , however, the device performance based on V-shaped n-type materials were not reported. Thus In chapter II, the synthesis of two angular-shaped n-type semiconductors is described. Their solution-processed OFET devices show varying electron mobilities, namely 0.01 and  $5 \times 10^{-4} \text{ cm}^2 \text{ V}^{-1} \text{ s}^{-1}$ . The leading reasons are also clear elucidated.

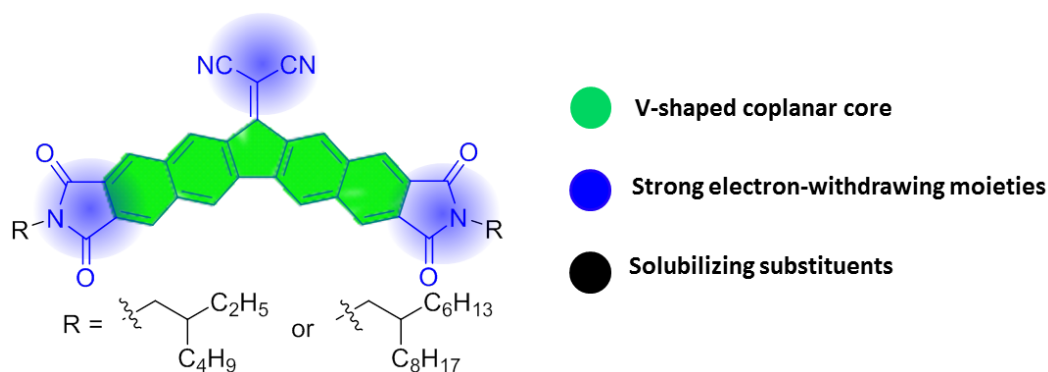


**Figure I-15.** Chemical structures of angular-shaped n-type semiconductors.

- ii) Bis-benzothiadiazole (BBT) has just emerged as a promising electron deficient building block for organic functional materials. An interesting topic should combine BBT units with electron-deficient cores or electron-rich acenes, such as anthracene, tetracene and pentacene to construct novel molecules, together with their single crystal analysis. In chapter III, linear benzoquinone-fused bis(benzothiadiazole) and V-shaped sulfone-fused bis(benzothiadiazole) demonstrate their potential as electron acceptors. Their different molecular geometries significantly influence the mode of crystal packing, which highlights the important role of molecular shape in organic conjugated materials.

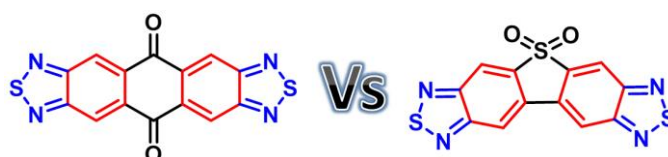


**Figure I-16.** Chemical structures of benzothiadiazole-based acceptors.

In chapter IV, the construction of four layered electron acceptors equipped with terminal 1,2,5-thiadiazole groups is illustrated. In such conjugated systems, their unique photophysical properties were discovered for the first time.

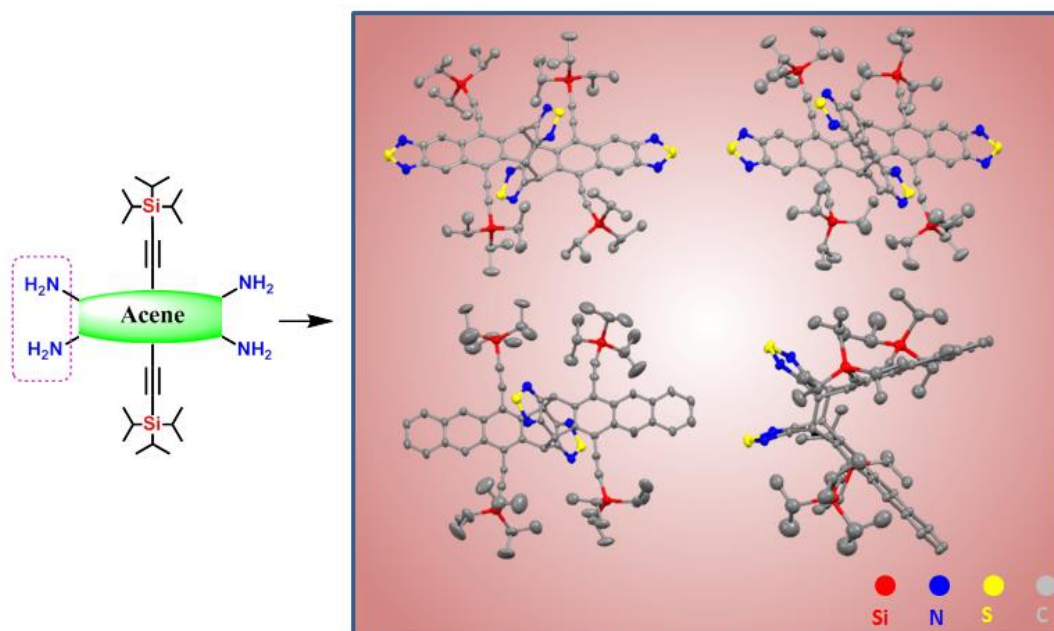


Figure I-17. Chemical structures of layered molecules.

- iii) The design and construction of spatially extended electron acceptors for isotropic charge<sup>[10]</sup> transfer like fullerene derivatives is an appealing topic. Indeed, the dicyanovinylene derivatives have already proven their potential as n-type organic semiconductors. Thus we predict that dicyanovinylene-substituted acceptors might also be a good candidate for fullerene-free OPVs. In chapter V and VI, the functionalization of the spiro-fluorenes is shown, yielding asymmetric and symmetric cruciform electron acceptors. Both molecules adopt 2D isotropic  $\pi$ -stacking and can serve as electron acceptors for fullerene-free OPVs.

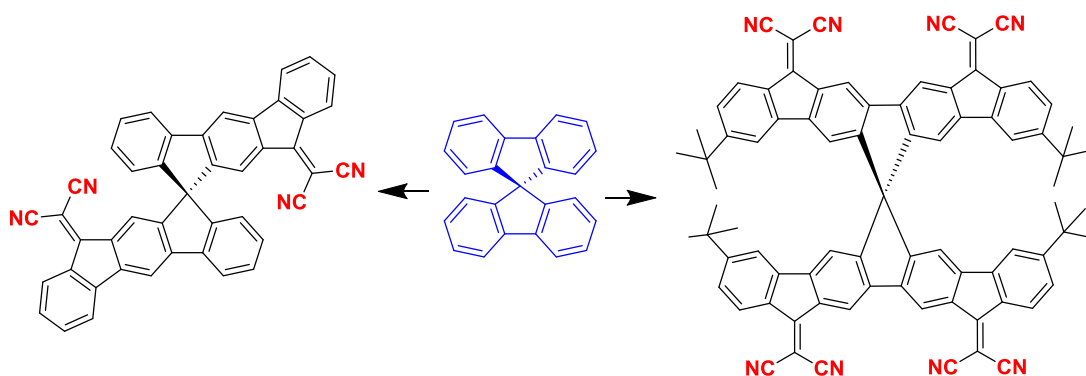


Figure I-18. Synthesis of spiro-fluorene based acceptors.

- iv) Spiro-fluorene is a well-known moiety for its thermal and electrochemical stability. Thus, it is expected to use such unit to construct more sterically rigid molecules for high efficient blue emitting OLEDs. In chapter VII, a unique design for blue light emitting materials is presented. Starting from commercial available building unit spiro-fluorene, dihydroindenofluorene-based and ladder-type tetra-p-phenylene-based blue emitters were synthesized with promising performances in OLED devices.

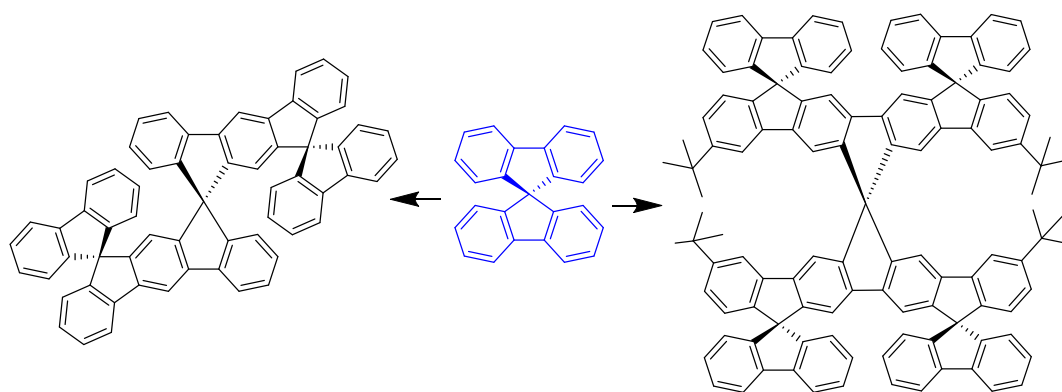


Figure I-19. Synthesis of spiro-fluorene based blue emitters.

## I.5 References

- [1] H. Shirakawa, E. J. Louis, A. G. MacDiarmid, C. K. Chiang, A. J. Heeger, *J. Chem. Soc., Chem. Commun.* **1977**, 578-580.
- [2] M. Muccini, *Nat. Mater.* **2006**, 5, 605-613.
- [3] C. Wang, H. Dong, W. Hu, Y. Liu, D. Zhu, *Chem. Rev.* **2012**, 112, 2208-2267.
- [4] X. Guo, M. Baumgarten, K. Müllen, *Prog. Polym. Sci.* **2013**, 38, 1832-1908.
- [5] C.-a. Di, F. Zhang, D. Zhu, *Adv. Mater.* **2013**, 25, 313-330.
- [6] F. C. Krebs, *Sol. Energ Mater. Sol. Cells* **2009**, 93, 394-412.
- [7] T. Sekitani, U. Zschieschang, H. Klauk, T. Someya, *Nat. Mater.* **2010**, 9, 1015-1022.
- [8] B. Comiskey, J. D. Albert, H. Yoshizawa, J. Jacobson, *Nature* **1998**, 394, 253-255.

- [9] G. H. Gelinck, H. E. A. Huitema, E. van Veenendaal, E. Cantatore, L. Schrijnemakers, J. B. P. H. van der Putten, T. C. T. Geuns, M. Beenhakkers, J. B. Giesbers, B.-H. Huisman, E. J. Meijer, E. M. Benito, F. J. Touwslager, A. W. Marsman, B. J. E. van Rens, D. M. de Leeuw, *Nat. Mater.* **2004**, *3*, 106-110.
- [10] J. Roncali, P. Leriche, A. Cravino, *Adv. Mater.* **2007**, *19*, 2045-2060.
- [11] A. Tsumura, H. Koezuka, T. Ando, *Appl. Phys. Lett.* **1986**, *49*, 1210-1212.
- [12] O. D. Jurchescu, J. Baas, T. T. M. Palstra, *Appl. Phys. Lett.* **2004**, *84*, 3061-3063.
- [13] H. Minemawari, T. Yamada, H. Matsui, J. y. Tsutsumi, S. Haas, R. Chiba, R. Kumai, T. Hasegawa, *Nature* **2011**, *475*, 364-367.
- [14] C. Luo, A. K. K. Kyaw, L. A. Perez, S. Patel, M. Wang, B. Grimm, G. C. Bazan, E. J. Kramer, A. J. Heeger, *Nano Lett.* **2014**, *14*, 2764-2771.
- [15] C. Reese, Z. Bao, *Adv. Mater.* **2007**, *19*, 4535-4538.
- [16] O. D. Jurchescu, M. Popinciuc, B. J. van Wees, T. T. M. Palstra, *Adv. Mater.* **2007**, *19*, 688-692.
- [17] E. Menard, V. Podzorov, S. H. Hur, A. Gaur, M. E. Gershenson, J. A. Rogers, *Adv. Mater.* **2004**, *16*, 2097-2101.
- [18] T. Ameri, P. Khoram, J. Min, C. J. Brabec, *Adv. Mater.* **2013**, *25*, 4245-4266.
- [19] Y. Lin, Y. Li, X. Zhan, *Chem. Soc. Rev.* **2012**, *41*, 4245-4272.
- [20] A. a. F. Eftaiha, J.-P. Sun, I. G. Hill, G. C. Welch, *J. Mater. Chem. A* **2014**, *2*, 1201-1213.
- [21] K. R. Graham, C. Cabanetos, J. P. Jahnke, M. N. Idso, A. El Labban, G. O. Ngongang Ndjawa, T. Heumueller, K. Vandewal, A. Salleo, B. F. Chmelka, A. Amassian, P. M. Beaujuge, M. D. McGehee, *J. Am. Chem. Soc.* **2014**, *136*, 9608-9618.
- [22] B. C. Thompson, J. M. J. Fréchet, *Angew. Chem. Int. Ed.* **2008**, *47*, 58-77.
- [23] Z. He, C. Zhong, S. Su, M. Xu, H. Wu, Y. Cao, *Nat. Photonics* **2012**, *6*, 591-595.
- [24] B. Kan, Q. Zhang, M. Li, X. Wan, W. Ni, G. Long, Y. Wang, X. Yang, H. Feng, Y. Chen, *J. Am. Chem. Soc.* **2014**, *136*, 15529-15532.
- [25] J. You, L. Dou, K. Yoshimura, T. Kato, K. Ohya, T. Moriarty, K. Emery, C.-C. Chen, J. Gao, G. Li, Y. Yang, *Nat. Commun.* **2013**, *4*, 1446.
- [26] T. Ameri, N. Li, C. J. Brabec, *Energy Environ. Sci.* **2013**, *6*, 2390-2413.

- [27] Y. Liu, C.-C. Chen, Z. Hong, J. Gao, Y. Yang, H. Zhou, L. Dou, G. Li, Y. Yang, *Sci. Rep.* **2013**, *3*, 3356.
- [28] D. Carsten, D. Vladimir, *Rep. Prog. Phys.* **2010**, *73*, 096401.
- [29] Y.-J. Cheng, S.-H. Yang, C.-S. Hsu, *Chem. Rev.* **2009**, *109*, 5868-5923.
- [30] C. W. Tang, *Appl. Phys. Lett.* **1986**, *48*, 183-185.
- [31] G. Yu, J. Gao, J. C. Hummelen, F. Wudl, A. J. Heeger, *Science* **1995**, *270*, 1789-1791.
- [32] J. K. Borchardt, *Mater. Today* **2004**, *7*, 42-46.
- [33] M. Pope, H. P. Kallmann, P. Magnante, *J. Chem. Phys.* **1963**, *38*, 2042-2043.
- [34] C. W. Tang, S. A. VanSlyke, *Appl. Phys. Lett.* **1987**, *51*, 913-915.
- [35] J. H. Burroughes, D. D. C. Bradley, A. R. Brown, R. N. Marks, K. Mackay, R. H. Friend, P. L. Burns, A. B. Holmes, *Nature* **1990**, *347*, 539-541.
- [36] M. A. Baldo, D. F. O'Brien, Y. You, A. Shoustikov, S. Sibley, M. E. Thompson, S. R. Forrest, *Nature* **1998**, *395*, 151-154.
- [37] H. Tian, Y. Deng, F. Pan, L. Huang, D. Yan, Y. Geng, F. Wang, *J. Mater. Chem.* **2010**, *20*, 7998-8004.
- [38] S. Wang, M. Wang, X. Zhang, X. Yang, Q. Huang, X. Qiao, H. Zhang, Q. Wu, Y. Xiong, J. Gao, H. Li, *Chem. Commun.* **2013**.
- [39] H. Li, F. S. Kim, G. Ren, E. C. Hollenbeck, S. Subramaniyan, S. A. Jenekhe, *Angew. Chem. Int. Ed.* **2013**, *52*, 5513-5517.
- [40] Y. Lin, Y. Li, X. Zhan, *Adv. Energy Mater.* **2013**, *3*, 724-728.
- [41] X.-F. Wu, W.-F. Fu, Z. Xu, M. Shi, F. Liu, H.-Z. Chen, J.-H. Wan, T. P. Russell, *Adv. Funct. Mater.* **2015**, *25*, 5954-5966.
- [42] S. M. McAfee, J. M. Topple, I. G. Hill, G. C. Welch, *J. Mater. Chem. A* **2015**, *3*, 16393-16408.
- [43] O. K. Kwon, J.-H. Park, S. K. Park, S. Y. Park, *Adv. Energy Mater.* **2015**, *5*, 1400929.
- [44] H. Li, T. Earmme, S. Subramaniyan, S. A. Jenekhe, *Adv. Energy Mater.* **2015**, *5*, 1402041.
- [45] X.-K. Liu, C.-J. Zheng, M.-F. Lo, J. Xiao, C.-S. Lee, M.-K. Fung, X.-H. Zhang, *Chem. Commun.* **2014**, *50*, 2027-2029.
- [46] H.-H. Chou, Y.-H. Chen, H.-P. Hsu, W.-H. Chang, Y.-H. Chen, C.-H. Cheng, *Adv. Mater.* **2012**, *24*, 5867-5871.

- [47] X.-C. Hang, T. Fleetham, E. Turner, J. Brooks, J. Li, *Angew. Chem. Int. Ed.* **2013**, *52*, 6753-6756.
- [48] Y. Sakamoto, T. Suzuki, M. Kobayashi, Y. Gao, Y. Fukai, Y. Inoue, F. Sato, S. Tokito, *J. Am. Chem. Soc.* **2004**, *126*, 8138-8140.
- [49] Y.-I. Park, J. S. Lee, B. J. Kim, B. Kim, J. Lee, D. H. Kim, S.-Y. Oh, J. H. Cho, J.-W. Park, *Chem. Mater.* **2011**, *23*, 4038-4044.
- [50] M.-C. Chen, Y.-J. Chiang, C. Kim, Y.-J. Guo, S.-Y. Chen, Y.-J. Liang, Y.-W. Huang, T.-S. Hu, G.-H. Lee, A. Facchetti, T. J. Marks, *Chem. Commun.* **2009**, 1846-1848.
- [51] J. A. Letizia, A. Facchetti, C. L. Stern, M. A. Ratner, T. J. Marks, *J. Am. Chem. Soc.* **2005**, *127*, 13476-13477.
- [52] S. Ando, R. Murakami, J.-i. Nishida, H. Tada, Y. Inoue, S. Tokito, Y. Yamashita, *J. Am. Chem. Soc.* **2005**, *127*, 14996-14997.
- [53] Y. Ie, M. Ueta, M. Nitani, N. Tohnai, M. Miyata, H. Tada, Y. Aso, *Chem. Mater.* **2012**, *24*, 3285-3293.
- [54] F. Zhang, Y. Hu, T. Schuettfort, C.-a. Di, X. Gao, C. R. McNeill, L. Thomsen, S. C. B. Mannsfeld, W. Yuan, H. Sirringhaus, D. Zhu, *J. Am. Chem. Soc.* **2013**, *135*, 2338-2349.
- [55] B. Yoo, B. A. Jones, D. Basu, D. Fine, T. Jung, S. Mohapatra, A. Facchetti, K. Dimmler, M. R. Wasielewski, T. J. Marks, A. Dodabalapur, *Adv. Mater.* **2007**, *19*, 4028-4032.
- [56] B. A. Jones, A. Facchetti, T. J. Marks, M. R. Wasielewski, *Chem. Mater.* **2007**, *19*, 2703-2705.
- [57] J. Chang, H. Qu, Z.-E. Ooi, J. Zhang, Z. Chen, J. Wu, C. Chi, *J. Mater. Chem. C* **2013**, *1*, 456-462.
- [58] Z. Wang, C. Kim, A. Facchetti, T. J. Marks, *J. Am. Chem. Soc.* **2007**, *129*, 13362-13363.
- [59] J. Li, J.-J. Chang, H. S. Tan, H. Jiang, X. Chen, Z. Chen, J. Zhang, J. Wu, *Chem. Sci.* **2012**, *3*, 846-850.
- [60] X. Gao, Y. Hu, *J. Mater. Chem. C* **2014**, *2*, 3099-3117.
- [61] T. M. Pappenfus, R. J. Chesterfield, C. D. Frisbie, K. R. Mann, J. Casado, J. D. Raff, L. L. Miller, *J. Am. Chem. Soc.* **2002**, *124*, 4184-4185.

- [62] S. Handa, E. Miyazaki, K. Takimiya, Y. Kunugi, *J. Am. Chem. Soc.* **2007**, *129*, 11684-11685.
- [63] Y. Qiao, Y. Guo, C. Yu, F. Zhang, W. Xu, Y. Liu, D. Zhu, *J. Am. Chem. Soc.* **2012**, *134*, 4084-4087.
- [64] Q. Wu, S. Ren, M. Wang, X. Qiao, H. Li, X. Gao, X. Yang, D. Zhu, *Adv. Funct. Mater.* **2013**, *23*, 2277-2284.
- [65] C. Zhang, Y. Zang, E. Gann, C. R. McNeill, X. Zhu, C.-a. Di, D. Zhu, *J. Am. Chem. Soc.* **2014**, *136*, 16176-16184.
- [66] Q. Wu, R. Li, W. Hong, H. Li, X. Gao, D. Zhu, *Chem. Mater.* **2011**, *23*, 3138-3140.
- [67] A. Mishra, P. Bäuerle, *Angew. Chem. Int. Ed.* **2012**, *51*, 2020-2067.
- [68] Y. Zhong, M. T. Trinh, R. Chen, G. E. Purdum, P. P. Khlyabich, M. Sezen, S. Oh, H. Zhu, B. Fowler, B. Zhang, W. Wang, C.-Y. Nam, M. Y. Sfeir, C. T. Black, M. L. Steigerwald, Y.-L. Loo, F. Ng, X. Y. Zhu, C. Nuckolls, *Nat. Commun.* **2015**, *6*.
- [69] D. Mori, H. Benten, I. Okada, H. Ohkita, S. Ito, *Adv. Energy Mater.* **2014**, *4*, 1301006.
- [70] Y. Zang, C.-Z. Li, C.-C. Chueh, S. T. Williams, W. Jiang, Z.-H. Wang, J.-S. Yu, A. K. Y. Jen, *Adv. Mater.* **2014**, *26*, 5708-5714.
- [71] A. Sharenko, D. Gehrig, F. Laquai, T.-Q. Nguyen, *Chem. Mater.* **2014**, *26*, 4109-4118.
- [72] A. M. Poe, A. M. Della Pelle, A. V. Subrahmanyam, W. White, G. Wantz, S. Thayumanavan, *Chem. Commun.* **2014**, *50*, 2913-2915.
- [73] Y. Liu, L. Zhang, H. Lee, H.-W. Wang, A. Santala, F. Liu, Y. Diao, A. L. Briseno, T. P. Russell, *Adv. Energy Mater.* **2015**, *5*, 1500195.
- [74] T. V. Pho, F. M. Toma, B. J. Tremolet de Villers, S. Wang, N. D. Treat, N. D. Eisenmenger, G. M. Su, R. C. Coffin, J. D. Douglas, J. M. J. Fréchet, G. C. Bazan, F. Wudl, M. L. Chabynyc, *Adv. Energy Mater.* **2014**, *4*, 1301007.
- [75] H. Li, T. Earmme, G. Ren, A. Saeki, S. Yoshikawa, N. M. Murari, S. Subramaniyan, M. J. Crane, S. Seki, S. A. Jenekhe, *J. Am. Chem. Soc.* **2014**, *136*, 14589-14597.

- [76] Y. Zhong, M. T. Trinh, R. Chen, W. Wang, P. P. Khlyabich, B. Kumar, Q. Xu, C.-Y. Nam, M. Y. Sfeir, C. Black, M. L. Steigerwald, Y.-L. Loo, S. Xiao, F. Ng, X. Y. Zhu, C. Nuckolls, *J. Am. Chem. Soc.* **2014**, *136*, 15215-15221.
- [77] Q. Yan, Y. Zhou, Y.-Q. Zheng, J. Pei, D. Zhao, *Chem. Sci.* **2013**, *4*, 4389-4394.
- [78] X. Zhang, C. Zhan, J. Yao, *Chem. Mater.* **2015**, *27*, 166-173.
- [79] X. Zhang, Z. Lu, L. Ye, C. Zhan, J. Hou, S. Zhang, B. Jiang, Y. Zhao, J. Huang, S. Zhang, Y. Liu, Q. Shi, Y. Liu, J. Yao, *Adv. Mater.* **2013**, *25*, 5791-5797.
- [80] Y. Liu, C. Mu, K. Jiang, J. Zhao, Y. Li, L. Zhang, Z. Li, J. Y. L. Lai, H. Hu, T. Ma, R. Hu, D. Yu, X. Huang, B. Z. Tang, H. Yan, *Adv. Mater.* **2015**, *27*, 1015-1020.
- [81] Y. Lin, Y. Wang, J. Wang, J. Hou, Y. Li, D. Zhu, X. Zhan, *Adv. Mater.* **2014**, *26*, 5137-5142.
- [82] J. Zhao, Y. Li, H. Lin, Y. Liu, K. Jiang, C. Mu, T. Ma, J. Y. Lin Lai, H. Hu, D. Yu, H. Yan, *Energy Environ. Sci.* **2015**, *8*, 520-525.
- [83] S. Holliday, R. S. Ashraf, C. B. Nielsen, M. Kirkus, J. A. Röhr, C.-H. Tan, E. Collado-Fregoso, A.-C. Knall, J. R. Durrant, J. Nelson, I. McCulloch, *J. Am. Chem. Soc.* **2015**, *137*, 898-904.
- [84] J. T. Bloking, T. Giovenzana, A. T. Higgs, A. J. Ponec, E. T. Hoke, K. Vandewal, S. W. Ko, Z. N. Bao, A. Sellinger, M. D. McGehee, *Adv. Energy Mater.* **2014**, *4*, 1301426.
- [85] O. K. Kwon, J.-H. Park, D. W. Kim, S. K. Park, S. Y. Park, *Adv. Mater.* **2015**, *27*, 1951-1956.
- [86] Y. Lin, J. Wang, Z.-G. Zhang, H. Bai, Y. Li, D. Zhu, X. Zhan, *Adv. Mater.* **2015**, *27*, 1170-1174.
- [87] M. Zhu, C. Yang, *Chem. Soc. Rev.* **2013**, *42*, 4963-4976.
- [88] C. Liu, Y. Gu, Q. Fu, N. Sun, C. Zhong, D. Ma, J. Qin, C. Yang, *Chem. Eur. J.* **2012**, *18*, 13828-13835.
- [89] S. L. Gong, Q. Fu, W. X. Zeng, C. Zhong, C. L. Yang, D. G. Ma, J. G. Qin, *Chem. Mater.* **2012**, *24*, 3120-3127.
- [90] Y. Li, Z. Wang, X. Li, G. Xie, D. Chen, Y.-F. Wang, C.-C. Lo, A. Lien, J. Peng, Y. Cao, S.-J. Su, *Chem. Mater.* **2015**.
- [91] J. Santos, J. H. Cook, H. A. Al-Attar, A. P. Monkman, M. R. Bryce, *J. Mater. Chem. C* **2015**, *3*, 2479-2483.

- [92] K. Albrecht, K. Matsuoka, K. Fujita, K. Yamamoto, *Angew. Chem. Int. Ed.* **2015**, *54*, 5677-5682.
- [93] M. Liu, Y. Seino, D. Chen, S. Inomata, S.-J. Su, H. Sasabe, J. Kido, *Chem. Commun.* **2015**, DOI: 10.1039/C1035CC05435D.
- [94] T. Nakagawa, S.-Y. Ku, K.-T. Wong, C. Adachi, *Chem. Commun.* **2012**, *48*, 9580-9582.
- [95] J. Huang, N. Sun, Y. Dong, R. Tang, P. Lu, P. Cai, Q. Li, D. Ma, J. Qin, Z. Li, *Adv. Funct. Mater.* **2013**, *23*, 2329-2337.
- [96] J. Huang, X. Yang, J. Wang, C. Zhong, L. Wang, J. Qin, Z. Li, *J. Mater. Chem.* **2012**, *22*, 2478-2484.
- [97] J. Huang, N. Sun, J. Yang, R. Tang, Q. Li, D. Ma, J. Qin, Z. Li, *J. Mater. Chem.* **2012**, *22*, 12001-12007.
- [98] J. N. Moorthy, P. Venkatakrisnan, D.-F. Huang, T. J. Chow, *Chem. Commun.* **2008**, 2146-2148.
- [99] T. Peng, G. Li, Y. Liu, Y. Wu, K. Ye, D. Yao, Y. Yuan, Z. Hou, Y. Wang, *Org. Electron.* **2011**, *12*, 1068-1072.
- [100] J.-Y. Hu, Y.-J. Pu, F. Satoh, S. Kawata, H. Katagiri, H. Sasabe, J. Kido, *Adv. Funct. Mater.* **2014**, *24*, 2064-2071.
- [101] Q. Zhang, B. Li, S. Huang, H. Nomura, H. Tanaka, C. Adachi, *Nat. Photonics* **2014**, *8*, 326-332.
- [102] M. Kim, S. K. Jeon, S.-H. Hwang, J. Y. Lee, *Adv. Mater.* **2015**, *27*, 2515-2520.



# Chapter II. Solution-Processable n-Type Angular-Shaped Organic Semiconductors

The angular-shaped n-type semiconductors 2-(12H-dibenzofluoren-12-ylidene)malononitrilediimide **2-5a** and **2-5b** were synthesized, and fully characterized by optical absorption and fluorescence, cyclic voltammetry, X-ray crystal structure analysis, XRD, and OFET device performance. The varying alkyl chain lengths of **2-5a** and **2-5b** caused different molecular orientations with respect to the substrate. Thus, **2-5a** presents an electron mobility of  $0.01 \text{ cm}^2 \text{ V}^{-1} \text{ s}^{-1}$ , whereas **2-5b** resulted in poor device performance with much lower electron mobility of  $5 \times 10^{-4} \text{ cm}^2 \text{ V}^{-1} \text{ s}^{-1}$ .

## II.1 Introduction

In comparison with hole transporting materials,<sup>[1-5]</sup> in order to obtain high performance materials for electron transport,<sup>[6-10]</sup> there are three key factors: 1) suitable lowest unoccupied molecular orbital (LUMO) energy levels allowing efficient electron injection from metal electrodes that can be achieved by introduction of electron-withdrawing groups or atoms (benzothiadiazole, dicyanovinylenes, imides, fluorines, *etc.*) into known p-type molecules;<sup>[11-17]</sup> 2) coplanarity favoring strong  $\pi$ - $\pi$  intermolecular interaction and thus improving the charge carrier transport in the solid state;<sup>[18-20]</sup> and 3) an edge-on molecular orientation with respect to the substrate usually result in high-performance OFET, due to minimized grain boundaries and charge traps.<sup>[4]</sup> As another factor, “shape” is, rarely considered, but especially important as it influences packing in the solid state. Almost all n-type organic

semiconductors reported so far adopt linear arrangements.<sup>[2, 5, 7]</sup> Therefore, exploration of angular-shaped n-type molecules might expand the potential applications in OFETs.

#### Known V-shaped p-type materials

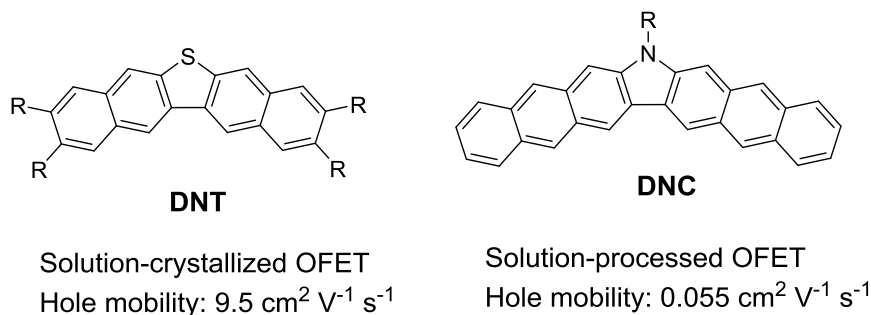


**Figure II-1.** Structures of **DNT** and **DNC**.

Very recently, V-shaped molecules with extended  $\pi$ -conjugation have revealed to be good candidates for p-type OFETs. For example, OFETs based on solution-crystallized dinaphtho-thiophene (**DNT**) (Figure II-1) showed extremely high hole mobility as  $9.5 \text{ cm}^2 \text{ V}^{-1} \text{ s}^{-1}$  because of the suitable molecular arrangements in the solid states.<sup>[21]</sup> In another study, dinaphthocarbazole (**DNC**) (Figure II-1) with seven fused rings presented good stability compared to the linear acene counterparts, arising from a stabilization of the highest occupied molecular orbital (HOMO). Additionally, **DNC** exhibited a hole mobility of  $0.055 \text{ cm}^2 \text{ V}^{-1} \text{ s}^{-1}$  from solution-processed OFETs.<sup>[22]</sup> Considering both the high mobility of **DNT** and the stability of the **DNC** of such V-shaped molecules, electron-withdrawing groups at the endpoints of the V-shaped coplanar core have been combined in the current design. This also enables to study the details of packing of these molecules between each other and with respect to the surface in comparison to linear fused acceptors.

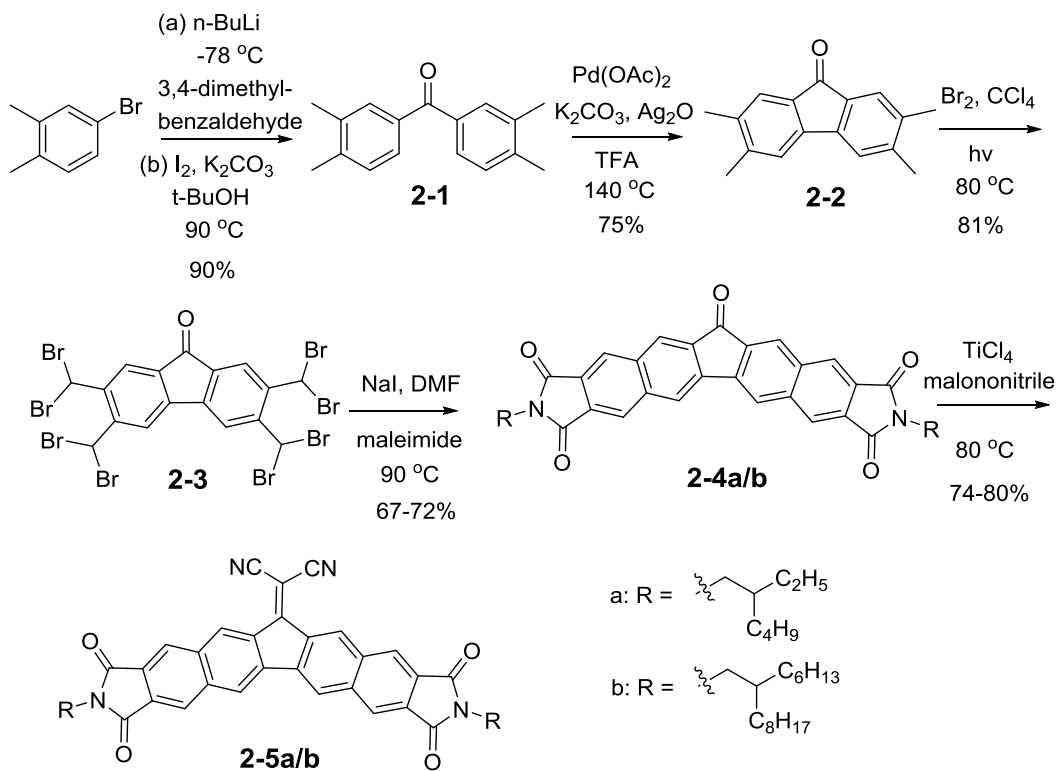
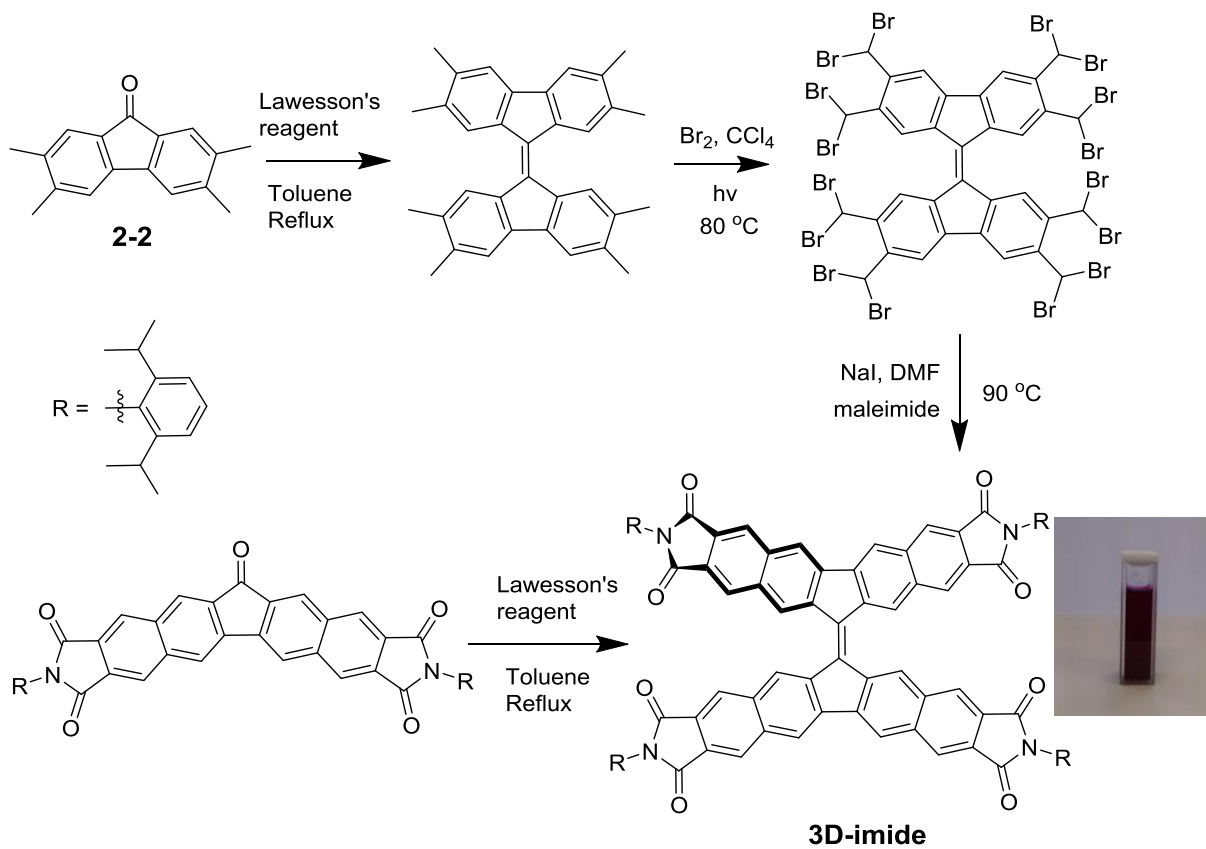
Based on such a molecular design, 2-(12H-dibenzofluoren-12-ylidene)malononitrilediimide (**1-5a/b**, Scheme1) are expected to be good candidates as solution-processable n-type materials according to the following considerations: 1) the electron-withdrawing dicarboximides and dicyanovinylene units will dramatically lower the LUMO energy level for effective electron injection; 2) alkyl chains can be easily attached at the nitrogen atoms of the end-capped dicarboximides to induce

solubility and formation of ordered thin films; and 3) the rigid and planar conjugated framework facilitates efficient intermolecular charge-transfer interaction.

## II.2 Synthesis

2,3,6,7-Tetramethyl-9H-fluoren-9-one (**2-2**) is the key building block for organic semiconductors, as extension of  $\pi$ -conjugation can be achieved by the functionalization of tetramethyl and carbonyl groups of **2-2**. Compound **2-2** was achieved in 75% yield through Pd-catalyzed dehydrogenative cyclization.<sup>[23]</sup> Note that the TFA amount could significantly influence the yield of **2-2**, which ranged from 20% to 80%. The best reaction concentration of **2-1** in TFA was 0.1 g/mL. Thereafter, radical bromination was done with bromine in CCl<sub>4</sub> upon irradiation with a 250 W halogen lamp, which afforded 2, 3, 6, 7-tetrakis(dibromomethyl)-9H-fluoren-9-one **2-3** as a yellow solid in 81% yield. After treatment of fluorenone **2-3** with NaI in DMF, a Diels–Alder cycloaddition with maleimides containing different alkyl chains afforded **2-4a/b** in 67-72% yield. As a matter of fact, hexyl linear chains were also introduced in the N atom positions aiming for achieving more planar molecules in comparison with **2-4a/b**. However, due to bad solubility, this target compound could not be purified by column chromatography. Finally, the target products **2-5a/b** were obtained in 74-80% yield by Knoevenagel condensation of **2-4a/b** with the Lehnert reagent<sup>[24-25]</sup> (TiCl<sub>4</sub>, malononitrile, pyridine). The chemical structures of all new compounds were fully supported by standard spectroscopic characterizations and high resolution mass spectrometry.

Apart from that, this two dimensional planar conjugated system can be spatially extended. As shown in Scheme II-2, **3D-imide** could also be obtained by two reaction routes, which was confirmed by H-NMR spectrum (Figure II-2). Note that the “below” reaction route was not very efficient due to the less reactivity reactant caused by electron deficient imide groups. Additionally, the angle of the two faces in **3D-imide** was calculated to be 35 °C and the color of the material is purple, which means it can harvest more photons. Therefore, it might be suitable used as electron acceptor for solar cells. Unfortunately, the compound decomposed slowly in deuterated chloroform, thus, this topic was not investigated further.

Scheme II-1. Synthesis of **2-4a/b** and **2-5a/b**.Scheme II-2. Synthesis of **3D-imide**.

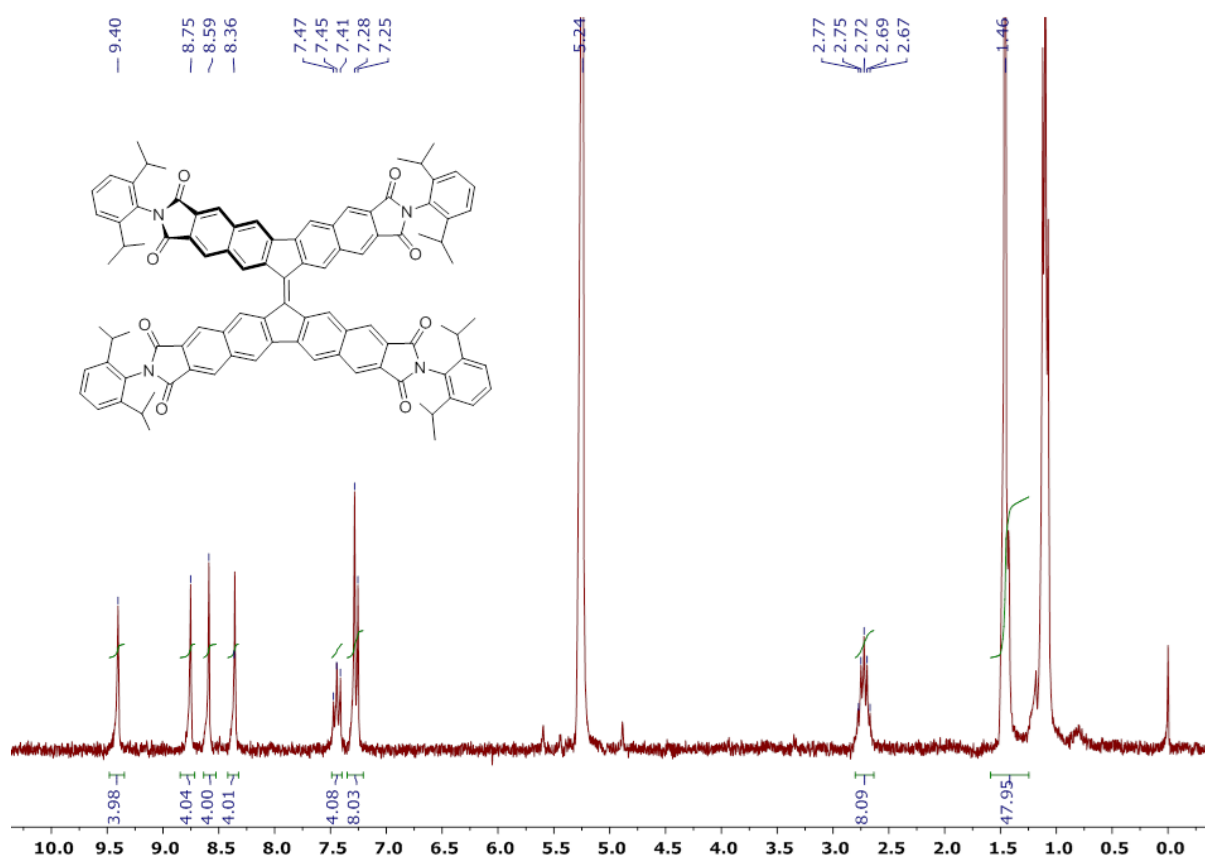
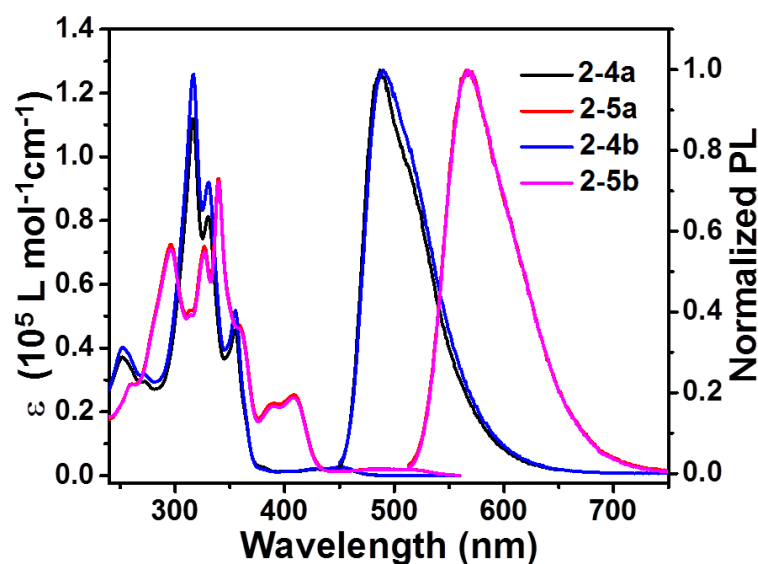


Figure II-2. H-NMR spectrum of **3D-imide**.

### II.3 Photophysical, electrochemical, and thermal properties

The UV-vis absorption and photoluminescence spectra of **2-4a/b** and **2-5a/b** were recorded in DCM solution (Figure II-3 and Table II-1). Compounds **2-4a** (**2-5a**) and **2-4b** (**2-5b**) displayed almost the same substructures in the absorption spectra and identical emission wavelengths because the alkyl chains do not influence the electronic properties in dilute solution.<sup>[26]</sup> The absorption bands for **2-4** (below 400 nm) and for **2-5** (below 450 nm) are contributed from  $\pi$ - $\pi^*$  transitions. Very weak absorption bands were also observed at lower energy ca. 428/452 nm for **2-4** and 485/516 nm for **2-5**, which were ascribed to symmetry forbidden  $n$ - $\pi^*$  transitions. The significant red-shift of both the absorption and emission spectra of **2-5** in comparison with **2-4** can be explained by the stronger electron withdrawing malononitrile group, which decreases the LUMO more than the HOMO energies.<sup>[27-30]</sup> The fluorescence

emission maxima of carbonyl-containing cores **2-4** and dicyanovinylene-containing **2-5** are located at 487 and 567 nm, respectively. Such large observed Stokes shifts are assigned to internal energy transfers between chromophore moieties in these molecules: the V-shaped conjugated core, the diimide, carbonyl/dicyano systems. Optical band gaps estimated from the onset of the absorption spectra are 2.60 eV and 2.25 eV for **2-4** and **2-5**, respectively.



**Figure II-3.** UV-vis absorption spectra and fluorescence spectra of **2-4a/b** and **2-5a/b** in dichloromethane.

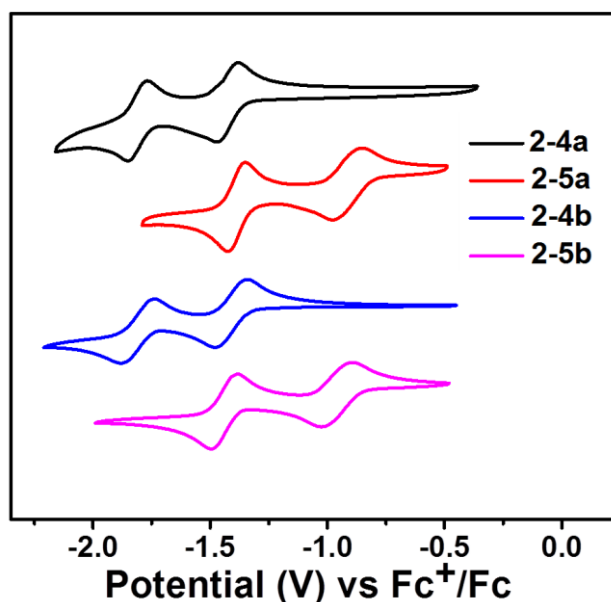


**Figure II-4.** Cyclic voltammetric profile of **2-4a/b** and **2-5a/b** in dichloromethane with 0.1 M  $\text{Bu}_4\text{NPF}_6$  as supporting electrolyte. Potentials are reported versus the  $\text{Fc}^+/\text{Fc}$  redox couple as an external standard, scan rate = 100 mV/s.

The redox properties of **2-4/a-b** and **2-5a/b** were studied using cyclic voltammetry. In Figure II-4, cyclic voltammograms of all compounds in DCM exhibited two reduction waves, with the  $E_{1/2}$  potential around -1.39V for **2-4** and -0.94 V for **2-5**, but no oxidation waves in the potential range available. The LUMO energies of **2-4** and **2-5** estimated through the equation  $E_{\text{LUMO}} = - [E_{\text{red}1/2} - E_{(\text{Fc}^+/\text{Fc})} + 4.8]$  eV were around -3.41 and -3.86 eV, respectively. The deeper LUMO level of **2-5** can be attributed to the stronger electron-withdrawing character of the dicyanovinylene group compared to that of the carbonyl moiety. The low-lying LUMO of **2-5** indicates that they could be well suited as n-type semiconductors with efficient electron injection.

**Table II-1.** Summary of photophysical and electrochemical properties of **2-4a/b** and **2-5a/b**.

	$E_{\text{red}1/2}$ vs $\text{Fc}^+/\text{Fc}$ (V) <sup>[a]</sup>	Absorption edge (nm)	LUMO (eV) <sup>[b]</sup>	HOMO (eV) <sup>[c]</sup>	$E_g$ (eV) <sup>[d]</sup>
<b>2-4a</b>	-1.38	477	-3.42	-6.02	2.60
<b>2-4b</b>	-1.40	477	-3.40	-6.00	2.60
<b>2-5a</b>	-0.92	550	-3.88	-6.13	2.25
<b>2-5b</b>	-0.95	550	-3.85	-6.10	2.25

[a] In  $\text{CH}_2\text{Cl}_2$ ,  $\text{Bu}_4\text{NPF}_6$  (0.1 M), 295 K, scan rate = 100 mV/s, versus  $\text{Fc}^+/\text{Fc}$ . [b] Determined from  $E_{\text{LUMO}} = - [E_{\text{red}1/2} - E_{(\text{Fc}^+/\text{Fc})} + 4.8]$  eV. [c] Calculated from  $E_{\text{HOMO}} = E_{\text{LUMO}} - E_{\text{gap}}$ . [d] Determined from the onset of absorption ( $1 \times 10^{-5}$  M).

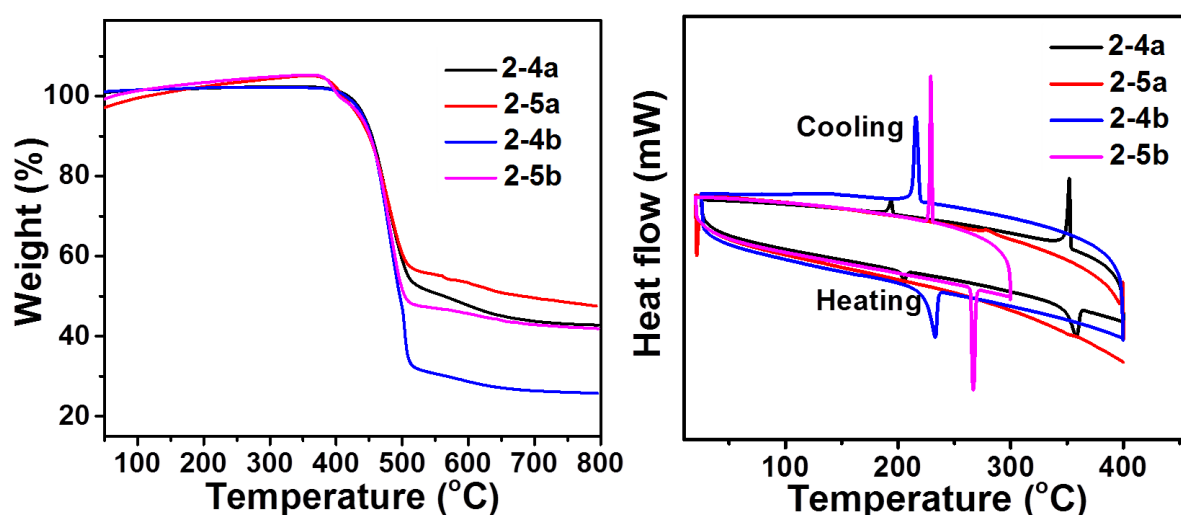


**Figure II-5.** TGA curves and DSC thermograms of the **2-4a/b** and **2-5a/b**.

Thermogravimetric analysis (TGA) revealed that **2-4a**, **2-4b**, **2-5a** and **2-5b** exhibit good thermal stability, with 5 wt% loss occurring at 442, 411, 441 and 404 °C,

respectively (Figure II-5). Differential scanning calorimetry (DSC) traces for **2-4a**, **2-4b**, **2-5a** and **2-5b** showed melting points at 359, 235, 359 and 266 °C, respectively (Figure II-4).

## II.4 Crystal structure analysis

The crystal growth of **2-5a** did not succeed via the slow evaporation method with different solvents, such as DCM, THF, and chloroform. A single crystal of **2-5b** was grown by slow evaporation of DCM. The crystal structure determined by X-ray diffraction is presented in Figure II-6. The crystal analysis experiment was carried out by ..... (Johannes Gutenberg-University, Mainz). The dicyanomethylene moiety is slightly twisted with respect to the backbone of the core, which can be caused by the close proximity of the cyano groups and the hydrogen atoms. The crystal structure of **2-5b** involves face-to-face stacked dimers, which interact with each other in a one-dimensional, slipped-stack arrangement as shown in Figure II-5 A. Furthermore, = O···H- (2.50 Å and 2.58 Å) and  $\equiv$  N···H- (2.38 Å) hydrogen bonds are an additional driving force contributing to the assembly of **2-5b**. This crystal arrangement is probably due to strong dipole–dipole interactions among the imide and cyano groups.

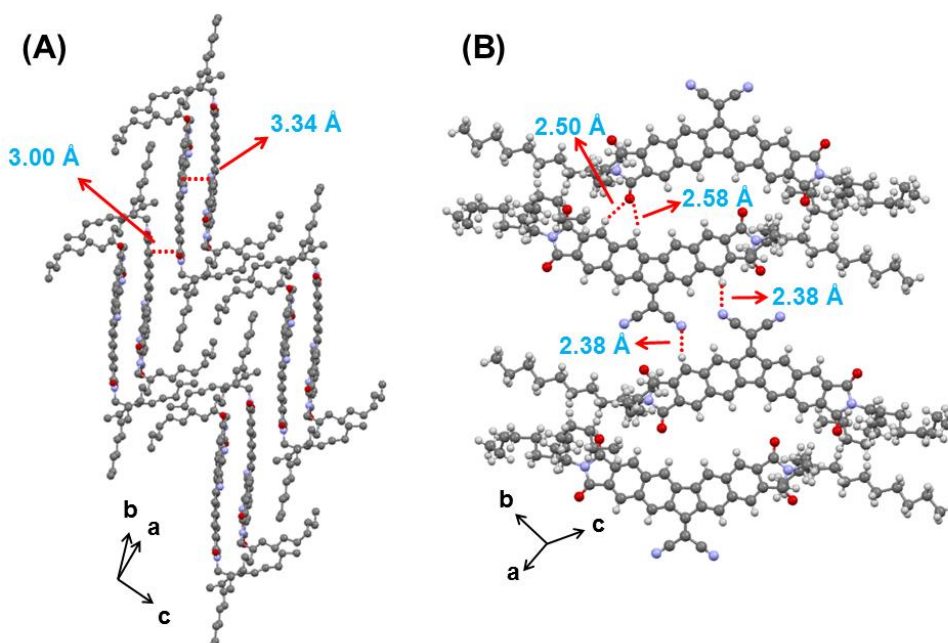


**Figure II-6.** Crystal packing of **2-5b**. (A) Face-to-face  $\pi$ - $\pi$  stacking with an interplanar distance of 3.34 Å. (B) = O···H- and  $\equiv$  N···H- hydrogen bonding between stacks.

## II.5 Density functional theory calculations

To gain more insights into the electronic properties of **2-4** and **2-5**, density functional theory (DFT) calculations were performed at the B3LYP/6-31G(d) level. As shown in Figure II-7, frontier molecular orbitals of both molecules contribute to the conjugated backbone, indicating effective  $\pi$ -conjugation in the fused systems. Moreover, the HOMOs of **2-4** and **2-5** demonstrate almost the same orbital distributions, as well as quasi-similar energy levels, which is in agreement with the CV results. In contrast, the LUMOs of **2-4** and **2-5** exhibit dramatically different energy levels and great contributions from the electron deficient groups, namely, carbonyl and the dicyanovinylene moieties. Note that carbonyl and cyano groups contribute almost similar to HOMOs, whereas their contributions to the LUMOs present huge differences. Consequently, the HOMO-LUMO gap of **2-5** is reduced relative to that of **2-4**. This finding can be attributed to the dicyanovinylene group, which stabilizes the LUMO levels.

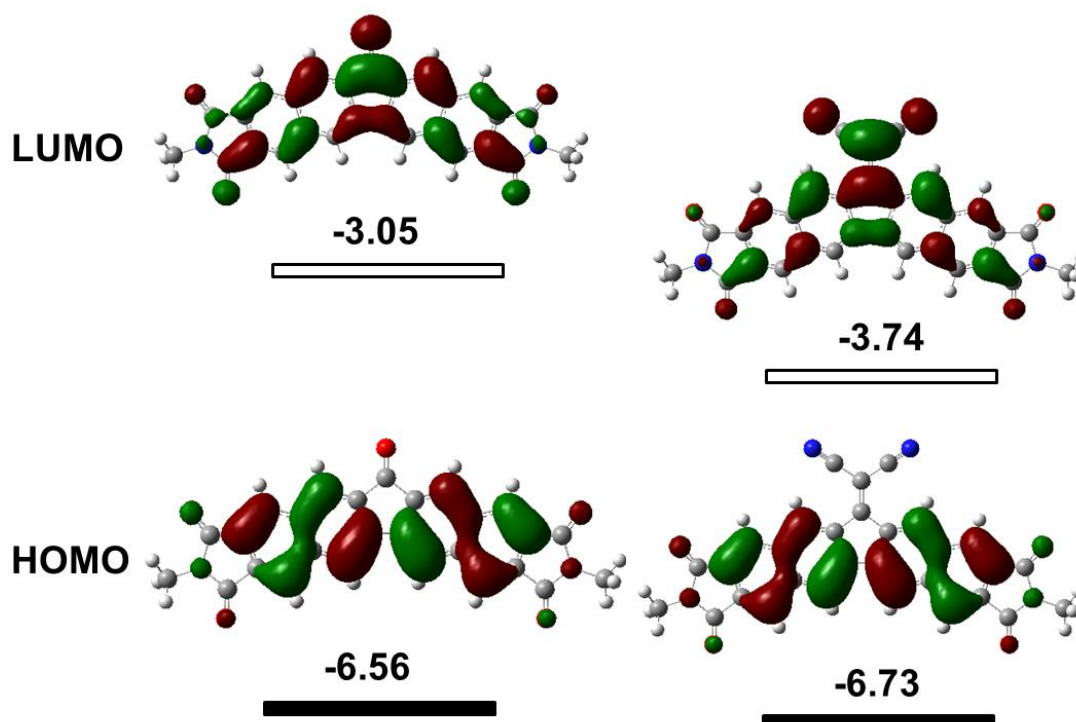


**Figure II-7.** Frontier molecular orbitals (FMOs) and their energies (in eV) for models of **2-4** and **2-5**.

## II.6 Self-organization

To understand the influence of the alkyl substitution of the V-shaped core on the surface self-organization of **2-5a** and **2-5b**, X-ray diffraction (XRD) of both polycrystalline samples was performed by ..... (Max Planck Institute for Polymer Research, Mainz). Zone-casting, a solution processing method, was utilized for the film deposition. This technique has been reported to yield homogenous and well-ordered polycrystalline films for various  $\pi$ -conjugated systems.<sup>[31-32]</sup> Figure II-8 presents XRD diffractograms obtained for zone-cast **2-5a** and **2-5b**. The interlayer distance of 2.60 nm for **2-5a** is determined from the main reflection (100 according to the Miller's index) observed at  $q_z = 0.24 \text{ \AA}^{-1}$ . Higher order reflections (up to 8<sup>th</sup>) imply long-range organization of the molecules in the out-of-plane direction of the film. This interlayer distance is in agreement with the theoretical length of the molecule (2.65 nm calculated by Cerius<sup>2</sup>).<sup>[33]</sup> This suggests that the long axis of the V-shaped molecule is arranged perpendicular to the silicon dioxide surface (Figure II-9 C). In this edge-on organization the  $\pi$ -stacking direction is oriented parallel to the surface which is beneficial for the charge carrier transport in field-effect transistors.

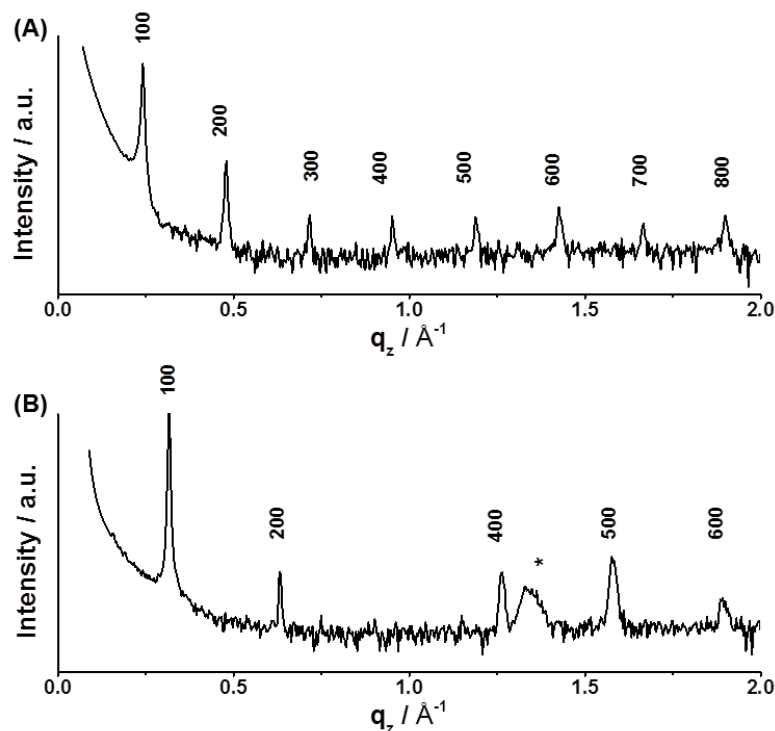


**Figure II-8.** XRD of zone-cast films of (A) **2-5a** and (B) **2-5b** (reflections are assigned by Miller's indexes). The additional peak (\*) at  $1.39 \text{ \AA}^{-1}$  is assigned to minor misalignment of the molecules.

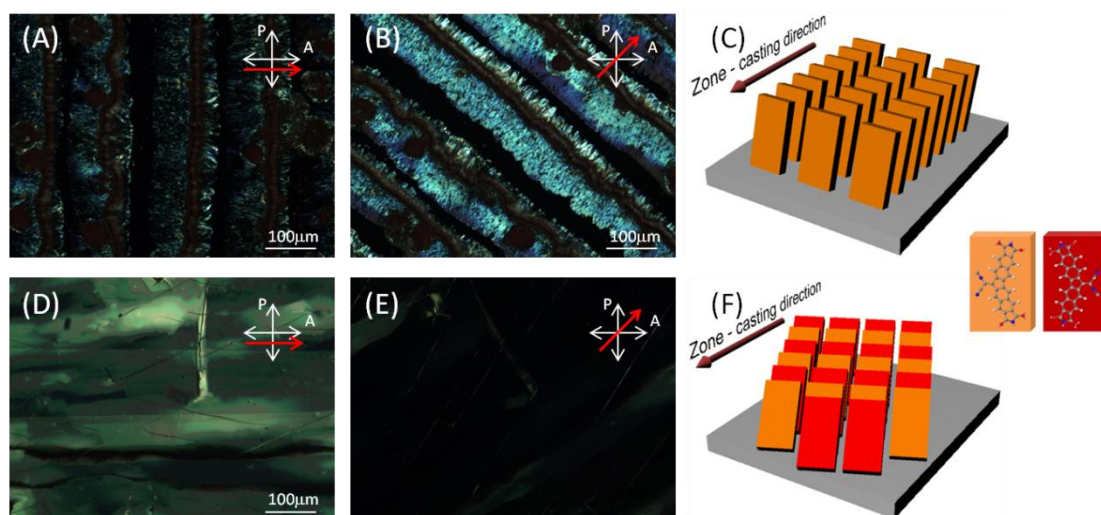


**Figure II-9.** Polarized optical microscopy images for **2-5a** (A and B) and **2-5b** (D and E) zone-cast layers. The red arrow indicates the zone-casting direction. Figure (C) and (F) illustrate schematically the organization of the **2-5a** and **2-5b** molecules on the surface. Red color suggests that the molecule is rotated by  $180^\circ$  with respect to the orange molecule (face-to-face organization).

For **2-5b** the main reflection (100 according to Miller's index, Figure II-9 B) corresponds to a d-spacing of 2.00 nm which is in agreement with the *c* parameter of the triclinic unit cell obtained for the single crystal (Figure II-6). It can be therefore concluded that the *c* axis is arranged in the out-of plane direction. In that case, **2-5b** is organized in a face-to-face stacked dimers which are tilted with respect to the surface (Figure II-9 F).

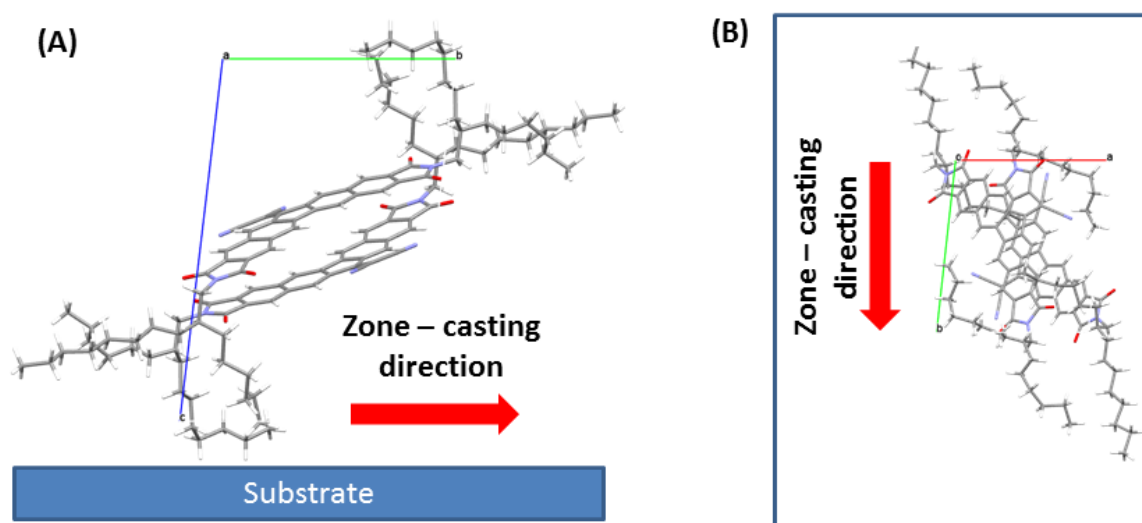


**Figure II-10.** Schematic illustration of the crystal orientation of **2-5b** in the zone-cast films.

In Figure II-9, an indirect evidence for the tilting of **2-5b** is provided by polarized optical microscopy (POM) performed for the zone-cast layers, which was done by ..... (Max Planck Institute for Polymer Research, Mainz). All polycrystalline layers exhibit birefringence between cross-polarizers. In the case of **2-5a**, the POM image remains dark when the crystal optical axis (or zone-casting direction) is arranged parallel to one of the polarizers ( $0^\circ$  and  $90^\circ$ ). Maximum birefringence is observed for the angle of  $45^\circ$ . In contrast, **2-5b** shows no light transmission for the angle of  $45^\circ$  indicating that axis b of the crystal is almost aligned parallel to the zone-casting direction (Figure II-10). In such a crystal arrangement, the axis of the molecules is oriented around  $45^\circ$  towards the alignment direction resulting in a reverse extinction under POM compared to **2-5a**.

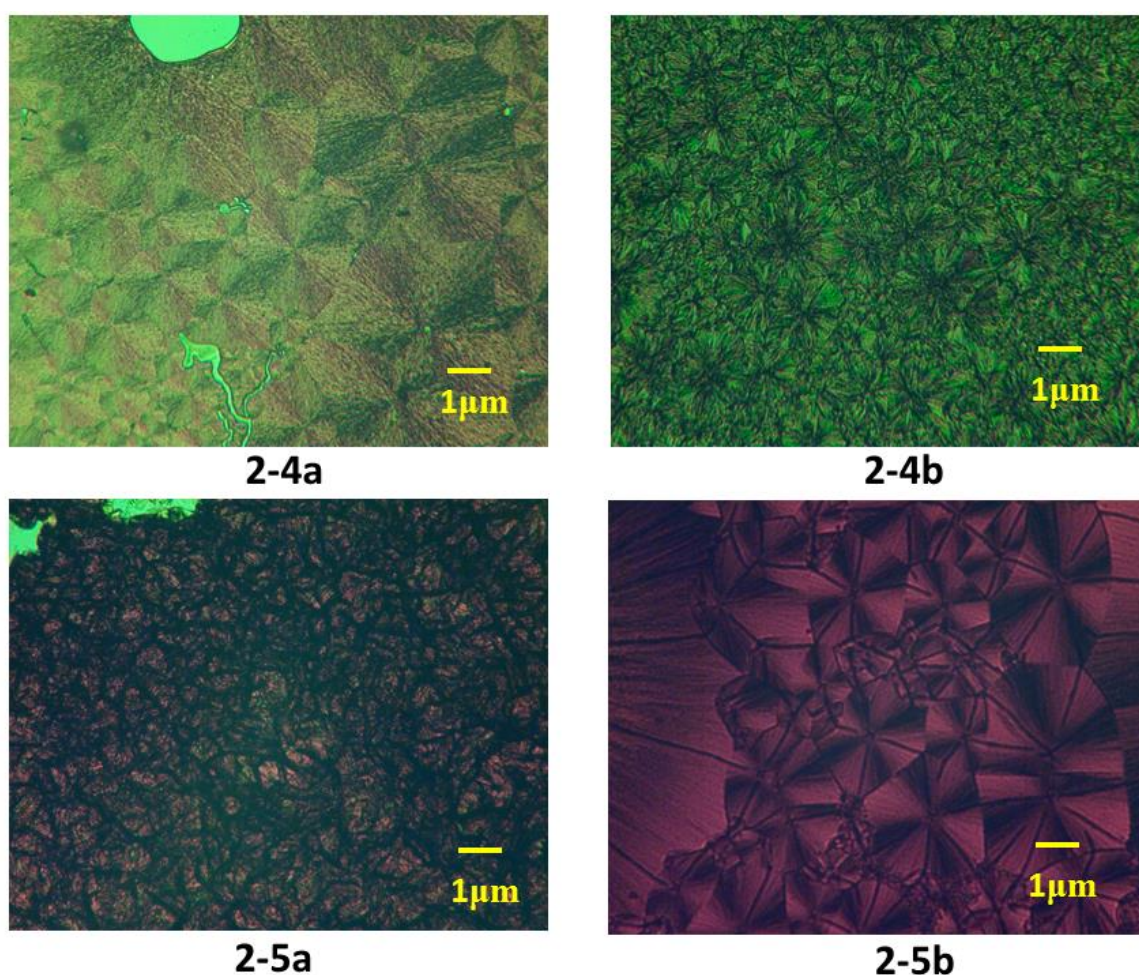


**Figure II-11.** Polarized optical microscopy images (drop-casting layers): **2-4a**, **2-5a**, **2-4b** and **2-5b** were heated to  $270^\circ\text{C}$ ,  $270^\circ\text{C}$ ,  $375^\circ\text{C}$  and  $375^\circ\text{C}$ , respectively, and then slowly cooled down to RT. The images were taken at  $25^\circ\text{C}$ .

To investigate the crystalline properties of the drop-casting layers, polarized optical microscopy (POM) was also performed by ..... (Max Planck Institute for Polymer Research, Mainz) (Figure II-11). POM studies revealed that all compounds showed crystalline properties. It was found that the alkyl chains played a significant role in the phase transition and self-assembly of these angular-shaped molecules in the solid state. Compound **2-4** and **2-5** with varying length of alkyl chains became fluid upon heating and entered into an isotropic phase at different temperatures. Upon slow cooling from the isotropic phase, mosaic textures were observed.

## II.7 OFET properties

The charge carrier transport of **2-5a** and **2-5b** was investigated by fabricating OFET devices in bottom-gate bottom-contact configuration, which was done by ..... (Max Planck Institute for Polymer Research, Mainz). Before drop-casting from 2 mg/mL chloroform solution, the silicon wafer with 300 nm thick thermally grown SiO<sub>2</sub> was functionalized by hexamethyldisilazane (HMDS) to minimize interfacial trapping sites. Au electrodes were evaporated as source and drain. The drop-cast films were annealed at 120 °C for 30 min to remove the residual solvent before OFET measurement. Figure II-12 shows the transfer and output characteristics of **2-5a** and **2-5b**, respectively.

In the positive drain mode of both compounds, the drain current ( $I_{DS}$ ) firstly exhibits a linear behavior with increasing the gate voltage ( $V_{GS}$ ) and then becomes saturated (Figures II-12 A and C). This transistor behavior is characteristic for an electron transporting semiconductor which can be attributed to the introduction of strong electron withdrawing moieties. The maximum saturated electron mobility of **2-5a** is  $0.01 \text{ cm}^2 \text{ V}^{-1} \text{ s}^{-1}$  and the on/off ratio is around  $10^4$ . The threshold voltage of 12 V is low compared to **2-5b** (see below). To the best of our knowledge, this is the first case of an electron transport by a semiconductor consisting of a V-shaped coplanar core. In comparison to **2-5a**, **2-5b** shows a relatively poor electron transport, with maximum mobility of  $5 \times 10^{-4} \text{ cm}^2 \text{ V}^{-1} \text{ s}^{-1}$  and on/off ratio of  $10^3$ . Additionally, the

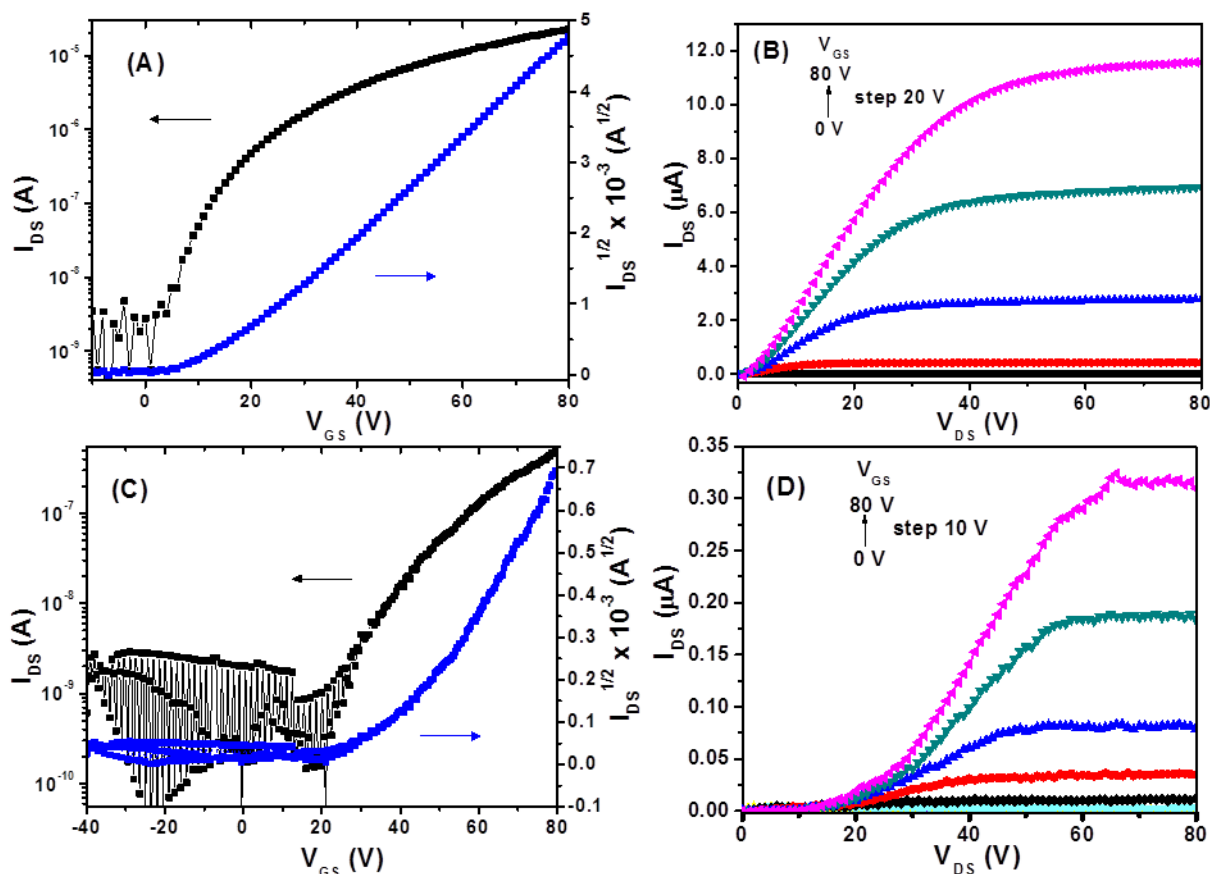


**Figure II-12.** Transfer and output characteristics of OFET devices fabricated by drop casting of **2-5a** (A, B) and **2-5b** (C, D). For B and D,  $V_{DS}=80$  V is applied.

threshold voltage is increased to 35 V. High contact resistance observed in the output characteristics of **2-5b** is possibly caused by disorder of the molecules close at the metal/semiconductor interface. The additional XRD peak at  $1.39 \text{ \AA}^{-1}$  (Figure II-8 B) indicates the minor molecular disorder in the **2-5b** films. This disorder can reduce the charge injection process from the metal electrode to the semiconductor layer resulting in an increase of the threshold voltage. Zone-casting only slightly improves the device performance of **2-5b** yielding charge carrier mobilities of  $1 \times 10^{-3} \text{ cm}^2 \text{ V}^{-1} \text{ s}^{-1}$ . The lower performance of drop-cast **2-5b** in comparison to **2-5a** is ascribed to the face-to-face organization of **2-5b** and molecular tilting induced by longer alkyl chains. Such organization of the molecules causes that the  $\pi$ -stacking interaction is not in-plane to the substrate.

## II.8 Conclusions

In conclusion, two novel angular n-type molecules **2-5a** and **2-5b** have been synthesized based on the 2,3,6,7-tetramethyl-9H-fluoren-9-one intermediate, which can also be extended to construct compound **3D-imide**. Electronic properties of **2-5a** and **2-5b** in diluted media are identical as proven by cyclic voltammetry and optical spectra with a low lying LUMO of -3.86 eV, indicating the different alky chains have no influence on the electronic properties of the planar core. However, the length of the alkyl chain plays a pivotal role in the molecular orientation relative to surface. For **2-5a**, the molecules adopt an edge-on orientation with an OFET electron mobility of  $0.01 \text{ cm}^2 \text{ V}^{-1} \text{ s}^{-1}$ , while **2-5b** with longer branched chains is tilted with respect to the substrate, thereby resulting in poor device performance. Even though such device performance is not good enough compared to that of p-type V-shaped dinaphthothiophene (**DNT**) based device,<sup>[21]</sup> it is still meaningful due to enriching the angular shaped n-type semiconductors. Regarding the electron-accepting capability for **2-5**, it is contributed mainly by cyano and imides groups. Thiadiazole is another good electron-withdrawing group, which will be illustrated in Chapter III.

## II.9 References

- [1] X. Guo, M. Baumgarten, K. Müllen, *Prog. Polym. Sci.* **2013**, *38*, 1832-1908.
- [2] J. Mei, Y. Diao, A. L. Appleton, L. Fang, Z. Bao, *J. Am. Chem. Soc.* **2013**, *135*, 6724-6746.
- [3] C. A. Di, F. Zhang, D. Zhu, *Adv. Mater.* **2013**, *25*, 313-330.
- [4] C. L. Wang, H. L. Dong, W. P. Hu, Y. Q. Liu, D. B. Zhu, *Chem. Rev.* **2012**, *112*, 2208-2267.
- [5] W. Jiang, Y. Li, Z. Wang, *Chem. Soc. Rev.* **2013**, *42*, 6113-6127.
- [6] Y. N. Li, P. Sonar, L. Murphy, W. Hong, *Energ. Environ. Sci.* **2013**, *6*, 1684-1710.
- [7] Z. Liu, G. Zhang, Z. Cai, X. Chen, H. Luo, Y. Li, J. Wang, D. Zhang, *Adv. Mater.* **2014**, *26*, 6965-6977.

- [8] M. Durso, D. Gentili, C. Bettini, A. Zanelli, M. Cavallini, F. De Angelis, M. Grazia Lobello, V. Biondo, M. Muccini, R. Capelli, M. Melucci, *Chem. Commun.* **2013**, 49, 4298--4300.
- [9] N. Yanai, T. Mori, S. Shinamura, I. Osaka, K. Takimiya, *Org. Lett.* **2014**, 16, 240-243.
- [10] T. Mori, N. Yanai, I. Osaka, K. Takimiya, *Org. Lett.* **2014**, 16, 1334-1337.
- [11] Q. Wu, S. Ren, M. Wang, X. Qiao, H. Li, X. Gao, X. Yang, D. Zhu, *Adv. Funct. Mater.* **2013**, 23, 2277-2284.
- [12] H. Li, F. S. Kim, G. Ren, E. C. Hollenbeck, S. Subramanian, S. A. Jenekhe, *Angew. Chem., Int. Ed.* **2013**, 52, 5513-5517.
- [13] Y. Koyama, S. Hiroto, H. Shinokubo, *Angew. Chem. Int. Ed.* **2013**, 52, 5740-5743.
- [14] J. M. Alonso, A. E. Díaz-Álvarez, A. Criado, D. Pérez, D. Peña, E. Guitián, *Angew. Chem. Int. Ed.* **2012**, 51, 173-177.
- [15] H. Usta, C. Kim, Z. Wang, S. Lu, H. Huang, A. Facchetti, T. J. Marks, *J. Mater. Chem.* **2012**, 22, 4459-4472.
- [16] X. Guo, S. R. Puniredd, M. Baumgarten, W. Pisula, K. Müllen, *Adv. Mater.* **2013**, 25, 5467-5472.
- [17] T. Kono, D. Kumaki, J.-i. Nishida, S. Tokito, Y. Yamashita, *Chem. Commun.* **2010**, 46, 3265-3267.
- [18] H. Tian, Y. Deng, F. Pan, L. Huang, D. Yan, Y. Geng, F. Wang, *J. Mater. Chem.* **2010**, 20, 7998-8004.
- [19] P. Gao, D. Beckmann, H. N. Tsao, X. Feng, V. Enkelmann, M. Baumgarten, W. Pisula, K. Müllen, *Adv. Mater.* **2009**, 21, 213-216.
- [20] Z. Liang, Q. Tang, R. Mao, D. Liu, J. Xu, Q. Miao, *Adv. Mater.* **2011**, 23, 5514-5518.
- [21] T. Okamoto, C. Mitsui, M. Yamagishi, K. Nakahara, J. Soeda, Y. Hirose, K. Miwa, H. Sato, A. Yamano, T. Matsushita, T. Uemura, J. Takeya, *Adv. Mater.* **2013**, 25, 6392-6397.
- [22] T. V. Pho, J. D. Yuen, J. A. Kurzman, B. G. Smith, M. Miao, W. T. Walker, R. Seshadri, F. Wudl, *J. Am. Chem. Soc.* **2012**, 134, 18185-18188.
- [23] H. Li, R.-Y. Zhu, W.-J. Shi, K.-H. He, Z.-J. Shi, *Org. Lett.* **2012**, 14, 4850-4853.
- [24] W. Lehnert, *Tetrahedron Lett.* **1970**, 11, 4723-4724.

- [25] W. Lehnert, *Synthesis* **1974**, 1974, 667-669.
- [26] J. Yin, H. Qu, K. Zhang, J. Luo, X. Zhang, C. Chi, J. Wu, *Org. Lett.* **2009**, 11, 3028-3031.
- [27] M. Kozaki, Y. Yonezawa, K. Okada, *Org. Lett.* **2002**, 4, 4535-4538.
- [28] H. Usta, A. Facchetti, T. J. Marks, *Org. Lett.* **2008**, 10, 1385-1388.
- [29] H. Usta, A. Facchetti, T. J. Marks, *J. Am. Chem. Soc.* **2008**, 130, 8580-8581.
- [30] E. Jacques, M. Romain, A. Yassin, S. Bebiche, M. Harnois, T. Mohammed-Brahim, J. Rault-Berthelot, C. Poriel, *J. Mater. Chem. C.* **2014**, 2, 3292-3302.
- [31] W. Pisula, A. Menon, M. Stepputat, I. Lieberwirth, U. Kolb, A. Tracz, H. Sirringhaus, T. Pakula, K. Müllen, *Adv. Mater.* **2005**, 17, 684-689.
- [32] T. Marszalek, A. Nosal, R. Pfattner, J. Jung, S. Kotarba, M. Mas-Torrent, B. Krause, J. Veciana, M. Gazicki-Lipman, C. Crickert, G. Schmidt, C. Rovira, J. Ulanski, *Org. Electron.* **2012**, 13, 121-128.
- [33] *Cerius 2 calculation; Accelrys, Inc.: San Diego, CA, 1998.*



# Chapter III. Fused Bis-Benzothiadiazoles as Electron Acceptors

Fused bis-benzothiadiazoles with different molecular geometries, namely linear benzoquinone-fused bis(benzothiadiazole) (**3-10**) and V-shaped sulfone-fused bis(benzothiadiazole) (**3-11**), were synthesized as novel electron acceptors. Single crystal analysis of **3-10** and **3-11** revealed profoundly distinct packing modes, which must be ascribed to the different molecular shapes. Experimental and theoretical studies indicated that both compounds give rise to electron-accepting materials. This work thus contributes to the diversity of electron acceptors based on bis-benzothiadiazole moieties and highlights the important role of molecular shape for the solid-state packing of organic conjugated materials.

## III.1 Introduction

Electron-deficient (hetero)aromatic moieties are key components of n-type organic semiconducting materials, as they can decrease the low-lying LUMO energy levels of materials to i) match the work function of the electrodes for efficient electron injection;<sup>[1]</sup> ii) broaden the light absorption to harvest more sunlight for obtaining high efficiency photovoltaics;<sup>[2]</sup> iii) be a strong acceptor for effective charge transfer with other donors.<sup>[3]</sup> Various electron acceptor moieties such as dicyanovinylene,<sup>[4-9]</sup> diketopyrrolopyrrole (DPP),<sup>[10-11]</sup> [1,2,5]-thiadiazolo[3,4-g]quinoxaline (TQ),<sup>[12-15]</sup>

benzothiadiazole (BT), perylene diimide (PDI),<sup>[16-18]</sup> naphthalene diimide (NDI) and isoindigo (IID) have already been developed. Among them, BT is a particularly popular case and has been introduced into oligomers and polymers for a variety of applications, such as organic light-emitting diodes (OLEDs),<sup>[19-22]</sup> organic photovoltaics (OPVs),<sup>[23-28]</sup> dye-sensitized solar cells (DSSCs),<sup>[29]</sup> and organic field-effect transistors (OFETs)<sup>[30-32]</sup>.

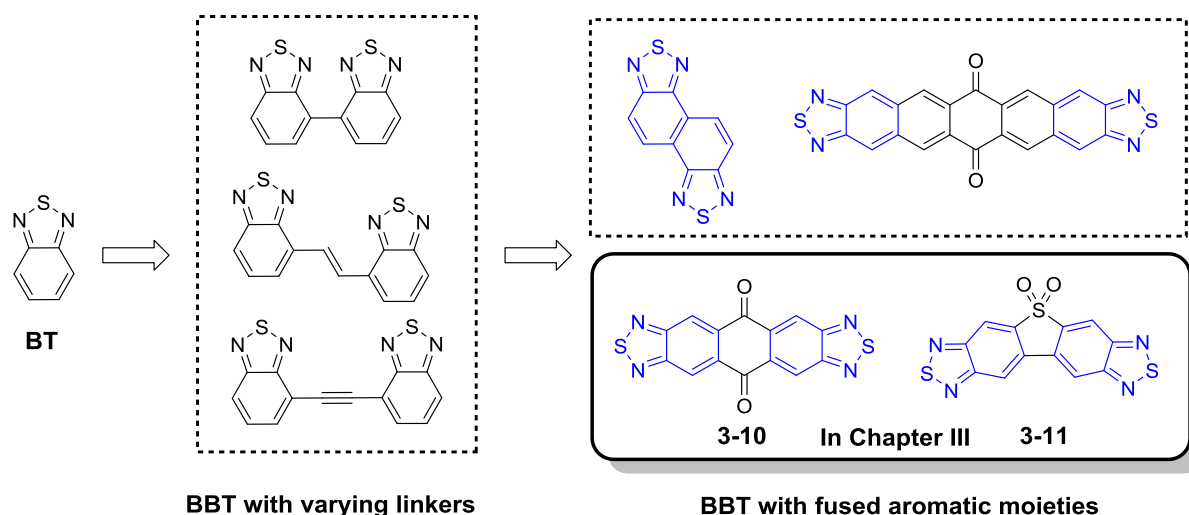


**Figure III-1.** Chemical structures of BT unit and BBT derivatives.

To further explore the potential of BT-based electron-accepting materials, several bis-benzothiadiazole (BBT) derivatives (Figure III-1), which should possess higher electron affinities, have been developed very recently. One approach is to connect two BT units via a single bond linker.<sup>[33-34]</sup> In this case, the large twist between the neighboring BT units hinders the effective inter- and intramolecular interaction, thus resulted in poor device performance ( $1 \times 10^{-3} \text{ cm}^2 \text{ V}^{-1} \text{ s}^{-1}$ ). To solve this problem, Yang's group firstly introduced the vinylene and acetylene  $\pi$ -spacers between the two BT, which facilitate the interchain packing of the resulting polymers and thereby their carrier mobilities were improved to  $0.32 \text{ cm}^2 \text{ V}^{-1} \text{ s}^{-1}$  and  $0.24 \text{ cm}^2 \text{ V}^{-1} \text{ s}^{-1}$ , respectively.

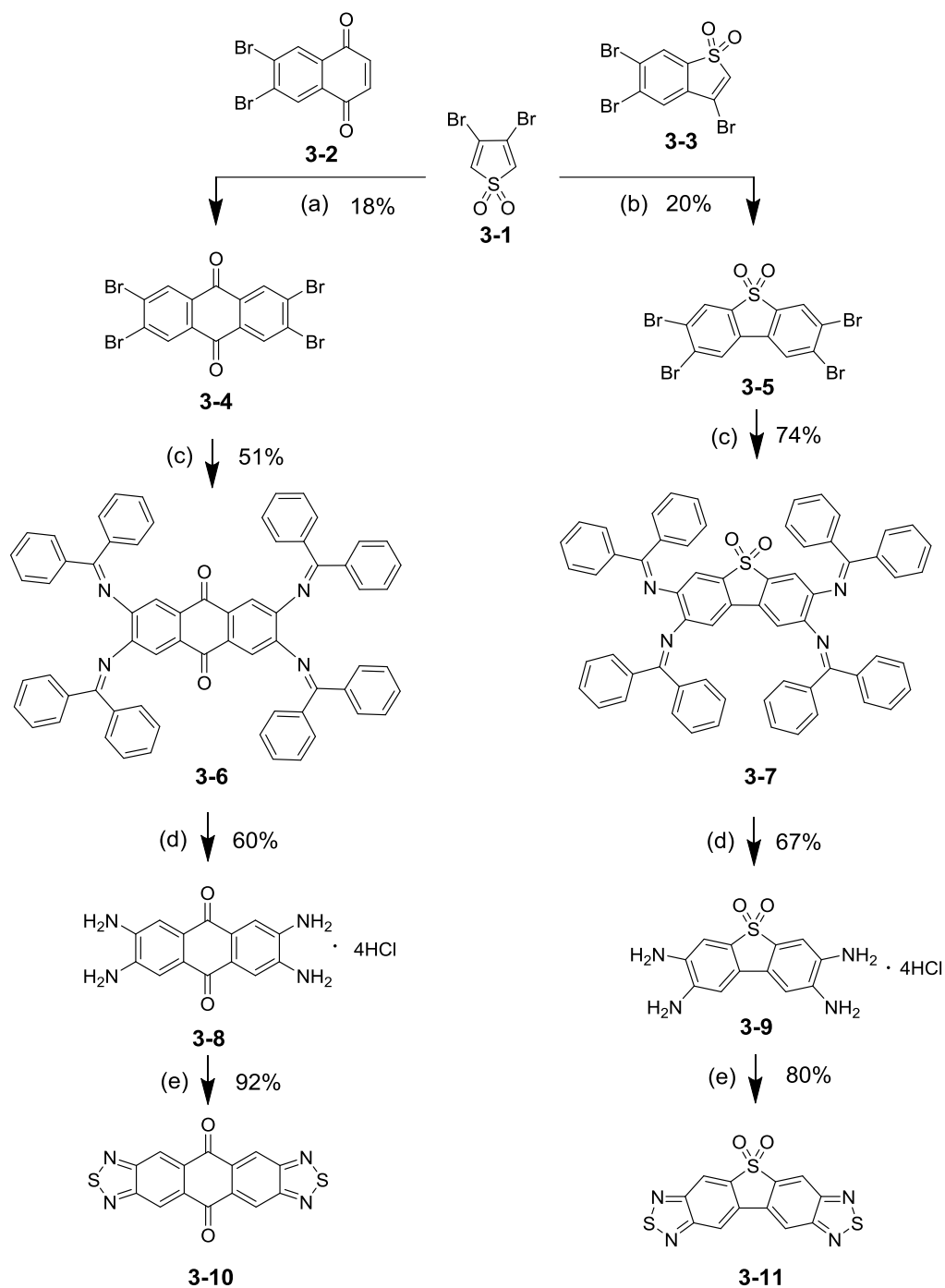
Another approach is to incorporate two BT units into fused aromatic systems, providing a better coplanarity and a more pronounced  $\pi$ -conjugation, affording the electron mobility up to  $0.11 \text{ cm}^2 \text{ V}^{-1} \text{ s}^{-1}$  in OFET devices reported by F. Perepichka's

group.<sup>[35]</sup> To the best of our knowledge, the synthesis of such important BBT-based electron-deficient cores has been seldom reported. Moreover, the structure-property relationship of such materials has never been clearly investigated regarding how molecular shapes and fused structures influence their solid-state packings and optoelectronic properties. Importantly, there is no crystal analysis report of such compounds to deeply explicate their intermolecular interactions in the solid state. Those promote us to focus attention on developing some small molecules.

Herein, we describe the synthesis, single crystal structures, photophysical and electrochemical properties of linear benzoquinone-fused BBT (**3-10**) and V-shaped sulfone-fused BBT (**3-11**) (see Scheme III-1). An unexpected precursor 2,3,7,8-tetrabromodibenzo[*b,d*]thiophene 5,5-dioxide (**3-5**) was discovered in the synthesis and used for the construction of novel V-shaped **3-11**. Single crystal X-ray analysis suggests that **3-10** and **3-11** exhibit dramatically different molecular arrangements. The low-lying LUMO levels and short  $\pi$ - $\pi$  distances of both molecules may render them suitable for n-type charge transport materials.

## III.2 Synthesis

A facile synthetic route to the two target molecules is illustrated in Scheme III-1. According to a procedure described in the literature,<sup>[36]</sup> 2,3,6,7-tetrabromoanthracene-9,10-dione (**3-4**) was synthesized in 18% yield. After changing reaction conditions, such as prolonging reaction time, altering the reactant ratio and microwave assistance, the reaction yield could not be further increased. The major byproduct 3,5,6-tribromobenzo[*b*]thiophene 1,1-dioxide (**3-3**) was discovered and obtained in 52% yield, whose formation was ascribed to homodimerization of 3,4-dibromothiophene 1,1-dioxide (**3-1**). Surprisingly, 2,3,7,8-tetrabromodibenzo[*b,d*]thiophene 5,5-dioxide (**3-5**) was also found, presumably due to further Diels-Alder reaction of compound **3-1** with **3-3**. However, the purification of **3-5** in such reaction system was a challenge, because of its bad solubility and low reaction yield. A ~2% yield of **3-5** was collected by multiple solid residue washing with acetone, since **3-5** showed kind of better solubility in acetone in comparison with



**Scheme III-1.** Synthesis of **3-10** and **3-11**. Reagents and conditions: a) para-benzoquinone, acetic acid, reflux. b) 3,5,6-tribromobenzo[*b*]thiophene 1,1-dioxide, acetic acid, reflux; c) benzophenone imine, *rac*-BINAP, Pd<sub>2</sub>(dba)<sub>3</sub>, *t*-BuONa, toluene, 110 °C; d) 2.0 M HCl, THF, RT. e) TMSCl, PhNSO, pyridine, 80 °C.

**3-4**. Indeed, an independent Diels-Alder reaction was carried out between compound **3-1** and **3-3**, producing **3-5** in a yield of 20%. Moreover, compound **3-5** could also be prepared in 10% yield only using **3-1** as the reactant in refluxing acetic acid. We assume that the reaction must proceed in a sequence of Diels-Alder reactions (see Figure III-2). Tetra(diphenylmethanimine) substituted **3-6** and **3-7** were synthesized by Buchwald-Hartwig aminations,<sup>[37]</sup> followed by hydrolysis to form the amino-substituted compounds **3-8** and **3-9** in the presence of 2.0 M HCl in THF. Finally, using the N-sulfinylaniline as the cyclization reagent, **3-10** and **3-11** were successfully synthesized in yields of 90% and 82%, respectively. At the beginning, the NMR characterization did not succeed with common deuterated solvents due to the bad solubility of **3-10** and **3-11**. Thereafter, the problem was solved using D<sub>2</sub>SO<sub>4</sub> to dissolve both compounds for NMR measurements.

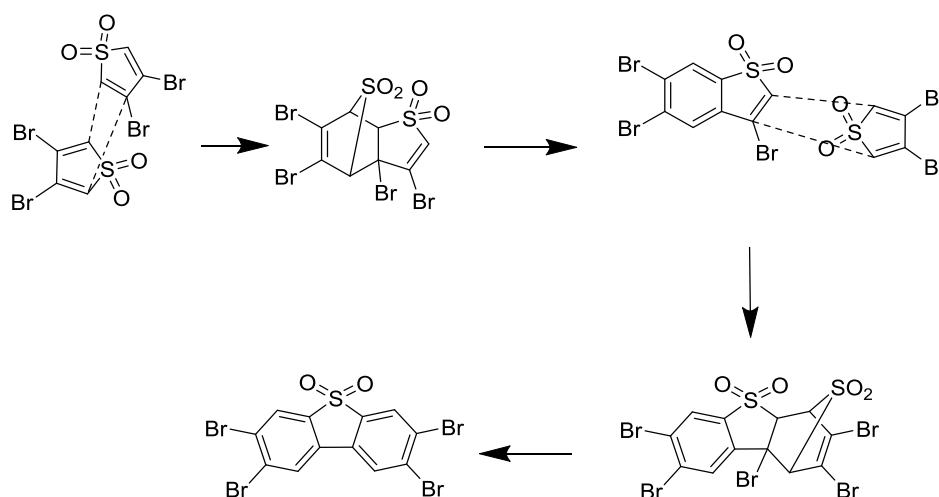


**Figure III-2.** Proposed reaction mechanism to produce compound **3-5**.

### III.3 Crystal structure analysis

By slow solvent evaporation method, single crystals of **3-10** and **3-11** suitable for X-ray analysis were grown from their THF solutions at room temperature. Note that this is the first crystal structure analysis of BBT-based conjugated systems. As depicted in Figure III-3, the conjugated backbones of **3-10** and **3-11** are essentially planar while the sulfone oxygen atoms of **3-11** are out of the  $\pi$ -plane with the S-O-S

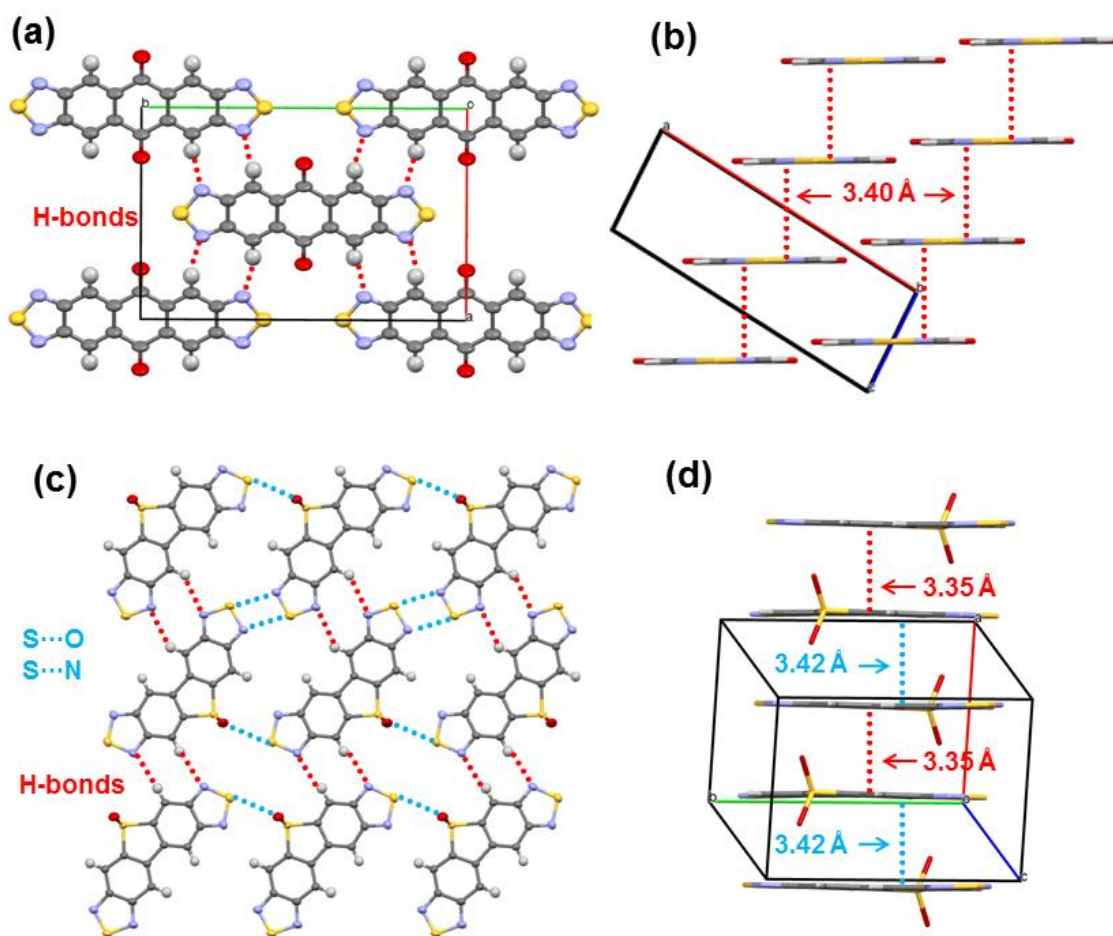


**Figure III-3.** Single crystal structure of **3-10**: (a) C-H...N hydrogen bonds as shown with dashed red lines; (b) slipped columnar  $\pi$ - $\pi$  stacking and single crystal structure of **3-11**: (c) C-H...N hydrogen bonds and intermolecular S...O/N interactions as shown with dashed red lines and dashed blue lines, respectively; (d) one-dimensional  $\pi$ - $\pi$  stacking.

angle of  $103.39^\circ$ . Each **3-10** is closely surrounded by four neighbors by virtue of eight hydrogen bonds, whose H...N distance is  $2.54 \text{ \AA}$  and the C-H...N angle is  $163.4^\circ$  (Figure III-3 a). Indeed, the crystal arrangement of **3-10** is almost the same as that of n-type semiconductor N-heteropentacenequinones, which indicates the potential of **3-10** applying in OFETs. Furthermore, **3-10** self-assembles in a slipped  $\pi$ -stacking with an average  $\pi$ - $\pi$  distance of  $3.40 \text{ \AA}$  (Figure III-3 b). Interestingly, due to the V-shaped backbone and out-of-plane oxygen atoms for **3-11**, it shows a unique crystal packing mode, which is unlike **3-10** and other BT-containing molecules.<sup>[38-39]</sup> First, C-H...N hydrogen bonds and Van der Waals bonds between the hetero atoms [(N...N ( $2.95 \text{ \AA}$ ), N...S ( $2.89 \text{ \AA}$ ) and O...S ( $3.20 \text{ \AA}$ )] are approved to be existed. Second, **3-11**

forms face-to-face stacked dimers with a short intermolecular  $\pi$ - $\pi$  distance (3.35 Å). Third, such stacked dimers interact with each other in a one-dimensional columnar arrangement with a longer  $\pi$ - $\pi$  distance (3.42 Å). Such dense molecular packing and close contacts between  $\pi$ -stacks of both **3-10** and **3-11** indicate their potential as good organic semiconductors.

### III.4 Photophysical and electrochemical properties

The photophysical properties of both novel compounds were also investigated. As shown in Figure III-4, the UV-vis absorption spectrum of **3-10** displays a broad absorption peaking at 304, 343, and 390 nm. According to the equation  $h\nu = \frac{1240}{\lambda}$  ( $\lambda$  represents the onset of absorption), the optical gap was calculated to be  $\sim 3.08$  eV. In the case of **3-11**, its absorption spectrum exhibits a significant vibronic structure ( $\lambda_{\text{max}} = 390$  nm) and a similar optical gap (3.05 eV). The different absorption intensities of these two molecules in the region of 360 nm – 390 nm are in good agreement with TD-DFT calculations, namely, the oscillator strength of **3-11** is around ten times higher than **3-10**. The normalized fluorescence spectra of **3-10** and **3-11** reveal almost the same profile with the maximum emission wavelength at 420 nm. As expected, the Stokes shifts for both compounds are small, which is in line with their rigidity.

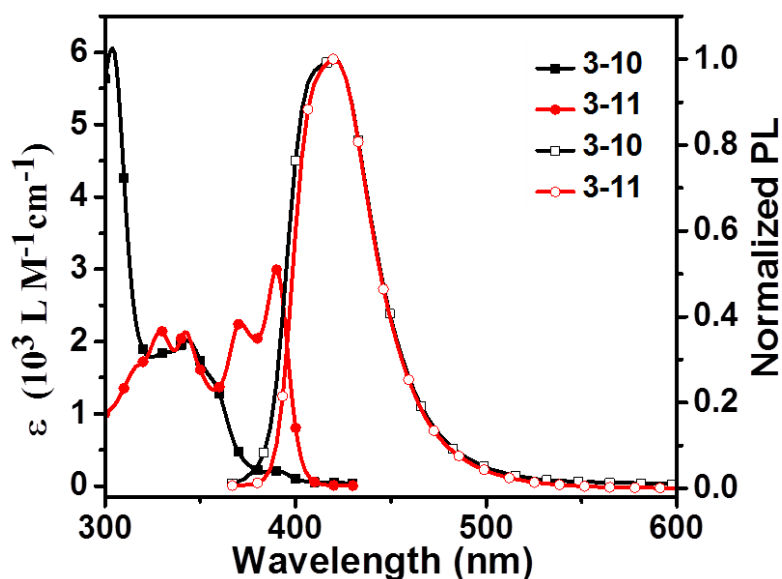


**Figure III-4.** Absorption (solid) and photoluminescence (hollow) spectra of **3-10** and **3-11** in THF ( $\lambda_{\text{Exc}} = 390$  nm).

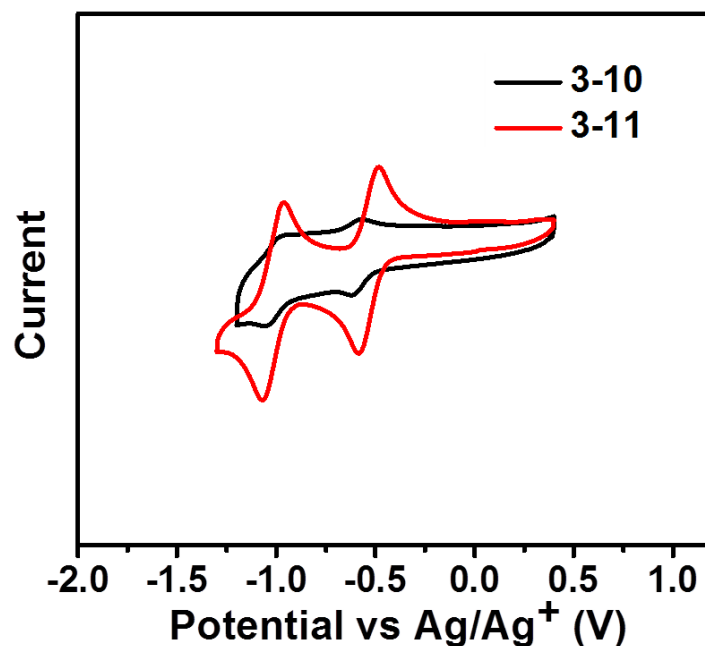


**Figure III-5.** Cyclic voltammograms of **3-10** and **3-11** in N-Methyl-2-pyrrolidone (NMP).

The electron-accepting properties of **3-10** and **3-11** were studied by electrochemical measurements. Previously, DCM was used as solvent for cyclic voltammetry measurement, whereas the experiment was not successful due to bad solubility of two compounds. Thereafter, N-methyl-2 pyrrolidone (NMP) was applied. In Figure III-5, two reversible reduction waves were observed for both compounds **3-10** and **3-11**, however no oxidation ones in the accessible potential range. The (lowest unoccupied molecular orbital) LUMO energy levels estimated from the onset of the first reduction peak are -3.77 eV for **3-10** and -3.81 eV for **3-11**. In comparison with the recently reported structurally related acceptors such as pentacenobis(thiadiazole)dione<sup>[35]</sup> and octafluoropentacenequinone,<sup>[40]</sup> **3-10** and **3-11** possess a lower LUMO level, which indicates the potential role of them using as n-type organic semiconductors. The low current value of **3-10** in the CV profile is ascribed to the low-concentration due to its poor solubility.

### III.5 Density functional theory calculations

To gain more insights into the electronic properties of **3-10** and **3-11**, the frontier molecular orbitals (FMOs) and the HOMO and LUMO levels were obtained by density

functional theory (DFT) calculations at the B3LYP/6-311G\*\* level of theory. As depicted in Figure III-6, frontier molecular orbitals of both molecules are delocalized over the whole molecules, indicating effective  $\pi$ -conjugation in the fused systems. Moreover, the LUMOs of **3-10** and **3-11** demonstrate similar energy levels, which is in accordance with the CV results. Also, the LUMOs of both molecules have a large contribution from the electron-accepting moieties, including BT, benzoquinone, and sulfone. In contrast, the HOMOs of **3-10** and **3-11** are mainly contributed by benzo rings in the conjugated backbone and their energy levels are different in comparison with the corresponding experimental values, which were possibly because they were not directly measured from oxidation waves in cyclic voltammograms but estimated from the optical HOMO-LUMO gaps and the LUMO energy levels.

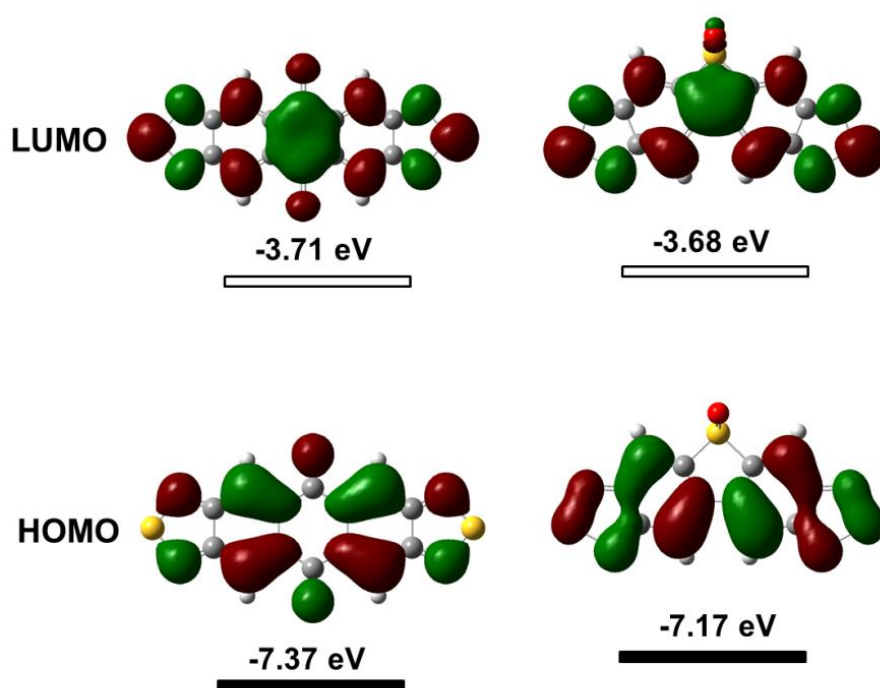


**Figure III-6.** Frontier molecular orbitals (FMOs) and their energies (in eV) for **3-10** and **3-11**.

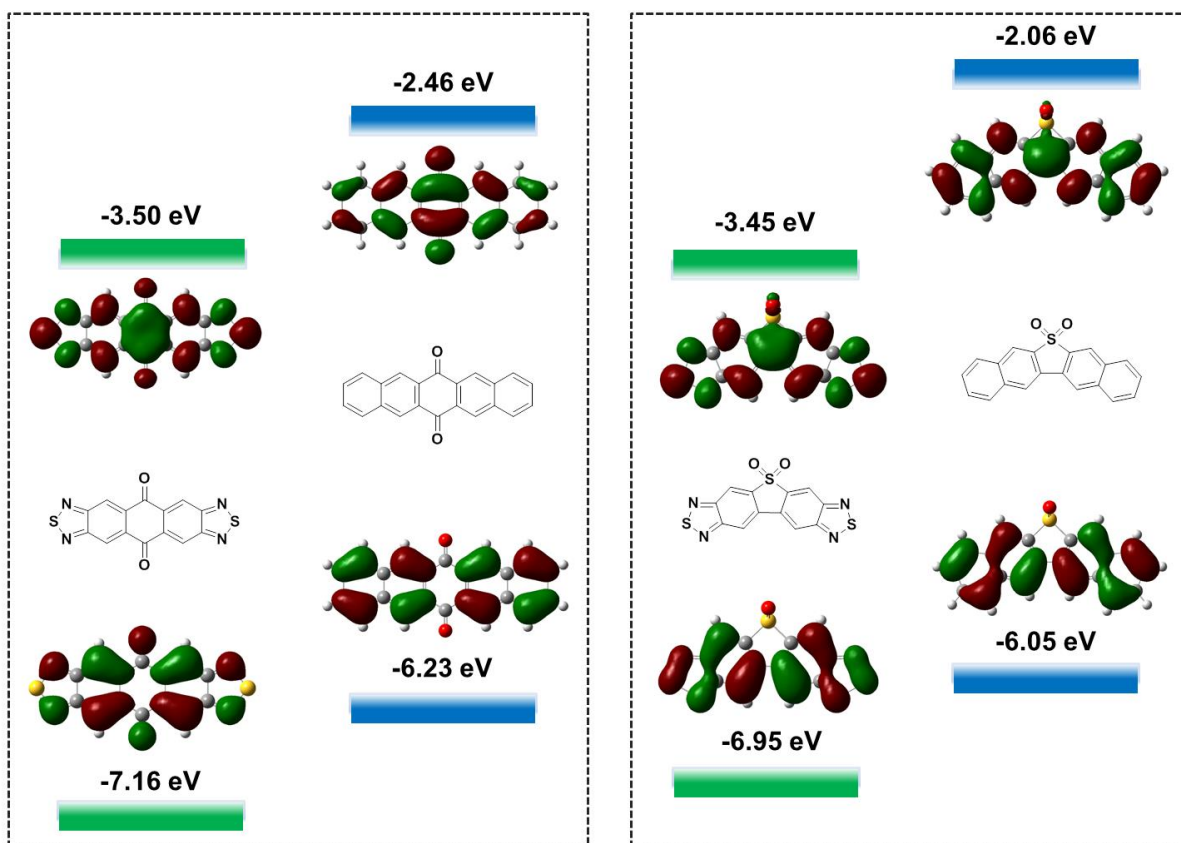


**Figure III-7.** Energy level diagram and frontier molecular orbitals according to DFT calculations at the B3LYP/6-31G (d) level.

Furthermore, as expected no matter for **3-10** or **3-11**, replacing thiazole rings in the backbones with benzene rings increase both HOMO and LUMO energy levels. The HOMO-LUMO gaps of **3-10** and **3-11** are reduced relative to those of their isoelectronic analogue pentacene-6,13-dione and dinaphthothiophene 6,6-dioxide, respectively (Figure III-7). This finding can be attributed to the peripheral thiadiazole rings, which stabilized the LUMO levels.

### III.6 Conclusions

In conclusion, we have prepared two novel bis-benzothiadiazole-based compounds with fused rings, namely linear **3-10** and V-shaped **3-11**. During the process, important precursor tetrabromodibenzothiophene dioxide (**3-5**) was firstly synthesized through Diels-Alder reaction with only reagent 3,4-dibromothiophene 1,1-

dioxide as starting material. The different molecular geometries of **3-10** and **3-11** significantly influence the mode of crystal packing. Moreover, a combination of experimental and theoretical studies reveals that both **3-10** and **3-11** are strong electron-withdrawing materials, which may find applications in organic field-effect transistors and solar cells in the future. In this chapter, the precursors, such as 2,3,6,7-tetrabromoanthracene-9,10-dione, tetra-amino substituted anthracene-9,10-dione and tetra-amino substituted dibenzo[b,d]thiophene 5,5-dioxide were synthesized and are also very important, which can be expanded to acene-like structures. Part of them will be shown in chapter IV.

### III.7 References

- [1] X. Shi, J. Chang, C. Chi, *Chem. Commun.* **2013**, *49*, 7135-7137.
- [2] B. Kohl, L. C. Over, T. Lohr, M. Vasylyeva, F. Rominger, M. Mastalerz, *Org. Lett.* **2014**, *16*, 5596-5599.
- [3] H. T. Black, D. F. Perepichka, *Angew. Chem. Int. Ed.* **2014**, *53*, 2138-2142.
- [4] R. Fitzner, E. Reinold, A. Mishra, E. Mena-Osteritz, H. Ziehlke, C. Körner, K. Leo, M. Riede, M. Weil, O. Tsaryova, A. Weiß, C. Urich, M. Pfeiffer, P. Bäuerle, *Adv. Funct. Mater.* **2011**, *21*, 897-910.
- [5] S. Haid, A. Mishra, M. Weil, C. Urich, M. Pfeiffer, P. Bäuerle, *Adv. Funct. Mater.* **2012**, *22*, 4322-4333.
- [6] R. Fitzner, E. Mena-Osteritz, K. Walzer, M. Pfeiffer, P. Bäuerle, *Adv. Funct. Mater.* **2015**, *25*, 1845-1856.
- [7] Y. Ie, K. Nishida, M. Karakawa, H. Tada, Y. Aso, *J. Org. Chem.* **2011**, *76*, 6604-6610.
- [8] T. Takahashi, K.-i. Matsuoka, K. Takimiya, T. Otsubo, Y. Aso, *J. Am. Chem. Soc.* **2005**, *127*, 8928-8929.
- [9] Y. Ie, M. Karakawa, S. Jinnai, H. Yoshida, A. Saeki, S. Seki, S. Yamamoto, H. Ohkita, Y. Aso, *Chem. Commun.* **2014**, *50*, 4123-4125.
- [10] Y. Lin, P. Cheng, Y. Li, X. Zhan, *Chem. Commun.* **2012**, *48*, 4773-4775.
- [11] C. B. Nielsen, M. Turbiez, I. McCulloch, *Adv. Mater.* **2013**, *25*, 1859-1880.

- [12] T. L. Dexter Tam, T. Salim, H. Li, F. Zhou, S. G. Mhaisalkar, H. Su, Y. M. Lam, A. C. Grimsdale, *J. Mater. Chem.* **2012**, *22*, 18528-18534.
- [13] H. Li, T. L. Tam, Y. M. Lam, S. G. Mhaisalkar, A. C. Grimsdale, *Org. Lett.* **2011**, *13*, 46-49.
- [14] M. Li, C. An, T. Marszalek, X. Guo, Y.-Z. Long, H. Yin, C. Gu, M. Baumgarten, W. Pisula, K. Müllen, *Chem. Mater.* **2015**, *27*, 2218-2223.
- [15] C. An, M. Li, T. Marszalek, D. Li, R. Berger, W. Pisula, M. Baumgarten, *Chem. Mater.* **2014**, *26*, 5923-5929.
- [16] X. Zhang, Z. Lu, L. Ye, C. Zhan, J. Hou, S. Zhang, B. Jiang, Y. Zhao, J. Huang, S. Zhang, Y. Liu, Q. Shi, Y. Liu, J. Yao, *Adv. Mater.* **2013**, *25*, 5791-5797.
- [17] Y. Zang, C.-Z. Li, C.-C. Chueh, S. T. Williams, W. Jiang, Z.-H. Wang, J.-S. Yu, A. K. Y. Jen, *Adv. Mater.* **2014**, *26*, 5708-5714.
- [18] Y. Lin, Y. Wang, J. Wang, J. Hou, Y. Li, D. Zhu, X. Zhan, *Adv. Mater.* **2014**, *26*, 5137-5142.
- [19] L. Chen, P. Li, Y. Cheng, Z. Xie, L. Wang, X. Jing, F. Wang, *Adv. Mater.* **2011**, *23*, 2986-2990.
- [20] L. Chen, B. Zhang, Y. Cheng, Z. Xie, L. Wang, X. Jing, F. Wang, *Adv. Funct. Mater.* **2010**, *20*, 3143-3153.
- [21] L. Chen, H. Tong, Z. Xie, L. Wang, X. Jing, F. Wang, *J. Mater. Chem.* **2011**, *21*, 15773-15779.
- [22] L. Chen, L. Wang, X. Jing, F. Wang, *J. Mater. Chem.* **2011**, *21*, 10265-10267.
- [23] Q. Peng, X. Liu, D. Su, G. Fu, J. Xu, L. Dai, *Adv. Mater.* **2011**, *23*, 4554-4558.
- [24] P. Sonar, S. P. Singh, Y. Li, M. S. Soh, A. Dodabalapur, *Adv. Mater.* **2010**, *22*, 5409-5413.
- [25] H. Zhou, L. Yang, A. C. Stuart, S. C. Price, S. Liu, W. You, *Angew. Chem. Int. Ed.* **2011**, *50*, 2995-2998.
- [26] N. Wang, Z. Chen, W. Wei, Z. Jiang, *J. Am. Chem. Soc.* **2013**, *135*, 17060-17068.
- [27] A. Mishra, P. Bäuerle, *Angew. Chem. Int. Ed.* **2012**, *51*, 2020-2067.
- [28] Y. Lin, H. Wang, Y. Li, D. Zhu, X. Zhan, *J. Mater. Chem. A* **2013**, *1*, 14627-14632.
- [29] M. Zhang, Y. Wang, M. Xu, W. Ma, R. Li, P. Wang, *Energ. Environ. Sci.* **2013**, *6*, 2944-2949.

- [30] G. Yang, C.-a. Di, G. Zhang, J. Zhang, J. Xiang, D. Zhang, D. Zhu, *Adv. Funct. Mater.* **2013**, *23*, 1671-1676.
- [31] Y. Zhang, C. Kim, J. Lin, T.-Q. Nguyen, *Adv. Funct. Mater.* **2012**, *22*, 97-105.
- [32] P. M. Beaujuge, H. N. Tsao, M. R. Hansen, C. M. Amb, C. Risko, J. Subbiah, K. R. Choudhury, A. Mavrinskiy, W. Pisula, J.-L. Brédas, F. So, K. Müllen, J. R. Reynolds, *J. Am. Chem. Soc.* **2012**, *134*, 8944-8957.
- [33] J. Lee, S. Cho, J. H. Seo, P. Anant, J. Jacob, C. Yang, *J. Mater. Chem.* **2012**, *22*, 1504-1510.
- [34] J. Kim, A. R. Han, J. Hong, G. Kim, J. Lee, T. J. Shin, J. H. Oh, C. Yang, *Chem. Mater.* **2014**, *26*, 4933-4942.
- [35] Z.-F. Shi, H. T. Black, A. Dadvand, D. F. Perepichka, *J. Org. Chem.* **2014**.
- [36] D. Bailey, V. E. Williams, *Tetrahedron Lett.* **2004**, *45*, 2511-2513.
- [37] L. Chen, J. Kim, T. Ishizuka, Y. Honsho, A. Saeki, S. Seki, H. Ihee, D. Jiang, *J. Am. Chem. Soc.* **2009**, *131*, 7287-7292.
- [38] A. L. Appleton, S. Miao, S. M. Brombosz, N. J. Berger, S. Barlow, S. R. Marder, B. M. Lawrence, K. I. Hardcastle, U. H. F. Bunz, *Org. Lett.* **2009**, *11*, 5222-5225.
- [39] T. Lei, Y. Zhou, C.-Y. Cheng, Y. Cao, Y. Peng, J. Bian, J. Pei, *Org. Lett.* **2011**, *13*, 2642-2645.
- [40] Z. Liang, Q. Tang, J. Liu, J. Li, F. Yan, Q. Miao, *Chem. Mater.* **2010**, *22*, 6438-6443.



## **Chapter IV. Layered Electron Acceptors from Dimerized Acenes End-capped with 1,2,5-Thiadiazoles**

Layered electron acceptors **4-7/8/9/10** equipped with terminal 1,2,5-thiadiazole groups have been constructed using a one-pot protocol of acene dimerization. Their molecular structures are determined using single crystal X-ray diffraction analysis. Photophysical and electrochemical properties of these molecules present a marked dependence on conjugation length and molecular geometry. An aggregation-induced emission peak and an intramolecular excimer emission (IEE) band were observed for **4-8** and **4-10**, respectively. This work paves the way for the efficient synthesis of nonplanar heteroacenes.

## IV.1 Introduction

As far as we know, certain modes of solid-state packing for common planar organic semiconductors can pose specific problems for device performance.<sup>[1-3]</sup> Therefore, to suppress those packing modes, exploring nonplanar or layered organic semiconductors could be helpful. To date, 9,9'-bianthryls<sup>[4]</sup> triptycenes,<sup>[5]</sup> and spirofluorenes with  $sp^3$  carbon connectors,<sup>[6]</sup> have been commonly adopted as cores to construct nonplanar conjugated molecules. Linear acenes such as anthracene, tetracene and pentacene were used to generate higher dimensional systems through the traditional  $[4\pi + 4\pi]$  photodimerization reaction.<sup>[7]</sup> However extended heteroacenes, especially electron-deficient molecules were hardly considered.<sup>[8-10]</sup> As far as we know, only one example of dimerized diazaacene was unexpectedly obtained in high yield (76%), which was explained by cycloaddition. This was reported by the group of Bunz when they attempted to generate diazaheptacene through oxidation of dihydrodiazahexacene.<sup>[11]</sup> Since there have not been effective synthetic methods of heteroacene-based nonplanar electron acceptors, new synthetic protocols need to be explored.

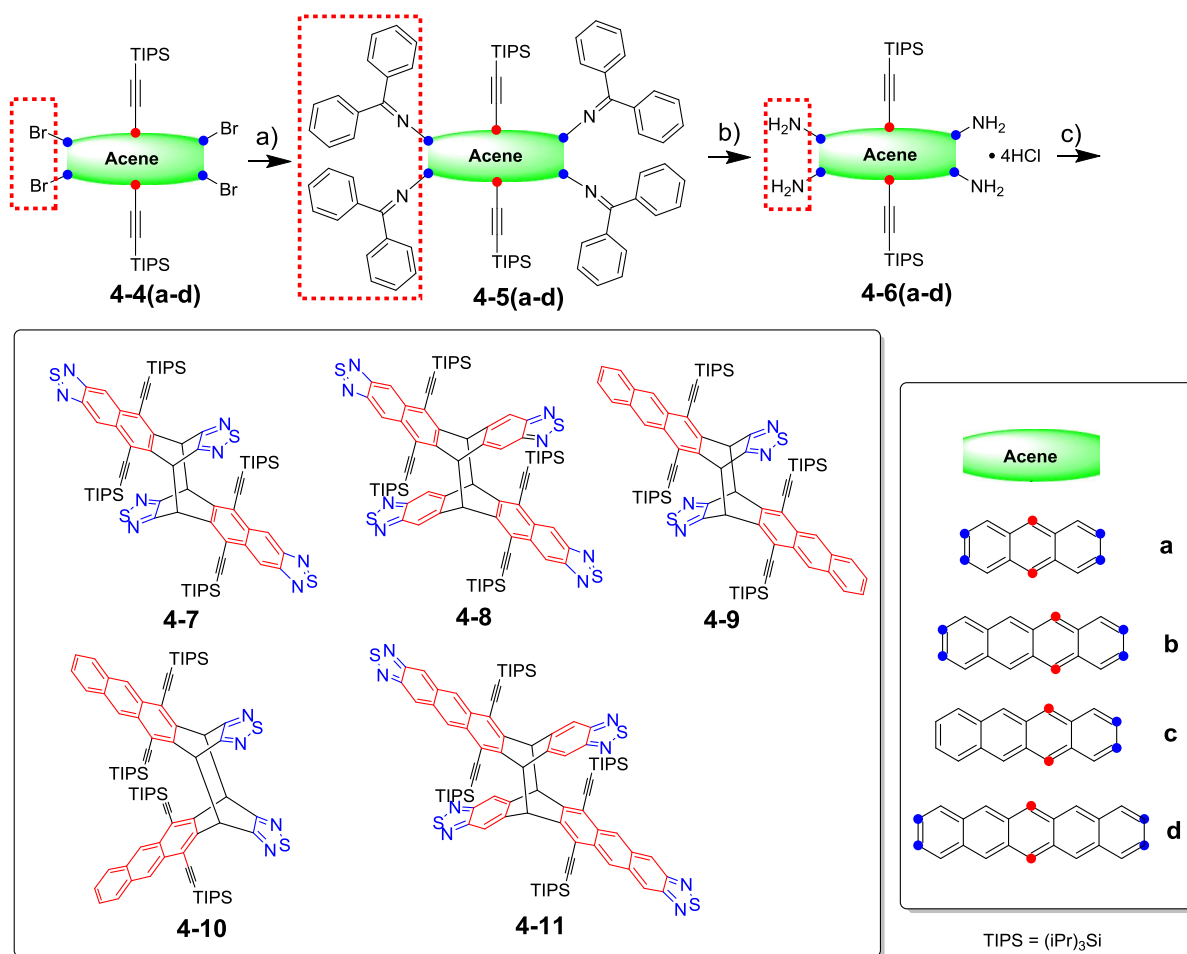
Among electron acceptor moieties, the five-membered ring 1,2,5-thiadiazole has proven to be strongly electron-deficient and its derivatives such as 2,1,3-benzothiadiazol, benzobisthiadiazole, [1,2,5]thiadiazolo[3,4-g]quinoxaline and naphtho[1,2-c:5,6-c]bis[1,2,5]-thiadiazole, have been widely used as key building blocks for organic semiconducting materials due to their planarity and strong electron-withdrawing capability. It is thus expected that incorporation of electron-deficient 1,2,5-thiadiazole units into layered molecules would present interesting inter-and intramolecular interactions as well as new optoelectronic properties, greatly enriching organic functional materials. Herein, we synthesized thiadiazole end-capped layered molecules **4-7/8/9/10/11** through dimerization of heteroacene. A one-pot reaction is employed in which formation of thiadiazole rings and dimerization is accomplished based on di- and tetraamino-substituted acene precursors **4-6(a-d)** (Scheme IV-1). It is believed that introduction of electron-withdrawing thiadiazole rings increase the quinoid character of the conjugated system,<sup>[12]</sup> and thus leads the dimerization step without the involvement of light or oxygen.<sup>[13-18]</sup> Therefore, the

developed electron-deficient heteroacene dimerization method becomes a useful tool for preparing novel layered molecules.

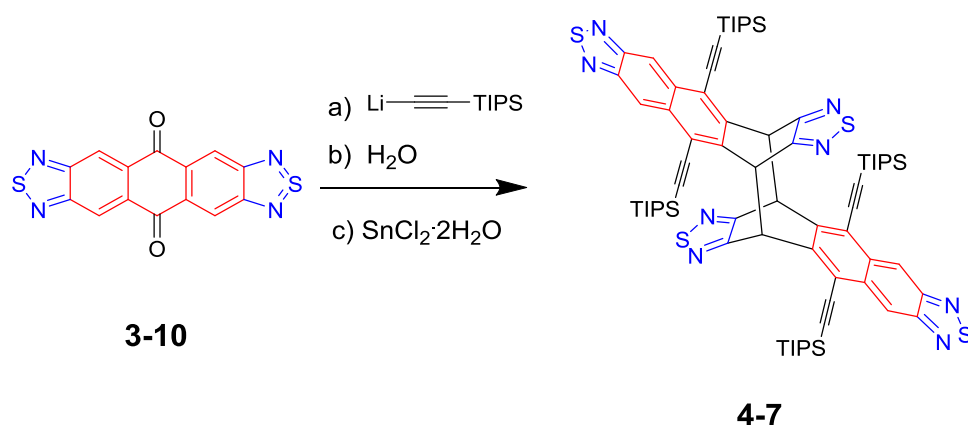
## IV.2 Synthesis

The synthesis is outlined in Scheme IV-1. Di- and tetrabrominated acenes **4-4(a-d)** were obtained by the reduction of the corresponding diol precursors, which were converted from the acene diones **3-4** and **4-1/2/3** by treatment with excess acetylide. The synthesis of diphenylmethaneimine substituted acenes **4-5(a-d)** were accomplished by reaction with benzophenone imine, applying tris(dibenzylideneacetone)dipalladium(0) as catalyst and *rac*-BINAP as ligand. Since such compounds are very sensitive to acidic conditions, which leads to decomposition during the purification by column chromatography based on silica gel. Such case could be prevented when silica columns were neutralized by trimethylamine previously. Then, amino substituted acenes **4-6(a-d)** were obtained after hydrolysis.<sup>[19]</sup> Note that, in this step, the amount and the concentration of hydrochloric acid have a significant impact on the reaction yield, especially for producing **4-6d**. The HCl molecules within **4-6(a-d)** could also be removed by adding them into trimethylamine. The chemical shifts of resulting products could be identified by NMR spectroscopy. Lastly, using N-sulfinylaniline as the cyclization reagent, **4-7** and **4-8** were successfully synthesized in 57-66% yields. Unlike the photoconversion of tetracene and pentacene derivatives, which produced isomeric dimers,<sup>[20-21]</sup> only the centrosymmetric **4-7** and **4-8** were obtained based on **4-6a** and **4-6b**, respectively. In case of the diamino substituted acene **4-6c** as the precursor, the reaction not only produced centrosymmetric **4-9** in 77% yield, but also the planosymmetric **4-10** in 15% yield. The isomeric **4-9** and **4-10** have different polarities, thus they could be separated by silica column. As far as we know, this is the first time report of such one-pot reaction, which involves cyclization reaction of di- or tetraamino acenes and dimerization of aceno[2,1,3]thiadiazoles. Signals in the range of 45 to 55 ppm in the <sup>13</sup>C NMR spectra of **4-7/8/9/10** proved the existence of saturated carbon atoms in the acene moieties. The structural details of all four compounds were confirmed by HRMS, <sup>1</sup>H NMR, <sup>13</sup>C NMR and X-ray crystallographic analysis. **4-11** was also prepared using the same procedure with pentacene as conjugated core.

Unfortunately, it could only be characterized by MALDI-TOF mass spectrometry because of its poor solubility in common solvents (Figure IV-1). Surprisingly, the monomer peak ( $m/z = 756$ ) could also be observed, which might indicate that the so-called dimer compound could break into two monomers by laser irradiation. This phenomenon also happened on the other dimers mentioned above.



**Scheme IV-1.** Synthetic route for **4-7/8/9/10/11**: a) benzophenone imine, *rac*-BINAP, Pd<sub>2</sub>(dba)<sub>3</sub>, *tert*-butoxide, toluene, 110 °C, 55-65%; b) 2.0 M HCl, THF, r.t. 90-95%; c) TMS-Cl, PhNSO, Py, 80 °C, 57-77% (**4-7/8/9**) and 15% (**4-10**). Blue and red dots on acenes a, b and c represent the substitution of corresponding functional groups.



**Scheme IV-2.** Another synthetic route for **4-7**.

Another method was also tried to construct molecule **4-7** as shown in Scheme IV-2. However, the solubility of **3-10** was quite bad. Furthermore, when the nucleophilic reaction was carried out, the mixture remained a suspension even though more THF was added, which indicated the less efficient nucleophilic reaction. Luckily, through the TLC plate monitoring and FD-Mass measurement, the formation of compound **4-7** was confirmed. The estimated reaction yield was less than 2%. This reaction result is another evidence to confirm that the originally designed monomer (III) is not stable and can dimerize immediately (Figure IV-2).

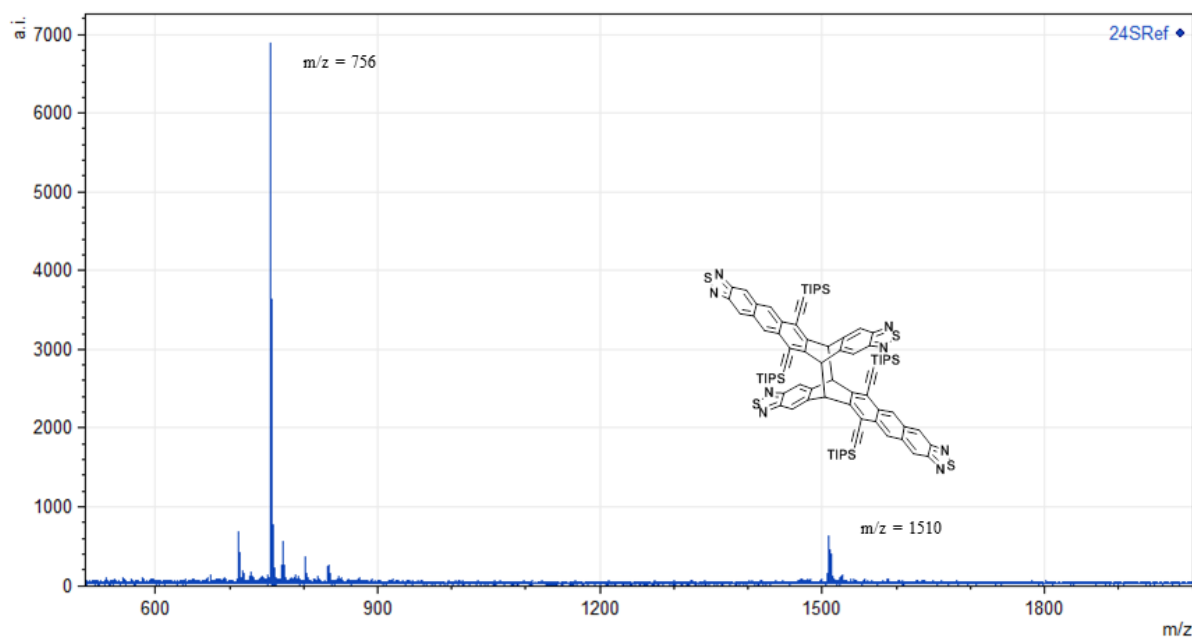


**Figure IV-1.** MALDI-TOF spectrum of **4-11**.

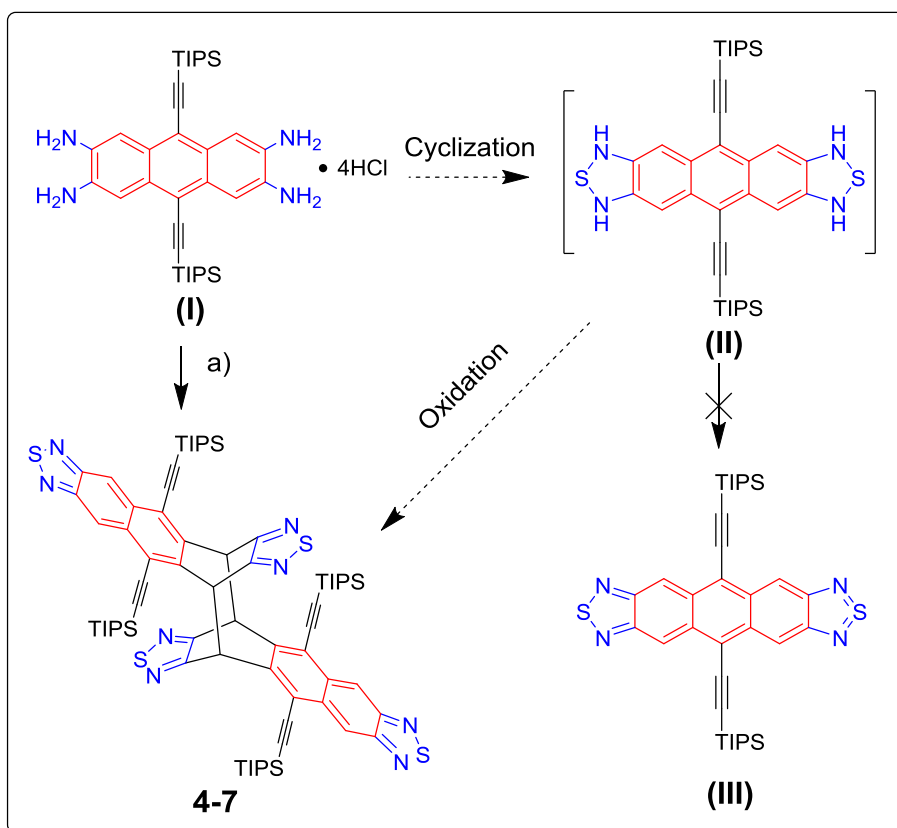
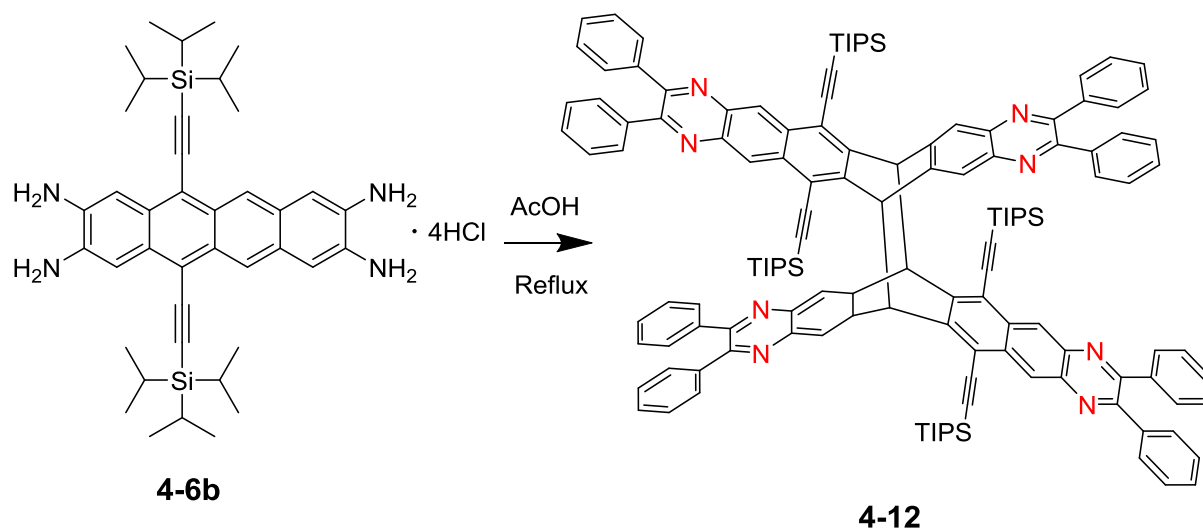


**Figure IV-2.** Proposed reaction mechanism with the anthracene case as an example; a) TMS-Cl, PhNSO, Py, 80 °C.

The two-step synthesis, namely, formation of 2,1,3-thiadiazole rings and dimer formation are successively completed in one pot, making this procedure convenient and efficient. Taking the anthracene case as an example (see Figure IV-2), we assume that firstly, the cyclization of amino substituted acene (**I**) occurs to form the bis-dihydro-2,1,3-thiadiazole anthracene (**II**), which is similar to the formation of dihydro-2,1,3-benzothiadiazole from *o*-phenylenediamine reported by Bryce.<sup>[22]</sup> Then, the intermediate (**II**) was converted directly to molecule **4-7** by oxidation reaction whereas intermediate monomer (**III**) could not be observed at all. Similar to the reported procedure, in the case of dihydrodiazahexacene, MnO<sub>2</sub> was used as oxidant to form acene dimer instead of diazahexacene.<sup>[11]</sup> Thus the oxidative condition seems to favor the cycloaddition adduct.



**Scheme IV-3.** The formation of novel dimeric compound **4-12**.

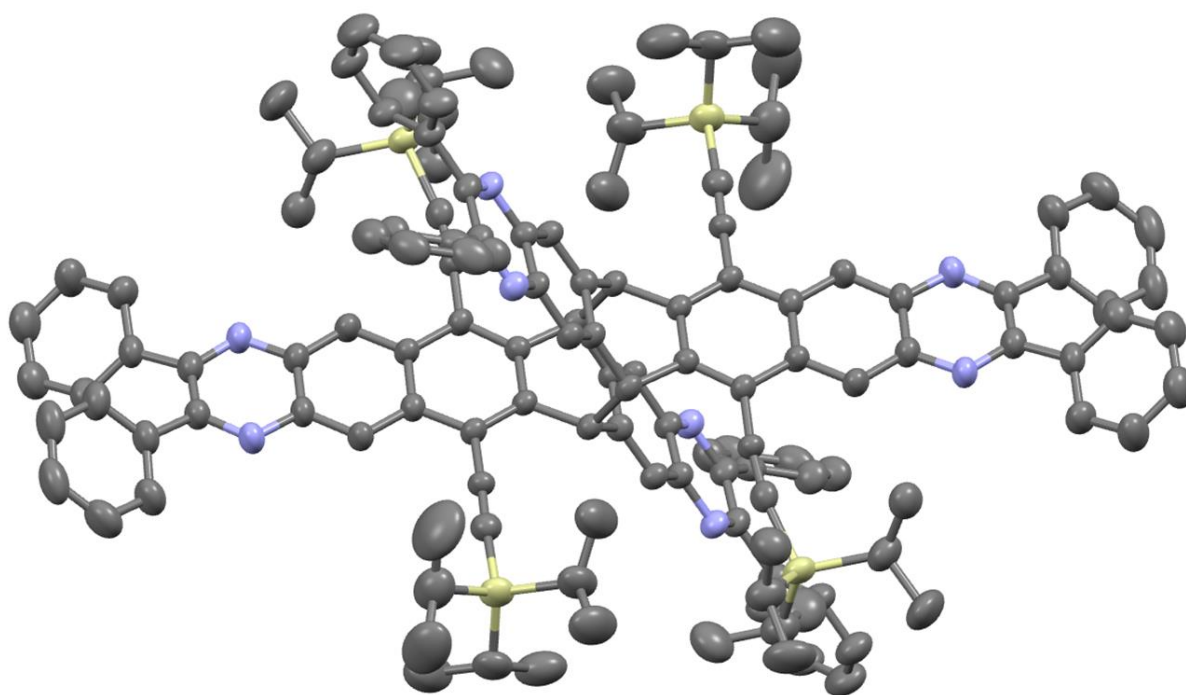
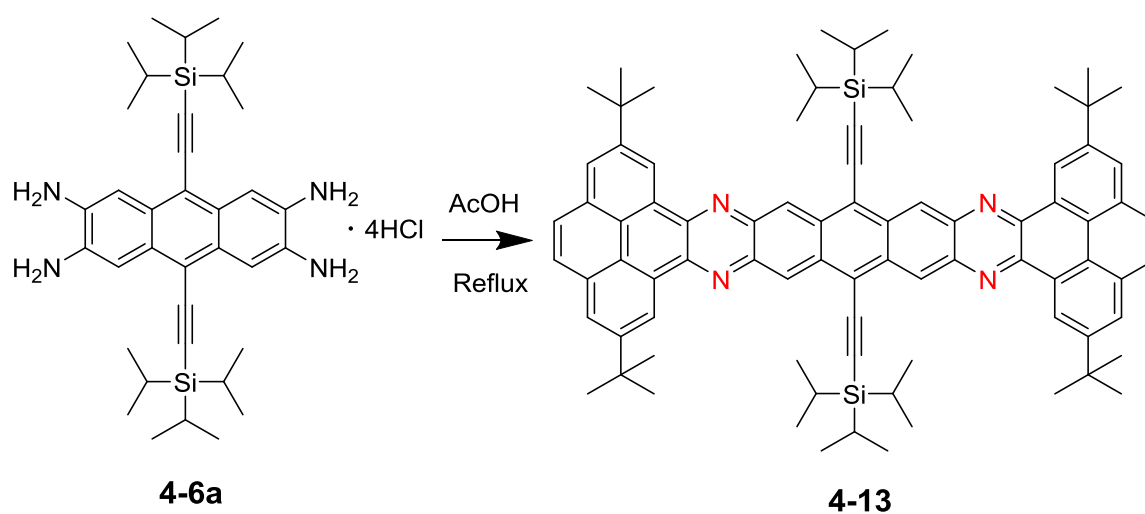


**Figure IV-3.** Single crystal structure of **4-12** (H atoms removed for clarity).

Long acenes, such as hexacene, heptacene, octacene and nonacene are more interesting species. They have smaller band gaps and potentially higher charge-carrier motilities, but they are also prone to oxidative degradation. Aiming for synthesizing longer N-heteroacenes, the condensation reaction between **4-6b** and diphenylethanedione was carried out. The reaction yield reached 85%, whereas there was no envisaged acene hint other than the dimeric compound, which might be

caused by photo-oxidation or photo-dimerization (Scheme IV-3). Clar's concept can explain the photophysical and chemical behavior of designed long acene as a polyene rather than as a poly-benzenoid compound, since only one sextet can be drawn in the molecular structure. Such decomposition might possibly be prevented by the introduction of bulky groups to the acene scaffold. From the other point of view, the obtained layered acene **4-12** might also show some special photophysical properties, which will be checked in the future. Single crystals were grown by solvent evaporation method from dichloromethane solution and were analyzed by ..... (Johannes Gutenberg-University, Mainz).



**Scheme IV-4.** The reaction route towards novel acene compound **4-13**.

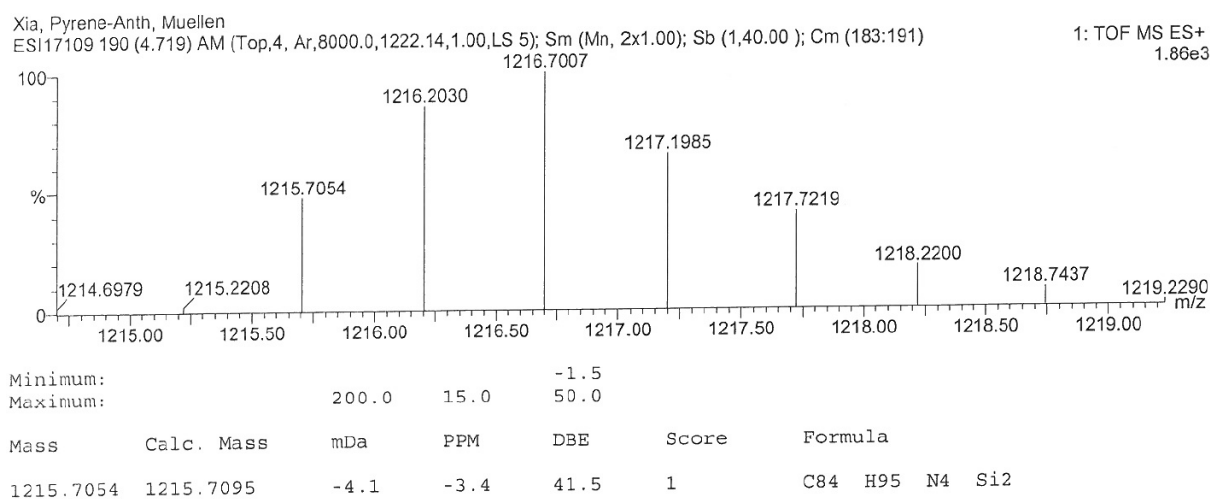


**Figure IV-4.** HR-Mass of compound **4-13**.

Interestingly, there was no indication of dimeric compound when the condensation reaction was carried out between **4-6a** and 4,5-pyrenedione, 2,7-bis(1,1-dimethylethyl) (Scheme IV-4). After purification during the air condition, the target molecule **4-13** is still stable; this was confirmed by HR-Mass as shown in Figure IV-4. Therefore, the longer acenes are expected to be constructed using condensation reaction between **4-6b/c** and 4,5-pyrenedione, 2,7-bis(1,1-dimethylethyl).

### IV.3 Crystal structure analysis

To investigate the intermolecular interaction in the solid state of dimerized acenes **4-7/8/9/10**, their crystals were grown by slow evaporation of tetrahydrofuran solutions. X-ray diffraction experiments were carried out by ..... (Johannes Gutenberg-University, Mainz). As expected based on the varying geometries of **4-7/8/9/10**, their packing modes are quite different. The crystal

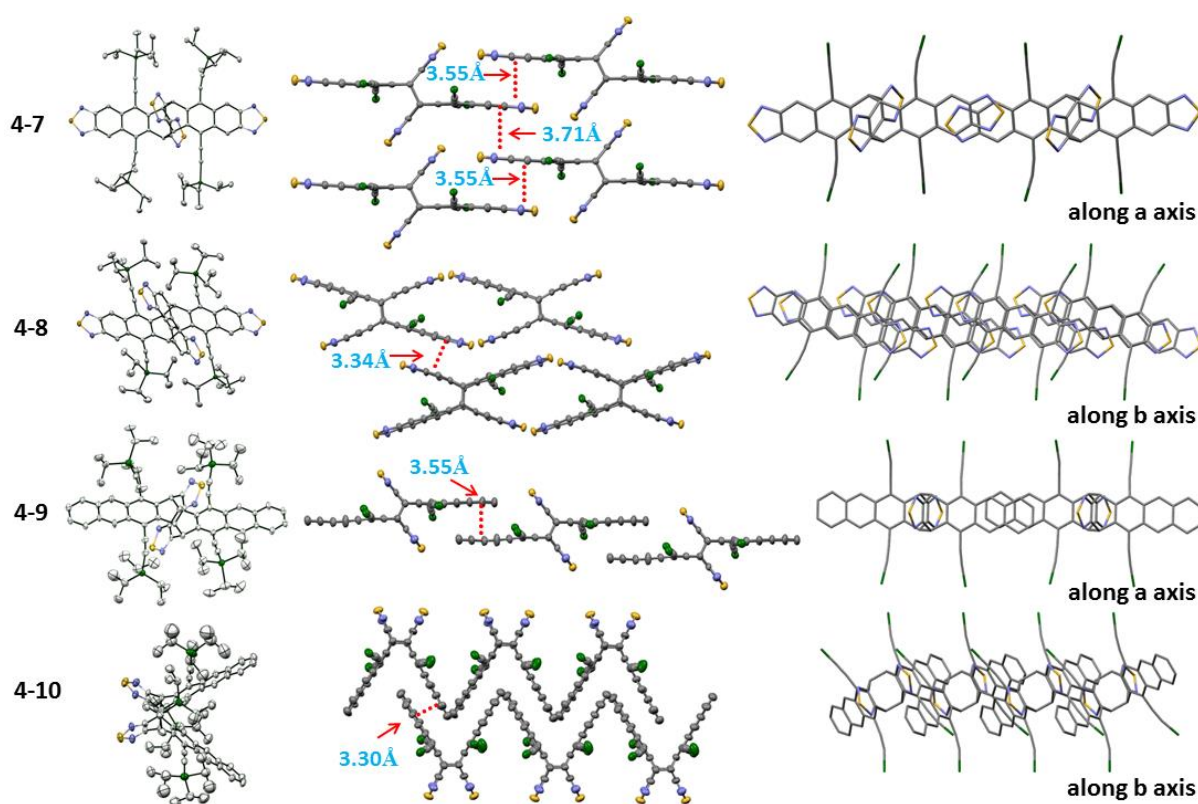


**Figure IV-5.** Structure (left), crystal packing (middle), and degree of  $\pi$ -face overlap (right) of four dimeric acenes (alkyl groups on Si removed for clarity).

structure of **4-7** exhibits columnar packing, where each molecule interacts with four nearest neighboring molecules by two types of symmetrical  $\pi$ - $\pi$  interactions with two interplanar distances (3.55 and 3.71 Å) (Figure IV-5). However, only with the extension of thiadiazole in **4-7** to benzothiadiazole in **4-8**, **4-8** adopts 2D slipped  $\pi$ -stacking motifs, where the fragments of benzothiadiazole interact with naphthothiadiazole fragment of the neighboring molecules. This packing mode favors the intermolecular charge transport in the solid. Thereby, considering its low LUMO energy levels, **4-8** presents the potential usefulness as an organic electron acceptor. **4-9** forms a brick wall type packing motif with  $\pi$ -stacking distance between anthracenes to the 3.55 Å. **4-10** packs in a 2D slipped  $\pi$ -stacking arrangement similar to that of **4-8**, with a shorter  $\pi$ -face separation of 3.30 Å. As far as we know, this is the first time report both crystal structures of two isomers based on acene dimers.

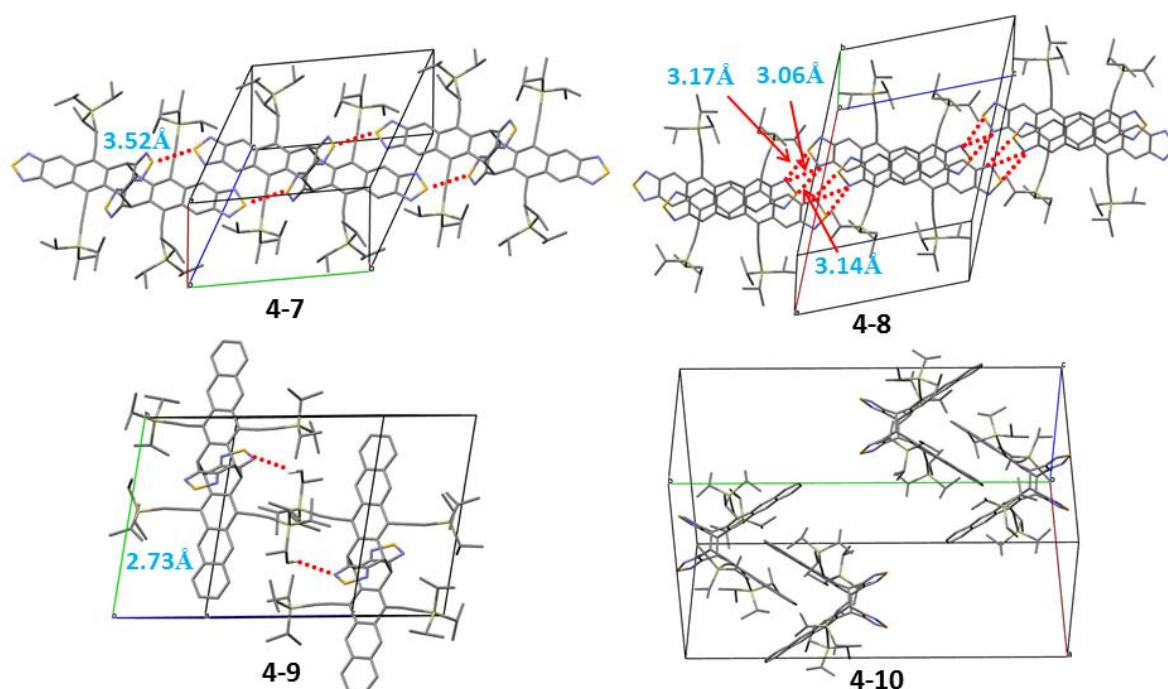


**Figure IV-6.** The involvement of heteroatoms for intermolecular interaction (red dash lines).

The heteroatoms also contribute differently to their crystal packing (Figure IV-6). For **4-7**, the distance [ $S\cdots S$  (3.52 Å)] between the two sulfur atoms of two neighboring molecules is shorter than the sum of their van der Waals radii (1.85 Å). In the case of

**4-8**, it is the first case to show the intermolecular interaction by head-to-tail contacts of the thiadiazole moieties with N...S interaction. In comparison with **4-7** and **4-8**, only **4-9** presents the intermolecular interactions between a hydrogen atom of an isopropyl group and a nitrogen atom of the thiadiazole [N...H (2.73 Å)]. However, for **4-10** no hydrogen bonds or intermolecular interactions between heteroatoms were observed at all. The crystallographic data and refinement details of the four compounds are summarized in Table IV-1.

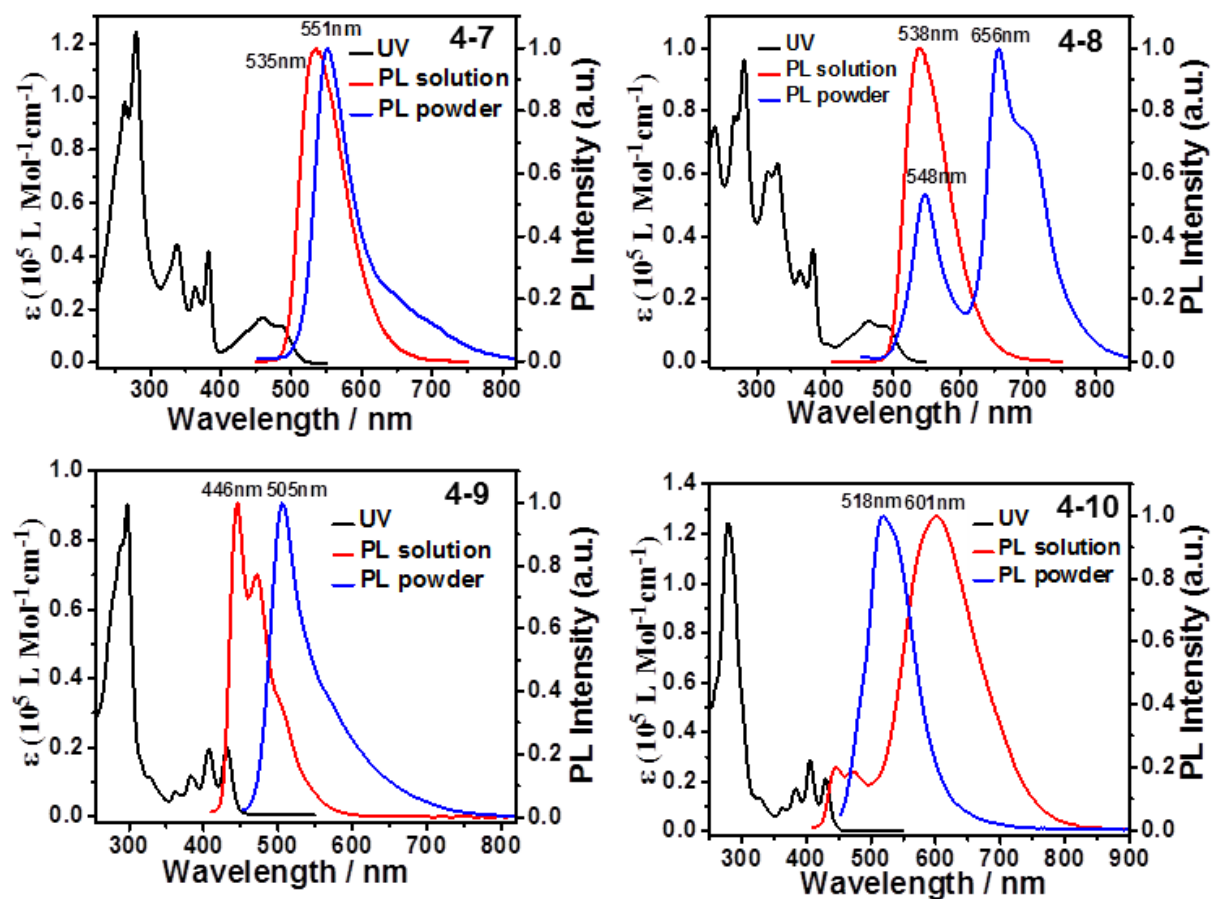
**Table IV-1.** Crystal structure data for compounds **4-7/8/9/10**

	Space group	A[Å]	b[Å]	c[Å]	$\alpha$ [deg]	$\beta$ [deg]	$\gamma$ [deg]	V[Å <sup>3</sup> ]	Z
<b>4-7</b>	P-1	7.769(1)	13.928(2)	17.208(3)	78.462(5)	86.683(5)	79.739(5)	1794.8(9)	1
<b>4-8</b>	P2 <sub>1</sub> /c	18.5577(8)	15.4895(6)	15.0011(7)		113.356(4)		3958.7(3)	2
<b>4-9</b>	P-1	14.5655(10)	14.7189(11)	18.6267(13)	86.867(6)	88.326(6)	74.024(6)	3833.0(5)	2
<b>4-10</b>	P2 <sub>1</sub> /c	18.7012(10)	33.6573(13)	12.8089(7)		106.214(4)		7741.7(7)	4

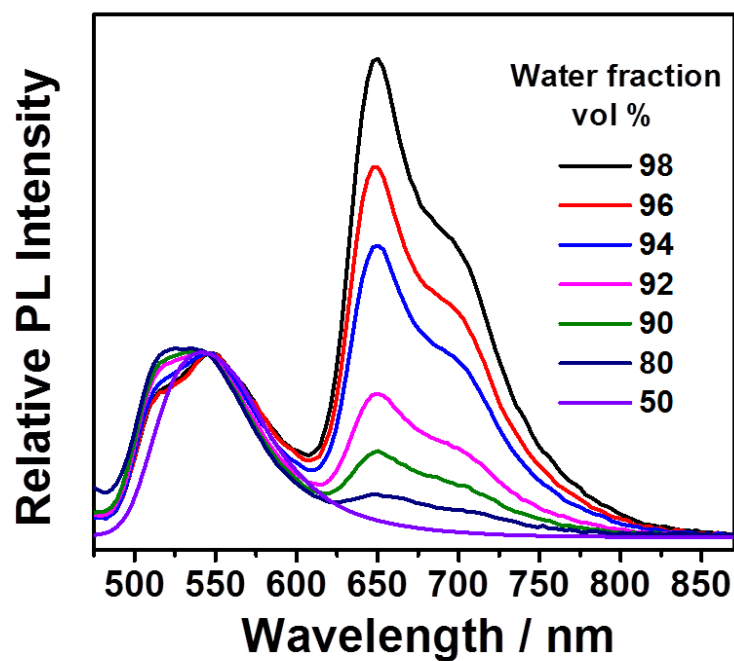
## IV.4 Photophysical and electrochemical properties

Figure IV-7 depicts the UV-vis and photoluminescence (PL) spectra for **4-7/8/9/10**. **4-7** and **4-8** show a similar absorption spectral shape, whereas their emission profiles are dramatically different. The absorption band of both molecules in the range of 265 – 380 nm arises from the  $\pi$ - $\pi^*$  transition of the aryl substituents. The other bands located between 400 and 530 nm can be assigned to the acetylene-substituted naphthothiadiazole chromophore. For **4-7**, the peak position shifts from 535 nm in solution to 551 nm in powder. Similarly, **4-8** shows an emission band as that of **4-7** in solution, yet surprisingly, apart from a slightly red-shifted emission band compared to **4-7**, an additional strong emission peak at 657 nm with a shoulder at 700 nm appears in the powder PL spectrum of **4-8**. To figure out the origin of this new band, we investigated the influence of aggregation effects on the fluorescence behavior by measuring the PL spectra of **4-8** in THF/water mixtures with different fractions of water (fw). As shown in Figure IV-8, the new emission peak appeared from fw  $\approx$  80 vol% and was relatively enhanced by further increasing the fraction of water (after normalization to 545 nm peak). Evidently, the new band is thus induced

by aggregation effect. Note that the overall fluorescence intensity decreased upon adding water. Similarly, the emission intensity decreased correspondingly with the concentration increasing of DCM solutions (Figure IV-9). A new peak appeared until the concentration increased to  $2 \times 10^{-3}$  mol/L, which might be ascribed to the intermolecular excimer emission.



**Figure IV-7.** Absorption (black line, in  $\text{CH}_2\text{Cl}_2$  solution) and PL spectra of **4-7** ( $\lambda_{\text{Exc}} = 337$  nm), **4-8** ( $\lambda_{\text{Exc}} = 382$  nm), **4-9** ( $\lambda_{\text{Exc}} = 380$  nm) and **4-10** ( $\lambda_{\text{Exc}} = 380$  nm) in  $\text{CH}_2\text{Cl}_2$  solution (red line) and powder (blue line).



**Figure IV-8.** PL spectra of **4-8** ( $10\mu\text{M}$ ) were measured in THF/water mixtures with different water fractions. Excitation wavelength = 382 nm.

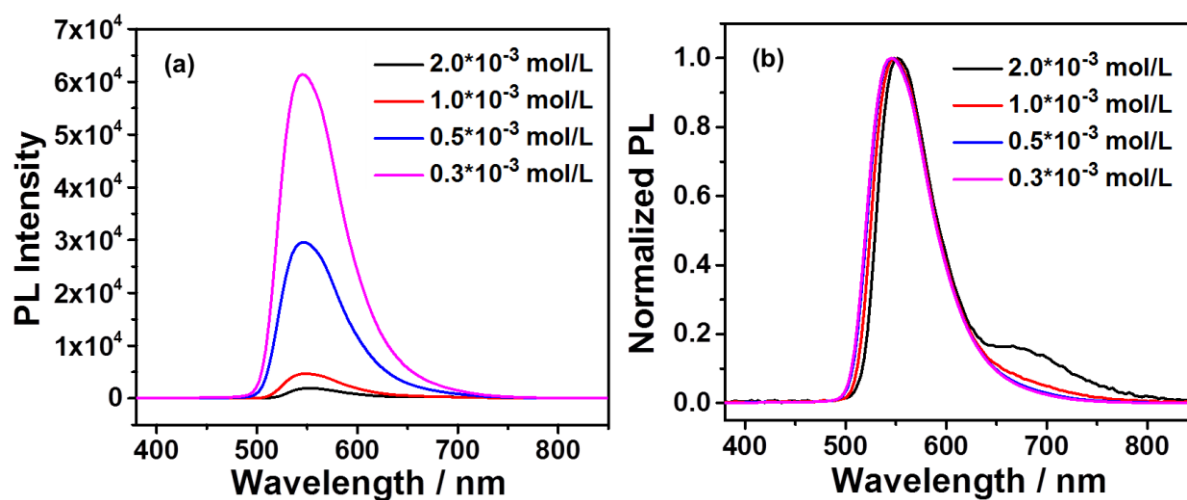


**Figure IV-9.** PL spectra of **4-8** were measured in DCM solutions with different concentrations. (a) Concentration dependent PL spectra; (b) Normalized PL spectra. Excitation wavelength = 382 nm.

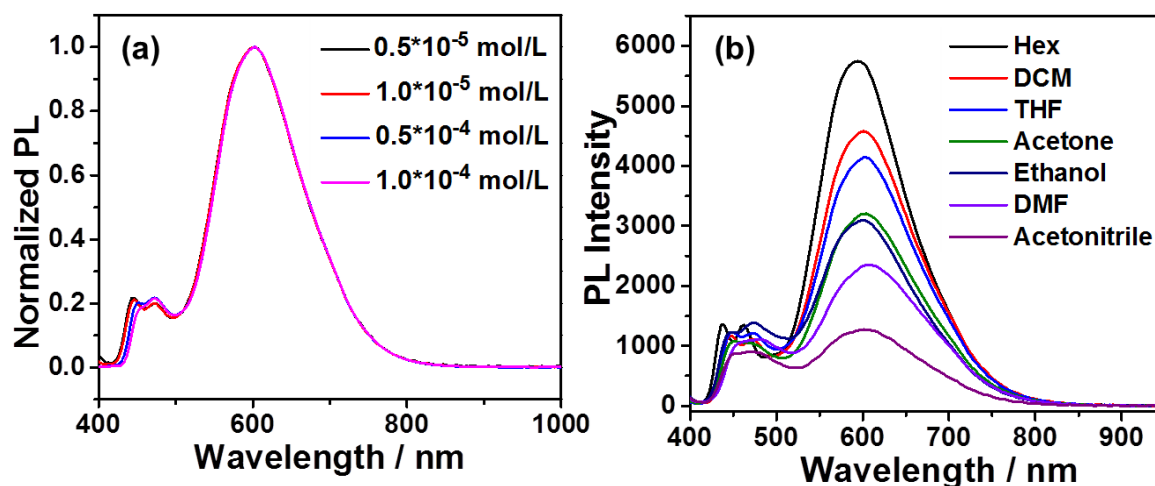


**Figure IV-10.** (a) PL spectra of **4-10** measured in CH<sub>2</sub>Cl<sub>2</sub> solution with varying concentrations. (b) PL spectra of **4-10** measured in different solvents with a concentration of 1.0×10<sup>-5</sup> M. ( $\lambda_{\text{Exc}} = 380$  nm).

While resolved vibrational sublevels well overlap for **4-9** and **4-10** in the absorption spectra (Figures IV-7) since they contain the same functional groups, their PL spectra are very different. In comparison with 446 and 472 nm emission peaks of **4-9**, **4-10** shows a new strong and red-shifted band ( $\lambda_{\text{max}} = 601$  nm), which does not originate from emission of the intermolecular excimer because: (i) the ratio between two emission bands of **4-10** is found to be constant at varying concentration in dichloromethane solution (Figure IV-10a); (ii) their ratio could be tuned in different solvents, as the intramolecular excimer emission is strongly dependent on the polarity of solvent (Figure IV-10b),<sup>[23-24]</sup> and (iii) under the same condition, intermolecular excimer emission have not been observed for **4-9**. Thus, we assign the red-shifted band to the intramolecular excimer emission (IEE)<sup>[16, 25]</sup> from the two opposite 1,4-bis((triisopropylsilyl)ethynyl)anthracene (anthra-TIPS) moieties. These phenomenon are in accordance with that of naphthalene-1,8:4,5-bis(dicarboximide) dimer, in which 515 nm fluorescence peak appears with a large Stokes shift and a lack of vibronic features.<sup>[26]</sup> The changes in fluorescence spectra on going from solution to solid state also differ dramatically for isomers **4-9** and **4-10**. For **4-9**, a significant bathochromic shift from 446 to 505 nm occurs when going from solution to powder spectra. In contrast, the maximum emission peak of powder **4-10** shifts hypsochromically to 518 nm. That can be assigned to the aggregation of anthra-TIPS. We tentatively attribute the disappearance of an IEE peak to its solid-state packing

motif as indicated by the single-crystal structure (see above), in which the two anthra-TIPS moieties within one molecule strongly interact with other two neighbours in the excimer formation zone. Figure IV-11 further confirmed that the intensity of the IEE peak reduced gradually with the increasing fraction of water, whereas the anthra-TIPS aggregation emission peak increased correspondingly.

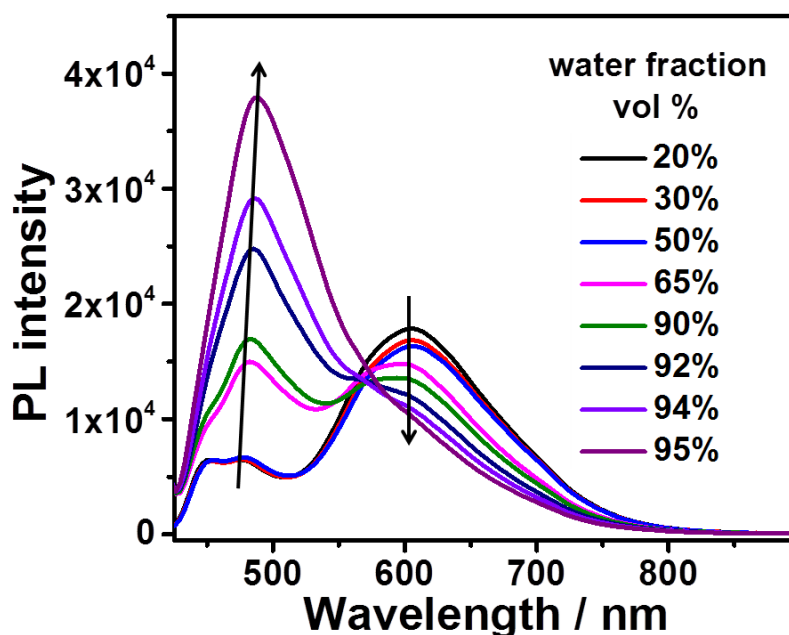


**Figure IV-11.** PL spectra of **4-10** (around 10 $\mu$ M) were measured in THF and water solution. Excitation wavelength = 380 nm.

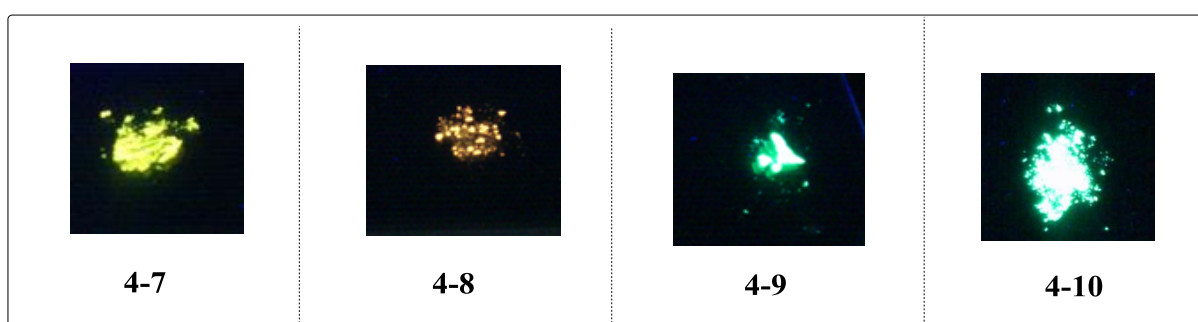


**Figure IV-12.** Solid-state **4-7/8/9/10** show strong fluorescence emission under 365 nm UV lamp.

The photoluminescent quantum yields (PLQYs) of **4-7/8**, and **4-9/10** were determined in DCM in reference to fluorescein ( $\Phi = 0.9$  in 0.1 M NaOH,  $\lambda_{\text{Exc}} = 460\text{nm}$ ) and 9,10-diphenylanthracene ( $\Phi = 0.7$  in toluene,  $\lambda_{\text{Exc}} = 365\text{nm}$ ), respectively. The

PLQYs of **4-7** and **4-8** are  $0.28\pm 0.02$  and  $0.36\pm 0.03$ , respectively. The PLQY of centrosymmetric **4-9** is  $0.21\pm 0.02$ , which is five times higher than that of its isomeric planosymmetric **4-10**. That might be caused by the intramolecular self-quenching between the two opposite anthra-TIPS. This phenomenon was also observed for syn-[2.2](4,7)benzothiadiazolophanes, due to a similar behavior between the two opposite benzothiadiazole rings.<sup>[27]</sup> All of the four materials in the solid state emit strong fluorescence as irradiated by UV light (365 nm) (Figure IV-12).

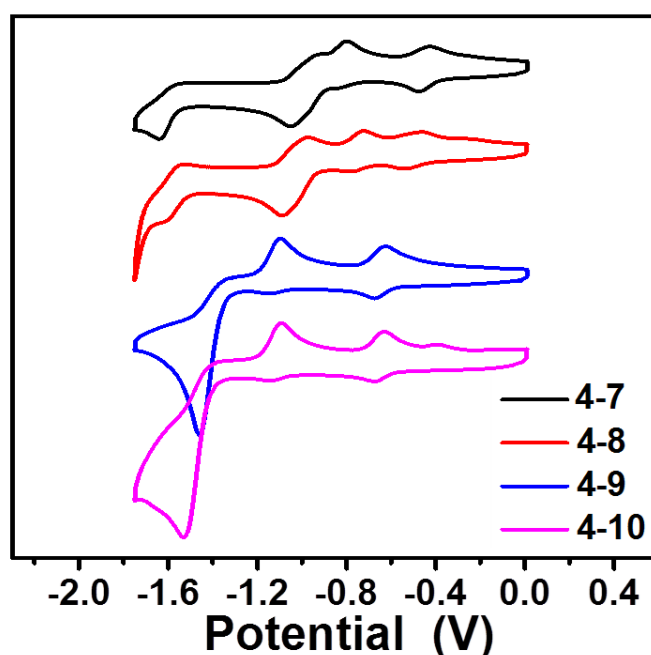


**Figure IV-13.** Cyclic voltammetric profiles of **4-7/8/9/10** in dichloromethane with 0.1 M  $\text{Bu}_4\text{NPF}_6$  as supporting electrolyte. Scan rate = 100 mV/s.

The cyclic voltammograms were measured versus  $\text{Fc}^+/\text{Fc}$  in  $\text{CH}_2\text{Cl}_2/0.1\text{M}$   $\text{Bu}_4\text{NPF}_6$  at a scan rate of 100 mV/s (Figure IV-13 and Table IV-2). **4-7** and **4-8** show reversible redox processes with the half-wave reduction potential  $E_{\text{red}1/2}$  vs  $\text{Fc}^+/\text{Fc} = -0.91$  V and  $E_{\text{red}1/2}$  vs  $\text{Fc}^+/\text{Fc} = -0.97$  V, respectively. The slightly smaller reduction potential for **4-7** suggests that the thiadiazole ring has a stronger electron-withdrawing ability in comparison with benzothiadiazole. **4-9** and **4-10** present quite similar profiles ( $E_{\text{red}1/2}$  vs  $\text{Fc}^+/\text{Fc} = -1.11$  V), which indicates no strong electronic interaction between face-to-face orientated aromatic rings (anthracene to anthracene, thiadiazole to thiadiazole or anthracene to thiadiazole).

**Table IV-2.** [a] In  $\text{CH}_2\text{Cl}_2$ ,  $\text{Bu}_4\text{NPF}_6$  (0.1 M), 295 K, scan rate = 100 mV/s, versus  $\text{Fc}^+/\text{Fc}$ . [b] Determined from  $E_{\text{LUMO}} = - [E_{\text{red1/2}} - E_{(\text{Fc}^+/\text{Fc})} + 4.8]$  eV. [c] Calculated from  $E_{\text{HOMO}} = E_{\text{LUMO}} - E_{\text{gap}}$ . [d] Determined from the onset of absorption ( $1 \times 10^{-5}\text{M}$ ). [e] DFT calculation results.

	$E_{\text{red1/2}}$ vs $\text{Fc}^+/\text{Fc}$ (V) [a]	absorption edge (nm)	LUMO (eV) [b]	HOMO (eV) [c]	$E_g$ (eV) [d]	LUMO (eV) [e]	HOMO (eV) [e]
<b>4-7</b>	-0.80	514	-4.00	-6.41	2.41	-3.14	-5.90
<b>4-8</b>	-0.86	521	-3.94	-6.32	2.38	-3.08	-5.83
<b>4-9</b>	-1.00	445	-3.80	-6.59	2.79	-2.47	-5.44
<b>4-10</b>	-1.00	445	-3.80	-6.59	2.79	-2.53	-5.50

## IV.5 Density functional theory calculations

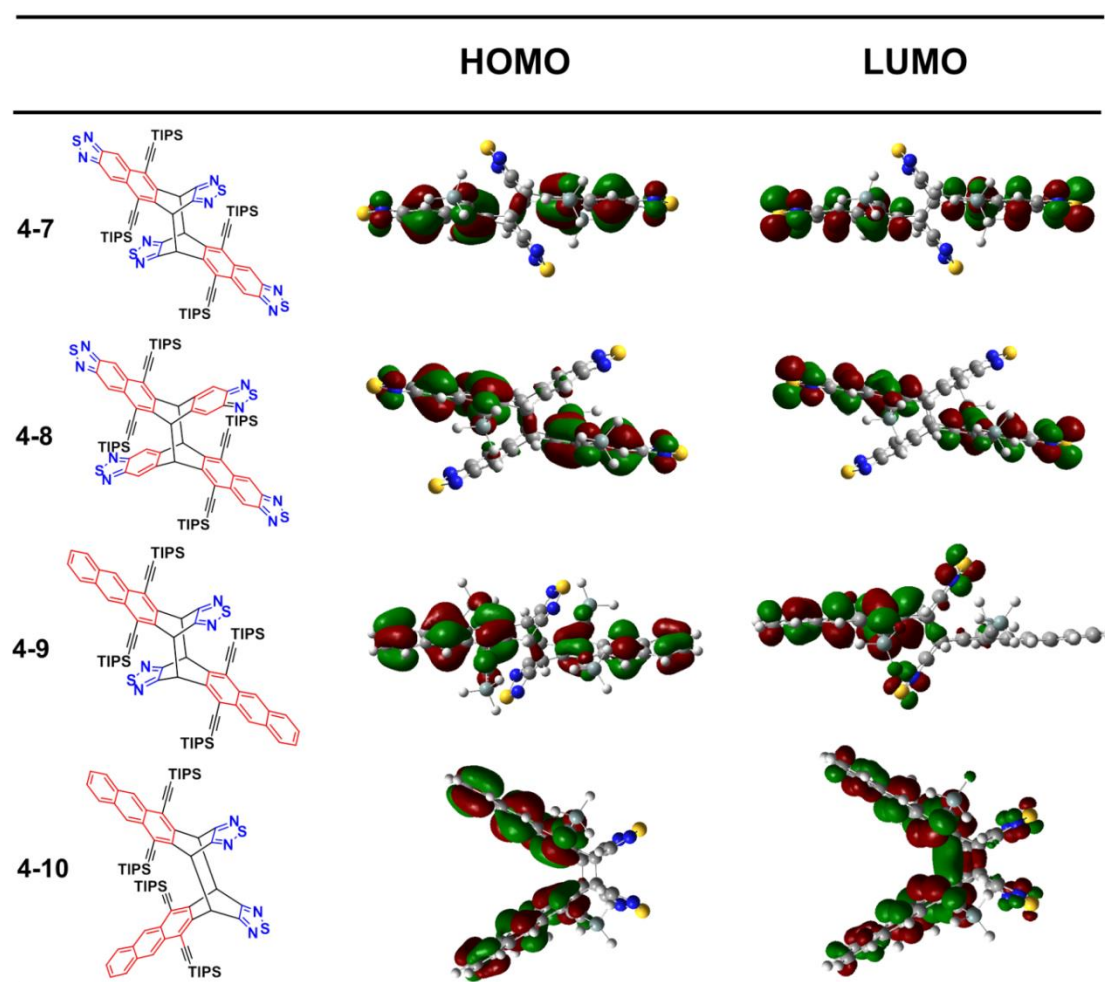


**Figure IV-14.** Calculated frontier molecular orbitals based on model compounds (omitted methyl groups) according to DFT calculations at the B3LYP/6-31G (d) level.

Furthermore, we used DFT calculations to investigate the electron delocalization and energy levels for the four molecules (Figure IV-14 and Table IV-2), which were done by ..... Electron cloud densities only locate on naphtho[2,3-c][1,2,5]thiadiazole moieties for both HOMO and LUMO of **4-7** and **4-8**. The contributions of thiadiazole units to these LUMOs are increased due to the electron-withdrawing inductive effect. Moreover, the HOMOs of **4-9** and **4-10** are delocalized only over the two anthracenes, whereas their LUMOs are contributed also by the thiadiazole units. Obviously, intramolecular overlaps were observed for **4-10** between two opposite anthracene moieties. This is in agreement with the DFT results found for a pentacene based cyclophane.<sup>[28]</sup>

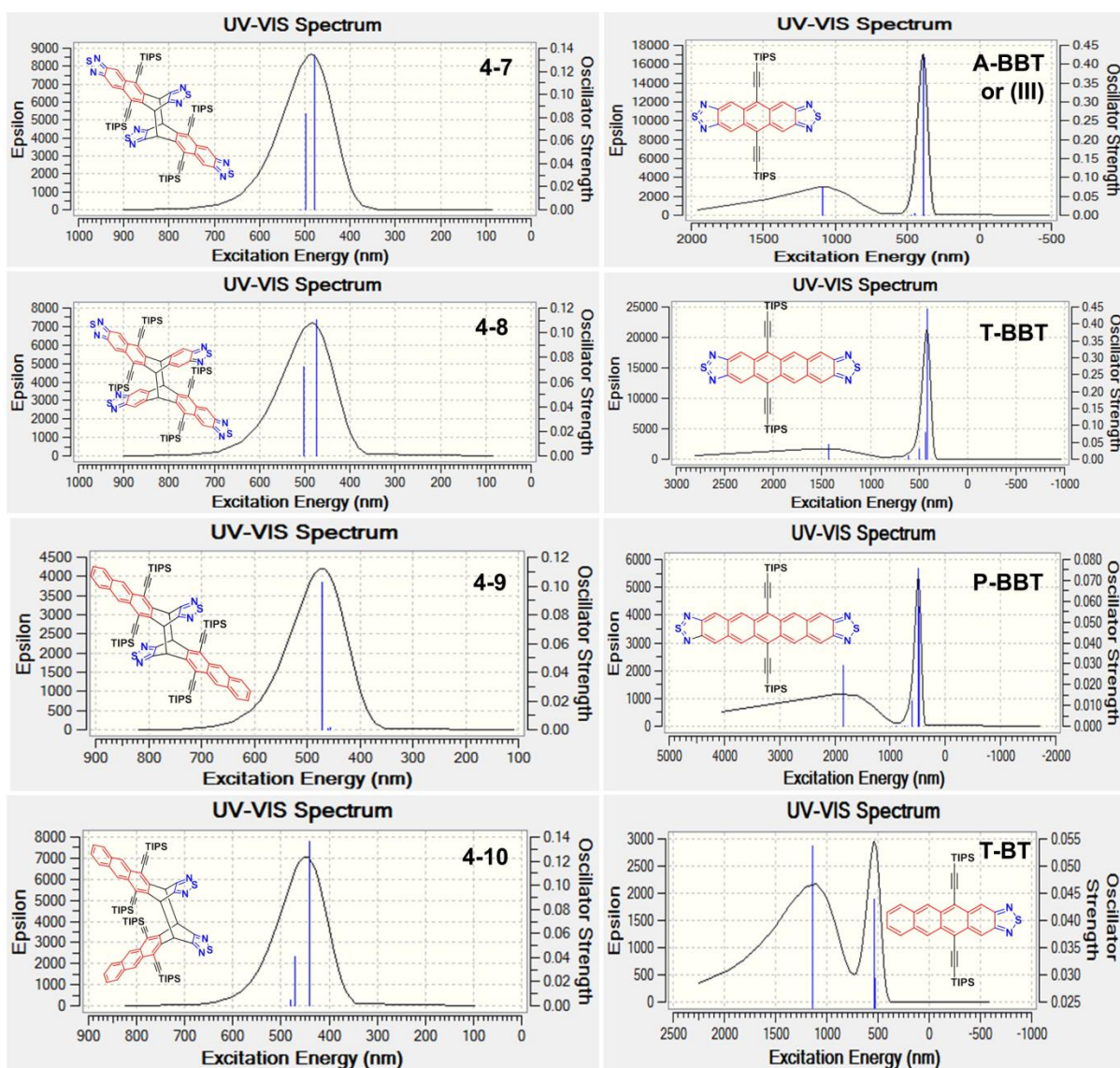


**Figure IV-15.** Calculated UV-vis spectra based on model compounds of **4-7/8/9/10** and envisaged monomers (omitted methyl groups) according to TD-DFT calculations at the B3LYP/6-31G (d) level.

For curiosity, with the help of ..... , the absorption spectra of the model structures of **4-7/8/9/10** and envisaged corresponding monomer compounds were also calculated, which present dramatically different properties (Figure IV-15). Taking the difference between compound **4-7** and A-BBT (III) as an example, the energy gap for **4-7** is around 2.75 eV, whereas the energy gap for A-BBT (III) is only 1.34 eV and maximum absorb at low energy region appears at 1086 nm. If the conjugated backbone was further extended to form T-BBT and P-BBT, the calculated maximum absorption wavelength can reach up to 1433 nm and 1855 nm, respectively. This behavior is similar to that of compounds with quinone structure.

## IV.6 Conclusions

In conclusion, we have demonstrated herein the synthesis of layered acceptors via dimerization of thiadiazole end-capped acenes together with their crystal structures and analysis of packing motifs. Interestingly, the four structurally similar compounds feature huge differences in their photophysical properties. In comparison with **4-7**, **4-8** with acene ring extension shows a new strong emission in the near-infrared region introduced by the aggregation effect. Compound **4-9** features only A-TIPS unit emission, whereas **4-10** is also characterized by intramolecular excimer fluorescence in solution. This finding provides a feasible molecular strategy to design novel molecules with aggregation or IEE effect. The photovoltaic properties and device fabrication of synthesized nonplanar acceptors and application of the present method to other polyacene systems are currently under study. In this chapter, we only studied molecules with layered structures. In the coming chapter, cruciform electron-accepting molecules will be presented. Note that the novel tetra-amino substituted acenes, such as anthracene, tetracene, and pentacene are very useful building blocks to construct long acenes or layered acenes, like the pre-research results, compounds **4-12** and **4-13**. Moreover, covalent organic frameworks (COF) can also be expected after the condensation between our tetra-amino precursors and cyclohexane-1,2,3,4,5,6-hexaone. The bulk COF crystals can be post-synthesized to form 2D nanosheets. Then the electronic and catalytic properties can be further studied. This topic can be also extended for pore engineering. It will be very interesting.

## IV.7 References

- [1] H. Xu, R. Chen, Q. Sun, W. Lai, Q. Su, W. Huang, X. Liu, *Chem. Soc. Rev.* **2014**, *43*, 3259-3302.
- [2] A. Mishra, P. Bäuerle, *Angew. Chem. Int. Ed.* **2012**, *51*, 2020-2067.
- [3] J. Roncali, P. Leriche, A. Cravino, *Adv. Mater.* **2007**, *19*, 2045-2060.
- [4] P. Zhang, W. Dou, Z. Ju, X. Tang, W. Liu, C. Chen, B. Wang, W. Liu, *Adv. Mater.* **2013**, *25*, 6112-6116.
- [5] P. Kissel, D. J. Murray, W. J. Wulfstange, V. J. Catalano, B. T. King, *Nat. Chem.* **2014**, *6*, 774-778.
- [6] D. Xia, D. Gehrig, X. Guo, M. Baumgarten, F. Laquai, K. Müllen, *J. Mater. Chem. A* **2015**, *3*, 11086-11092.
- [7] H. Bouas-Laurent, A. Castellán, J.-P. Desvergne, R. Lapouyade, *Chem. Soc. Rev.* **2001**, *30*, 248-263.
- [8] B. Kohl, F. Rominger, M. Mastalerz, *Org. Lett.* **2014**, *16*, 704-707.
- [9] U. Mueller, M. Baumgarten, *J. Am. Chem. Soc.* **1995**, *117*, 5840-5850.
- [10] J. Heinze, *Angew. Chem. Int. Ed.* **1981**, *20*, 202-203.
- [11] J. U. Engelhart, B. D. Lindner, O. Tverskoy, F. Rominger, U. H. F. Bunz, *Chem. Eur. J.* **2013**, *19*, 15089-15092.
- [12] C. H. Suresh, S. R. Gadre, *J. Org. Chem.* **1999**, *64*, 2505-2512.
- [13] S. H. Chan, H. K. Lee, Y. M. Wang, N. Y. Fu, X. M. Chen, Z. W. Cai, H. N. C. Wong, *Chem. Commun.* **2005**, 66-68.
- [14] B. Purushothaman, S. R. Parkin, J. E. Anthony, *Org. Lett.* **2010**, *12*, 2060-2063.
- [15] J. U. Engelhart, O. Tverskoy, U. H. F. Bunz, *J. Am. Chem. Soc.* **2014**, *136*, 15166-15169.
- [16] J. Reichwagen, H. Hopf, A. Del Guerso, J.-P. Desvergne, H. Bouas-Laurent, *Org. Lett.* **2004**, *6*, 1899-1902.
- [17] P. Coppo, S. G. Yeates, *Adv. Mater.* **2005**, *17*, 3001-3005.
- [18] O. Berg, E. L. Chronister, T. Yamashita, G. W. Scott, R. M. Sweet, J. Calabrese, *J. Phys. Chem. A* **1999**, *103*, 2451-2459.
- [19] L. Chen, J. Kim, T. Ishizuka, Y. Honsho, A. Saeki, S. Seki, H. Ihee, D. Jiang, *J. Am. Chem. Soc.* **2009**, *131*, 7287-7292.

- [20] S. S. Zade, M. Bendikov, *J. Phys. Org. Chem.* **2012**, *25*, 452-461.
- [21] S. S. Zade, N. Zamoshchik, A. R. Reddy, G. Fridman-Marueli, D. Sheberla, M. Bendikov, *J. Am. Chem. Soc.* **2011**, *133*, 10803-10816.
- [22] M. R. Bryce, *J. Chem. Soc., Perkin Trans. 1* **1984**, 2591-2593.
- [23] T. Hayashi, T. Suzuki, N. Mataga, Y. Sakata, S. Misumi, *Chem. Phys. Lett.* **1976**, *38*, 599-601.
- [24] C. Hippus, I. H. M. van Stokkum, E. Zangrando, R. M. Williams, M. Wykes, D. Beljonne, F. Würthner, *J. Phys. Chem. C* **2008**, *112*, 14626-14638.
- [25] C. A. van Walree, V. E. M. Kaats-Richters, L. W. Jenneskens, R. M. Williams, I. H. M. van Stokkum, *Chem. Phys. Lett.* **2002**, *355*, 65-70.
- [26] Y. Wu, M. Frasconi, D. M. Gardner, P. R. McGonigal, S. T. Schneebeli, M. R. Wasielewski, J. F. Stoddart, *Angew. Chem. Int. Ed.* **2014**, *53*, 9476-9481.
- [27] M. Watanabe, K. Goto, M. Fujitsuka, S. Tojo, T. Majima, T. Shinmyozu, *Bull. Chem. Soc. Jpn.* **2010**, *83*, 1155-1161.
- [28] Y. Koyama, S. Hiroto, H. Shinokubo, *Angew. Chem. Int. Ed.* **2013**, *52*, 5740-5743.



# Chapter V. A Cruciform Electron Acceptor for Solution Processed Non-fullerene Organic Solar Cells

In this chapter, a novel electron acceptor, namely 2,2'-(12H,12'H-10,10'-spirobi[indeno[2,1-b] fluorene]-12,12'-diylidene) dimalononitrile (**5-3**), exhibiting cruciform molecular structure was synthesized and its thermal, photophysical, electrochemical, crystal, and photovoltaic properties were investigated. The novel acceptor exhibits excellent thermal stability with a decomposition temperature of 460 °C, an absorption extending to 600 nm, and a LUMO level of -3.72 eV. Solution processed bulk-heterojunction (BHJ) organic solar cells were fabricated using **5-3** as acceptor and polythieno[3,4-b]-thiophene-co-benzodithiophene (PTB7) as donor polymer. The effect of the donor-to-acceptor ratio and processing conditions on device performance was investigated. A device processed from tetrachloroethane with a donor to acceptor weight ratio of 1:1 yielded a power conversion efficiency (PCE) of 0.80 %.

## V.1 Introduction

Organic photovoltaic cells have attracted huge attention in the past decades.<sup>[1-18]</sup> In the ongoing search for non-fullerene acceptors special attention has been paid to small molecule acceptors.<sup>[19-30]</sup> Compared to one-dimensional (1D) analogues, spatially extended acceptors have attracted much more scientific interest because of

their unique advantages, specifically: The strong self-aggregation propensity of acceptors<sup>[31]</sup> might be prevented by such arrangement, e.g. perylenediimide substituted spiro-bifluorene, thiophene or triphenylamine,<sup>[32-34]</sup> which could avoid undesirable large scale phase separation from the donor. Furthermore, isotropic electron transport pathways as exhibited by fullerene derivatives are formed in BHJ OPVs, enhancing the exciton diffusion/separation efficiencies and the PCE of the devices.<sup>[35-36]</sup>

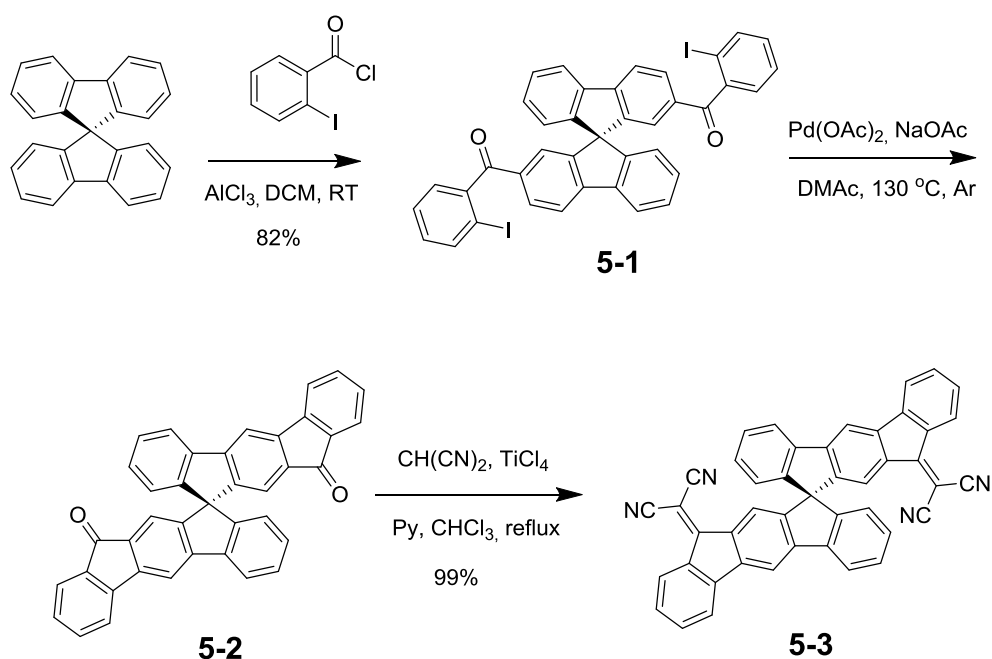
Non-fullerene spatially extended electron-withdrawing materials have shown good performance in OPVs including diketopyrrolopyrrole,<sup>[37]</sup> benzothiadiazole,<sup>[38]</sup> perylenediimide,<sup>[32-34][35, 39]</sup> naphthalene diimide and bifluorenylidene derivatives used as acceptors.<sup>[40-42]</sup> However, to our knowledge, there have been no reports on dicyanovinylene-substituted acceptors based on spiro-fluorene for OPVs, even though dicyanovinylene derivatives have already proven their potential as n-type organic semiconductors.<sup>[43-46]</sup>

In this chapter, we describe the synthesis and characterization of a novel small-molecule acceptor 2,2'-(12H, 12'H-10, 10'-spirobi[indeno[2,1-b]fluorene]-12,12'-diylidene) dimalononitrile (**5-3**) (Scheme 1). We also demonstrate its potential as a non-fullerene electron acceptor in BHJ solar cells. Using a simple spin-coating fabrication technique, with polythieno[3,4-b]-thiophene-co-benzodithiophene (PTB7)<sup>[47]</sup> as electron donor, the best device efficiency was obtained when processed from tetrachloroethane, while further solvent additives like diiodooctane did not improve the performance further.

## V.2 Synthesis and characterization

The synthetic route towards 2,2'-(12H,12'H-10,10'-spirobi[indeno [2,1-b]fluorene]-12,12'-diylidene)dimalononitrile (**5-3**) is shown in Scheme V-1. 9,9-Spiro-bifluorene was acylated by 2-iodobenzoyl chloride to yield 9,9'-spirobi[fluorene]-2,2'-diylbis((2-iodophenyl)methadone) (**5-1**) in 82%. Unfortunately, the envisaged tetra-((2-iodophenyl)methadone) substituted compound was not observed at all. By altering the reaction conditions, such as using nitrobenzene as solvent, high reaction temperature (140 °C) and prolonging reaction time, the main product is still **5-1**.

When the reaction time was extended to 72 hours, and tetrachloroethane was used as solvent in 100 °C reaction condition, tri- rather than tetra-((2-iodophenyl)methadone) substituted product could be obtained together with the main product **5-1**. This is mainly due to the low reaction activity of the spiro-bifluorene after acylation. Then, the intermediate compound 12H,12'H-10,10'-spirobi[indeno[2,1-b]fluorene]-12,12'-dione (**5-2**) was synthesized by a cyclization reaction using palladium acetate as catalyst and sodium acetate as base. Furthermore, we also approved that there was no reaction between **5-2** and 2-iodobenzoyl chloride at room temperature in tetrachloroethane with aluminum trichloride as catalyst. Finally, the target product **5-3** was obtained in 99% yield by Knoevenagel condensation of **5-2** with the Lehnert reagent<sup>[48-49]</sup> (TiCl<sub>4</sub>, malononitrile, pyridine). We have discovered that reaction yield of the last step is strongly depending on the amount of TiCl<sub>4</sub> and malononitrile adding. In this case, the same amount of reactant and reagent were added every 4 hours, until there was no **5-2** left, resulting in such high reaction yield.



**Scheme V-1.** Synthetic route towards **5-3**.

To assign the positions of protons, 2D NMR studies were performed by ..... (Max Planck Institute for Polymer Research, Mainz). Firstly, H-NMR spectra were obtained for both compounds **5-2** and **5-3**. As we can see from Figure V-1, switching from carbonyls to dicyanovinylene units leads to an impressive deshielding

effect for the hydrogen atoms in their  $\beta$  positions. That can be explained by the stronger electron-withdrawing strength of dicyanovinylene vs carbonyl. Secondly, H-C HMBC spectrum of **5-3** was implemented in order to detect hydrogens, which were closed to the spiro carbon. Consequently, two cross-peaks were observed for the spiro carbon atom corresponding to three-bond correlations with  $H_F$  (7.69 ppm) and  $H_J$  (6.85 ppm). Obviously, the other single peak ascribe to  $H_E$ . Furthermore, the other important information was obtained by H-H NOESY, which shows the chemical shift of 7.72 ppm belonging to  $H_D$ , since it was correlated with  $H_E$ . Lastly, from the H-H COSY spectrum, the other protons,  $H_A$ ,  $H_B$ ,  $H_C$ ,  $H_G$ ,  $H_H$  and  $H_I$  can be easily assigned.

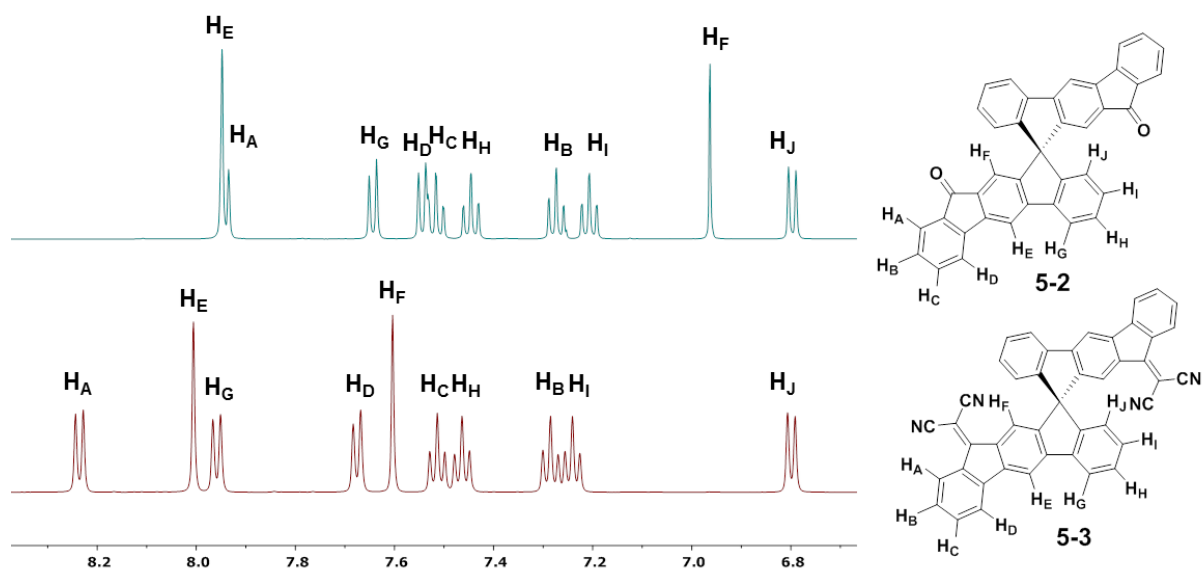


**Figure V-1.** Aromatic region of the <sup>1</sup>H-NMR spectra of **5-2** (top) and **5-3** (bottom).

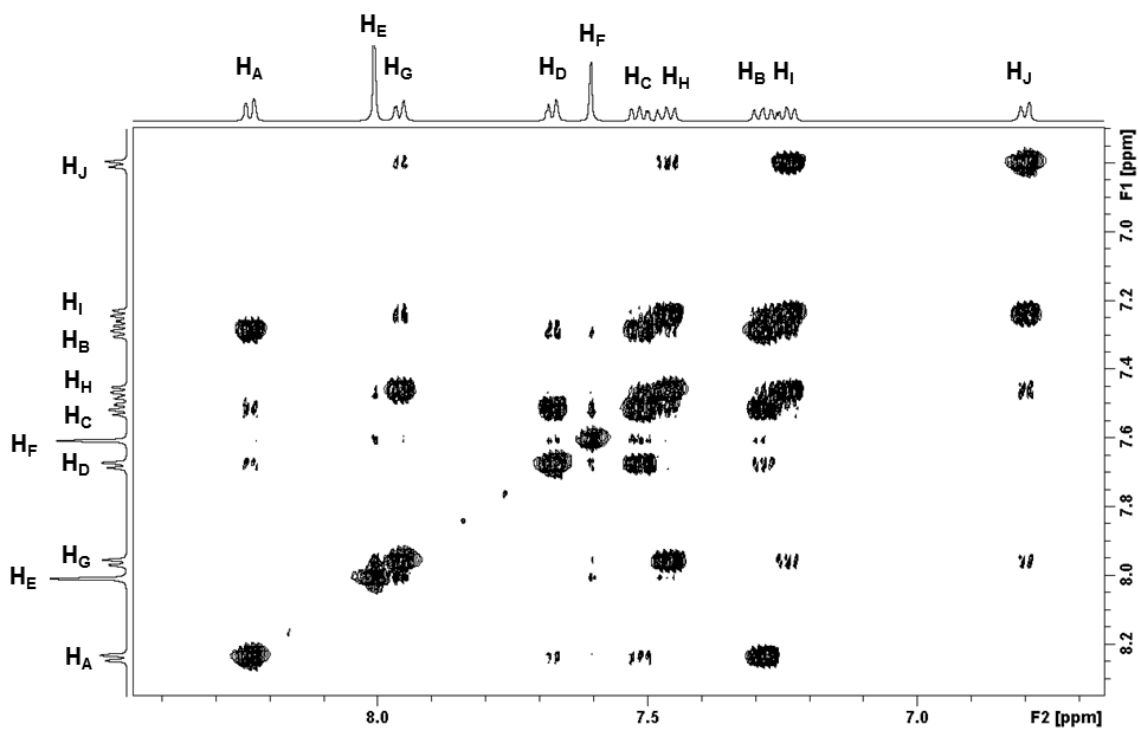


Figure V-2. Aromatic region of H-H COSY spectrum of 5-3.

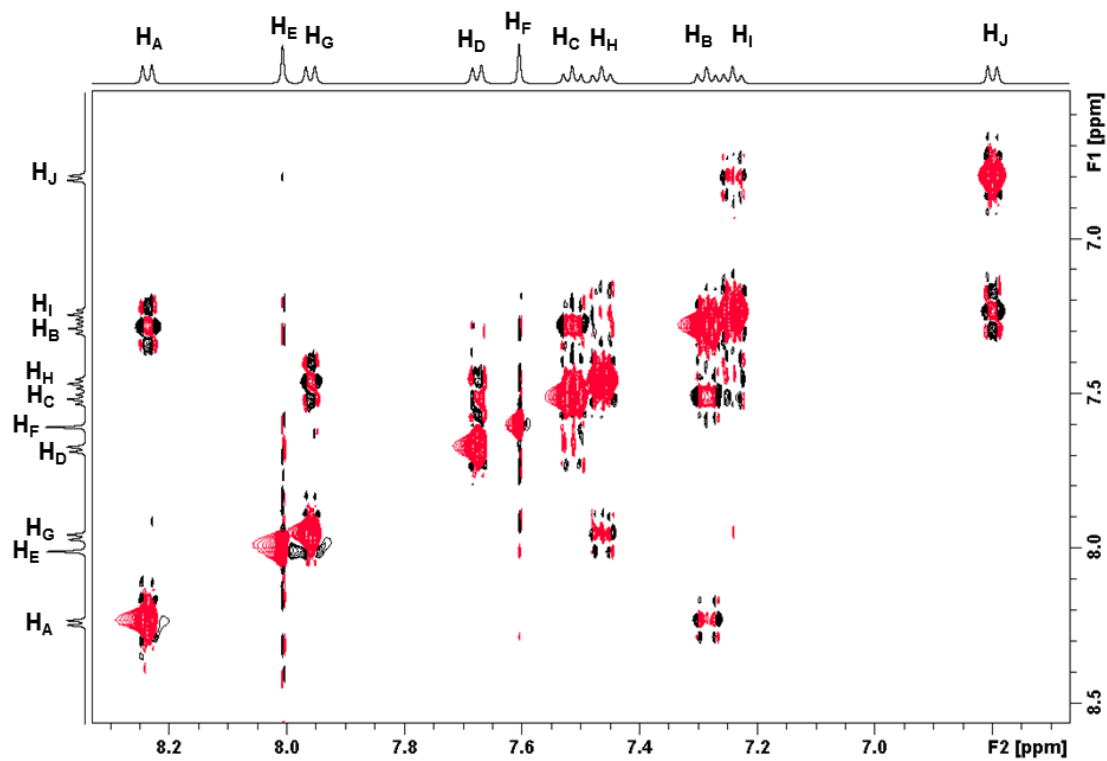
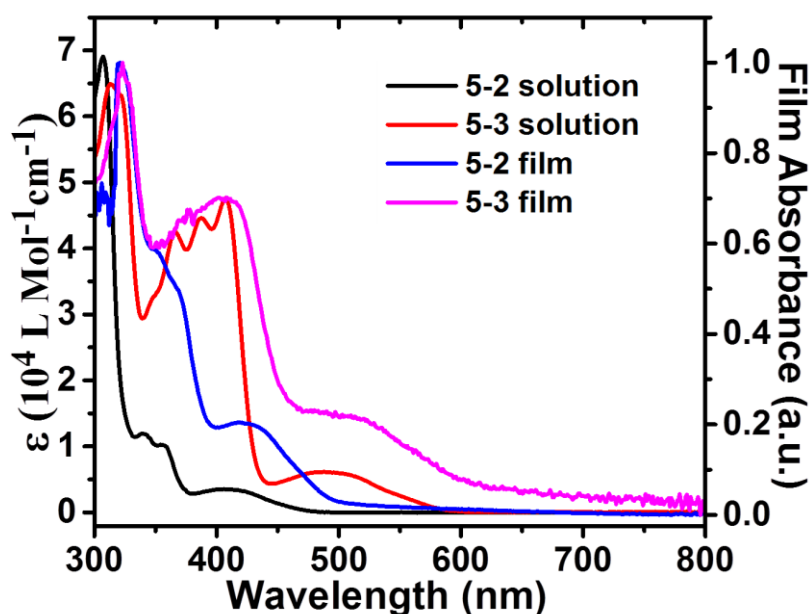


Figure V-3. Aromatic region of H-H NOESY spectrum of 5-3.

### V.3 Photophysical, electrochemical, and thermal properties

Figure V-4 shows the absorption spectra of **5-2** and **5-3** in dichloromethane solution and as thin solid film. The absorption bands of **5-2** and **5-3** in the thin film spectra are only slightly red-shifted compared to those in solution. This is different from the previously reported star-shaped materials, whose absorption bands are significantly red-shifted in solid state, which might be due to the different electron donating and electron withdrawing groups (push-pull effect). The optical gap ( $E_g$ ) estimated from the absorption edge of the solution spectrum is 2.56 eV for **5-2** and 2.08 eV for **5-3**, respectively.



**Figure V-4.** UV-vis absorption spectra of **5-2** and **5-3** in dichloromethane solution and in thin film.

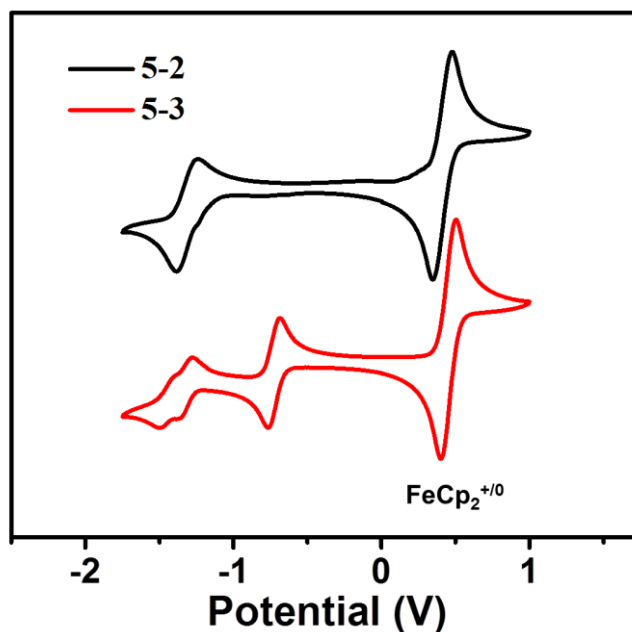


**Figure V-5.** Cyclic voltammograms of **5-2** and **5-3** in dichloromethane/0.1 M  $\text{Bu}_4\text{NPF}_6$  at  $100 \text{ mV s}^{-1}$ .

The electrochemical properties of **5-2** and **5-3** were investigated by cyclic voltammetry (CV) in dichloromethane solution with 0.1 M  $\text{Bu}_4\text{NPF}_6$  as supporting electrolyte. As shown in Figure V-5, both **5-2** and **5-3** exhibit reversible reduction waves. No oxidation waves could be observed in the measured potential range. The half-wave potential of **5-2** is -1.29 V. Upon dicyanovinylene functionalization, the reduction potentials of **5-3** shift to more positive values with the  $E_{1/2}$  potentials at -0.72, -1.31 and -1.44 V, respectively. The overlapping second and third reduction waves of **5-3** with a lower associated current are similar to those of dicyanovinylene-functionalized(bis)indenofluorenes.<sup>[43]</sup> The LUMO energy level of **5-2** and **5-3** estimated from the equation  $E_{\text{LUMO}} = - [E_{\text{red}1/2} - E_{\text{Fc}1/2} + 4.8] \text{ eV}$  are -3.09 eV and -3.63 eV, respectively. The strong electron-withdrawing character of the dicyanovinylene causes a low LUMO level of **5-3**, which guarantees sufficient driving force for exciton dissociation in OPV devices. The HOMO energy of **5-2** and **5-3** are virtually identical to the value of -5.80 eV, calculated from the optical gap according to the equation  $\text{HOMO} = \text{LUMO} - E_g$ .

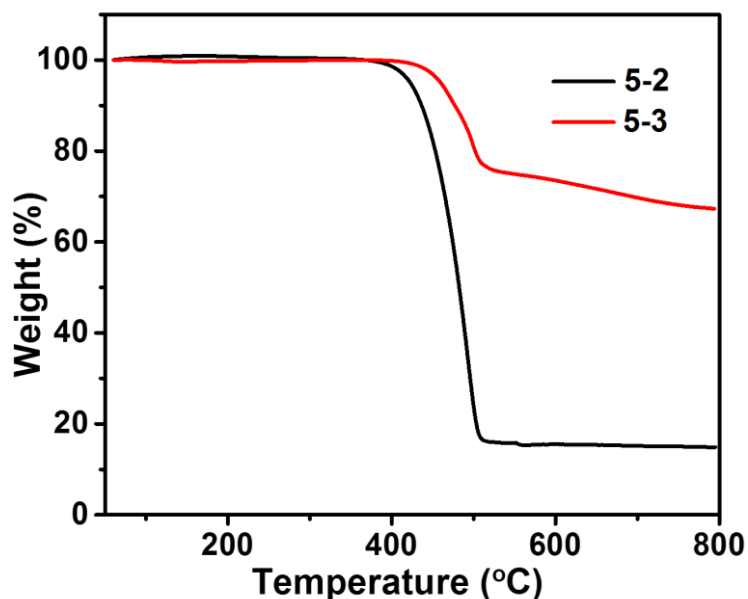


**Figure V-6.** TGA curves of **5-2** and **5-3**.

As shown in Figure V-6, thermogravimetric analysis (TGA) of **5-2** and **5-3** revealed excellent thermal stability, with 5% weight loss occurring at 423 °C and 460 °C, respectively.

## V.4 Crystal structure analysis

Single crystals of the new compounds **5-2** and **5-3** were grown by slow evaporation of the solvent mixture dichloromethane/hexane, and pure dichloromethane, respectively. In Figure V-7, the crystal structure determined by X-ray diffraction is presented, which was done by ..... (Johannes Gutenberg-University, Mainz). The functionalized 9,9-spiro-bifluorene consists of two identical fluorene  $\pi$ -systems, which are perpendicular to each other via a common  $sp^3$ -hybridized carbon atom. Crystal packing of the two molecules is dominated by  $\pi$ - $\pi$  stacking interactions. The  $\pi$ -stacking of **5-2** obviously extends into three dimensions in the single crystal, as it can clearly be seen from the packing structure (Figure V-7a). Three  $\pi$ -stacking axes are almost perpendicular to each other. This is another example of an organic semiconductor that can adopt a 2D  $\pi$ -stacking. In case of the acceptor **5-3**  $\pi$ -stacking with interplanar distances of *ca.* 3.48 and 3.40 Å along the *a* axis and *b* axis (Figure V-7b) was observed. Therefore, the packing

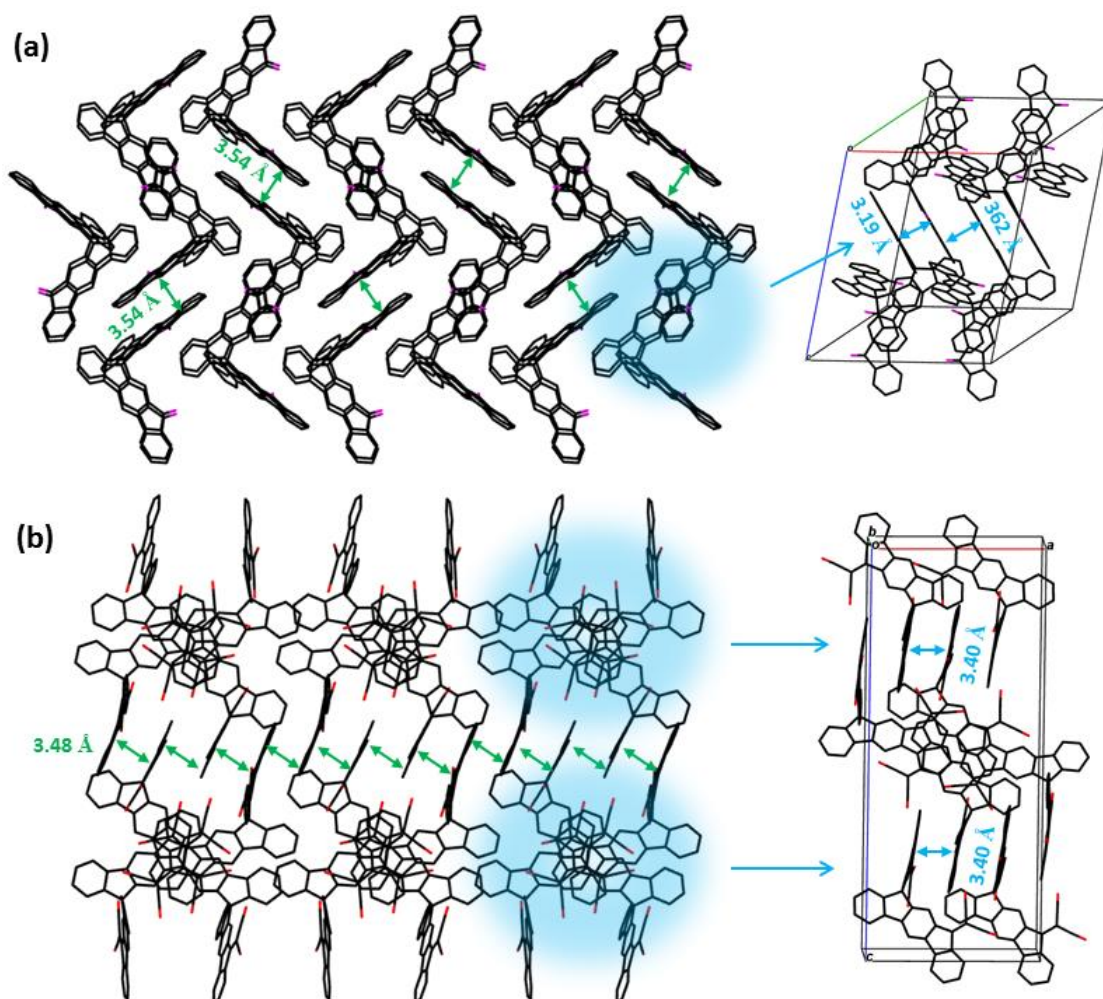


**Figure V-7.** Crystal packing diagrams of **5-2** (a) and **5-3** (b) projected along a axis. C, black; O, purple; N, red.

geometry of the two compounds indicates the possibility of  $\pi$ - $\pi$  interaction, implying that isotropic electron transport pathways as in fullerene derivatives could potentially be formed in donor-acceptor BHJ solar cells.

## V.5 OPV properties

To demonstrate the potential application of **5-3** as acceptor, the photovoltaic device fabrication and measurement were done by ..... (Max Planck Institute for Polymer Research, Mainz). It was blended with PTB7 as electron donor polymer, whose absorption band is more red-shifted than that of P3HT and partially complementary to the absorption of **5-3**. BHJ OPV cells of the structure

ITO/PEDOT:PSS/PTB7:5-3/Ca/Al were prepared. In addition, the effects of varying processing solvents and blend composition were investigated. Table V-1 summarizes the obtained open-circuit voltage ( $V_{oc}$ ), short-circuit current density ( $J_{sc}$ ), fill factor (FF), and PCE of the devices.

**Table V-1.** Photovoltaic parameters of the solar cell devices obtained under AM1.5G-like conditions at 0.7 suns illumination intensity.

Blend ratio(A/D)	solvent	$V_{oc}$ [V]	$J_{sc}$ [mA/cm <sup>2</sup> ]	FF [%]	PCE [%]
1:2	TCE	0.87	1.13	0.49	0.64
1:1	TCE	0.89	1.41	0.48	0.80
1:1	TCE/DCB	0.89	0.22	0.19	0.05
1:1	DCB	0.09	0.10	0.09	0.01
1:1	TCE/3%DIO	0.42	0.03	0.20	0.00

TCE: tetrachloroethane    DCB: dichlorobenzene

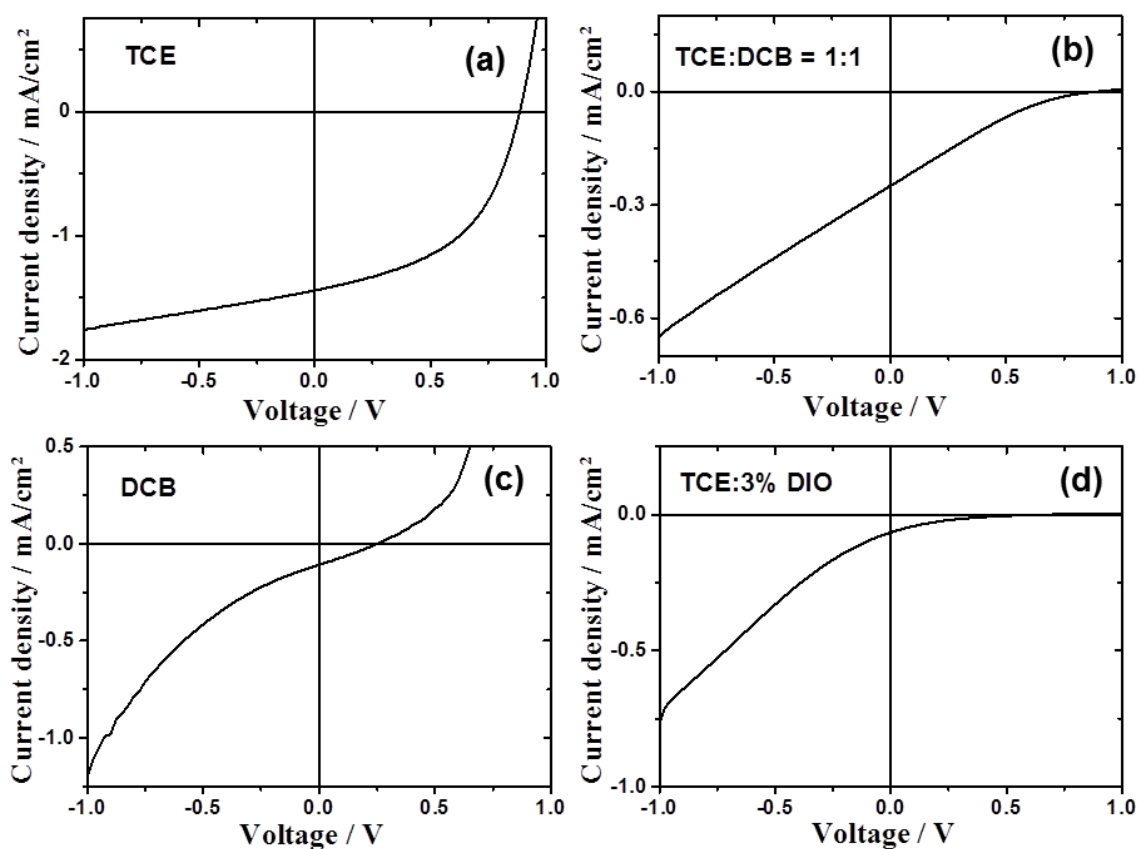


**Figure V-8.** Current density-voltage (J-V) curves of the OPVs processed by different solvents: (a) tetrachloroethane; (b) tetrachloroethane/DCB; (c) DCB; (d) tetrachloroethane/3% DIO.

The device prepared from tetrachloroethane with a donor-acceptor weight ratio of 1:2 exhibited an open-circuit voltage of 0.87 V, a short-circuit current density of 1.13 mA cm<sup>-2</sup>, a fill factor of 0.49, and a power conversion efficiency of 0.64% (Figure V-8a). Encouragingly, the blend at a donor-acceptor weight ratio of 1:1 demonstrated an increased PCE of up to 0.80% with a  $V_{oc}$ ,  $J_{sc}$  and FF of 0.89 V, 1.41 mA cm<sup>-2</sup> and 0.48, respectively. We note, that tetrachloroethane is a rather uncommon solvent in photovoltaic device preparation, however, TCE is also a good solvent for the acceptors used in the present study. AFM height images show a homogeneous surface structure of the blend with demixing on the length scale of exciton diffusion, which ensures efficient exciton quenching and dissociation (Figure V-9a). We have also tried further device optimization including the use of solvent additives. In fact, a small amount of 1,8-diiodooctane (DIO) in a volume ratio of 3% was used as solvent additive to improve the photovoltaic performance in PTB7:PCBM devices.<sup>[47]</sup> However, in the present case the device prepared with the additive exhibited no response to light at all, even though the AFM images indicated a rather uniform surface structure (Figure V-9b). This implies that other processes such as geminate recombination of interfacial charge-transfer (CT) states or insufficient charge carrier transport due to a lack of charge carrier percolation pathways limit the photovoltaic performance. Furthermore, we have also investigated the device performance upon using DCB as solvent or a mixture of DCB and tetrachloroethane. However, in these cases, the AFM images indicated the formation of large crystallites as high RMS values were observed. This is detrimental for device efficiency (Figure V-9c/d) as demonstrated also by the low PCE value. We note that even for the optimized device only a moderate short circuit current and fill factor were obtained compared to devices that use fullerene as acceptor. The latter is a consequence of the pronounced bias dependence of the current density, which does not even saturate at high negative bias, as previously also observed by us for a polymer-PDI blends.<sup>[50]</sup>

To better understand the origin of the former, that is, the moderate short circuit current of the PTB7:5-3 blends spun from C<sub>2</sub>D<sub>2</sub>Cl<sub>4</sub>, transient absorption (TA) spectroscopy was performed on the picosecond to nanosecond timescale. This experiment was carried out by ..... (Max Planck Institute for Polymer Research, Mainz). The transient absorption spectra shown in Figure V-10a) are dominated by a positive feature in the spectral region from 540 to 830 nm peaking at 685 nm, which

we assigned to a combination of the ground-state bleaching (GSB) of PTB7, as it coincides with the ground state absorption of the polymer and stimulated emission (SE) of PTB7 singlet excitons. The observation of SE points towards inefficient exciton quenching in these blends, in part explaining the lower device performance compared to PTB7:fullerene blends. Figure V-10b) shows the decay dynamics of the GSB at various excitation intensities. Clearly, the signal decay is independent of the excitation intensity pointing towards geminate recombination of charges that do not manage to entirely dissociate into free charges. We note that a substantial fraction of  $> 80\%$  of the initially created excited states decays on the sub-ns timescale and consequently does not contribute to the photocurrent of the device. Thus, we conclude that the devices are limited by both inefficient exciton quenching as well as pronounced geminate recombination of bound charges on the sub-ns timescale.

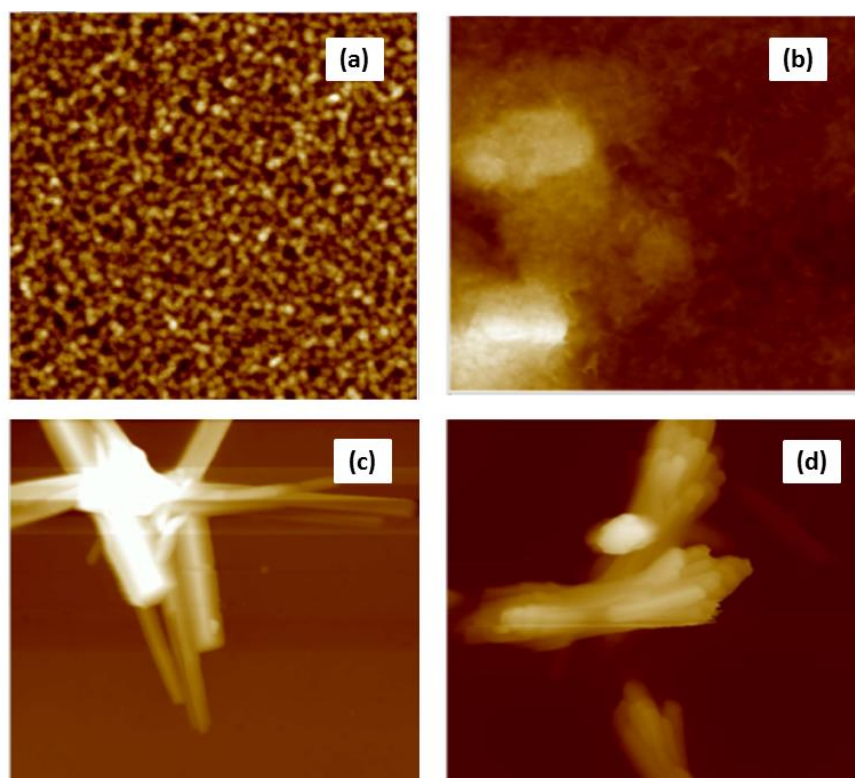


**Figure V-9.** AFM height images of PTB7:5-3 (1:1, w/w) blend processed by different solvents: (a) tetrachloroethane; (b) tetrachloroethane/3% DIO; (c) DCB; (d) tetrachloroethane/DCB.

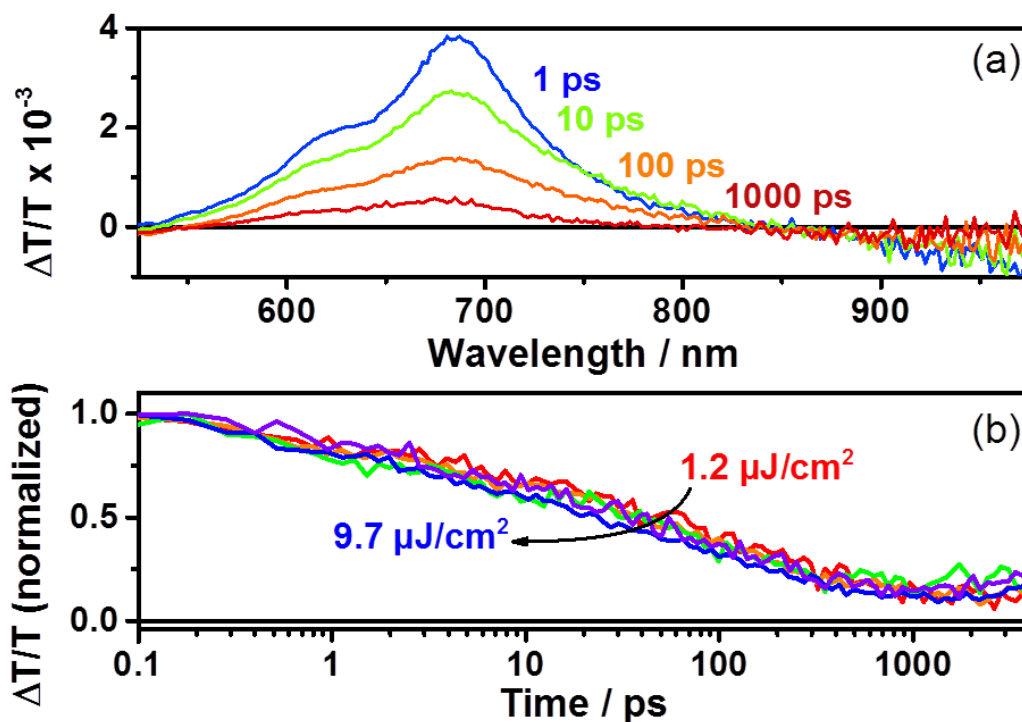


**Figure V-10.** a) ps-ns transient absorption spectra at different time delays after photoexcitation at 650 nm with a fluence of 6.0  $\mu\text{J}/\text{cm}^2$  and b) ground-state bleaching (680-700 nm) dynamics at various excitation densities.

## V.7 Conclusions

In conclusion, a novel cruciform acceptor **5-3** containing spiro-bifluorene as core was synthesized and its thermal, photophysical, electrochemical, crystal, and photovoltaic properties were fully investigated. As revealed by single-crystal analysis, the new compound presents the possibility of isotropic charge transport, which is similar to the situation in fullerene derivatives. The solar cells based on PTB7:**5-3** processed from tetrachloroethane yields the highest PCE of 0.80%. Our results demonstrated for the first time that dicyanovinylene substituted **5-3** could be served as nonfullerene acceptors. However, we also observed that device performance is limited by incomplete exciton quenching and fast geminate recombination on the sub-ns timescale. Further experiments are required to determine whether the bias dependence of the photocurrent is caused by field-dependent charge generation or limited by a low charge carrier mobility leading to a competition of charge extraction and non-geminate recombination or a combination of both processes. Finally, future

work will aim towards new acceptor structures to improve charge separation and to overcome the limits set by geminate recombination. In this chapter, we tried different reaction conditions to synthesize tetra-((2-iodophenyl)methadone) substituted spiro-fluorene, aiming for symmetric acceptors. However, the Friedel-Crafts reaction cannot occur further after the introduction of two electron-withdrawing benzoyl units, caused by low reactivity. Therefore, another reaction route towards a novel cruciform electron-deficient molecule was designed, which will be presented in the next chapter.

## V.8 References

- [1] R. Fitzner, C. Elschner, M. Weil, C. Urich, C. Körner, M. Riede, K. Leo, M. Pfeiffer, E. Reinold, E. Mena-Osteritz, P. Bäuerle, *Adv. Mater.* **2012**, *24*, 675-680.
- [2] A. Mishra, D. Popovic, A. Vogt, H. Kast, T. Leitner, K. Walzer, M. Pfeiffer, E. Mena-Osteritz, P. Bäuerle, *Adv. Mater.* **2014**, *26*, 7217-7223.
- [3] R. Fitzner, E. Reinold, A. Mishra, E. Mena-Osteritz, H. Ziehlke, C. Körner, K. Leo, M. Riede, M. Weil, O. Tsaryova, A. Weiß, C. Urich, M. Pfeiffer, P. Bäuerle, *Adv. Funct. Mater.* **2011**, *21*, 897-910.
- [4] T. R. Andersen, H. F. Dam, M. Hosel, M. Helgesen, J. E. Carle, T. T. Larsen-Olsen, S. A. Gevorgyan, J. W. Andreasen, J. Adams, N. Li, F. Machui, G. D. Spyropoulos, T. Ameri, N. Lemaitre, M. Legros, A. Scheel, D. Gaiser, K. Kreul, S. Berny, O. R. Lozman, S. Nordman, M. Valimaki, M. Vilkmann, R. R. Sondergaard, M. Jorgensen, C. J. Brabec, F. C. Krebs, *Energ. Environ. Sci.* **2014**, *7*, 2925-2933.
- [5] G. D. Spyropoulos, P. Kubis, N. Li, D. Baran, L. Lucera, M. Salvador, T. Ameri, M. M. Voigt, F. C. Krebs, C. J. Brabec, *Energ. Environ. Sci.* **2014**, *7*, 3284-3290.
- [6] A. K. K. Kyaw, D. H. Wang, V. Gupta, J. Zhang, S. Chand, G. C. Bazan, A. J. Heeger, *Adv. Mater.* **2013**, *25*, 2397-2402.
- [7] J. Zhou, X. Wan, Y. Liu, Y. Zuo, Z. Li, G. He, G. Long, W. Ni, C. Li, X. Su, Y. Chen, *J. Am. Chem. Soc.* **2012**, *134*, 16345-16351.

- [8] Y. Zhang, X.-D. Dang, C. Kim, T.-Q. Nguyen, *Adv. Energy Mater.* **2011**, *1*, 610-617.
- [9] K. R. Graham, C. Cabanetos, J. P. Jahnke, M. N. Idso, A. El Labban, G. O. Ngongang Ndjawa, T. Heumueller, K. Vandewal, A. Salleo, B. F. Chmelka, A. Amassian, P. M. Beaujuge, M. D. McGehee, *J. Am. Chem. Soc.* **2014**, *136*, 9608-9618.
- [10] J. E. Coughlin, Z. B. Henson, G. C. Welch, G. C. Bazan, *Acc. Chem. Res.* **2013**, *47*, 257-270.
- [11] L. Ye, S. Zhang, L. Huo, M. Zhang, J. Hou, *Acc. Chem. Res.* **2014**, *47*, 1595-1603.
- [12] A. Mishra, P. Bäuerle, *Angew. Chem. Int. Ed.* **2012**, *51*, 2020-2067.
- [13] C. D. Wessendorf, G. L. Schulz, A. Mishra, P. Kar, I. Ata, M. Weidelenner, M. Urdanpilleta, J. Hanisch, E. Mena-Osteritz, M. Lindén, E. Ahlswede, P. Bäuerle, *Adv. Energy Mater.* **2014**, *4*, 1400266.
- [14] Z. He, C. Zhong, S. Su, M. Xu, H. Wu, Y. Cao, *Nat. Photonics* **2012**, *6*, 593-597.
- [15] F. G. Brunetti, R. Kumar, F. Wudl, *J. Mater. Chem.* **2010**, *20*, 2934-2948.
- [16] R. B. Ross, C. M. Cardona, D. M. Guldi, S. G. Sankaranarayanan, M. O. Reese, N. Kopidakis, J. Peet, B. Walker, G. C. Bazan, E. Van Keuren, B. C. Holloway, M. Drees, *Nat. Mater.* **2009**, *8*, 208-212.
- [17] G. Zhao, Y. He, Y. Li, *Adv. Mater.* **2010**, *22*, 4355-4358.
- [18] Y. He, Y. Li, *Phys. Chem. Chem. Phys.* **2011**, *13*, 1970-1983.
- [19] L. Chen, L. Huang, D. Yang, S. Ma, X. Zhou, J. Zhang, G. Tu, C. Li, *J. Mater. Chem. A* **2014**, *2*, 2657-2662.
- [20] Y. Zhou, L. Ding, K. Shi, Y.-Z. Dai, N. Ai, J. Wang, J. Pei, *Adv. Mater.* **2012**, *24*, 957-961.
- [21] Y.-Q. Zheng, Y.-Z. Dai, Y. Zhou, J.-Y. Wang, J. Pei, *Chem. Commun.* **2014**, *50*, 1591-1594.
- [22] Y. Zhou, Y.-Z. Dai, Y.-Q. Zheng, X.-Y. Wang, J.-Y. Wang, J. Pei, *Chem. Commun.* **2013**, *49*, 5802-5804.
- [23] Y. Lin, Y. Li, X. Zhan, *Adv. Energy Mater.* **2013**, *3*, 724-728.
- [24] A. Sharenko, D. Gehrig, F. Laquai, T.-Q. Nguyen, *Chem. Mater.* **2014**, *26*, 4109-4118.

- [25] A. Sharenko, C. M. Proctor, T. S. van der Poll, Z. B. Henson, T.-Q. Nguyen, G. C. Bazan, *Adv. Mater.* **2013**, *25*, 4403-4406.
- [26] Y. Lin, Y. Li, X. Zhan, *Chem. Soc. Rev.* **2012**, *41*, 4245-4272.
- [27] P. Sonar, J. P. Fong Lim, K. L. Chan, *Energ. Environ. Sci.* **2011**, *4*, 1558-1574.
- [28] A. a. F. Eftaiha, J.-P. Sun, I. G. Hill, G. C. Welch, *J. Mater. Chem. A* **2014**, *2*, 1201-1213.
- [29] J. E. Anthony, *Chem. Mater.* **2010**, *23*, 583-590.
- [30] K. Cnops, B. P. Rand, D. Cheyns, B. Verreert, M. A. Empl, P. Heremans, *Nat Commun* **2014**, *5*.
- [31] V. Kamm, G. Battagliarin, I. A. Howard, W. Pisula, A. Mavrinskiy, C. Li, K. Müllen, F. Laquai, *Adv. Energy Mater.* **2011**, *1*, 297-302.
- [32] X. Zhang, Z. Lu, L. Ye, C. Zhan, J. Hou, S. Zhang, B. Jiang, Y. Zhao, J. Huang, S. Zhang, Y. Liu, Q. Shi, Y. Liu, J. Yao, *Adv. Mater.* **2013**, *25*, 5791-5797.
- [33] Q. Yan, Y. Zhou, Y.-Q. Zheng, J. Pei, D. Zhao, *Chem. Sci.* **2013**, *4*, 4389-4394.
- [34] Y. Lin, Y. Wang, J. Wang, J. Hou, Y. Li, D. Zhu, X. Zhan, *Adv. Mater.* **2014**, *26*, 5137-5142.
- [35] Y. Ie, T. Sakurai, S. Jinnai, M. Karakawa, K. Okuda, S. Mori, Y. Aso, *Chem. Commun.* **2013**, *49*, 8386-8388.
- [36] R. Shivanna, S. Shoaee, S. Dimitrov, S. K. Kandappa, S. Rajaram, J. R. Durrant, K. S. Narayan, *Energ. Environ. Sci.* **2014**, *7*, 435-441.
- [37] Y. Lin, P. Cheng, Y. Li, X. Zhan, *Chem. Commun.* **2012**, *48*, 4773-4775.
- [38] Y. Lin, H. Wang, Y. Li, D. Zhu, X. Zhan, *J. Mater. Chem. A* **2013**, *1*, 14627-14632.
- [39] Y. Zang, C.-Z. Li, C.-C. Chueh, S. T. Williams, W. Jiang, Z.-H. Wang, J.-S. Yu, A. K. Y. Jen, *Adv. Mater.* **2014**, *26*, 5708-5714.
- [40] F. G. Brunetti, X. Gong, M. Tong, A. J. Heeger, F. Wudl, *Angew. Chem. Int. Ed.* **2010**, *49*, 532-536.
- [41] H. U. Kim, J.-H. Kim, H. Suh, J. Kwak, D. Kim, A. C. Grimsdale, S. C. Yoon, D.-H. Hwang, *Chem. Commun.* **2013**, *49*, 10950-10952.
- [42] X. Gong, M. Tong, F. G. Brunetti, J. Seo, Y. Sun, D. Moses, F. Wudl, A. J. Heeger, *Adv. Mater.* **2011**, *23*, 2272-2277.
- [43] H. Usta, C. Risko, Z. Wang, H. Huang, M. K. Delimeroglu, A. Zhukhovitskiy, A. Facchetti, T. J. Marks, *J. Am. Chem. Soc.* **2009**, *131*, 5586-5608.

- [44] X. Shi, J. Chang, C. Chi, *Chem. Commun.* **2013**, *49*, 7135-7137.
- [45] H. Tian, Y. Deng, F. Pan, L. Huang, D. Yan, Y. Geng, F. Wang, *J. Mater. Chem.* **2010**, *20*, 7998-8004.
- [46] Q. Wu, S. Ren, M. Wang, X. Qiao, H. Li, X. Gao, X. Yang, D. Zhu, *Adv. Funct. Mater.* **2013**, *23*, 2277-2284.
- [47] Y. Liang, Z. Xu, J. Xia, S.-T. Tsai, Y. Wu, G. Li, C. Ray, L. Yu, *Adv. Mater.* **2010**, *22*, E135-E138.
- [48] W. Lehnert, *Tetrahedron Lett.* **1970**, *11*, 4723-4724.
- [49] W. Lehnert, *Synthesis* **1974**, *1974*, 667-669.
- [50] D. W. Gehrig, S. Roland, I. A. Howard, V. Kamm, H. Mangold, D. Neher, F. Laquai, *J. Phys. Chem. C* **2014**, *118*, 20077-20085.



# Chapter VI. Novel Cruciform Electron-Deficient Molecule with Dicyanovinylene Substitution

In this chapter, a novel electron-deficient cruciform acceptor embedding dicyanovinylene functionality was designed and synthesized, and its optical and electrochemical properties were characterized. It exhibits optical band gap of 2.02 eV and low LUMO energy of  $-3.60$  eV, representing a promising small molecule for n-type electronic materials. Single crystal analysis indicates such molecule can achieve 2D isotropic charge transfer in the solid state.

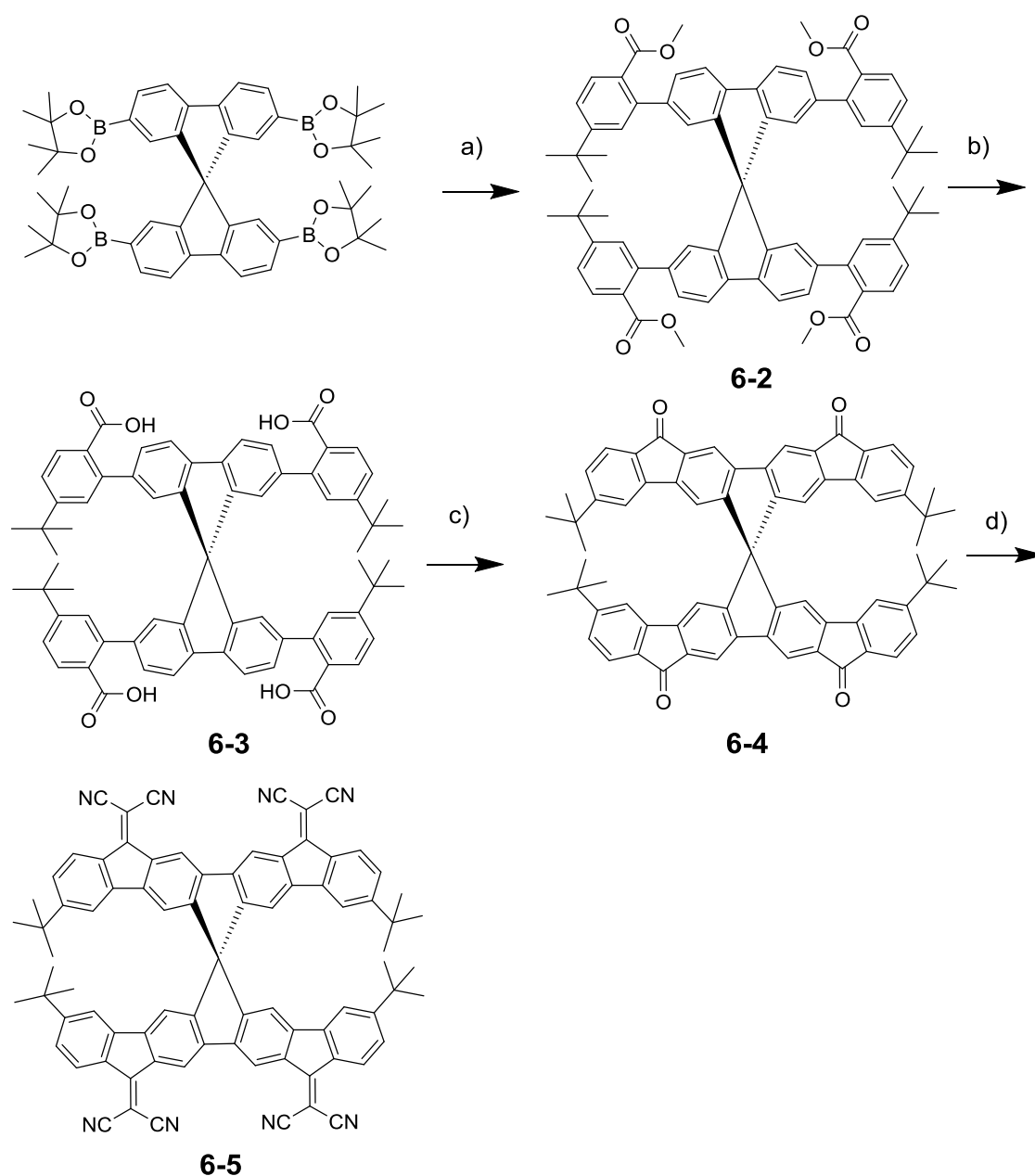
## VI.1 Introduction

The development of three-dimensional (3D) charge transporting materials is a vital subject for the achievement of high-performance organic devices.<sup>[1-8]</sup> It is believed that there are two efficient methods to facilitate charge transfer, namely, tuning the frontier molecular orbital levels<sup>[9-15]</sup> and manipulating the material packing mode in the solid state.<sup>[16-21]</sup> Nowadays, the former method is much easier to be achieved via introducing functional groups with different electron negativities, whereas the latter technique only limited reports are available. In recent years, some spatially extended p-type molecules, such as **3D-1**<sup>[4]</sup> and **3D-2**<sup>[3]</sup> in Figure VI-1 were constructed, both of which adopt two-dimensional  $\pi$ -stacking in their crystals. This packing mode indeed favors two-dimensional isotropic charge transport.<sup>[22]</sup> However, as far as we know, such kind of n-type materials have not been reported.<sup>[23]</sup>



## VI.2 Synthesis and characterization

The synthetic route to **6-4** and **6-5** is shown in Scheme VI-1. Actually, the original target molecules are without tert-butyl substitutions, which were obtained and have bad solubility, thus they cannot be purified by column chromatography. In Scheme VI-1, the first step of this synthetic approach starts with Suzuki-Miyaura cross-coupling of methyl 2-bromo-4-(tert-butyl)benzoate (**6-1**) and 2,2',7,7'-tetrakis(4,4,5,5-



**Scheme VI-1.** Synthetic route towards **6-4** and **6-5**: a) methyl 2-bromo-4-(tert-butyl)benzoate, Pd(PPh<sub>3</sub>)<sub>4</sub>, K<sub>2</sub>CO<sub>3</sub>, toluene, 110 °C, 74%; b) NaOH aq, ethanol, reflux, 99%; c) First, oxalyl chloride, DMF, DCM; Second, AlCl<sub>3</sub>, DCM, 82%. d) TiCl<sub>4</sub>, CH(CN)<sub>2</sub>, Py, CHCl<sub>3</sub>, reflux, 90%.

tetramethyl-1,3,2-dioxaborolan-2-yl)-9,9'-spirobi[fluorene] to afford high yields (74%) of tetramethyl 2,2',2'',2'''-(9,9'-spirobi[fluorene]-2,2',7,7'-tetrayl)tetrakis(4-(tert-butyl)benzoate) (**6-2**). The hydrolysis of **6-2** followed by acidification lead to the formation of its corresponding spirobi[fluorene]-tetrabenzoic acid **6-3**, which was pure enough and did not need further purification. Initially, we also tried the Suzuki-Miyaura cross-coupling between 2-bromo-4-(tert-butyl)benzoic acid and tetra boronic ester substituted-spiro-fluorene, which was successful. However we could not overcome the purification issue arise from the similar polarity of byproducts and products. Compound **6-3** was converted into its carboxylic acid chloride by reaction with oxalyl chloride and catalytic amount of DMF in dry dichloromethane. Subsequent intramolecular Friedel-Craft acylation with aluminum chloride afforded the desired tetraketone **6-4** in 82% yield. Finally, the target product **6-5** was obtained in 90% yield by the Knoevenagel condensation of **6-4** with the Lehnert reagent (TiCl<sub>4</sub>, malononitrile, pyridine).<sup>[29-30]</sup> Such high reaction yield could be achieved by adding a large amount of malononitrile, which could be washed away later by acetone. (see experimental part). Besides standard characterizations, such as HRMass and NMR for proof of molecules, also their crystal structures could be obtained.

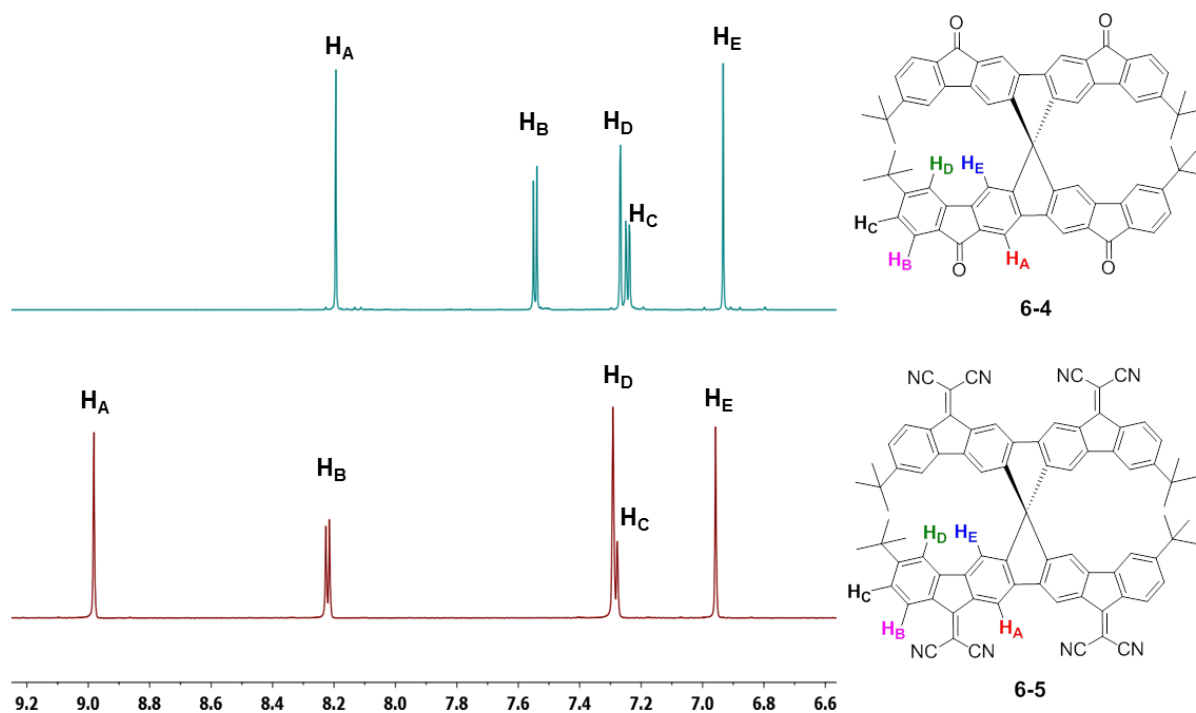


**Figure VI-2.** Aromatic region of the <sup>1</sup>H-NMR spectra of **6-4** (top) and **6-5** (bottom) (C<sub>2</sub>D<sub>2</sub>Cl<sub>4</sub>, 700 MHz).

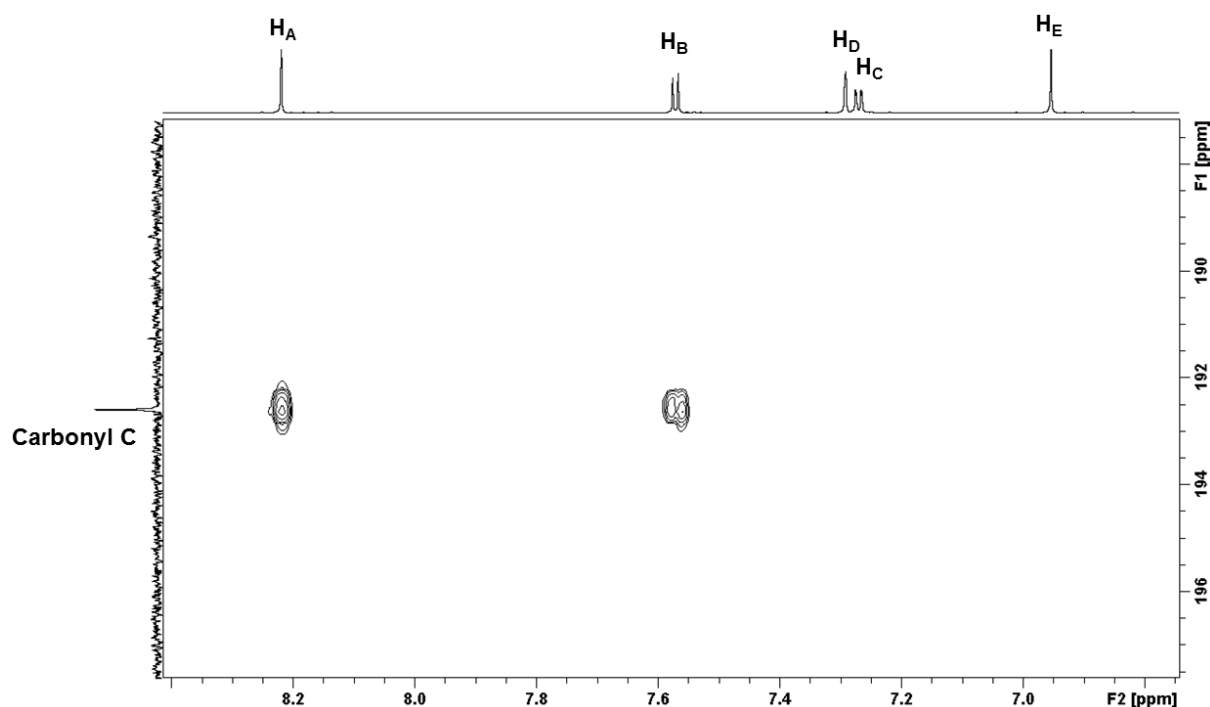


**Figure VI-3.** Portion of the HMBC spectrum of **6-4** ( $C_2D_2Cl_4$ , 850 MHz).

In collaboration with ..... (Max Planck Institute for Polymer Research, Mainz), the compounds **6-4** and **6-5** were also proven by NMR spectroscopy. The  $^1H$ -NMR (Figure VI-2) reveals the remarkable symmetry of both molecules and also evaluates the strength of electron withdrawing moieties. The hydrogen atoms  $H_A$  and  $H_B$  in the  $\beta$  positions of the dicyanovinylene units of **6-5** are in the low magnetic field region, because of the stronger deshielding effect. For molecule **6-4**, HMBC spectrum (Figure VI-3) was performed to investigate correlations between carbonyl carbons and their neighboring hydrogens. Consequently,  $H_A$  and  $H_B$  is assigned to the single peak with the chemical shift of 8.20 ppm and double peaks with the chemical shift of 7.55 ppm, respectively. Switching from carbonyl to dicyanovinylene units leads to a stronger deshielding effect for the hydrogen atoms  $H_A$  and  $H_B$  of **6-5** with the chemical shift of 8.98 ppm and 8.22 ppm, respectively. Nevertheless, the chemical shift of  $H_C$ ,  $H_D$  and  $H_E$  are almost the same for both **6-4** and **6-5**, indicating that the electronic effect arising from electro withdrawing groups, namely carbonyl and dicyanovinylene, is dramatically reduced in these positions. Obviously, the double peak with the chemical shift 7.24 ppm arises from  $H_C$ , as it is correlated with the known proton  $H_B$ . To investigate in detail the specific H/H contacts and assign hydrogen atoms  $H_D$  and  $H_E$  to the exact

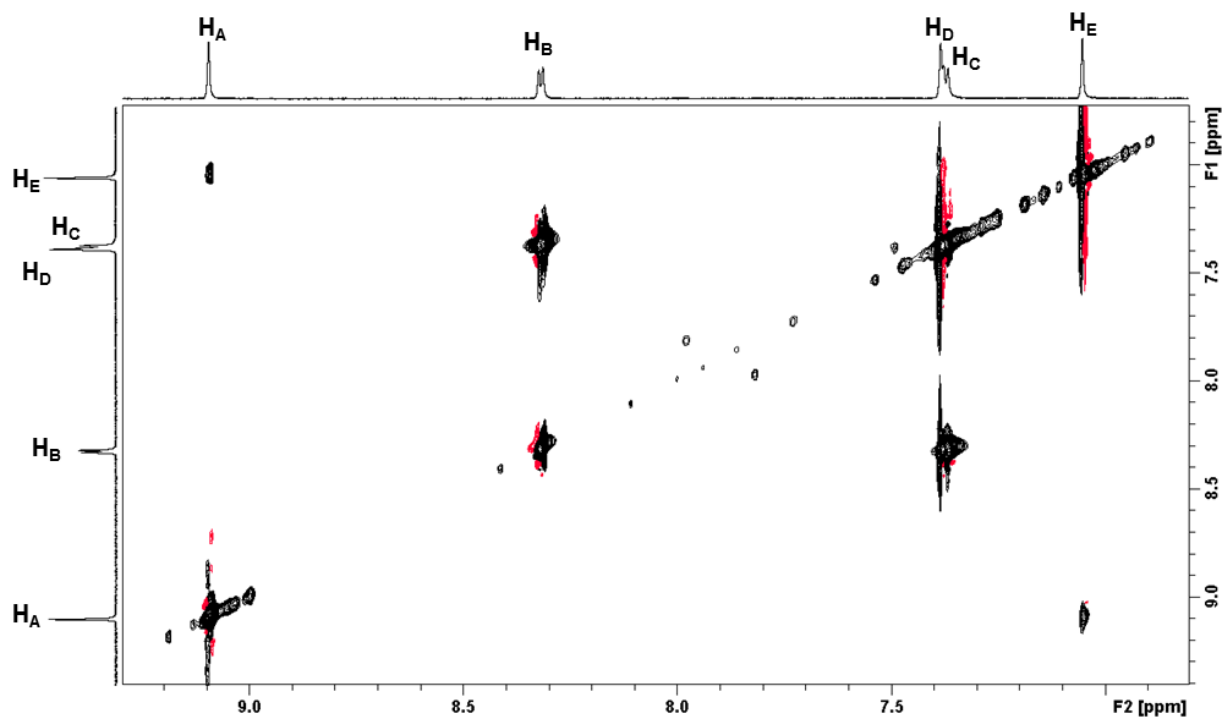


Figure VI-4. Aromatic region of H-H TOCSY spectrum of **6-5** (100 °C, C<sub>2</sub>D<sub>2</sub>Cl<sub>4</sub>, 850 MHz).

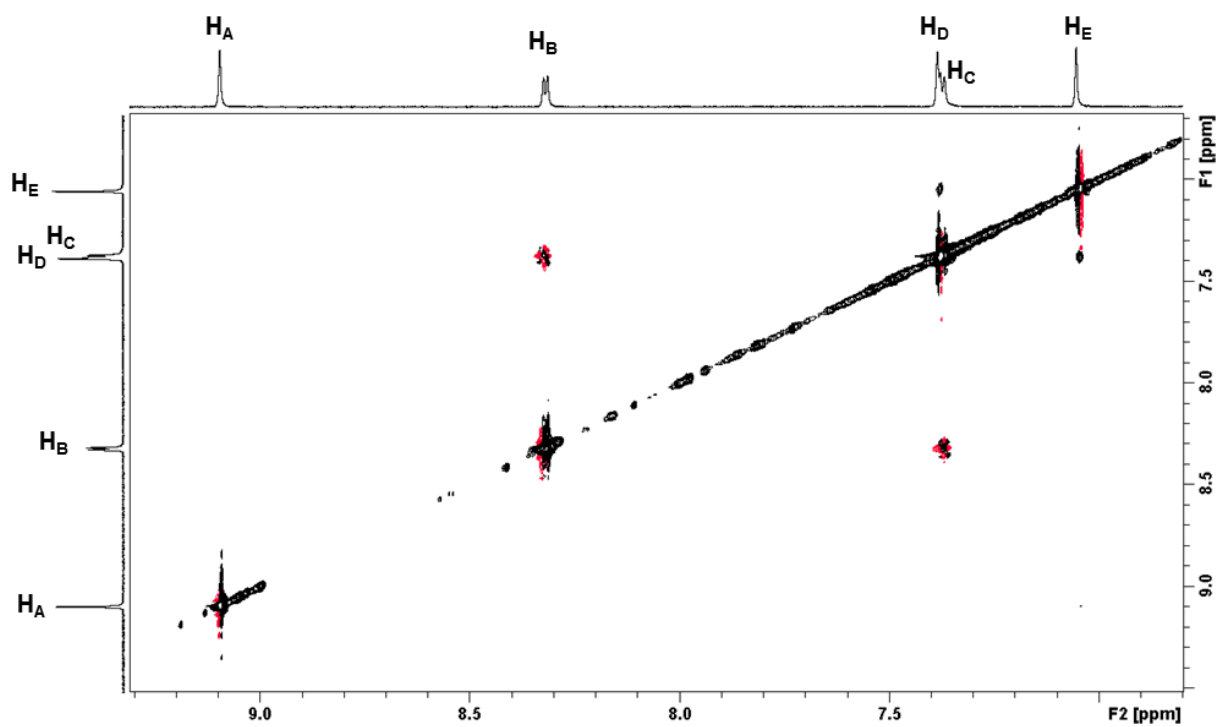
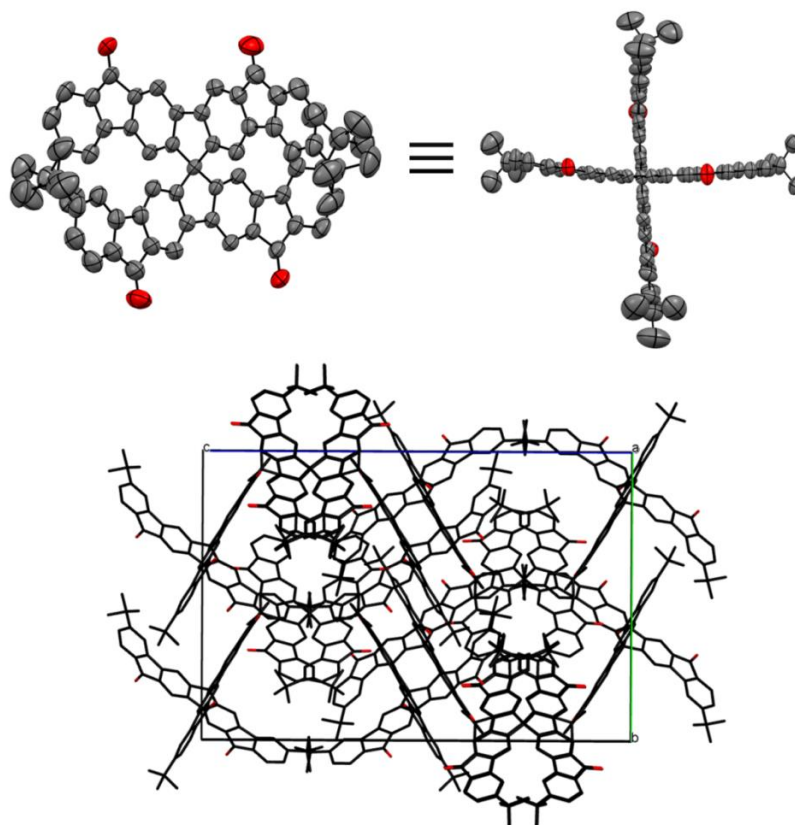


Figure VI-5. Aromatic region of H-H NOESY spectrum of **6-5** (100 °C, C<sub>2</sub>D<sub>2</sub>Cl<sub>4</sub>, 850 MHz).

positions within both molecules, 2D-NMR experiments, such as H-H TOCSY and H-H NOESY, were performed. Herein, molecule **6-5** is taken as an example for the hydrogen assignment purpose. As shown in H-H TOCSY spectrum (Figure VI-4), apart from the expected correlation between the proton  $H_B$  and the proton  $H_C$ , the correlation also happens between the known proton  $H_A$  and the proton  $H_E$ . Therefore, the proton  $H_E$  and  $H_D$  is assigned to the single peak with the chemical shift around 6.96 ppm and 7.28 ppm, respectively. To further support this finding, a H-H NOESY spectrum was recorded (Figure VI-5). In this spectrum, through-space couplings are observed between  $H_D$  and  $H_E$ , as well as  $H_B$  and  $H_C$ , which indicates the protons are close to each other in space correspondingly. Evidently, the single peak (8.99 ppm) is ascribed to  $H_A$ , since there is no through-space coupling signal.

### VI.3 Crystal structure analysis

The solid-state packing structures of **6-4** and **6-5** were studied by crystallographic analysis, which was performed by ..... (Johannes Gutenberg-University, Mainz). Single crystals of both molecules suitable for X-ray diffraction analysis were grown by slow evaporation of the corresponding dichloromethane solutions. Figure VI-6 presents a single crystal structure and the packing pattern of molecule **6-4**. Two  $\pi$ -conjugated bisfluorenone units are connected via a  $sp^3$  carbon, which results in the formation of a cruciform structure. As expected, the  $\pi$ -conjugated bisfluorenone units can form slipped face-to-face  $\pi$  stacking with those of neighboring molecules, leading to a typical  $\pi$ - $\pi$  separation of 3.35 Å (Figure VI-7). Surprisingly, in one molecule, only one bisfluorenone unit is parallel to the other bisfluorenone unit of its neighboring molecule. The other bisfluorenone unit which is unparallel to the neighboring bisfluorenone unit interacts with other two neighboring molecules via Van der Waals forces. As shown in Figure VI-7, there are three types of intermolecular interactions in different directions, namely, C...C (a), C...C (b), and C...O (c), with distances of 3.32 Å, 3.32 Å and 3.16 Å, respectively. By virtue of the  $\pi$ ... $\pi$  interaction and multiple weak noncovalent interactions, compound **6-4** self-assembles into such a special packing structure in the solid state.



**Figure VI-6.** X-ray diffraction structure of **6-4**. Top: single molecule. Bottom: crystal packing viewed along a-axis. Hydrogen atoms are omitted for clarity.

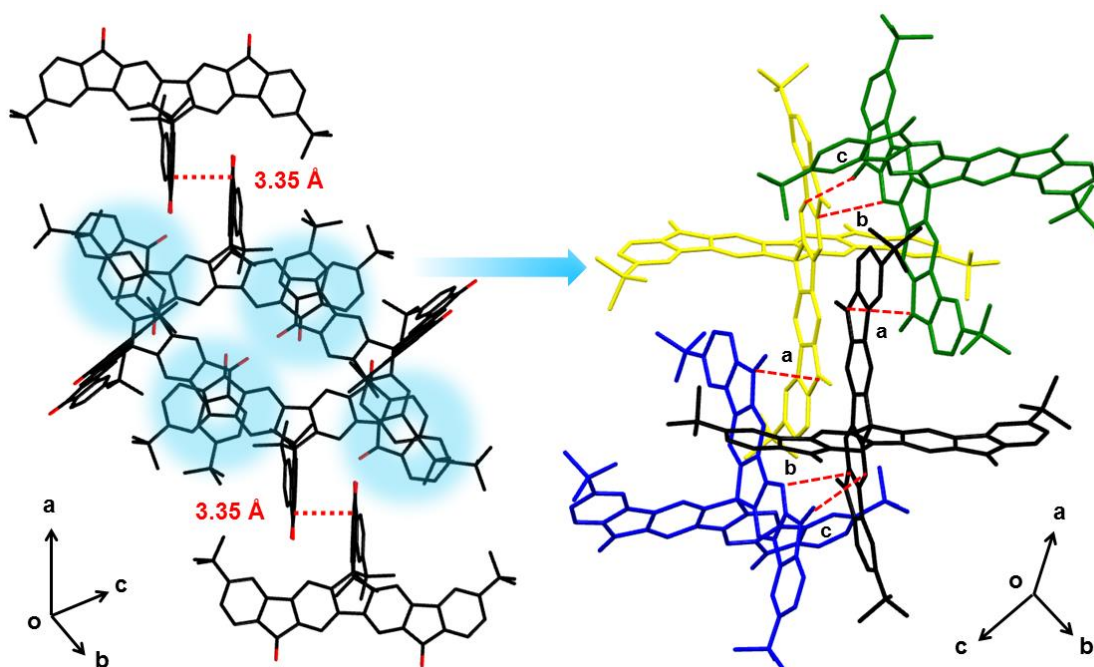


**Figure VI-7.** X-ray diffraction structure of **6-4**. Left: molecular stacking pattern. Right: intermolecular distances: a: 3.32 Å (C...C); b: 3.32 Å (C...C); c: 3.16 Å (C...O). Hydrogen atoms are omitted for clarity.

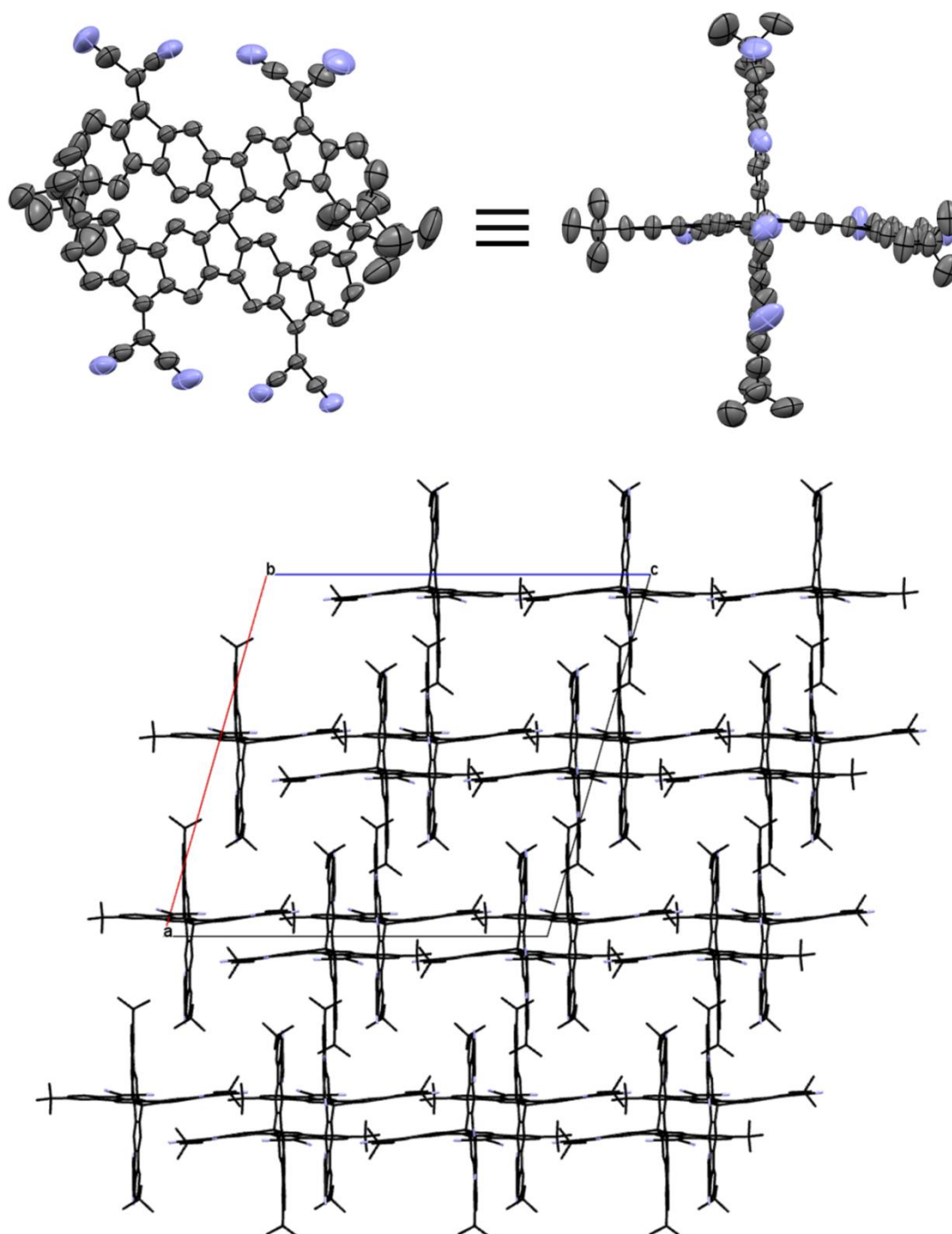


**Figure VI-8.** X-ray diffraction structure of **6-5**. Top: single molecule. Bottom: crystal packing viewed along b-axis. Hydrogen atoms and solvent molecules ( $\text{CH}_2\text{Cl}_2$ ) are omitted for clarity.

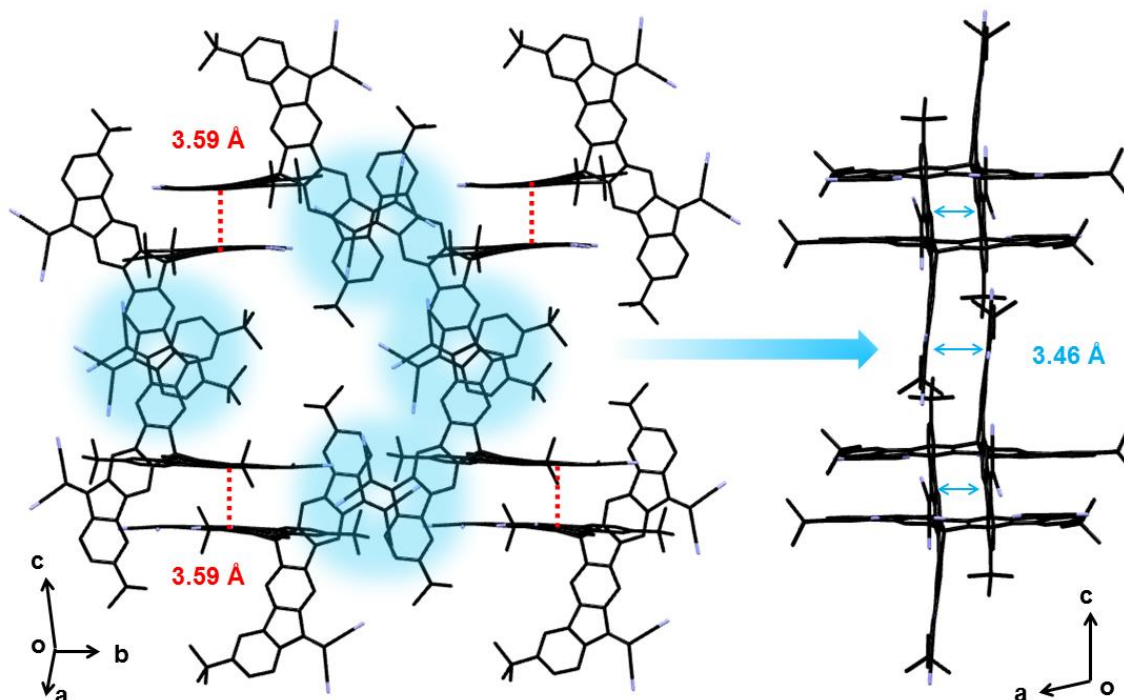


**Figure VI-9.** Molecular stacking patterns of **6-5**. Hydrogen atoms and solvent molecules ( $\text{CH}_2\text{Cl}_2$ ) are omitted for clarity.

In Figure VI-8, **6-5** with cruciform structure shows a 2D  $\pi$ - $\pi$  stacking with two types of packing motifs, arising from the effective parallel of the aromatic rings between neighboring molecules. As shown in Figure VI-9, the two bis-indenofluorene units in one molecule contribute differently to the crystal packing. One bis-indenofluorene unit is involved in a face-to-face  $\pi$ - $\pi$  interaction with neighboring bis-indenofluorene unit, whereas the other bis-indenofluorene unit interacts with other two neighboring indenofluorene units. The interplane distances for these two types of stacking are 3.59 Å and 3.46 Å, respectively. In the single crystal, the two  $\pi$ -stacking axes run in two directions and are perpendicular to each other. To the best of our knowledge, **6-4** and **6-5** are the longest cruciform phenylene oligomers to date that have been characterized by X-ray diffraction. Considering their unique packing structures and the strong intermolecular interactions, **6-4** and **6-5** are expected to show 2D isotropic charge transport and have potential applications for thin-film OFETs. The compound **6-5** with the combination of isotropic electron transport pathways and low LUMO levels (see below) should also be a good candidate for nonfullerene acceptors in donor-acceptor bulk-heterojunction solar cells.

## V.4 Photophysical and electrochemical properties

Figure VI-10 shows the absorption spectra of **6-4** and **6-5** in dichloromethane solution. The absorption band of both molecules in the range of 280 – 400 nm arises from the  $\pi$ - $\pi^*$  transition of the conjugated backbones. The other bands located between 400 and 600 nm can be assigned to the symmetry forbidden  $n$ - $\pi^*$  transition. However, the intensity of  $n$ - $\pi^*$  absorptions are relatively low in comparison to their analogues, which might be caused by the solvent effects. Both of the high-energy absorption and long-wavelength absorptions of **6-5** are redshifted in comparison with those of **6-4**. This mainly is attributed to the decrease of the LUMO levels arising from the stronger electron-withdrawing nature of dicyanovinylene versus carbonyl substituents. The optical gap ( $E_g$ ) estimated from the absorption edge of the solution spectrum is 2.46 eV for **6-4** and 2.02 eV for **6-5**, respectively.

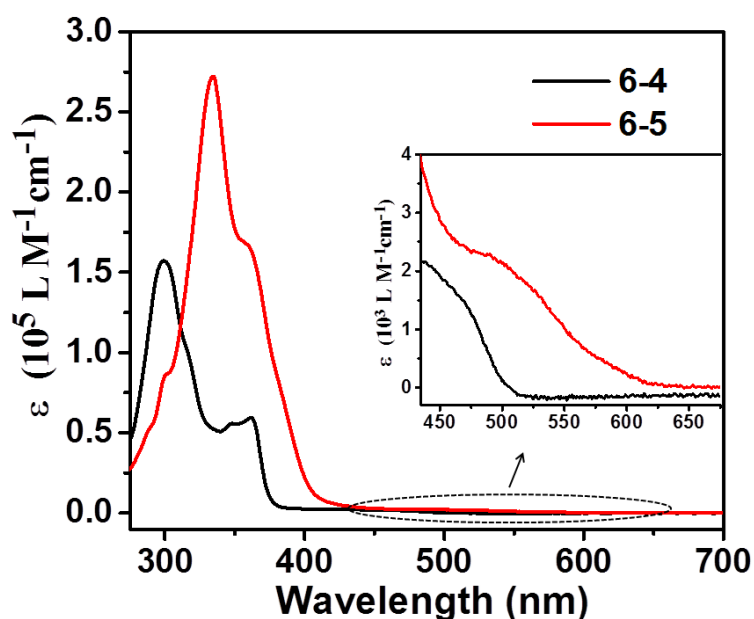


**Figure VI-10.** UV-vis absorption spectra of **6-4** (black line) and **6-5** (red line) in  $\text{CH}_2\text{Cl}_2$  solution. The inset shows the UV-vis spectra in the region 440 - 680 nm ( $n$ - $\pi^*$  transitions).

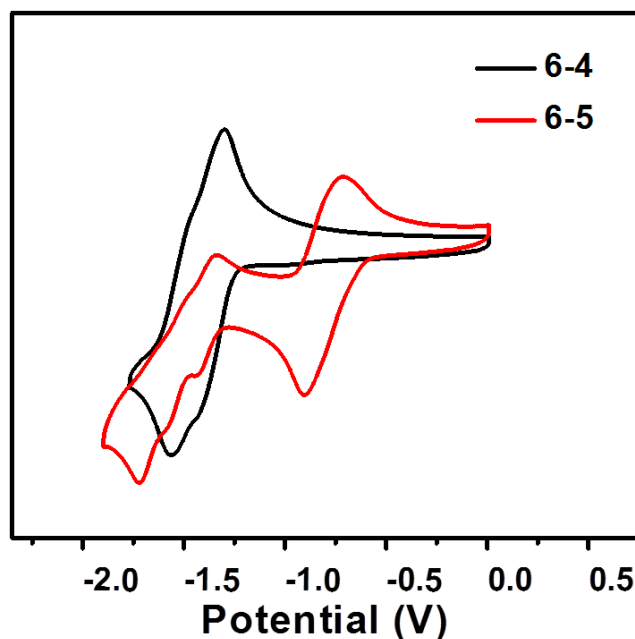


**Figure VI-11.** Cyclic voltammograms of **6-4** and **6-5** in DCM containing 0.1 M  $\text{Bu}_4\text{NPF}_6$  as the supporting electrolyte, Ag as the reference electrode, a glassy carbon as the working electrode, Pt wire as the counter electrode, and a scan rate of 100 mV/s. The potential was externally calibrated against the ferrocene/ferrocenium couple.

The electrochemical properties of **6-4** and **6-5** were investigated by cyclic voltammetry in DCM solutions. As shown in Figure VI-11, **6-4** and **6-5** presented reversible reduction waves with first half-wave potentials -1.36 and -0.81 eV, respectively, while no oxidation waves were observed in the measured potential range. Accordingly, LUMO energy levels were estimated to be -3.05 eV for **6-4** and -3.60 eV for **6-5**. The deeper LUMO energy levels can be attributed to the stronger electron-withdrawing character of the dicyanovinylene groups than for the ketone. The HOMOs energy levels of **6-4** and **6-5** are -5.51 and -5.62 eV, respectively, calculated from their optical gaps according to the equation  $\text{HOMO} = \text{LUMO} - E_g$ .

## VI.5 Density functional theory calculations

To further understand the electronic structures and optical properties of the two acceptors, density functional theory (DFT) calculations were carried out at the B3LYP/6-311G (d, p) level. The electron density distributions are shown in Figure VI-12. Electron cloud densities of their HOMOs are uniformly distributed on the conjugated poly(para-phenylene) backbones, whereas their LUMOs are also

contributed to carbonyl groups for **6-4** and cyanovinylene units for **6-5**. In comparison with **6-4**, **6-5** is a stronger acceptor, since cyano is a stronger electron withdrawing group than carbonyl. The calculated LUMO energy level of **6-5** is -3.45 eV, which is in agreement with the CV results.

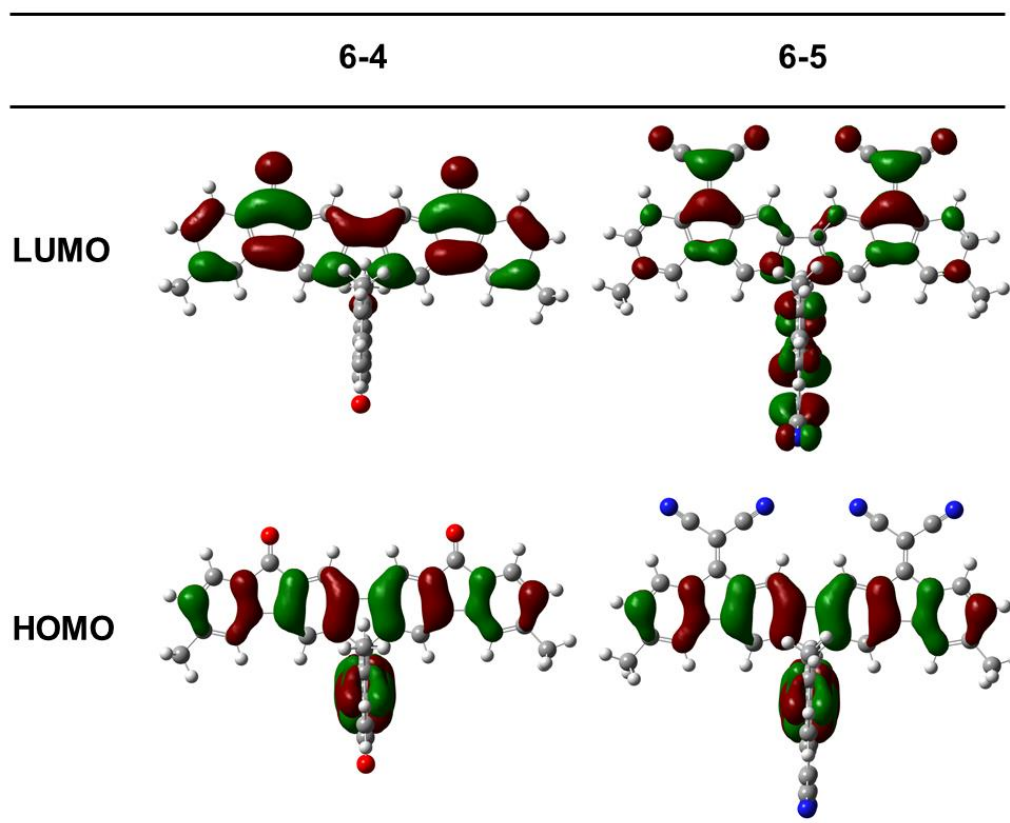


**Figure VI-12.** The electron density distribution on models of **6-4** and **6-5**.

## VI.6 Conclusions

In conclusion, cruciform molecules **6-4** and **6-5** were synthesized and fully characterized. The introduction of tert-butyl groups is essential, since without them the solubility issue could not be overcome. The assignment of protons was elucidated through 2D NMR spectroscopy. Packing mode in crystals of both two molecules might favor the 2D isotropic charge transfer, like orthogonally linked bis-pentacene with hole mobilities of  $0.01 \text{ cm}^2 \text{ V}^{-1} \text{ s}^{-1}$ . Note that this mobility is not strongly dependent on the molecular orientation to substrates due to the unique crystal packing mode (two-directional isotropic face-to-face  $\pi$  stacking).<sup>[3]</sup> The CV

experiment and DFT calculations indicate compound **6-5** can serve as electron acceptor, which is also the first cruciform acceptor, as far as we know. The device fabrication and measurement are currently undergoing. In this chapter, compound **6-4** with ketone functional groups is a key building block, which can also be used to construct spatially extended blue-emitting materials. Details will be shown in next chapter.

## VI.7 References

- [1] A. Wakamiya, H. Nishimura, T. Fukushima, F. Suzuki, A. Saeki, S. Seki, I. Osaka, T. Sasamori, M. Murata, Y. Murata, H. Kaji, *Angew. Chem. Int. Ed.* **2014**, *53*, 5800-5804.
- [2] A. Lv, M. Stolte, F. Würthner, *Angew. Chem. Int. Ed.* **2015**, 10512-10515.
- [3] X. Zhang, X. Jiang, J. Luo, C. Chi, H. Chen, J. Wu, *Chem. Eur. J.* **2010**, *16*, 464-468.
- [4] I. A. Wright, A. L. Kanibolotsky, J. Cameron, T. Tuttle, P. J. Skabara, S. J. Coles, C. T. Howells, S. A. J. Thomson, S. Gambino, I. D. W. Samuel, *Angew. Chem. Int. Ed.* **2012**, *51*, 4562-4567.
- [5] S. Ma, Y. Fu, D. Ni, J. Mao, Z. Xie, G. Tu, *Chem. Commun.* **2012**, *48*, 11847-11849.
- [6] J. Roncali, P. Leriche, A. Cravino, *Adv. Mater.* **2007**, *19*, 2045-2060.
- [7] A. L. Kanibolotsky, I. F. Perepichka, P. J. Skabara, *Chem. Soc. Rev.* **2010**, *39*, 2695-2728.
- [8] S. Roquet, R. de Bettignies, P. Leriche, A. Cravino, J. Roncali, *J. Mater. Chem.* **2006**, *16*, 3040-3045.
- [9] X. Shi, J. Chang, C. Chi, *Chem. Commun.* **2013**, *49*, 7135-7137.
- [10] J. Mei, Y. Diao, A. L. Appleton, L. Fang, Z. Bao, *J. Am. Chem. Soc.* **2013**, *135*, 6724-6746.
- [11] Z. Liang, Q. Tang, R. Mao, D. Liu, J. Xu, Q. Miao, *Adv. Mater.* **2011**, *23*, 5514-5518.
- [12] Z. Liang, Q. Tang, J. Liu, J. Li, F. Yan, Q. Miao, *Chem. Mater.* **2010**, *22*, 6438-6443.

- [13] J. Li, Y. Xiong, Q. Wu, S. Wang, X. Gao, H. Li, *Eur. J. Org. Chem.* **2012**, 2012, 6136-6139.
- [14] J. Yin, H. Qu, K. Zhang, J. Luo, X. Zhang, C. Chi, J. Wu, *Org. Lett.* **2009**, 11, 3028-3031.
- [15] O. K. Kwon, J.-H. Park, S. K. Park, S. Y. Park, *Adv. Energy Mater.* **2015**, 5, 1400929.
- [16] S. H. Etschel, A. R. Waterloo, J. T. Margraf, A. Y. Amin, F. Hampel, C. M. Jager, T. Clark, M. Halik, R. R. Tykwinski, *Chem. Commun.* **2013**, 49, 6725-6727.
- [17] J. E. Anthony, *Angew. Chem. Int. Ed.* **2008**, 47, 452-483.
- [18] R. Fitzner, C. Elschner, M. Weil, C. Uhrich, C. Körner, M. Riede, K. Leo, M. Pfeiffer, E. Reinold, E. Mena-Osteritz, P. Bäuerle, *Adv. Mater.* **2012**, 24, 675-680.
- [19] Y.-F. Lim, Y. Shu, S. R. Parkin, J. E. Anthony, G. G. Malliaras, *J. Mater. Chem.* **2009**, 19, 3049-3056.
- [20] R. K. Hallani, K. J. Thorley, A. K. Hailey, S. R. Parkin, Y.-L. Loo, J. E. Anthony, *J. Mater. Chem. C* **2015**, 3, 8956-8962.
- [21] T. Miki, A. Saeki, H. Masuda, N. Ikuma, K. Kokubo, S. Seki, *J. Mater. Chem. A* **2015**, 3, 1152-1157.
- [22] J. E. Anthony, J. S. Brooks, D. L. Eaton, S. R. Parkin, *J. Am. Chem. Soc.* **2001**, 123, 9482-9483.
- [23] D. Xia, D. Gehrig, X. Guo, M. Baumgarten, F. Laquai, K. Müllen, *J. Mater. Chem. A* **2015**, 3, 11086-11092.
- [24] E. Jacques, M. Romain, A. Yassin, S. Bebiche, M. Harnois, T. Mohammed-Brahim, J. Rault-Berthelot, C. Poriel, *J. Mater. Chem. C* **2014**, 2, 3292-3302.
- [25] H. Usta, A. Facchetti, T. J. Marks, *Org. Lett.* **2008**, 10, 1385-1388.
- [26] H. Usta, A. Facchetti, T. J. Marks, *J. Am. Chem. Soc.* **2008**, 130, 8580-8581.
- [27] H. Usta, C. Risko, Z. Wang, H. Huang, M. K. Delimeroglu, A. Zhukhovitskiy, A. Facchetti, T. J. Marks, *J. Am. Chem. Soc.* **2009**, 131, 5586-5608.
- [28] H. Usta, A. Facchetti, T. J. Marks, *Acc. Chem. Res.* **2011**, 44, 501-510.
- [29] W. Lehnert, *Synthesis* **1974**, 1974, 667-669.
- [30] W. Lehnert, *Tetrahedron Lett.* **1970**, 11, 4723-4724.



# Chapter VII. Spiro-Fluorene Based Blue Fluorescent Emitters

## VII.1 Introduction

Since the first organic light-emitting diodes (OLEDs) were demonstrated in 1987,<sup>[1]</sup> they have attracted considerable attention due to their potential applications in flat-panel displays and solid-state lightings.<sup>[2-9]</sup> With respect to red and green emitters,<sup>[10-11]</sup> it is a big challenge to develop blue counterparts with excellent efficiency and color purity, which is due to the intrinsic wide gap causing inevitably inefficient charge injection to an emitting layer.<sup>[12]</sup> Therefore, great efforts should be paid on the design and synthesis of stable blue emitters to promote the commercialization of OLED technology.

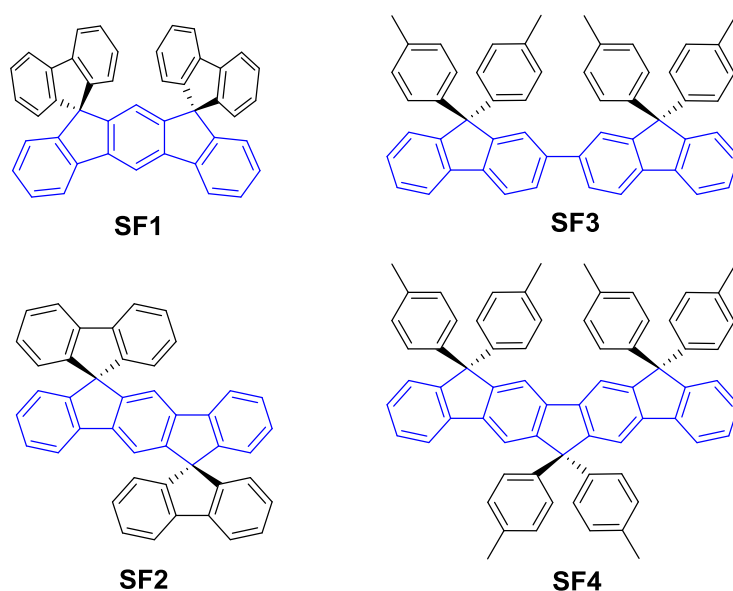


**Figure VII-1.** Examples of fluorene based blue-emitting molecules found in literature.

Fluorene is one widely used building block to construct molecules used not only as blue emitting materials but also as host materials.<sup>[9, 13-19]</sup> In recent years, its

derivatives (Figure VII-1), such as dihydroindenofluorene (e.g. blue backbone of **SF1** and **SF2**),<sup>[20-23]</sup> bi(9,9-diarylfluorene) (e.g. **SF3**)<sup>[24]</sup> and ladder-type poly-p-phenylene (e.g. blue backbone of **SF4**)<sup>[25-27]</sup> have attracted particular interests, due to their relatively rigid and planar structures. However, in some cases, the excimer emission<sup>[28-29]</sup> and ketone defects<sup>[30-31]</sup> happened in the solid states, with the evidence of the emission in the long-wave length region. Thus, the corresponding device efficiencies decreased dramatically.

To solve this problem, the introduction of a rigid spiro linkage, such as spirobifluorene, into the polymer/oligomer backbone is one of the most efficient ways. Simultaneously, thermal stabilities were increased; solubility was improved; and the quantum yields were also enhanced. With the guidance, we came up with a new idea, namely, connecting two dihydroindenofluorene or ladder-type poly-p-phenylene units via a sp<sup>3</sup>-hybridized carbon atom, which has not been reported before. We believe that should be a challenge and also more meaningful work, considering the following aspects: (1) the advantages as we discussed above will be kept, favoring device engineering; (2) molecules we expect indeed will be spatially extended, and thus the intermolecular aggregation should be reduced theoretically, together with the high quantum yield increasing; (3) the study on their crystals and intermolecular interactions of such spatially extended molecules in the solid state is also appealing and will provide direct data for other scientists.

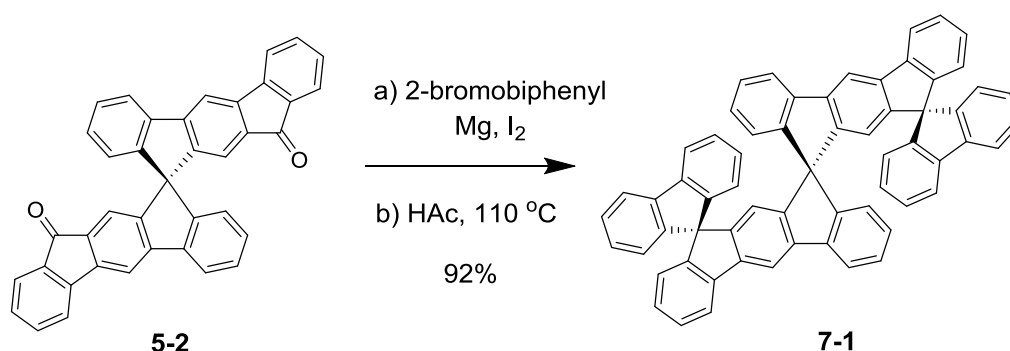
Herein, we divide the research content into two parts, namely so called “dihydroindenofluorene” part (VII.2) and “ladder-type tetra-p-phenylene” part (VII.3). In both parts, we describe the synthesis, characterization, photophysical and electrochemical properties, crystal analysis, together with the density functional theory (DFT) calculations.

## VII.2 Blue emitter based on dihydroindenofluorene units

### VII.2.1 Synthesis and characterization

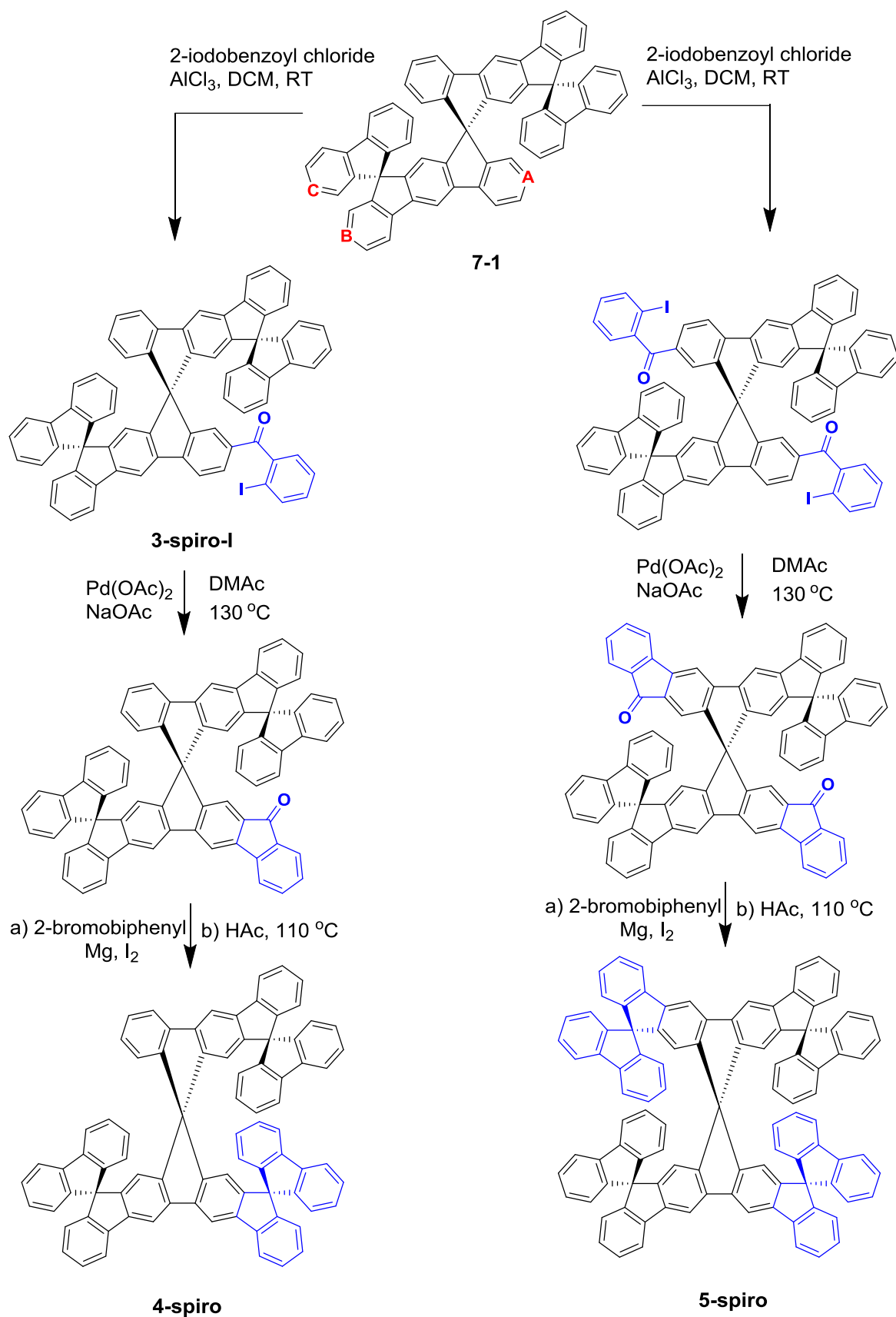
The synthetic route is presented in Scheme VII-1. It is based on a nucleophilic reaction between 12H,12'H-10,10'-spirobi[indeno[2,1-b]fluorene]-12,12'-dione **5-2**

and [1,1'-biphenyl]-2-ylmagnesium bromide, followed by an intramolecular cyclization reaction under the reflux condition using acetic acid as solvent. To obtain high reaction yield, ten equivalent of 2-bromobiphenyl was used, which ensured the complete nucleophilic substitution on **5-2**. Therefore, 92% reaction yield was achieved. The molecule **7-1** possesses two fluorene rings and two dihydroindeno[2,1-b]fluorenyl moieties, which are connected via the spiro linkage. As far as we know, molecule **7-1** appears to be the first case of a spiro-linked two dihydroindeno[2,1-b]fluorenyl fragments.



Scheme VII-1. Synthetic route towards **7-1**.

The compound **7-1** can be further extended to form bigger rigid structures. At the beginning, we assumed that the Friedel-Crafts reaction should occur in the C position (see Scheme VII-2), considering the reactivity of fluorene. In order to confirm the chemical structure, single crystals were grown by slowly evaporation of the DCM and hexane mixed solution and analyzed by Dr. Dieter Schollmeyer (Johannes Gutenberg-University, Mainz). The crystal structure shows that the Friedel-Crafts reaction happened prior to the A position rather than B and C positions (Figure IIV-2). Additionally, through altering the amount of 2-iodobenzoyl chloride adding, the formation of mono- or di- (2-iodophenyl)methanone substituted spiro-fluorene can be reached (see Scheme VII-2). Thereafter, 4-spiro and 5-spiro could be formed, which were only characterized by FD Mass. However, the purification of such compounds by column chromatography was quite a challenge. The problem could be possible solved by using recycling GPC. Anyway, this reaction route was confirmed working well.



Scheme VII-2. Synthetic route towards 4-spiro and 5-spiro.

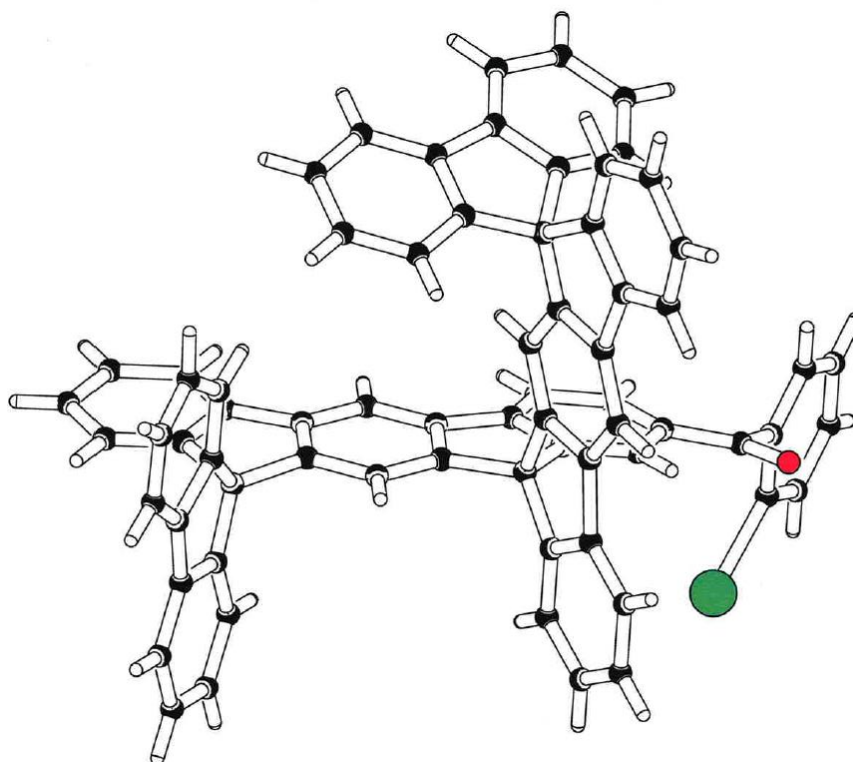


Figure VII-2. Single crystal structure of 3-spiro-I

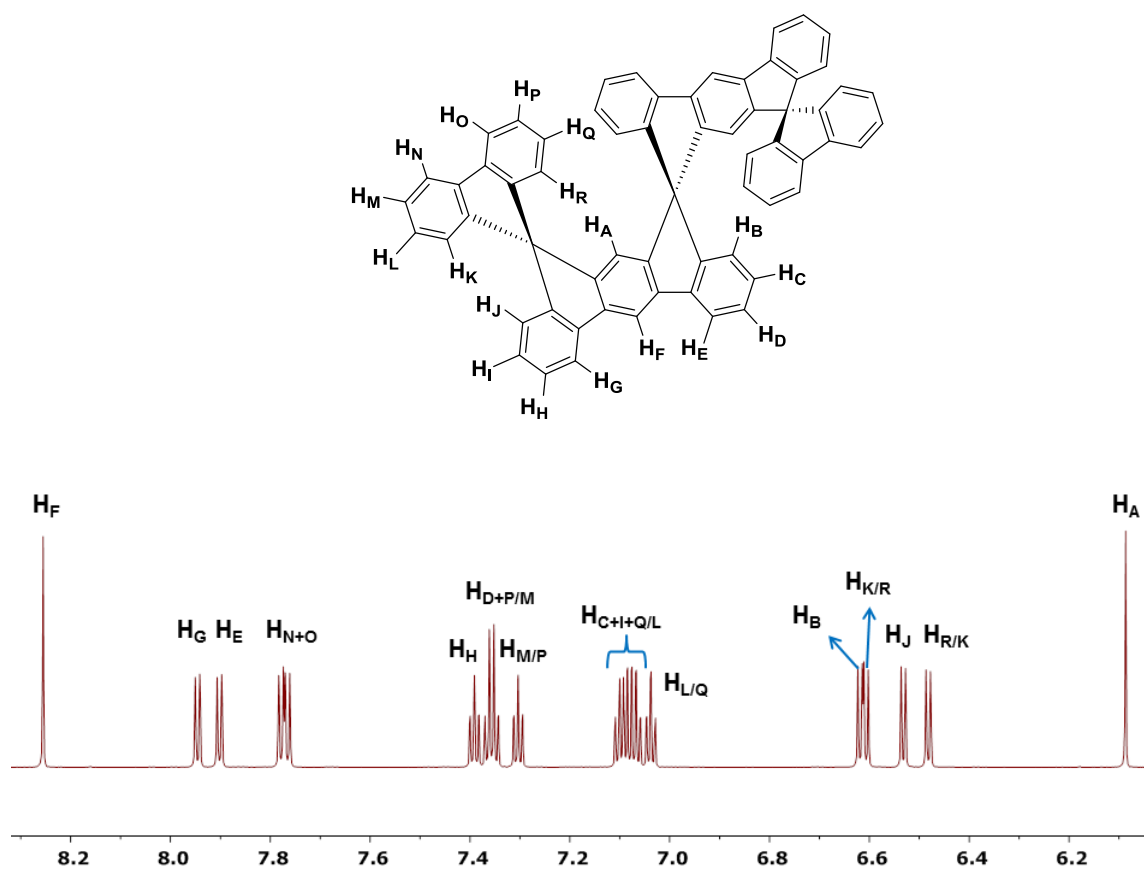
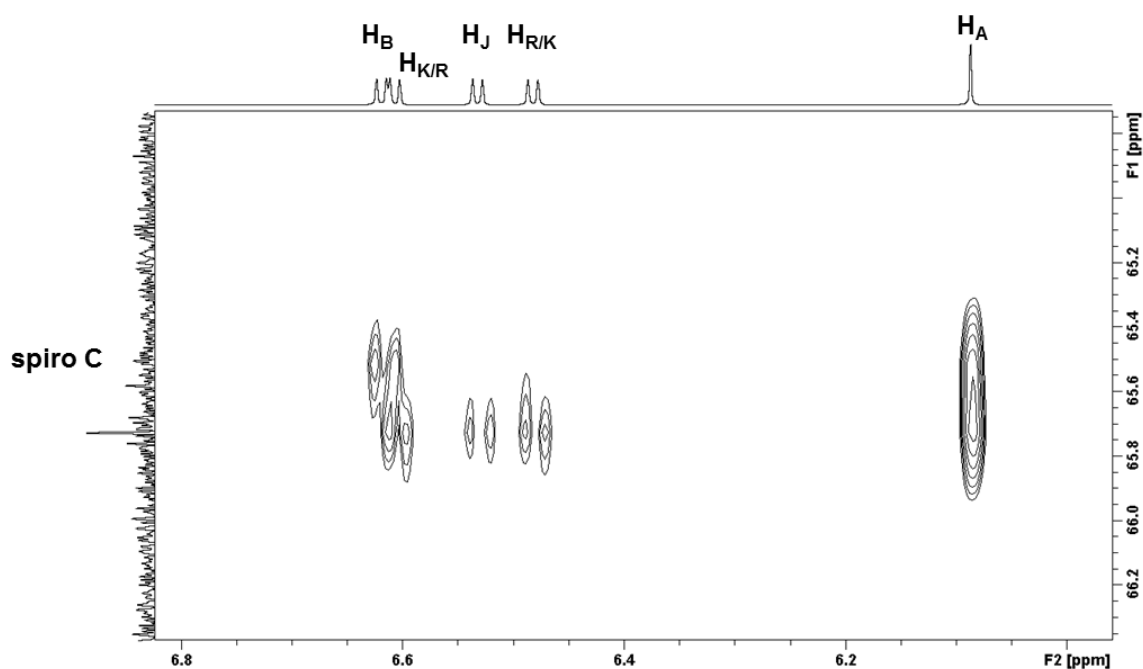


Figure VII-3. Aromatic region of H-NMR spectrum of 7-1 (CD<sub>2</sub>Cl<sub>2</sub>, 850 MHz).

The structure of **7-1** was also proven by NMR spectroscopy. As shown in Figure VII-3, the different protons can be assigned to different moieties and exact positions within the molecule. That was supported and ascertained by 2D-NMR experiments, such as HMBC (Figure VII-4), NOESY (Figure VII-5), COSY (Figure VII-6) and TOCSY (Figure VII-7), which were performed by ..... (Max Planck Institute for Polymer Research, Mainz). Firstly, HMBC spectrum was performed to investigate correlations between spiro carbons and their neighboring hydrogens. Consequently, H<sub>A</sub> and H<sub>B</sub> are assigned to the single peak with the chemical shift of 6.09 ppm and double peaks with the chemical shift of 6.62 ppm, respectively. Obviously, the other single peak (8.26 ppm) is ascribed to proton H<sub>F</sub>. Thereafter, H<sub>G</sub> and H<sub>E</sub> can also be assigned to the double peaks with chemical shift of 7.95 and 7.90 ppm, respectively, since both protons have correlations with H<sub>F</sub> in the NOESY spectrum and only proton H<sub>E</sub> has correlation with known H<sub>B</sub> in the TOCSY spectrum. Through the COSY spectrum, the assignment of the other protons on the dihydroindeno[2,1-b]fluorenyl moieties is straightforward. Those are H<sub>H</sub> (7.39 ppm) and H<sub>J</sub> (6.53 ppm). Regarding the H<sub>C</sub>, H<sub>D</sub> and H<sub>I</sub>, their peaks are mixed with the peaks arising from protons of two fluorene units. Unfortunately, the attempt to specify the proton positions of fluorene was failed. However, the roughly prediction of their positions was achieved.



**Figure VII-4.** Portion of the H-C HMBC spectrum of **7-1** (CD<sub>2</sub>Cl<sub>2</sub>, 850 MHz).

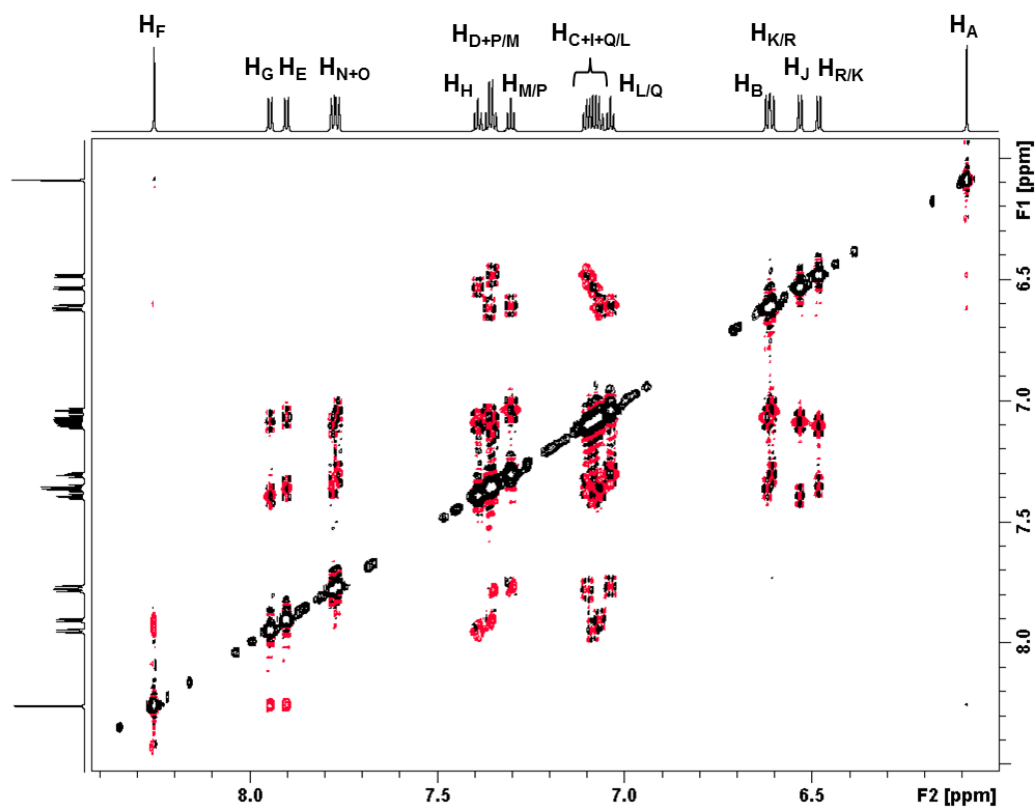


Figure VII-5. Aromatic region of H-H NOESY spectrum of 7-1 (CD<sub>2</sub>Cl<sub>2</sub>, 850 MHz).

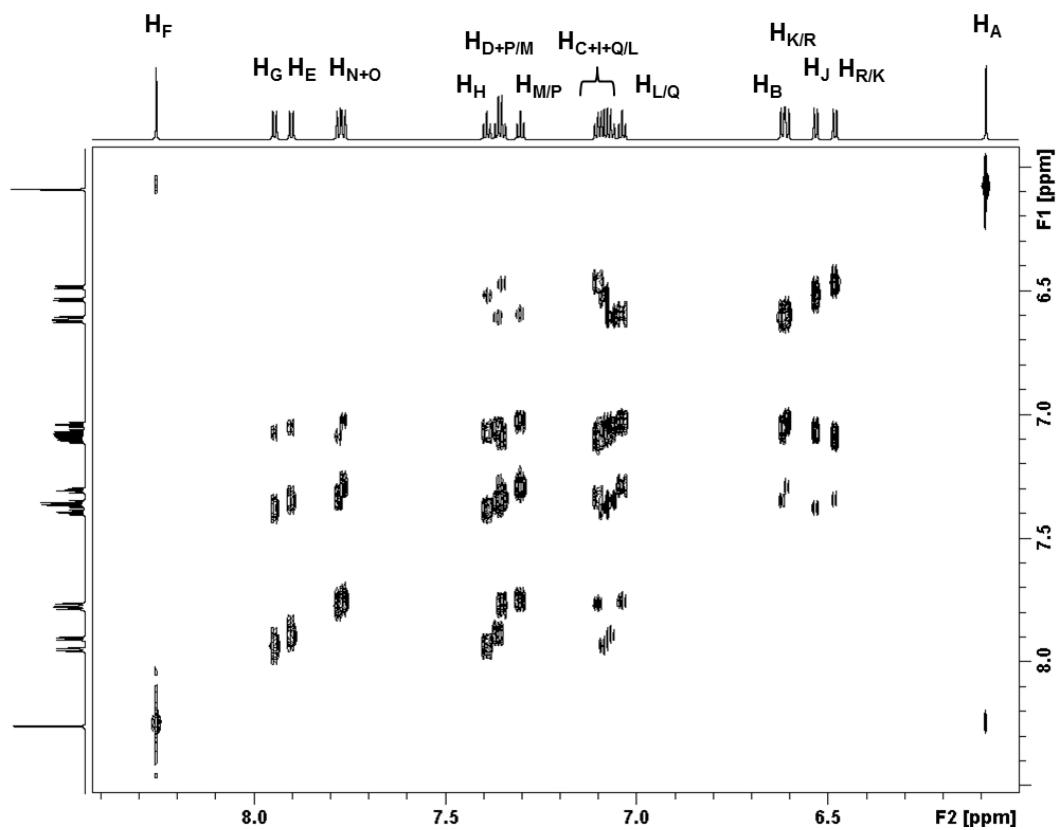


Figure VII-6. Aromatic region of H-H COSY spectrum of 7-1 (CD<sub>2</sub>Cl<sub>2</sub>, 850 MHz).

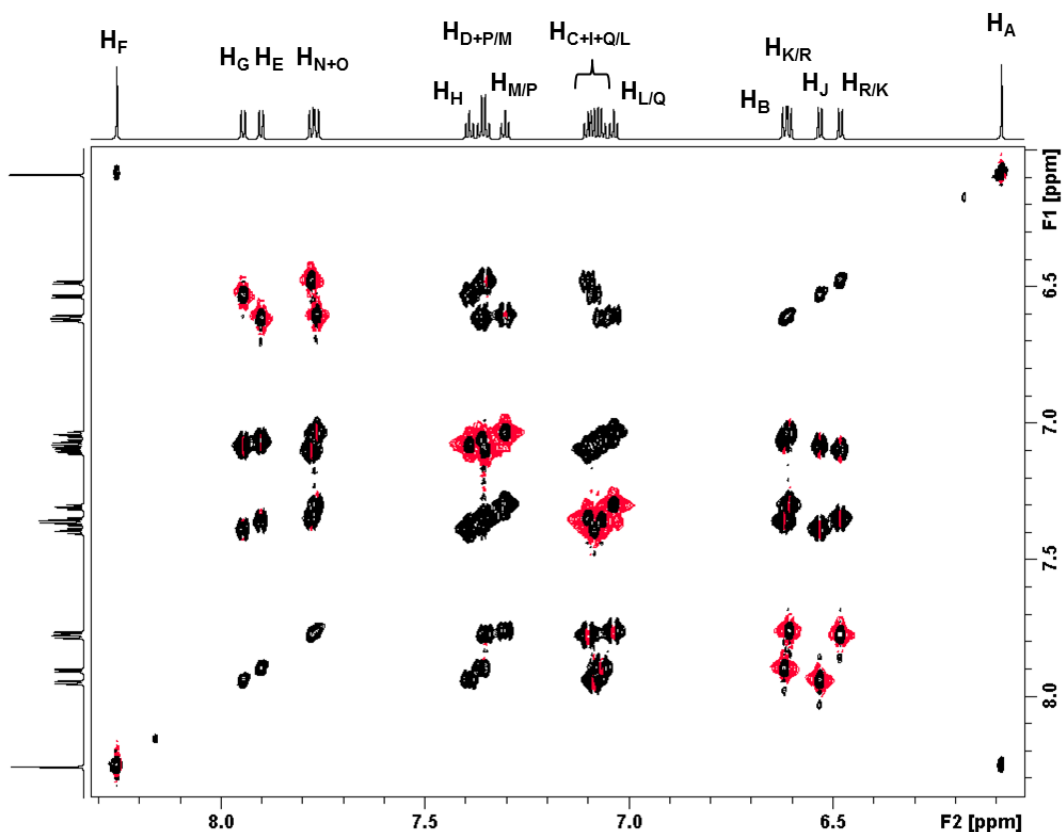
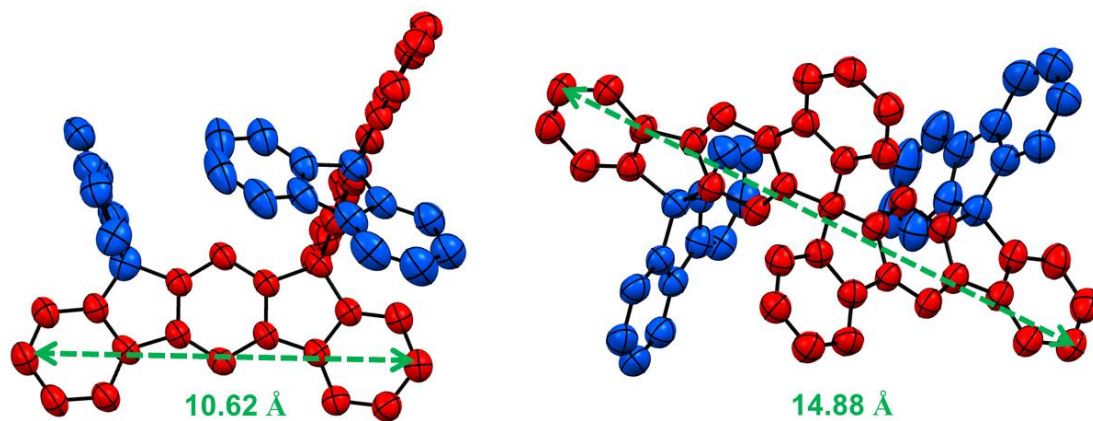


Figure VII-7. Aromatic region of H-H TOCSY spectrum of **7-1** ( $\text{CD}_2\text{Cl}_2$ , 850 MHz).

## VII.2.2 Crystal structure analysis

Single crystals of **7-1** suitable for X-ray diffraction analysis were successfully grown by slow evaporation of the hexane and dichloromethane mixed solution. Crystal structure analysis was carried out by ..... (Johannes Gutenberg-University, Mainz). In Figure VII-8, **7-1** presents the rigid three-dimensional structure, which could efficiently prevent the intermolecular self-aggregation and thus reduce or eliminate the quenching of the luminance. The dihydroindeno[2,1-b]fluorenyl core of **7-1** has a maximum length of 10.6 Å, which is similar to its derivatives.<sup>[22]</sup> The diameter of the molecule is up to 14.88 Å (distance between endcapped carbons of the dihydroindeno [2,1-b]fluorenyl core, see Figure VII-8 right). As shown in Figure VII-9, three types of intermolecular interactions in different directions are observed, namely, C···H (a), H···H (b), and C···H (c), with a distance of 2.88 Å, 2.29 Å and 2.80 Å, respectively. Surprisingly, no intermolecular  $\pi$ - $\pi$  interaction is observed in such crystals, even though large planar aromatic rings, such as fluorene and

dihydroindeno [2,1-b]fluorenyl core exist in this system. That can be explained by the steric hindrance effect.



**Figure VII-8.** X-ray diffraction structure of 7-1. Hydrogen atoms are omitted for clarity.

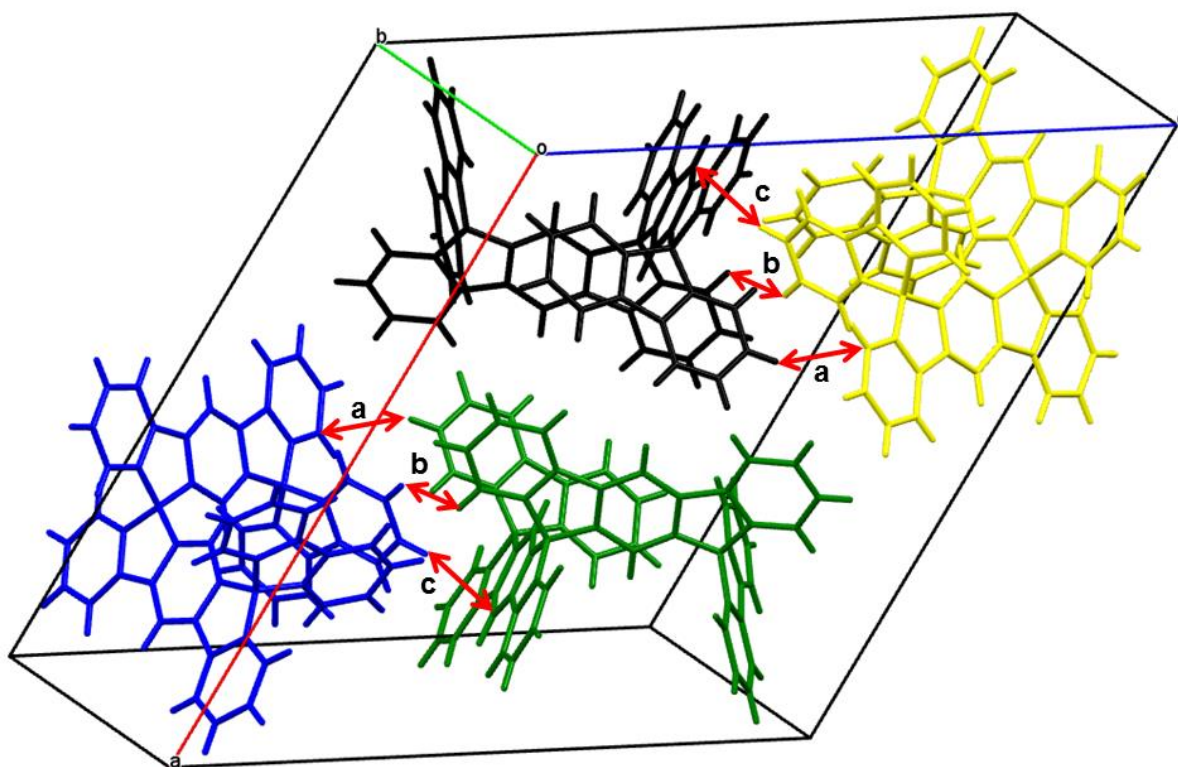


**Figure VII-9.** X-ray diffraction structure of 7-1. Intermolecular distances: a: 2.88 Å (C...H); b: 2.29 Å (H...H); c: 2.80 Å (C...H).

### VII.2.3 Photophysical, electrochemical, and thermal properties

As depicted in Figure VII-10, the UV-vis absorption spectrum of **7-1** in CH<sub>2</sub>Cl<sub>2</sub> displays six characteristic bands (269, 297, 311, 328, 334, and 344 nm) that are very similar to those previously observed for its analogue, such as dispiro[fluorene-9,10'-indeno[2,1-b]fluorene-12',9''-fluorene].<sup>[22]</sup> The absorption bands of **7-1** in the thin film spectrum are only slightly red-shifted (4 nm) compared to that in solution. The fluorescence spectrum of **7-1** in CH<sub>2</sub>Cl<sub>2</sub> is with the maximum emission peak at 351 nm and thus with a narrow Stokes shift of 8 nm. This is indicative of an extremely rigid chromophore, in which the vibrational relaxation of the excited state is dramatically restricted. The feature is also related to the high quantum yield of approximately 0.45, especially for the violet emitter, which could also be used as host for the sky-blue emitting phosphorescent material. In the neat film, however, the emission behavior are different. On going from solution to the solid state, **7-1** displays a redshift of about 20 nm, together with the appearance of a long tail in the range of  $\lambda = 400-600$  nm. This indicates the existence of strong intermolecular interactions. To prevent this phenomenon in the future, more bulk groups, such as dendrimer, could be introduced in the core.

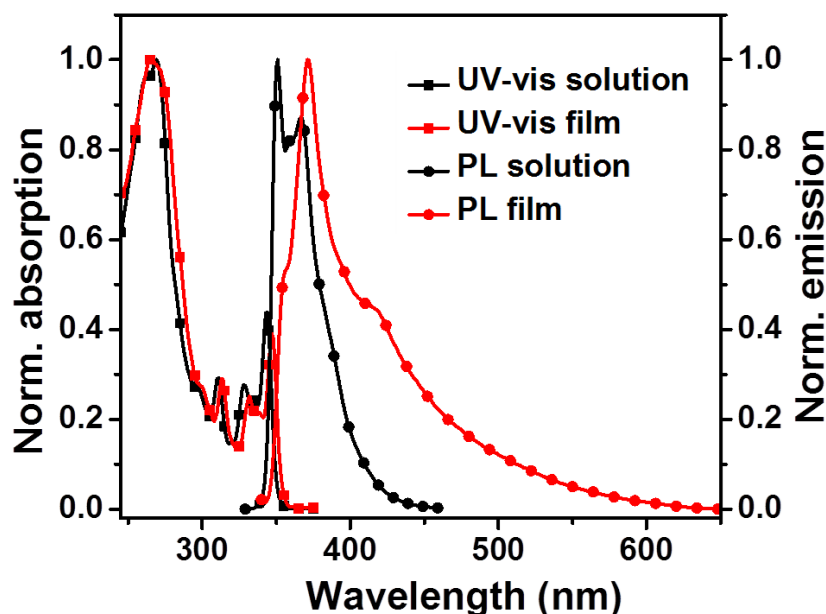


**Figure VII-10.** Absorption (square) and photoluminescence (circle) spectra of **7-1** in DCM ( $\lambda_{\text{Exc}} = 330$  nm) and thin film ( $\lambda_{\text{Exc}} = 270$  nm).

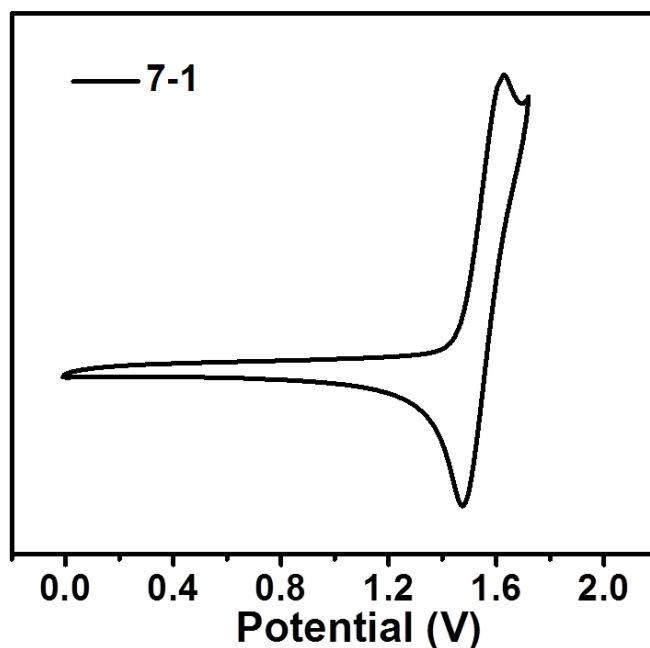


**Figure VII-11.** Cyclic voltammetric profile of **7-1** in dichloromethane at a scan rate of 100 mV/s with 0.1 M  $\text{Bu}_4\text{NPF}_6$  as supporting electrolyte.

To design the configurations of the OLED devices with high emitting efficiency, it is essential to determine the HOMO and LUMO energy levels of the chromophore in the emissive layer (EML). Thereafter, materials for hole and electron transporting layers can be chosen for efficient charge carrier transfer from the electrodes to the EML. The electrochemical behavior was investigated by cyclic voltammetry. Cyclic voltammograms (Figure VII-11) of **7-1** in DCM exhibited only one oxidation wave, with the  $E_{1/2}$  potential around 1.54 V, arising from the oxidation of the dihydroindenofluorenyl units. The HOMO energy level estimated through the equation  $E_{\text{HOMO}} = - [E_{\text{oxd}1/2} - E_{(\text{Fc}^+/\text{Fc})} + 4.8]$  eV was around -5.84 eV. This HOMO energy level is almost the same to that of reported analogue dispiro[fluorene-9,10'-indeno[2,1-b]fluorene-12',9''-fluorene]<sup>[22]</sup>. However, in the accessible potential range, we have not observed the reduction wave. The LUMO energy was calculated from the optical gap to be -2.30 eV, according to the equation  $\text{LUMO} = \text{HOMO} + E_g$ . The optical gap was calculated from the onset of the absorption spectrum.

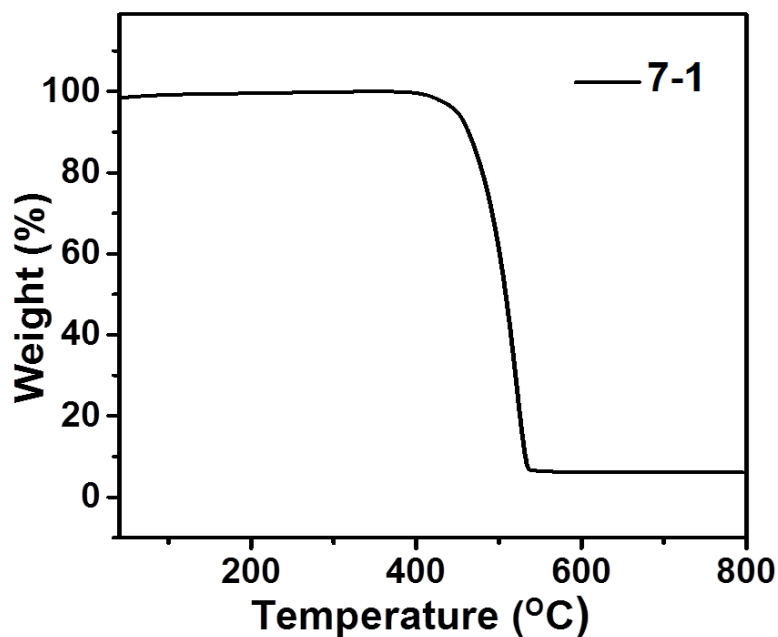


**Figure VII-12.** TGA curve for **7-1** measured under a nitrogen atmosphere at a heating rate of 10 °C/min.

The thermal stability of **7-1** was investigated by thermogravimetric analysis (TGA), which is shown in Figure VII-12. **7-1** exhibited an excellent thermal stability at 450 °C with 5% weight loss. The differential scanning calorimetry (DSC) curves of this compound did not show any phase transition in the range from 30 °C to 400 °C.

## VII.2.4 Density functional theory calculations

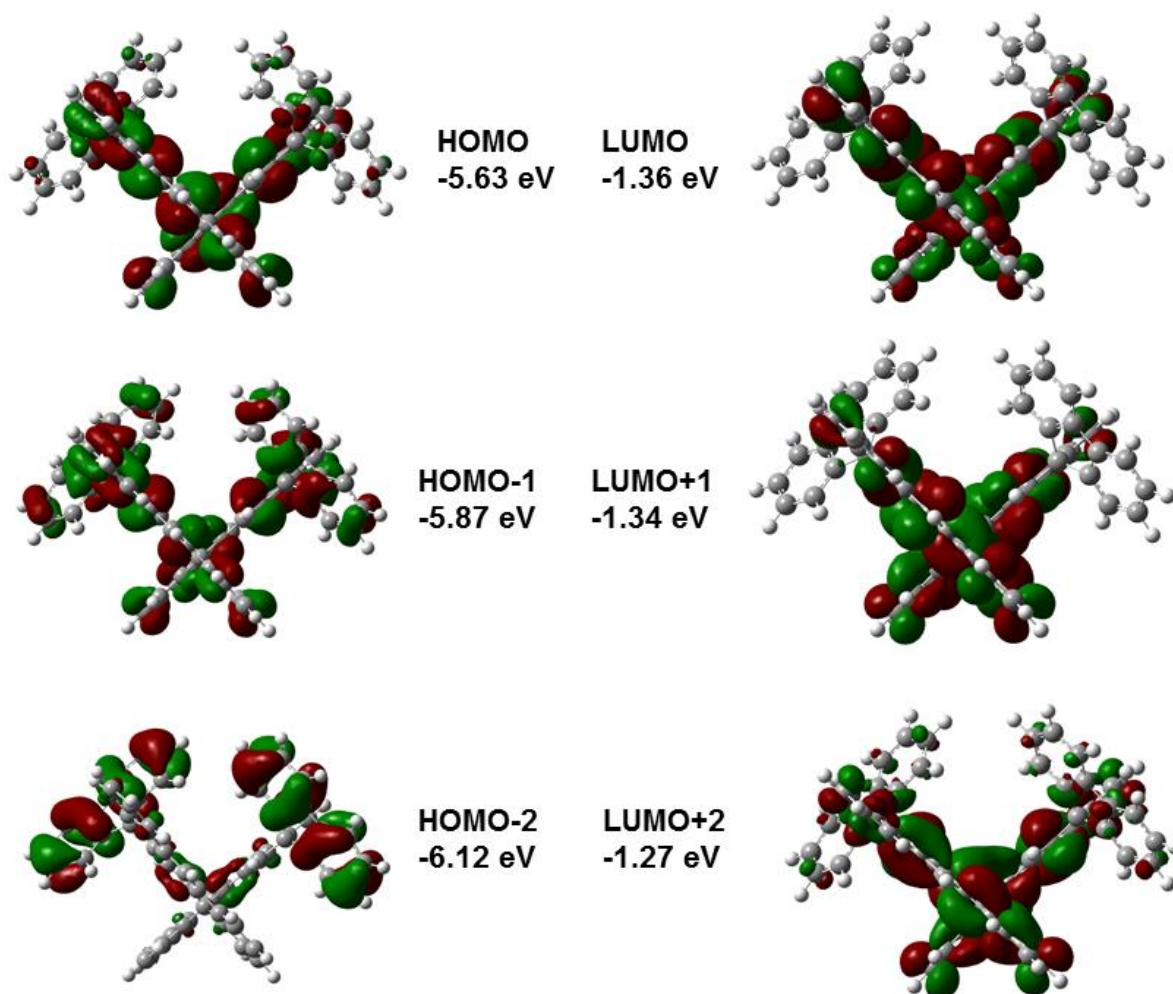


**Figure VII-13.** Frontier molecular orbitals calculated by DFT B3LYP/6-311G + (d, p) for 7-1 after geometry optimization.

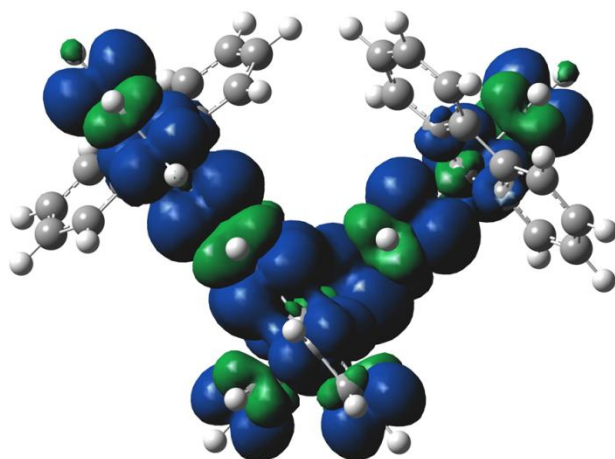


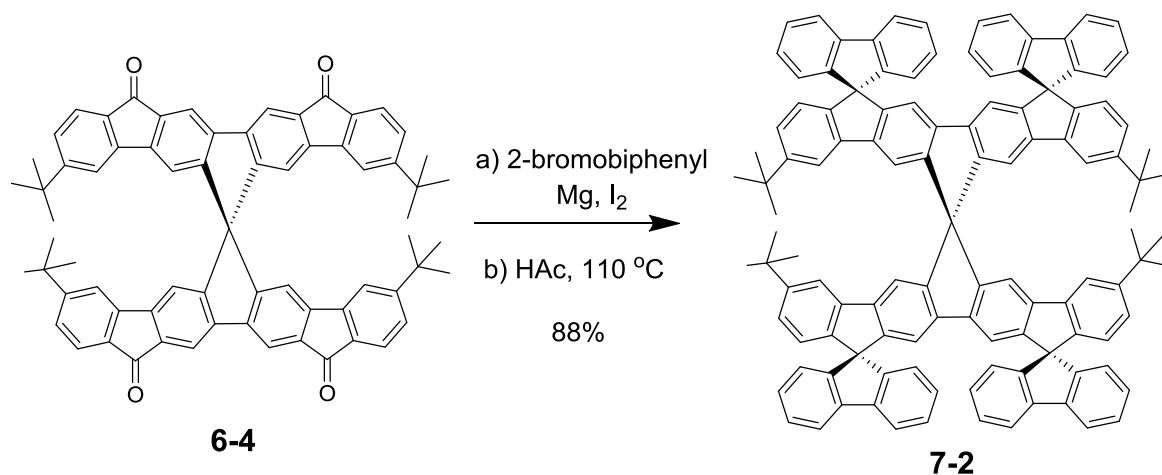
**Figure VII-14.** DFT-simulated triplet spin density distribution of 7-1.

The frontier orbital distribution of **7-1** was investigated by DFT calculations (Figure VII-13 and VII-14). The HOMO and LUMO is mainly located on dihydroindenofluorene units, with the energy levels of -5.63 and -1.36 eV, respectively. This electron delocalization phenomenon and calculated results of energy levels are similar to those for its analogue dispiro[fluorene-9,10'-indeno[2,1-b]fluorene-12',9''-fluorene].<sup>[22]</sup> This indicates that the spiro linkage can keep the original properties of its connected fragments. Ongoing from HOMO to HOMO-1 and HOMO-2, the dispersion of electron cloud densities are increased to fluorene moieties correspondingly. Simultaneously, the energy levels of occupied molecular orbitals HOMO-1 and HOMO-2 are decreased to -5.87 and -6.12 eV, respectively. The energy levels of its LUMO and LUMO+1 are almost degenerated, in which the electron density extends exclusively along the dihydroindenofluorene units. In LUMO+2, small amount of electron dispersion on fluorene can be observed. This feature clearly indicates the main involvement of the dihydroindenofluorene fragments for electron injection in devices. The  $T_1$  energy levels of **7-1** was estimated as the energy gaps between its ground state and  $T_1$  excited state to be 3.19 eV, which is around 0.30 eV higher than that of the traditional used host N,N'-dicarbazolyl-3,5-benzene (mCP). That indicates **7-1** expands the varieties of being used as host for other blue-emitting materials with high triplet energies.

## VII.3 Cruciform blue emitter based on ladder-type tetra-p-phenylene units

### VII.3.1 Synthesis and characterization

The synthetic route is presented in Figure VII-14. The target compound **7-2** was prepared based on a two-step reaction. Firstly, nucleophilic reaction happened between 3,3',9,9'-Tetra-tert-butyl-6,6'-spirobi[cyclopenta[2,1-b:3,4-b']difluorene]-12,12',15,15'-tetraone **6-4** and [1,1'-biphenyl]-2-ylmagnesium bromide. Then, **7-2** was produced in a 88% yield by an intramolecular cyclization reaction under acetic acid reflux condition. The product was purified by column chromatography.



**Scheme VII-3.** Synthetic route towards **7-2**.

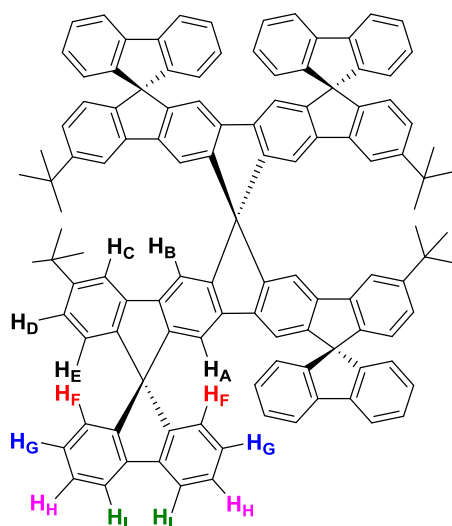


**Figure VII-15.** Labeling protons of **7-2**.

To assign hydrogen atoms to the exact positions within **7-2**, 2D-NMR experiments, such as H-H COSY (Figure VII-16), H-H NOESY (Figure VII-17), and H-H TOCSY (Figure VII-18) were performed by ..... (Max Planck Institute for Polymer Research, Mainz). Firstly, NOESY spectrum was recorded, which can ascertain proton H<sub>A</sub> with the chemical shift of 7.01 ppm, as its through-space couplings with other single peaks was not observed. Consequently, the other two single peaks arise from H<sub>B</sub> and H<sub>C</sub>. Secondly, considering the H-H correlations between H<sub>C</sub> and other two protons (H<sub>D/E</sub>) in TOCSY spectrum, we identify H<sub>B</sub> and H<sub>C</sub> with the chemical shift of 7.25 and 7.60 ppm, respectively. At the same time, the chemical shifts of H<sub>D</sub> and H<sub>E</sub> are roughly determined. Thereafter, when we go back to see the NOESY

spectrum, the  $H_D$  and  $H_E$  are defined with the chemical shift of 6.56 and 7.04 ppm, respectively, since  $H_E$  correlated with two protons ( $H_{D/F}$ ). Obviously, the double peak with the chemical shift of 6.87 ppm is assigned to proton  $H_F$ . Lastly,  $H_G$  (7.13 ppm),  $H_H$  (7.36 ppm) and  $H_I$  (7.84 ppm) can also be determined based on the analysis of the COSY spectrum.

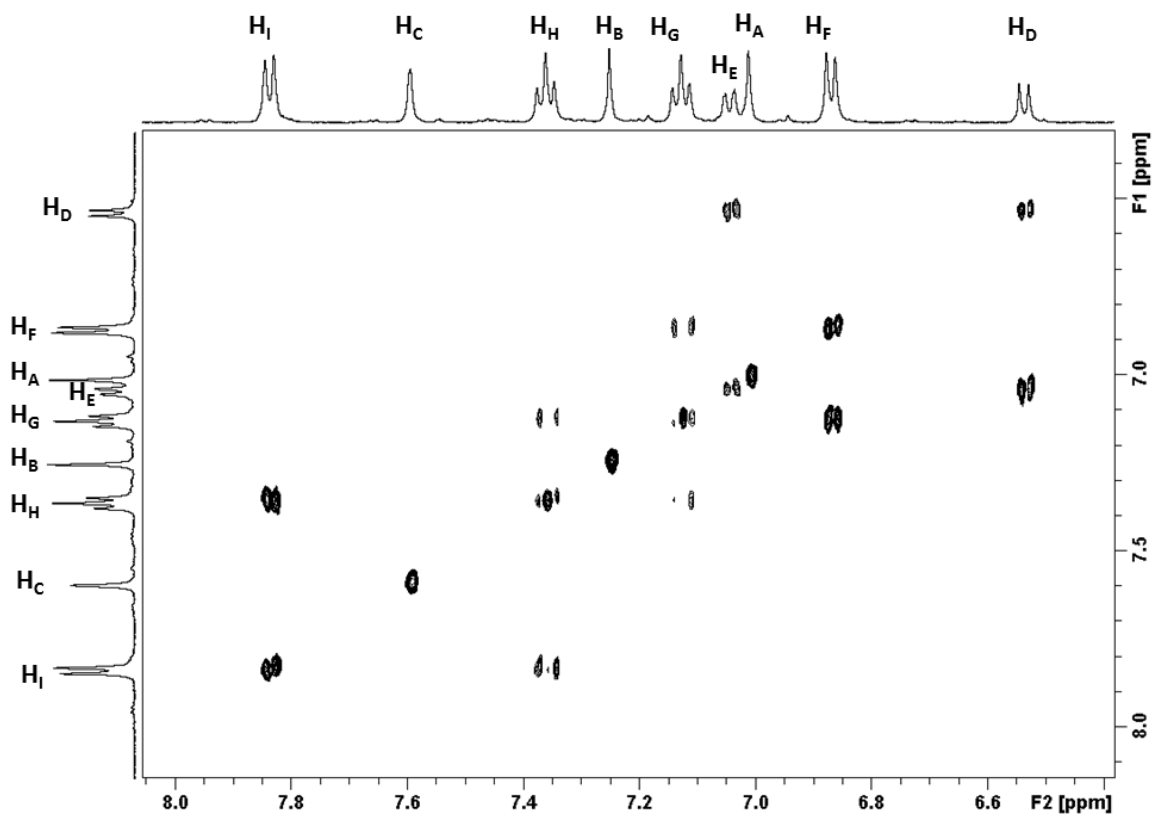


**Figure VII-16.** Aromatic region of H-H COSY spectrum of 7-2 ( $C_2D_2Cl_4$ , 500 MHz).

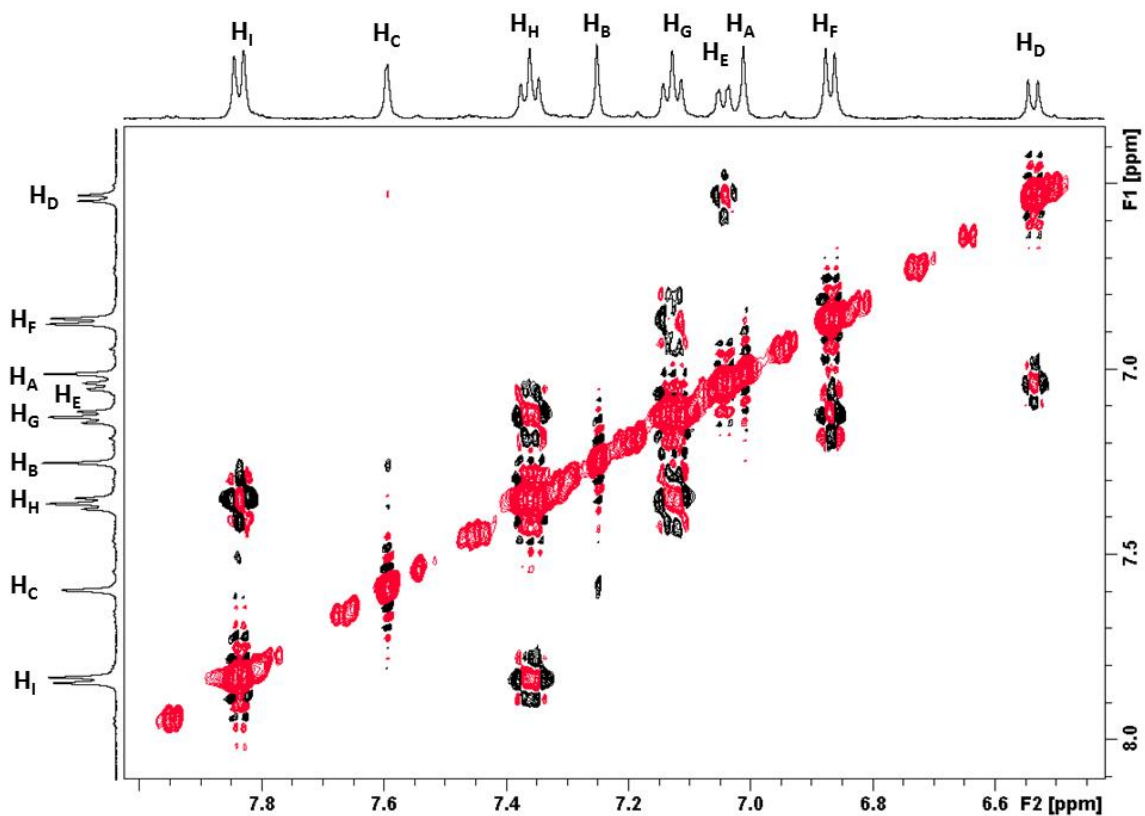


Figure VII-17. Aromatic region of H-H NOESY spectrum of 7-2 ( $C_2D_2Cl_4$ , 500 MHz).

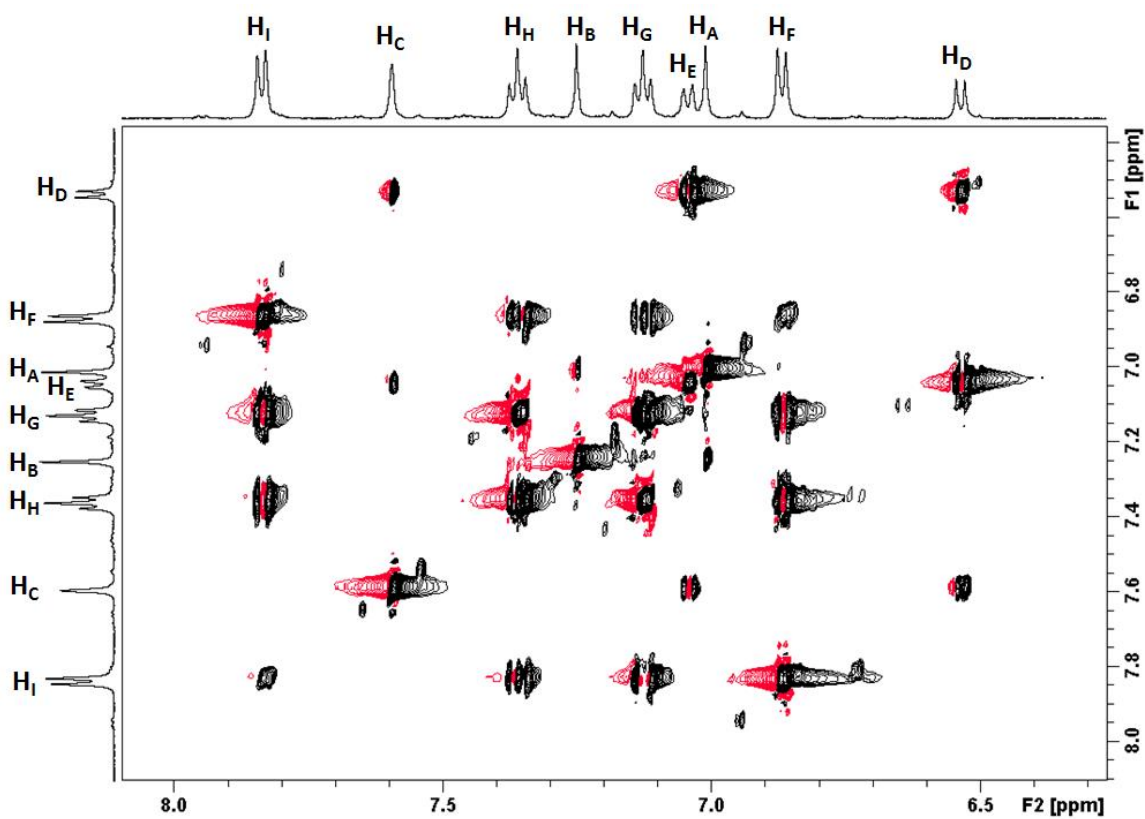
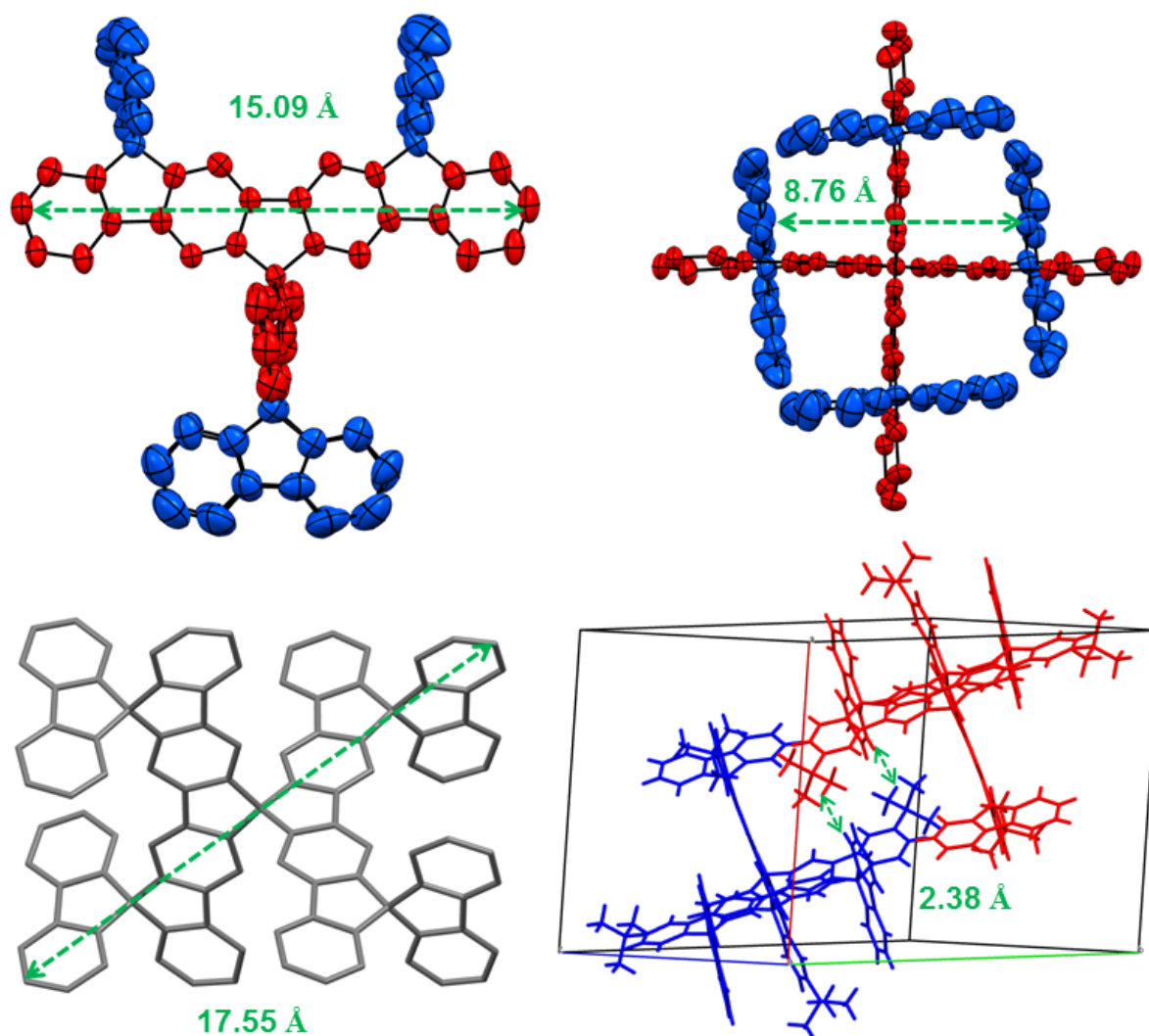


Figure VII-18. Aromatic region of H-H TOCSY spectrum of 7-2 ( $C_2D_2Cl_4$ , 500 MHz).

### VII.3.2 Crystal structure analysis

Suitable crystals for X-ray diffraction analysis were grown in pentane solution by slow evaporation and were analyzed by ..... (Johannes Gutenberg-University, Mainz). As depicted in Figure VII-19, the two conjugated poly(para-phenylene) backbones with the length of 15.09 Å are perpendicular to each other. Like its reported analogue, the  $\pi$ -system does not adopt a strictly coplanar configuration. Two distortions were observed on both sides. Moreover, two opposite fluorene groups directly connected to the poly(para-phenylene) backbone are parallel



**Figure VII-19.** X-ray diffraction structure of 7-2. Top and bottom-left: single molecule structure. Hydrogen atoms are omitted for clarity. Bottom-right: Unit cell.

to each other and with the distance of 8.76 Å. Furthermore, to the best of our knowledge, **7-2** is the largest three-dimensional poly(para-phenylene)-based structure that has been characterized using X-ray crystallography, with the diameter up to 17.55 Å. In the crystal-packing diagram (bottom right) of **7-2**, only interactions between hydrogen atom of the tert-butyl and hydrogen atom of the phenyl group are observed, which are shorter than the sum of the van der Waals radii of the hydrogen (1.20 Å). As expected, the packing diagram indicates the lack of effective intermolecular  $\pi$ - $\pi$  interactions in the solid state, despite molecule **7-2** presents two long  $\pi$  systems. We assign the reason to the steric hindrance arising from the tert-butyl groups and fluorene units.

### VII.3.3 Photophysical, electrochemical, and thermal properties

The absorption and PL spectra of **7-2** are shown in Figure VII-20. The UV-vis absorption spectrum taken in DCM shows four characteristic peaks (312, 334, 360, 379 nm) that are very similar to those earlier observed for its analogue hexa-p-tolyl-12,15-dihydro-6H-cyclopenta[2,1-b:3,4-b']difluorene.<sup>[25]</sup> Thus, we confirm that those absorption bands arise from the conjugated backbone. The PL spectrum recorded in DCM presents a well-resolved emission, with a maximum recorded at 406 nm. The maximum emission peak of film spectrum is only 7 nm redshift in comparison to that of solution, which is due to the prevention of the strong intermolecular aggregation in the solid state. However, a long tail in the range of  $\lambda = 480$ -600 nm appeared, which suggests the existence of the intermolecular interactions. The photoluminescence quantum yield (PLQY) of **7-2** is measured relative to a fluorescent standard material 9,10-diphenylanthracene ( $\Phi = 0.9$  in cyclohexane,  $\lambda_{\text{Exc}} = 325$  nm). The PLQY is as high as 0.76, which has a significant close relationship with the rigid structure.

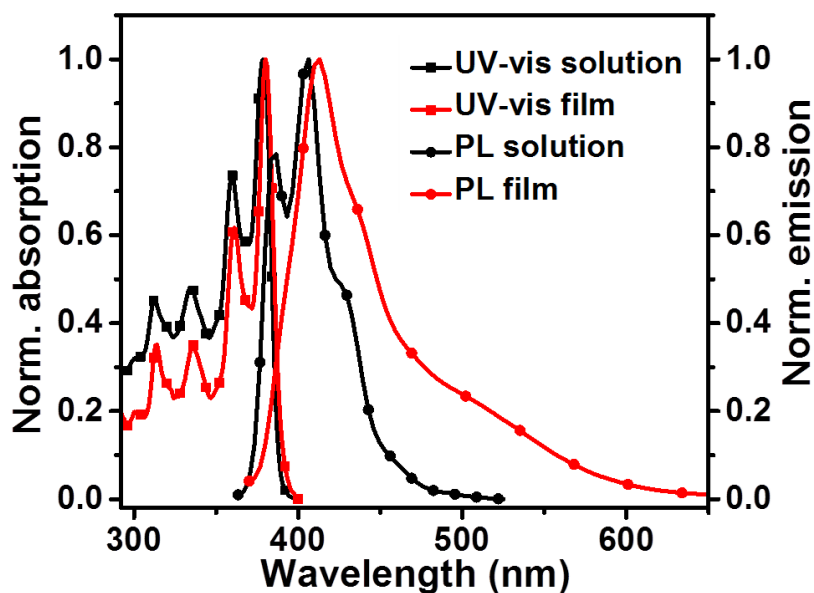


**Figure VII-20.** Absorption (square) and photoluminescence (circle) spectra of **7-2** in DCM ( $\lambda_{\text{Exc}} = 360$  nm) and thin film ( $\lambda_{\text{Exc}} = 310$  nm).

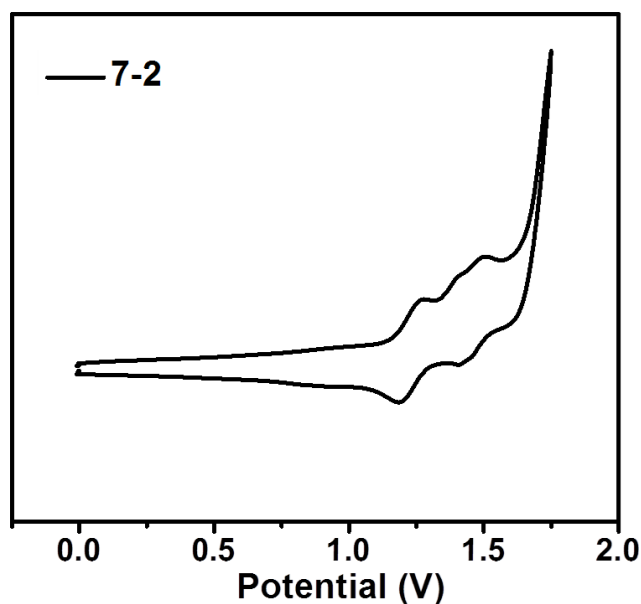


**Figure VII-21.** Cyclic voltammetric profile of **7-2** in dichloromethane at a scan rate of 100 mV/s with 0.1 M  $\text{Bu}_4\text{NPF}_6$  as supporting electrolyte.

The electrochemical property of **7-2** was investigated by cyclic voltammetry. Cyclic voltammograms (Figure VII-21) showed three reversible oxidation waves, with the  $E_{1/2}$  potentials 1.27, 1.40 and 1.48 V, respectively. Moreover, the first half wave potential of **7-1** is the same as the reported data of its analogue.<sup>[25]</sup> Thus, we assign the first wave to the oxidation of the poly(para-phenylene) backbones. Accordingly,

HOMO energy levels were calculated to be -5.62 eV. The higher level HOMO of **7-1** relative to that of 9,9-di(p-tolyl)bifluorene<sup>[24]</sup> is also consistent with the coplanar structure having an greater degree of  $\pi$ -conjugation. In the case of LUMO, we have not observed a reduction wave in the potential range. The LUMO energy was calculated from the optical gap to be -2.43 eV, according to the equation  $LUMO = HOMO + E_g$ .

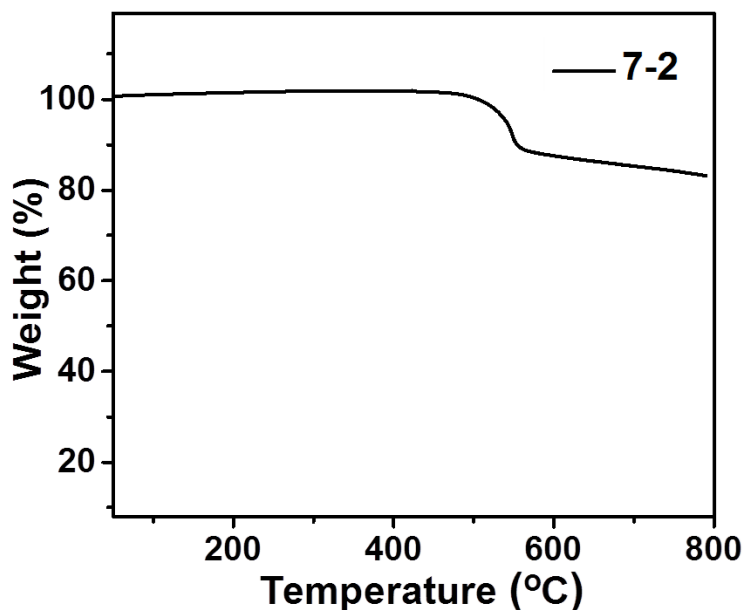


**Figure VII-22.** TGA curve for **7-2** measured under a nitrogen atmosphere at a heating rate of 10 °C/min.

The thermal property of **7-2** was investigated by TGA as shown in Figure VII-22. **7-2** exhibited excellent thermal stability, with 5% weight loss upon heating at 540 °C. When the temperature was raised to 580 °C, the tert-butyl alkyl chains were firstly decomposed. The weight loss up to 580 °C was around 12%, which is approximately in agreement with the alkyl chains weight ratio 15% in **7-2**. The DSC curves of this compound did not show any phase transition in the range from 30 °C to 450 °C.

### VII.3.4 Density functional theory calculations

DFT simulation was performed to get an insight into the nature of the optoelectronic characteristics of **7-2**. As shown in Figure VII-23 and VII-24, electron cloud densities of its HOMO, HOMO-1, LUMO and LUMO-1 are extended to almost whole of the conjugated poly(para-phenylene) backbones, while the fluorene units are not involved in the corresponding frontier orbitals. Therefore, this feature clearly indicates the conjugated backbones play a pivotal role for both hole and electron injection in OLED devices. Moreover, in the case of HOMO+2 and LUMO-2, the main electron cloud densities are predominately contributed by the fluorene moieties, together with the big energy levels change. The triplet energy level is calculated to be

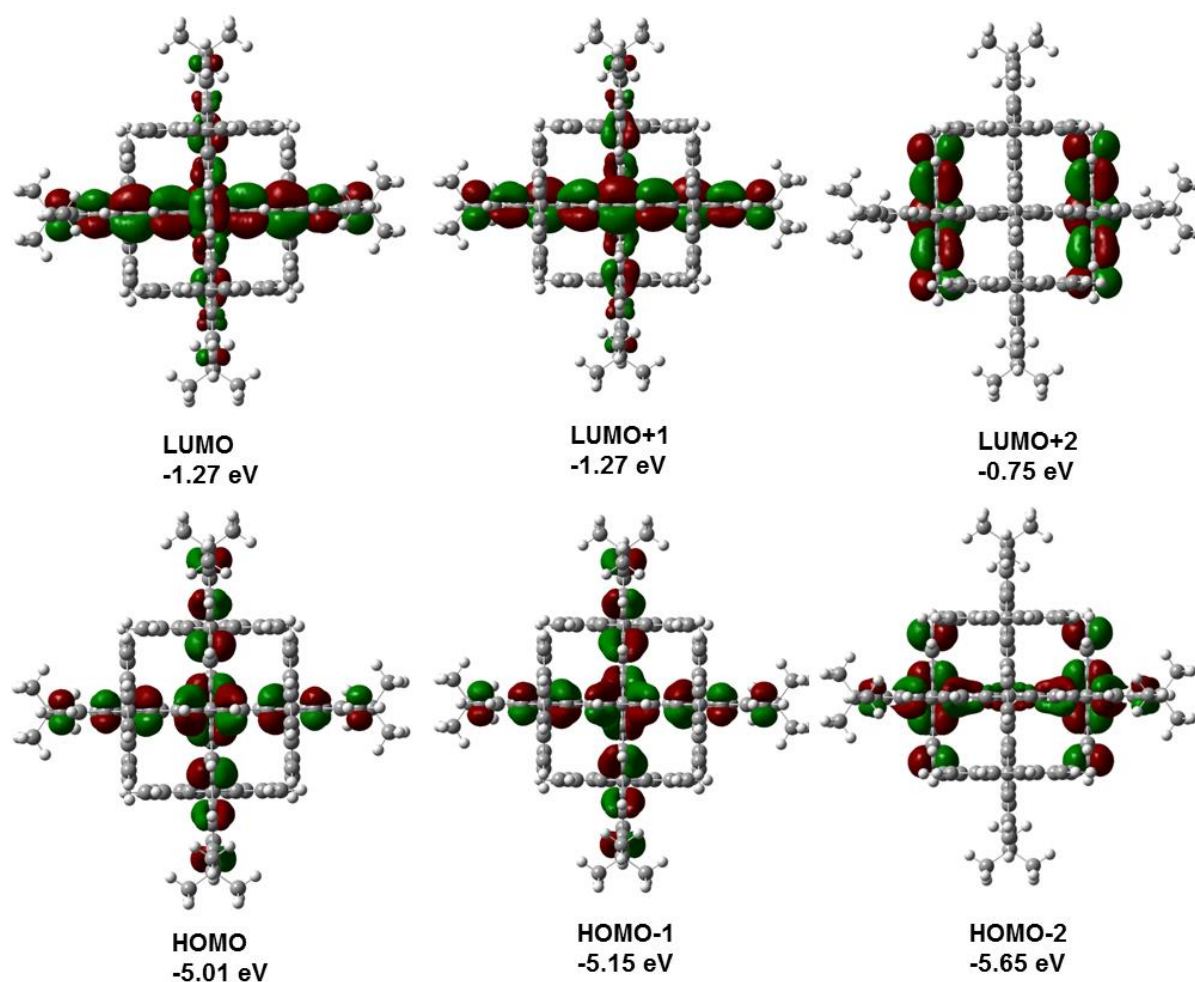


**Figure VII-23.** Frontier molecular orbitals calculated by DFT B3LYP/6-31G (d) for **7-2** after geometry optimization.

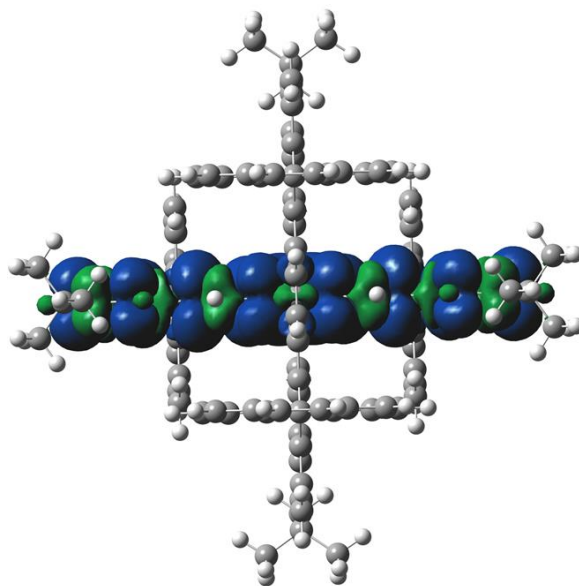


**Figure VII-24.** DFT-simulated triplet spin density distribution of **7-2**.

-2.31 eV, which is relatively low, indicating material **7-2** is not suitable to be used as host for other blue-emitting materials (guest). That is because triplet excitons may migrate from the guest to **7-2** (host) by Dexter energy transfer, resulting in poor OLED performance.<sup>[32]</sup> On the other side, **7-2** can be served as guest, and many other materials could easily meet the demand for being its host.

## VII.4 Conclusions

In conclusion, the connections between two dihydroindenofluorenyl units to construct **7-1**, as well as two ladder-type poly-p-phenylene groups to synthesize **7-2**, was initially achieved via a  $sp^3$  carbon linkage. Friedel–Crafts reaction can happen between **7-1** and 2-iodobenzoyl chloride. Furthermore, the acylation occurred primarily in the A carbon, which was confirmed by single crystal analysis. By altering the amount of 2-iodobenzoyl chloride, one- and two-position substitution products were obtained. Thereafter, the reaction routes toward **4-spiro** and **5-spiro** were approved to work well. The novel two rigid compounds **7-1** and **7-2** present excellent thermal and electrochemical stability and high PLQYs. Through analysis of different triplet energy levels **7-1** and **7-2**, the former can be used not only as the deep-blue emitter also as host for other normal fluorescent or phosphorescent materials,

whereas latter can only be employed as a blue emitter. The device application of both compounds is currently undergoing.

## VII.5 References

- [1] C. W. Tang, S. A. VanSlyke, *Appl. Phys. Lett.* **1987**, *51*, 913-915.
- [2] H. Xu, R. Chen, Q. Sun, W. Lai, Q. Su, W. Huang, X. Liu, *Chem. Soc. Rev.* **2014**, *43*, 3259-3302.
- [3] M. A. Baldo, M. E. Thompson, S. R. Forrest, *Nature* **2000**, *403*, 750-753.
- [4] Y. Sun, N. C. Giebink, H. Kanno, B. Ma, M. E. Thompson, S. R. Forrest, *Nature* **2006**, *440*, 908-912.
- [5] C. C. Wu, Y. T. Lin, K. T. Wong, R. T. Chen, Y. Y. Chien, *Adv. Mater.* **2004**, *16*, 61-65.
- [6] K. T. Kamtekar, A. P. Monkman, M. R. Bryce, *Adv. Mater.* **2010**, *22*, 572-582.
- [7] B. Kobin, F. Bianchi, S. Halm, J. Leistner, S. Blumstengel, F. Henneberger, S. Hecht, *Adv. Funct. Mater.* **2014**, 7717-7727.
- [8] T. Qin, J. Ding, L. Wang, M. Baumgarten, G. Zhou, K. Müllen, *J. Am. Chem. Soc.* **2009**, *131*, 14329-14336.
- [9] E. Mondal, W.-Y. Hung, H.-C. Dai, K.-T. Wong, *Adv. Funct. Mater.* **2013**, 3096-3105.
- [10] J. Ding, B. Wang, Z. Yue, B. Yao, Z. Xie, Y. Cheng, L. Wang, X. Jing, F. Wang, *Angew. Chem. Int. Ed.* **2009**, *48*, 6664-6666.
- [11] G. Zhou, W.-Y. Wong, B. Yao, Z. Xie, L. Wang, *Angew. Chem. Int. Ed.* **2007**, *46*, 1149-1151.
- [12] M.-T. Lee, H.-H. Chen, C.-H. Liao, C.-H. Tsai, C. H. Chen, *Appl. Phys. Lett.* **2004**, *85*, 3301-3303.
- [13] J.-Y. Hu, Y.-J. Pu, F. Satoh, S. Kawata, H. Katagiri, H. Sasabe, J. Kido, *Adv. Funct. Mater.* **2013**, 2064-2071.
- [14] C. Liu, Q. Fu, Y. Zou, C. Yang, D. Ma, J. Qin, *Chem. Mater.* **2014**, *26*, 3074-3083.
- [15] J.-H. Jou, S. Kumar, P.-H. Fang, A. Venkateswararao, K. R. J. Thomas, J.-J. Shyue, Y.-C. Wang, T.-H. Li, H.-H. Yu, *J. Mater. Chem. C* **2015**, *3*, 2182-2194.

- [16] X. Wang, L. Zhao, S. Shao, J. Ding, L. Wang, X. Jing, F. Wang, *Macromolecules* **2014**, *47*, 2907-2914.
- [17] J. Santos, J. H. Cook, H. A. Al-Attar, A. P. Monkman, M. R. Bryce, *J. Mater. Chem. C* **2015**, *3*, 2479-2483.
- [18] K. S. Yook, J. Y. Lee, *Adv. Mater.* **2014**, 4218-4233.
- [19] M. Zhu, C. Yang, *Chem. Soc. Rev.* **2013**, *42*, 4963-4976.
- [20] M. Romain, S. Thiery, A. Shirinskaya, C. Declairieux, D. Tondelier, B. Geffroy, O. Jeannin, J. Rault-Berthelot, R. Métivier, C. Poriel, *Angew. Chem. Int. Ed.* **2015**, *54*, 1176-1180.
- [21] N. Cocherel, C. Poriel, J. Rault-Berthelot, F. Barrière, N. Audebrand, A. M. Z. Slawin, L. Vignau, *Chem. Eur. J.* **2008**, *14*, 11328-11342.
- [22] M. Romain, D. Tondelier, J.-C. Vanel, B. Geffroy, O. Jeannin, J. Rault-Berthelot, R. Métivier, C. Poriel, *Angew. Chem. Int. Ed.* **2013**, *125*, 14397-14401.
- [23] M. Romain, D. Tondelier, B. Geffroy, O. Jeannin, E. Jacques, J. Rault-Berthelot, C. Poriel, *Chem. Eur. J.* **2015**, *21*, 9426-9439.
- [24] T. C. Chao, Y. T. Lin, C. Y. Yang, T. S. Hung, H. C. Chou, C. C. Wu, K. T. Wong, *Adv. Mater.* **2005**, *17*, 992-996.
- [25] K.-T. Wong, L.-C. Chi, S.-C. Huang, Y.-L. Liao, Y.-H. Liu, Y. Wang, *Org. Lett.* **2006**, *8*, 5029-5032.
- [26] A. C. Grimsdale, K. Müllen, *Angew. Chem. Int. Ed.* **2005**, *44*, 5592-5629.
- [27] A. C. Grimsdale, K. Müllen, *Macromol. Rapid. Commun.* **2007**, *28*, 1676-1702.
- [28] V. N. Bliznyuk, S. A. Carter, J. C. Scott, G. Klärner, R. D. Miller, D. C. Miller, *Macromolecules* **1999**, *32*, 361-369.
- [29] J.-I. Lee, G. Klärner, R. D. Miller, *Chem. Mater.* **1999**, *11*, 1083-1088.
- [30] L. Romaner, A. Pogantsch, P. Scandiucci de Freitas, U. Scherf, M. Gaal, E. Zojer, E. J. W. List, *Adv. Funct. Mater.* **2003**, *13*, 597-601.
- [31] M. Gaal, E. J. W. List, U. Scherf, *Macromolecules* **2003**, *36*, 4236-4237.
- [32] G. L. Schulz, X. Chen, S.-A. Chen, S. Holdcroft, *Macromolecules* **2006**, *39*, 9157-9165.



# **Chapter VIII. Experimental Section**

## **VIII.1 Reagents and analytical techniques**

### **Materials**

All starting materials, solvents and catalysts were purchased from companies Aldrich, Acros, Fluka, Merck and TIC. All of them were used as received without purification.

### **Chromatography**

Silica gel with particle size of 0.063-0.200 mm or 0.04-0.063 mm was used for preparing column chromatography. A combination of thin layer chromatography (TLC) and ultraviolet Lamp was used as analytical technique. For eluents, the technical hexane was distilled and used together with the analytically pure solvents. Gel permeation chromatography (GPC) was performed on Bio-Beads S-X1beads, provided by Bio-Rad Laboratories Inc. Chloroform (HPLC) was used as eluent.

## NMR spectroscopy

$^1\text{H}$ -NMR,  $^{13}\text{C}$ -NMR,  $^1\text{H},^1\text{H}$ -COSY,  $^1\text{H},^1\text{H}$ -NOESY,  $^1\text{H},^1\text{H}$ -TOCSY and  $^1\text{H},^{13}\text{C}$ -HMBC spectra were recorded in  $\text{CD}_2\text{Cl}_2$ ,  $\text{C}_2\text{D}_2\text{Cl}_4$ ,  $\text{THF-}d_8$ ,  $\text{DMSO-}d_6$  or  $\text{D}_2\text{SO}_4$  on a Bruker DPX 250, 300, 500, 700 or 850 spectrometer. Chemical shifts ( $\delta$ ) were expressed in parts per million (ppm) using tetramethylsilane as internal standard. Unless otherwise stated, the measurements were carried out at room temperature.

## Mass spectrometry

Field-desorption mass (FD-MS) spectra were recorded on a ZAB 2 SE-FPD spectrometer (range 110-3300). High Resolution Mass Spectra (HRMS) were carried out by a maXis ESI-Q-TOF system in Johannes Gutenberg-University, Mainz. Electrospray ionization and matrix assisted laser desorption-ionization (ESI-MALDI) was performed on Bruker Daltonics solariX system in Swiss Federal Institute of Technology, Zurich.

## UV-vis and photoluminescence spectroscopy

UV-vis spectra and photoluminescence spectra were recorded on a Perkin Elmer Lambda 15 spectrophotometer and a SPEX-Fluorolog II (212) spectrometer, respectively. Photoluminescence quantum yields (PLQYs) were measured relative to a fluorescent standard material with a known PLQY. Essentially, solutions of the standard and test samples were prepared with identical absorbance less than 0.1 at the same excitation wavelength. Hence, the PLQYs were calculated through the varying ratio of the integrated fluorescence intensities of the two solutions according to the following equation:

$$\Phi_x = \Phi_s \left( \frac{A_x}{A_s} \right) \left( \frac{\eta_x}{\eta_s} \right)^2$$

Where the subscripts X and S represent test and standard, respectively;  $\Phi$ , A, and  $\eta$  denotes PLQY, the integrated fluorescence intensity, and refractive index of the solvent, respectively.

## Cyclic voltammetry

Cyclic voltammetry measurements were carried out on a computer-controlled GSTAT12 in a three-electrode cell in anhydrous solution of tetrabutylammonium hexafluorophosphate (0.1 M) with a scan rate of 100 mV/s at room temperature, using glassy carbon discs as the working electrode, Pt wire as the counter electrode, Ag/AgCl electrode as the reference electrode. The used solvents were reported for the respective measurement. Ferrocene (Fc) was employed as standard. The HOMO and LUMO energy levels were estimated from the half-wave potential of the first oxidation peak and the first reduction peak, respectively, according to the corresponding equation  $E_{\text{HOMO}} = - [E_{\text{oxd1/2}} - E_{(\text{Fc}^+/\text{Fc})} + 4.8] \text{ eV}$  and  $E_{\text{LUMO}} = - [E_{\text{red1/2}} - E_{(\text{Fc}^+/\text{Fc})} + 4.8] \text{ eV}$ .

## Thermogravimetric analysis and differential scanning calorimetry

Thermogravimetric analysis (TGA) was carried out on a Mettler 500 at a heating rate of 10 °C/min under nitrogen flow. Differential scanning calorimetry (DSC) was performed on a Mettler DSC 30 at a heating/cooling rate of 10 °C/min under nitrogen flow.

## Melting point

Melting points were measured on a Büchi hot stage apparatus (B-545) under ambient atmosphere

## Computational methods

The geometry optimizations were performed using Gaussian 09, Revision B.04 quantum chemistry program at the B3LYP level of theory. 6-31G, 6-31G\* or 6-31G\*\* basis sets were chosen for different molecules.

## **Single crystal X-ray diffraction crystallography**

Single crystal X-ray diffraction measurements and structure solutions were performed by Dr. Dieter Schollmeyer at Johannes Gutenberg-University. The crystallographic data were collected on smart CCD diffractometer with Mo-K $\alpha$  radiation or STOE IPDS 2T diffractometer with Cu-K $\alpha$  radiation. The structures were solved by direct method and refined by a full-matrix program (SHELXL).

## **OFET devices fabrication and measurements**

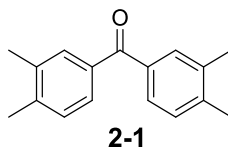
OFETs in this study were fabricated with the bottom-gate/bottom-contact architecture, employing gold as the source/drain electrode and Si/SiO<sub>2</sub> as gate dielectric. The gate dielectric was functionalized by hexamethyldisilazane (HMDS) to minimize interfacial trapping sites. Semiconductors in chloroform were drop-casted on substrates under nitrogen atmosphere, followed by annealing at 120 °C for 30 min. All the electrical measurements were performed in a glovebox using Keithley 4200 SCS under nitrogen atmosphere.

## **OPV devices fabrication and measurements**

Solar cells were fabricated on patterned ITO-coated glass substrates (Präzisions Glas & Optik GmbH, Germany). The samples were treated with an argon plasma before spincoating a ~40 nm thick poly(3,4-ethylene-dioxythiophene):poly(styrenesulfonate) (PEDOT:PSS) (Clevios P VP al 4083, H.C. Stark) layer. The substrates were heated to 120 °C for 30 min in a nitrogen-filled glovebox. The active layer was deposited via spin-coating a 1:1 mixture of donor and acceptor. Subsequent to the active layer deposition, a bilayer of 5 nm calcium and 100 nm aluminum was evaporated through a shadow mask. IV characteristics were obtained under illumination with a solar simulator (K.H. Steuernagel Lichttechnik GmbH, Germany) using a 575 W metal halide lamp in combination with a filter system to create a spectrum according to AM1.5G conditions. Yet, the intensity was at 70 mW cm<sup>-2</sup>. Current-voltage curves were measured with a Keithley 236 Source Measure Unit (SMU) within a glovebox. The light intensity was measured with a calibrated silicon photodiode.

## VIII.2 Material Synthesis

### Bis(3,4-dimethylphenyl)methanone (2-1)



n-Butyllithium (1.60 M solution in hexane, 18.56 mL, 29.70 mmol) was added dropwise to a solution of 4-bromo-1,2-dimethylbenzene (5.00 g, 27.00 mmol) in THF (100 mL) at -78 °C for 40 min. Then, 3, 4-dimethylbenzaldehyde (3.76 mL, 28.35 mmol) was added to the mixture at -78 °C and the obtained mixture was stirred at room temperature overnight. After removal of the solvent, I<sub>2</sub> (6.85 g, 43.20 mmol), K<sub>2</sub>CO<sub>3</sub> (11.18 g, 81.00 mmol), and *t*-BuOH (70 mL) were added and the obtained mixture was stirred at a refluxing condition for 8 h. The reaction mixture was quenched with 100 mL Na<sub>2</sub>SO<sub>3</sub> solution and was extracted with 200 mL dichloromethane three times. The organic layer was washed with brine three times and dried over Na<sub>2</sub>SO<sub>4</sub> for 6 hours. The solvent had been completely removed by rotary evaporator, affording 6.10 g product white powder in a yield of 95%.

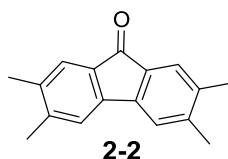
<sup>1</sup>H NMR (250 MHz, C<sub>2</sub>D<sub>2</sub>Cl<sub>2</sub>): δ 7.60 (s, 2H), 7.52 (dd, *J* = 7.8, 1.9 Hz, 2H), 7.28 (d, *J* = 7.7 Hz, 2H), 2.39 (s, 6H), 2.37 (s, 6H).

<sup>13</sup>C NMR (63 MHz, C<sub>2</sub>D<sub>2</sub>Cl<sub>2</sub>): δ 196.61, 142.07, 137.14, 136.10, 131.29, 129.63, 128.09, 20.12, 19.91.

HR-MS (MALDI) *m/z*: calculated for C<sub>17</sub>H<sub>19</sub>O [M<sup>+</sup>] 239.1430. Found 239.1430.

Elemental analysis for C<sub>17</sub>H<sub>18</sub>O: calculated: C, 85.67; H, 7.61. Found: C, 85.68; H, 7.67.

Melting point: 145.0 – 145.7 °C.

**2,3,6,7-Tetramethyl-9H-fluoren-9-one (2-2)**

Under air atmosphere, palladium acetate (100 mg, 0.44 mmol),  $\text{Ag}_2\text{CO}_3$  (3.06 g, 13.23 mmol),  $\text{K}_2\text{CO}_3$  (3.04 g, 22.65 mmol) and **2-1** (2.10 g, 8.82 mmol) were added into a Schlenktube dried by a hot-gun. The tube was stopped and degassed with argon for three times. Then, trifluoroacetic acid (20.00 mL, 262 mmol) was added by syringe. The mixture was stirred under argon atmosphere at 140 °C for 24 h. Then the mixture was cooled down to room temperature and 500 mL water was added and extracted by 200 mL dichloromethane three times, further purified by flash chromatography on silica gel with dichloromethane as eluent to give the product (1.56 g, 75%) as yellow solid.

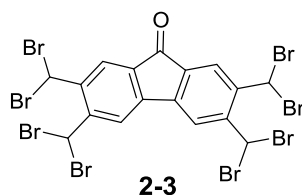
$^1\text{H NMR}$  (250 MHz,  $\text{C}_2\text{D}_2\text{Cl}_2$ ):  $\delta$  7.25 (s, 2H), 7.17 (s, 2H), 2.24 (s, 6H), 2.19 (s, 6H).

$^{13}\text{C NMR}$  (63 MHz,  $\text{C}_2\text{D}_2\text{Cl}_2$ ):  $\delta$  194.24, 144.34, 142.93, 137.49, 133.01, 125.33, 121.73, 20.83, 19.98.

**HR-MS** (MALDI)  $m/z$ : calculated for  $\text{C}_{17}\text{H}_{16}\text{O}$  [ $\text{M}^+$ ] 236.1196. Found 236.1196.

**Elemental analysis** for  $\text{C}_{17}\text{H}_{16}\text{O}$ : calculated: C, 86.40; H, 6.82. Found: C, 86.29; H, 7.09.

**Melting point**: 229.2 – 229.9 °C.

**2,3,6,7-Tetrakis(dibromomethyl)-9H-fluoren-9-one (2-3)**

The tetramethyl fluorenone **2-2** (0.36 g, 1.56 mmol) was added into a flask filled with Ar. Then,  $\text{CCl}_4$  (25 mL) was injected. The mixture was heated to reflux and irradiated

with a 250 W light bulb. Bromine (3.22 mL, 62.3 mmol) was slowly added dropwise to the solution. After 2 days, the mixture was cooled down to room temperature and the yellow product was collected by filtration and washed with chloroform to give the product **2-3** 1.10 g with a 81% yield.

$^1\text{H NMR}$  (250 MHz, THF- $d_8$ ):  $\delta$  8.49 (s, 1H), 8.11 (s, 1H), 7.64 (s, 1H), 7.59 (s, 1H).

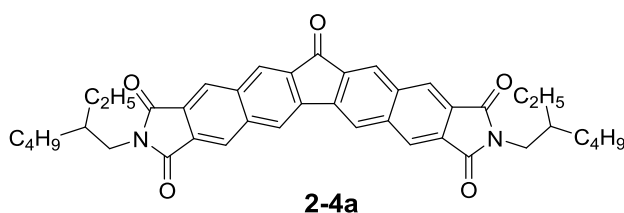
$^{13}\text{C NMR}$  (63 MHz, THF- $d_8$ ):  $\delta$  188.35, 143.87, 138.81, 135.62, 124.60, 123.51, 123.22, 35.66.

**HR-MS** (MALDI)  $m/z$  calculated for  $\text{C}_{17}\text{H}_9\text{Br}_8\text{O}$  [ $\text{M}^+$ ] 860.4415. Found 860.4127.

**Elemental analysis** for  $\text{C}_{17}\text{H}_8\text{Br}_8\text{O}$ : calculated: C, 23.54; H, 0.93. Found: C, 23.54; H, 0.68.

**Melting point**: 288.6 – 289.5 °C, decomposed.

### 2,9-Bis(2-ethylhexyl)-1H-fluoreno[2,3-f:6,7-f']diisoindole-1,3,8,10,13(2H,9H)-pentaone (**2-4a**)



To a solution of **2-3** (0.46 g, 0.53 mmol) in dry DMAc (15 mL), NaI (0.79 g, 5.30 mmol) and maleimide (R= 2-ethylhexyl) (0.28 g, 1.32 mmol) were added. Then the mixture was heated at 80 °C under Ar for 20 hours. After cooling, 20 mL water was added into the mixture. The product was collected by filtration, and washed with 30 mL water four times. The compound **2-4a** was purified by short column chromatography with THF as eluent to give the product **2-4a** in 67% yield.

$^1\text{H NMR}$  (500 MHz,  $\text{C}_2\text{D}_2\text{Cl}_2$ ):  $\delta$  8.47 (s, 2H), 8.40 (s, 2H), 8.38 (s, 2H), 8.37 (s, 2H), 3.68 (d,  $J = 7.0$  Hz, 4H), 1.90 – 1.96 (m, 2H), 1.44 – 1.28 (m, 16H), 0.98 (t,  $J = 7.4$  Hz, 6H), 0.92 (t,  $J = 6.6$  Hz, 6H).

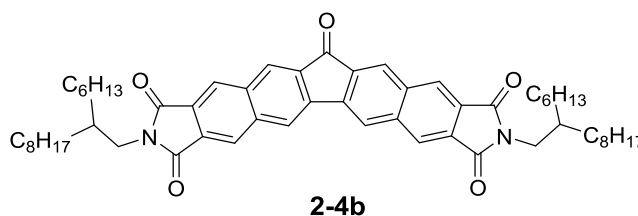
**$^{13}\text{C}$  NMR** (126 MHz,  $\text{C}_2\text{D}_2\text{Cl}_2$ ):  $\delta$  190.18, 167.39, 167.33, 140.81, 139.77, 136.56, 136.13, 131.19, 129.49, 127.29, 126.36, 124.53, 122.37, 42.72, 38.64, 31.06, 28.73, 24.43, 22.88, 13.84, 10.59.

**HR-MS** (MALDI)  $m/z$  calculated for  $\text{C}_{41}\text{H}_{43}\text{N}_2\text{O}_5$  [ $\text{M}^+$ ] 643.3166. Found 643.3166.

**Elemental analysis** for  $\text{C}_{41}\text{H}_{43}\text{N}_2\text{O}_5$ : calculated: C, 76.61; H, 6.59; N, 4.36. Found: C, 75.41; H, 6.93; N, 4.26.

**Melting point:** 359.0 – 359.7 °C.

**2,9-Bis(2-hexyldecyl)-1H-fluoreno[2,3-f:6,7-f']diisoindole-1,3,8,10,13(2H,9H)-pentaone (2-4b)**



Compound **2-4b** was synthesized according to the previously method used to synthesize **2-4a**. Yield: 72%.

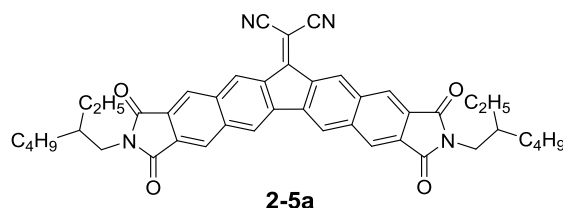
**$^1\text{H}$  NMR** (250 MHz,  $\text{C}_2\text{D}_2\text{Cl}_4$ ):  $\delta$  8.45 (s, 2H), 8.37 (s, 4H), 8.36 (s, 2H), 3.60 (d,  $J$  = 7.2 Hz, 4H), 1.81 – 1.88 (m, 2H), 1.35 – 1.21 (m, 48H), 0.80 – 0.84 (m, 12H).

**$^{13}\text{C}$  NMR** (63 MHz,  $\text{C}_2\text{D}_2\text{Cl}_2$ ):  $\delta$  190.83, 167.85, 167.78, 140.95, 139.89, 136.60, 136.12, 131.29, 129.57, 127.42, 126.50, 124.83, 122.84, 43.05, 37.47, 32.30, 32.23, 31.91, 30.37, 30.06, 29.96, 29.71, 26.68, 26.65, 23.07, 23.06, 23.06, 14.27, 14.26.

**HR-MS** (MALDI)  $m/z$  calculated for  $\text{C}_{57}\text{H}_{75}\text{N}_2\text{O}_5$  [ $\text{M}^+$ ] 867.5670. Found 867.5671.

**Elemental analysis** for  $\text{C}_{57}\text{H}_{75}\text{N}_2\text{O}_5$ : calculated: C, 78.94; H, 8.60; N, 3.23. Found: C, 78.57; H, 8.99; N, 3.17.

**Melting point:** 235.2 – 235.8 °C.

**2-(2,9-Bis(2-ethylhexyl)-1,3,8,10-tetraoxo-1,2,3,8,9,10-hexahydro-13H-fluoreno[2,3-f:6,7-f']diisoindol-13-ylidene)malononitrile (2-5a)**

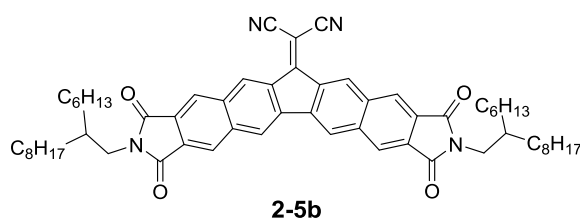
To a stirred mixture of **2-4a** (90 mg, 140  $\mu\text{mol}$ ) and malononitrile (28 mg, 420  $\mu\text{mol}$ ) in 60 mL  $\text{CHCl}_3$  was slowly added 1 mol/L  $\text{TiCl}_4$  (0.42 mL, 420  $\mu\text{mol}$ ) followed by dried pyridine (66 mg, 840  $\mu\text{mol}$ ). The mixture was refluxed for 36 hours under Ar. Every 5 hours, identical amounts of malononitrile,  $\text{TiCl}_4$  and pyridine were added. After cooling down, the mixture was poured on ice/water and extracted with DCM. The combined organic layers were dried with  $\text{Na}_2\text{SO}_4$  for five hrs. The solvent was removed under vacuum and the residue was purified by column chromatography using DCM/Methanol (200:1) as eluent to obtain **2-5a** as orange solid. Finally the solid was washed with 300 mL acetone to give the pure product in a 74% yield.

**$^1\text{H NMR}$**  (250 MHz,  $\text{CD}_2\text{Cl}_2$ ):  $\delta$  9.17 (s, 2H), 8.39 (s, 4H), 8.32 (s, 2H), 3.57 (d,  $J = 7.5$  Hz, 4H), 1.78 – 1.82 (m, 2H), 1.19 – 1.32 (m, 16H), 0.79 – 0.89 (m, 12H).

**$^{13}\text{C NMR}$**  (63 MHz,  $\text{C}_2\text{D}_2\text{Cl}_2$ ):  $\delta$  167.78, 167.66, 139.62, 139.24, 136.36, 135.94, 131.97, 130.55, 129.97, 126.68, 124.73, 122.94, 113.74, 77.29, 42.70, 38.77, 30.95, 28.92, 24.28, 23.41, 14.24, 10.61.

**HRMS** (TOF MS ES<sup>+</sup>):  $m/z$  calculated for  $\text{C}_{44}\text{H}_{43}\text{N}_4\text{O}_4$  691.3284. Found 691.33254.

**Melting point:** 359.1 – 359.6  $^\circ\text{C}$ .

**2-(2,9-Bis(2-hexyldecyl)-1,3,8,10-tetraoxo-1,2,3,8,9,10-hexahydro-13H-fluoreno[2,3-f:6,7-f']diisoindol-13-ylidene)malononitrile (2-5b)**

Compound **2-5b** was synthesized according to the previously method used to synthesize **2-5a**. Yield: 80%.

**<sup>1</sup>H NMR** (250 MHz, C<sub>2</sub>D<sub>2</sub>Cl<sub>4</sub>): δ 9.19 (s, 2H), 8.43 (s, 2H), 8.41 (s, 2H), 8.36 (s, 2H), 3.62 (d, J = 7.2 Hz, 4H), 1.84 – 1.88 (m, 2H), 1.21 – 1.28(m, 48H), 0.80 – 0.85 (m, 12H).

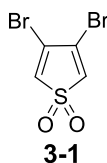
**<sup>13</sup>C NMR** (63 MHz, C<sub>2</sub>D<sub>2</sub>Cl<sub>2</sub>): δ 167.64, 167.52, 139.45, 139.13, 136.26, 135.74, 131.98, 130.41, 129.98, 126.57, 124.65, 122.85, 113.62, 77.23, 32.30, 32.23, 31.90, 30.37, 30.05, 29.96, 29.71, 26.67, 23.08, 23.06, 14.28, 14.26.

**HRMS** (TOF MS ES<sup>+</sup>): m/z calculated for C<sub>60</sub>H<sub>75</sub>N<sub>4</sub>O<sub>4</sub> 915.5788. Found 915.5759.

**Melting point:** 266.2 – 266.9 °C.

**Crystallographic data** (CCDC deposition number): CCDC 1042607

### 3,4-Dibromothiophene 1,1-dioxide (**3-1**)



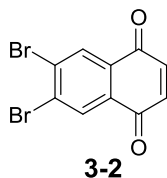
**3-1** was prepared using a modified procedure reported by Bailey. A flask equipped with a dropping funnel was charged with 30% H<sub>2</sub>O<sub>2</sub> 33 mL and the mixture was stirred in ice bath. Then, trifluoroacetic anhydride (70 mL, 517 mmol) was added dropwise. 30 minutes later, (10 g, 41 mmol) of 3,4-dibromothiophene in 50 mL of dichloromethane was added all at once. The reaction mixture was allowed to warm to room temperature and stirred for 2.5 h. The saturated sodium carbonate was slowly added to bring the pH up to around 9. The mixture was extracted with dichloromethane (3 × 50 mL) and dried over anhydrous sodium sulfate, filtered, and then the solvent was completely removed. The remaining yellowish-orange oil was mixed with dichloromethane and hexane. After 2 hours, pale yellow crystals were collected. (7.5 g, 67% yield).

**<sup>1</sup>H-NMR** (250 MHz, CD<sub>2</sub>Cl<sub>2</sub>): δ 6.80 (s, 2H).

$^{13}\text{C}$  NMR (75 MHz,  $\text{C}_2\text{D}_2\text{Cl}_2$ ):  $\delta$  131.00, 129.23.

FD-Mass (8 KV): calculated for  $\text{C}_4\text{H}_2\text{Br}_2\text{O}_2\text{S}$  273.93. Found 274.0

### 6,7-Dibromonaphthalene-1,4-dione (**3-2**)



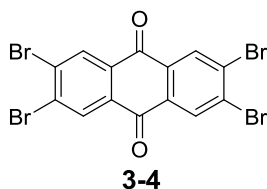
**3-1** (7.5 g, 27 mmol) and benzoquinone (5.3 g, 49 mmol) were dissolved in 400ml acetic acid and refluxed for 14 hours. The solution was poured into water. The mixture was extracted with dichloromethane (3  $\times$  50 mL). Then, the organic layer was washed with water three times, dried over anhydrous sodium sulfate, filtered, and then the solvent was completely removed. **3-2** was purified by column chromatography using Hex/EA (10:1) as eluent and the product was washed with acetone to yield an off-white solid. (3 g, 35% yield).

$^1\text{H}$ -NMR (250 MHz,  $\text{CD}_2\text{Cl}_2$ ):  $\delta$  8.22 (s, 2H), 6.91(s, 2H).

$^{13}\text{C}$  NMR (75 MHz,  $\text{C}_2\text{D}_2\text{Cl}_2$ ):  $\delta$  183.60, 138.97, 132.04, 131.92, 131.60.

FD-Mass (8 KV): calculated for  $\text{C}_{10}\text{H}_4\text{Br}_2\text{O}_2$  315.95. Found 316.0.

### 2,3,6,7-Tetrabromoanthracene-9,10-dione (**3-4**)



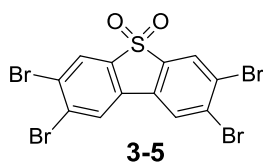
3,4-Dibromothiophene 1,1-dioxide (**3-1**) (5.0 g, 18.3 mmol) and 6,7-dibromonaphthalene-1,4-dione (**3-2**) (0.90 g, 8.29 mmol) were dissolved in 200 mL acetic acid and refluxed for 24 hours. After the reaction, around 150 mL solvent was evaporated and then 150 mL of water were poured into the mixture. The mixture was

filtered, and then the solid washed with acetone to yield black color product **3-4** 0.8 g with 18% yield. The major byproduct of this reaction is 3-bromobenzo[b]thiophene 1,1-dioxide **3-3**, which can also be obtained by the Diels–Alder reaction of 3,4-dibromothiophene 1,1-dioxide itself with the acetic acid reflux method. Purification of compound **3-4** was difficult owing to its low solubility in most organic solvents.

**FD-Mass:** calculated for  $C_{14}H_4Br_4O_2$  523.80. Found 523.8.

**Melting point** has not been observed below 300 °C.

### 2,3,7,8-Tetrabromodibenzo[b,d]thiophene 5,5-dioxide (**3-5**)



3-Bromobenzo[b]thiophene 1,1-dioxide (**3-3**) (2.0 g, 5.0 mmol) and 3,4-dibromothiophene 1,1-dioxide (**3-1**) (1.64 g, 5.97 mmol) was mixed together and reflux in acetic acid for 48 hours. Solid was formed, followed by the filtration. 300 mg crude product is obtained with 13% yield.

$^1\text{H NMR}$  (250 MHz, THF-*d*8):  $\delta$  8.52 (s, 2H), 7.38 (s, 2H).

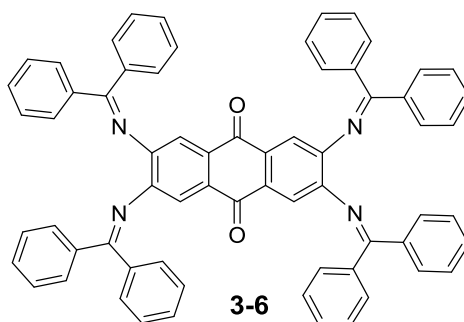
$^{13}\text{C NMR}$  spectra cannot be obtained due to the bad solubility.

**FD-Mass:** calculated for  $C_{12}H_4Br_4O_2S$  527.7. Found 528.0.

**MALDI-ESI:** calculated for  $C_{12}H_4NaO_2S$  550.6558. Found 550.6553.

**Melting point** has not been observed below 300 °C.

**3-6** and **3-7** were synthesized using the following general method, taking **3-6** for example.

**2,3,6,7-Tetrakis((diphenylmethylene)amino)anthracene-9,10-dione (3-6)**

A mixture of tris(dibenzylideneacetone)dipalladium(0) (40 mg, 0.045 mmol), *rac*-BINAP (56 mg, 0.09 mmol) and toluene (15 mL) was stirred at 110 °C for 0.5 h under argon. After cooling at RT, the mixture was added with benzophenone imine (0.19 mL, 1.20 mmol), sodium *tert*-butoxide (0.12 g, 1.21 mmol), and **3-4** (0.10 g, 0.19 mmol). The mixture was stirred at 110 °C overnight. After the reaction, toluene was evaporated, then the residue was subjected to column chromatography on silica gel with Hex/EA (4:1), including 1% trimethylamine (avoiding decomposition) as eluent to afford light green solid (90 mg, 51%).

**<sup>1</sup>H NMR** (700 MHz, CD<sub>2</sub>Cl<sub>2</sub>): δ 7.73 (s, 8H), 7.48 (s, 4H), 7.40 – 7.33 (m, 20H), 7.25 (s, 4H), 7.17 (s, 4H).

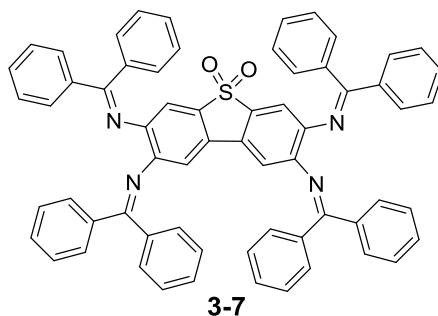
**<sup>13</sup>C NMR** (176 MHz, CD<sub>2</sub>Cl<sub>2</sub>): δ 181.48, 168.84, 147.60, 138.69, 136.10, 131.01, 129.63, 129.53, 129.26, 128.49, 128.49, 128.04, 118.11.

**HRMS** (TOF MS ES<sup>+</sup>): *m/z* calculated for C<sub>66</sub>H<sub>45</sub>N<sub>4</sub>O<sub>2</sub> 925.3543. Found 925.3533.

**Melting point:** 268 – 270 °C, decomposed.

**Crystallographic data** (CCDC deposition number): CCDC 1410009.

**2,3,7,8-Tetrakis((diphenylmethylene)amino)dibenzo[b,d]thiophene 5,5-dioxide (3-7)**



Yield: 74%.

**<sup>1</sup>H NMR** (700 MHz, CD<sub>2</sub>Cl<sub>2</sub>): δ 7.78 – 7.65 (m, 8H), 7.54 – 7.44 (m, 4H), 7.43 – 7.31 (m, 20H), 7.20 (s, 4H), 7.03 (dd, *J* = 11.4, 7.2 Hz, 4H), 6.69 (d, *J* = 7.0 Hz, 2H), 6.62 (d, *J* = 7.0 Hz, 2H).

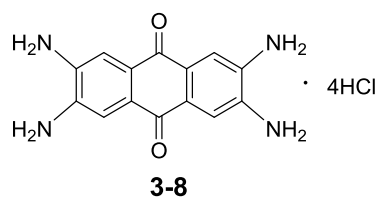
**<sup>13</sup>C NMR** (176 MHz, CD<sub>2</sub>Cl<sub>2</sub>): 169.05, 147.99, 142.35, 138.98, 138.85, 136.25, 135.81, 132.49, 131.04, 130.94, 129.50, 129.44, 129.35, 129.24, 128.85, 128.84, 128.11, 128.05, 127.14, 113.51, 112.54.

**HRMS** (TOF MS ES<sup>+</sup>): *m/z* calculated for C<sub>64</sub>H<sub>45</sub>N<sub>4</sub>O<sub>2</sub>S 933.3263. Found 933.3260.

**Melting point:** 258 – 260 °C, decomposed.

**3-8 and 3-9** were synthesized using the following general method, taking **3-8** for example.

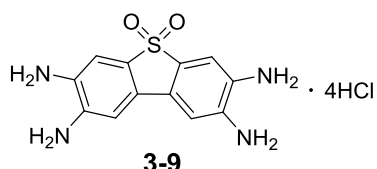
**2,3,6,7-Tetraaminoanthracene-9,10-dione (3-8)**



3 mL 2 mol/L Hydrochloric acid was added to a 30ml THF solution of **3-6** (0.30 g, 0.32 mmol). The mixture was stirred for 10 h at RT. Then the THF was evaporated

and residue was dried under freeze drier condition. The dark color solid was washed with hexane to give the rough product 80 mg with 60% yield. The rough product was used directly as the starting material in the next reaction without further purification.

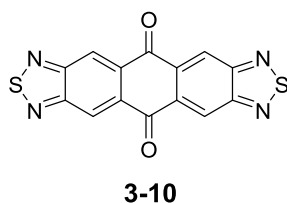
### 2,3,7,8-Tetraaminodibenzo[b,d]thiophene 5,5-dioxide (3-9)



Yield: 67%.

**3-10** and **3-11** were synthesized using the following general method, taking **3-10** for example.

### 5H,11H-Anthra[2,3-c:6,7-c']bis([1,2,5]thiadiazole)-5,11-dione (3-10)



**3-8** (25 mg, 0.06 mmol) was dissolved in 10 mL pyridine, then N-sulfinylaniline (0.04 mL, 0.38 mmol) and chlorotrimethylsilane (0.05 mL, 0.41 mmol) were added. The mixture was stirred under argon at 80 °C overnight. After the reaction, the mixture was filtrated. The affording material on filter paper was washed with acetone to give light yellow solid product (18 mg, 92%).

$^1\text{H NMR}$  (250 MHz,  $\text{D}_2\text{SO}_4$ ):  $\delta$  9.22 (s, 4H).

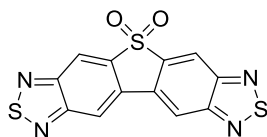
$^{13}\text{C NMR}$  (63 MHz,  $\text{D}_2\text{SO}_4$ ):  $\delta$  182.13, 150.64, 136.73, 123.78.

**HR-MS** (MALDI)  $m/z$  calculated for  $\text{C}_{14}\text{H}_4\text{N}_4\text{O}_2\text{S}_2$  [ $\text{M}^+$ ] 323.9776. Found 324.9847.

**Melting point** has not been observed below 300 °C.

**Crystallographic data** (CCDC deposition number): CCDC 1400306.

**Dibenzo[1,2,5]thiadiazolethiophene 5,5-dioxide (3-11)**



**3-11**

Yield: 80%.

**<sup>1</sup>H NMR** (500 MHz, D<sub>2</sub>SO<sub>4</sub>): δ 8.87 (s, 2H), 8.84 (s, 2H).

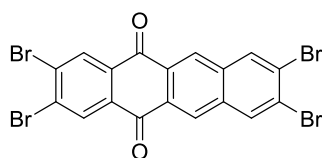
**<sup>13</sup>C NMR** (126 MHz, D<sub>2</sub>SO<sub>4</sub>): δ 144.79, 143.13, 135.93, 129.01, 113.16, 109.07.

**HR-MS** (MALDI) m/z calculated for C<sub>12</sub>H<sub>4</sub>N<sub>4</sub>O<sub>2</sub>S<sub>3</sub> [M<sup>+</sup>] 331.9496. Found 332.2009.

**Melting point** has not been observed below 300 °C.

**Crystallographic data** (CCDC deposition number): CCDC 1400305.

**2,3,8,9-Tetrabromo-5,12- tetracenequinone (4-1)**



**4-1**

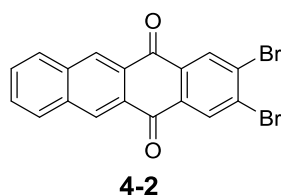
To a flame-dried flask cooled under nitrogen was added α,α,α',α',4,5-Hexabromo-o-xylene (2.8 g, 4.8 mmol), **3-2** (1.5 g, 4.7 mmol), and sodium iodide (3.65 g, 24.4 mmol). Then the dry dimethylacetamide (60 mL) was added. The mixture was stirred at 90 °C for 48 h. The mixture was then filtered, and the yellow solid was rinsed with water and acetone. The yellow solid was then dried under vacuum, which is insoluble in normal organic solvents (1.5 g, 56% yield).

$^1\text{H}$  NMR and  $^{13}\text{C}$  NMR spectra cannot be obtained because of the bad solubility of the compound.

**MALDI-TOF:** Calculated for  $\text{C}_{18}\text{H}_6\text{Br}_4\text{O}_2$  573.86. Found 573.66.

**Melting point** has not been observed below 300 °C.

### 2,3-Dibromo-5,12- tetracenequinone (4-2)



To a flame-dried flask cooled under nitrogen was added 1,2-bis(dibromomethyl)benzene (0.64 g, 1.52 mmol), **3-2** (0.40 g, 1.27 mmol), and sodium iodide (0.94 g, 6.35 mmol). Then the dry dimethylacetamide (15 mL) was added. The mixture was stirred at 90 °C for 24 h. 20 mL acetone was added. The mixture was then filtered, and the yellow solid was rinsed with water and acetone. The yellow solid was then dried under vacuum, yield 72%.

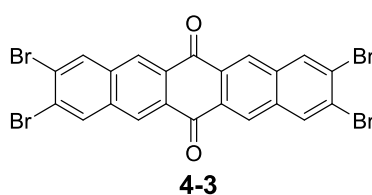
$^1\text{H-NMR}$  (250 MHz,  $\text{C}_2\text{D}_2\text{Cl}_4$ ):  $\delta$  8.84 (s, 2H), 8.59 (d,  $J = 1.5$  Hz, 2H), 8.11 (dd,  $J = 6.2, 3.3$  Hz, 2H), 7.72 (dd,  $J = 6.3, 3.2$  Hz, 2H).

$^{13}\text{C}$  NMR (63 MHz,  $\text{C}_2\text{D}_2\text{Cl}_4$ ):  $\delta$  181.01, 135.46, 134.10, 132.69, 132.09, 130.16, 129.84, 129.379, 129.60.

**HRMS** (TOF MS ES<sup>+</sup>):  $m/z$  calculated for  $\text{C}_{16}\text{H}_8\text{O}_2\text{Br}_2\text{Na}$  436.8789. Found 436.8789.

**Melting point** has not been observed below 300 °C.

### 3,4,10,11-Tetrabromo-7,14- pentacenequinone (4-3)



**4-3** was prepared according to the reported procedure.

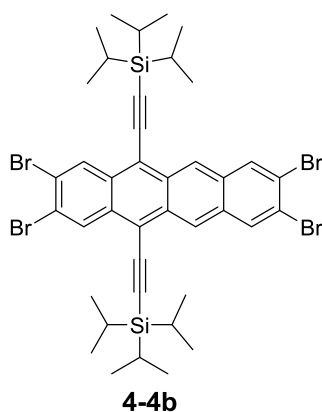
A dried round bottom flask was added 50 mL of dry N,N-dimethylacetamide. The solvent was purged for 30 minutes with argon. 4,5-Dibromo- $\alpha,\alpha,\alpha',\alpha'$ -tetrabromo-o-xylene (5.00 g, 8.63 mmol) was added to the mixture, followed by 1,4-benzoquinone (0.45 g, 4.30 mmol), and NaI (6.5g, 44 mmol). The mixture was stirred vigorously at 90°C for 30 hours. Water was added to the reaction mixture and then filtered. The crude yellow solid was rinsed with water and acetone separately. 0.84 g target compound was obtained in a yield of 31%.

**FD-Mass** (8KV): calculated for C<sub>22</sub>H<sub>8</sub>Br<sub>4</sub>O<sub>2</sub> 623.92. Found: 623.9.

**Melting point** has not been observed below 300 °C.

**4-4(a-d)** were synthesized using the following general method, taking **4-4b** for example.

**2,3,8,9-Tetrabromo-5,12-bis-(triisopropylsilylethynyl)tetracene (4-4b)**



To a flame-dried flask cooled under nitrogen was added dry ether 35 mL in ice bath. Triisopropylsilyl acetylene (1.2 mL, 5.8 mmol) was then added to the flask, followed by n-BuLi (2.2 mL, 3.4 mmol). The mixture was stirred for 35 minutes, and then 2,3,8,9-tetrabromo-5,11-tetracenequinone (0.5 g, 0.87 mmol) was added to the mixture, followed by 35 mL of anhydrous THF. The mixture was stirred over night at room temperature. The mixture was then quenched with wet ether, and the solvent

was evaporated. The diol was dissolved in THF/CH<sub>3</sub>CN and stannous chloride was added until the mixture turned a dark purple color. The reaction was stirred for six hours at room temperature, and then the solvent was evaporated. The residue was dissolved in DCM and filtered through a short silica column. The crude product was further purified by column chromatography with hexane as the eluent to afford dark purple solid 0.7 g in a yield of 89%.

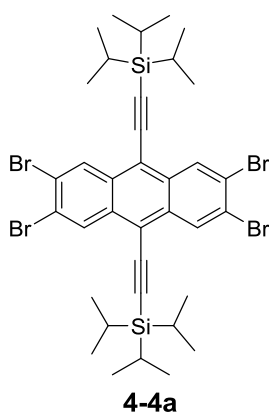
**<sup>1</sup>H-NMR** (250 MHz, CD<sub>2</sub>Cl<sub>2</sub>): δ 9.19 (s, 2H), 9.02 (s, 2H), 8.41 (s, 2H), 1.32 – 1.40 (m, 42H).

**<sup>13</sup>C NMR** (126 MHz, CD<sub>2</sub>Cl<sub>2</sub>): δ 132.59, 132.10, 131.92, 131.46, 130.58, 126.02, 124.10, 122.89, 118.29, 108.32, 102.36, 18.68, 11.53.

**HRMS** (TOF MS ES+): m/z calculated for C<sub>40</sub>H<sub>49</sub>Si<sub>2</sub>Br<sub>4</sub> 901.0106. Found 901.0106.

**Melting point** has not been observed below 300 °C.

### 2,3,7,8-Tetrabromo-5,10-bis-(triisopropylsilylethynyl)anthracene (4-4a)



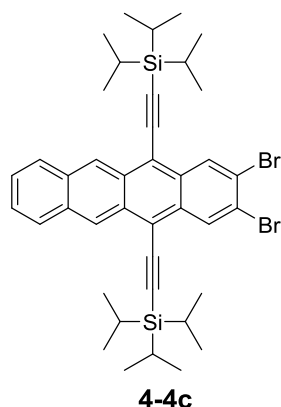
Yield: 42%.

**<sup>1</sup>H NMR** (250 MHz, CD<sub>2</sub>Cl<sub>2</sub>): δ 8.84 (s, 4H), 1.15 – 1.26 (m, 42H).

**<sup>13</sup>C NMR** (63 MHz, CD<sub>2</sub>Cl<sub>2</sub>): δ 132.34, 132.26, 125.01, 117.62, 108.24, 101.63, 18.97, 11.83.

**HRMS** (TOF MS ES+): m/z calculated for C<sub>36</sub>H<sub>47</sub>Si<sub>2</sub>Br<sub>4</sub> 850.9950. Found 850.9949.

**Melting point** has not been observed below 300 °C.

**2,3-Dibromo-5,12-bis-(triisopropylsilylethynyl)tetracene (4-4c)**

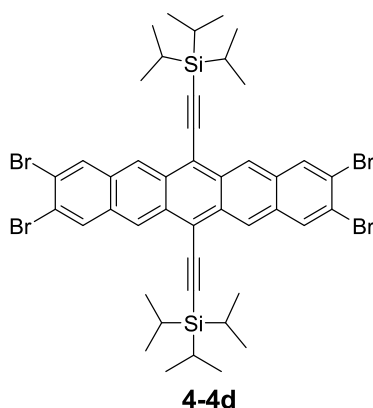
Yield: 62%.

**<sup>1</sup>H-NMR** (250 MHz, CD<sub>2</sub>Cl<sub>2</sub>): δ 9.17 (s, 2H), 8.90 (s, 2H), 7.95 (dd, J = 6.5, 3.3 Hz, 2H), 7.43 (dd, J = 6.5, 3.3 Hz, 2H), 1.21 – 1.26 (m, 42H).

**<sup>13</sup>C NMR** (63 MHz, C<sub>2</sub>D<sub>2</sub>Cl<sub>4</sub>): δ 133.02, 132.27, 131.99, 130.61, 128.85, 127.04, 126.88, 123.78, 118.39, 107.94, 103.18, 19.07, 11.95.

**HRMS** (TOF MS ES<sup>+</sup>): m/z calculated for C<sub>40</sub>H<sub>50</sub>Si<sub>2</sub>Br<sub>2</sub> 744.1818. Found 744.1833.

**Melting point:** 293.1 – 294.2 °C.

**3, 4, 10, 11-Tetrabromo-7, 14-bis-(triisopropylsilylethynyl)pentacene (4-4d)**

Yield: 60%.

**<sup>1</sup>H NMR** (250 MHz, CD<sub>2</sub>Cl<sub>2</sub>): δ 9.13 (s, 2H), 8.25 (s, 2H), 1.25 – 1.33(m, 42H).

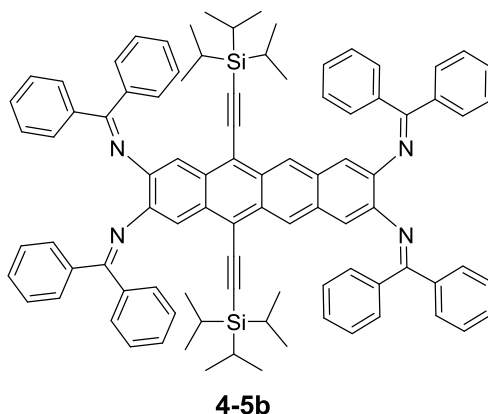
**<sup>13</sup>C NMR** (63 MHz, CD<sub>2</sub>Cl<sub>2</sub>) δ 132.64, 131.33, 131.01, 125.97, 122.73, 119.18, 108.84, 103.71, 19.03, 11.61.

**HRMS** (TOF MS ES<sup>+</sup>): *m/z* calculated for C<sub>44</sub>H<sub>51</sub>Si<sub>2</sub>Br<sub>4</sub> 951.0263. Found 951.0276.

**Melting point** has not been observed below 300 °C.

**4-5(a-d)** were synthesized using the following general method, taking **4-5b** for example.

***N*<sup>2</sup>,*N*<sup>3</sup>,*N*<sup>8</sup>,*N*<sup>9</sup>-Tetrakis(diphenylmethylene)amina-5,12-bis-(triisopropylsilylethynyl) tetracene (4-5b)**



A mixture of tris(dibenzylideneacetone)dipalladium(0) (62 mg, 0.07 mmol), *rac*-BINAP (84 mg, 0.14 mmol) and toluene (10 mL) was stirred at 110 °C for 0.5 h under argon. After cooling at r.t., the mixture was added with benzophenone imine (0.3 mL, 1.75 mmol), sodium *tert*-butoxide (0.17 g, 1.75 mmol), and **4-4b** (0.25 g, 0.28 mmol). The mixture was stirred at 110 °C overnight. After the reaction, toluene was evaporated, then the residue was subjected to column chromatography on silica gel with Hex/EA (10:1), including 1% trimethylamine (avoiding decomposition) as eluent to afford dark purple solid 0.22 g in a yield of 65%.

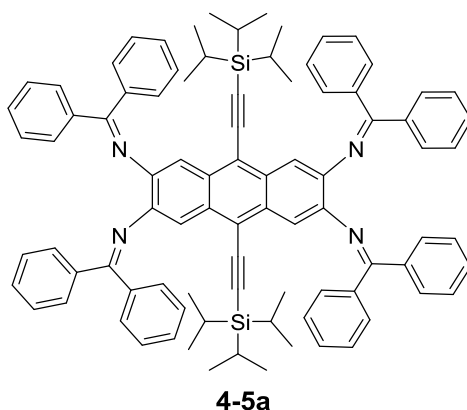
**<sup>1</sup>H-NMR** (700 MHz, CD<sub>2</sub>Cl<sub>2</sub>): δ 8.67 (s, 2H), 7.80 (d, *J* = 7.00 Hz, 8H), 7.47 – 7.50 (m, 8H), 7.43 (d, *J* = 7.00Hz, 8H), 7.42 (s, 2H), 7.31 (s, 16H), 6.89 (s, 2H), 1.25 – 1.30 (m, 42H).

**<sup>13</sup>C NMR** (126 MHz, CD<sub>2</sub>Cl<sub>2</sub>): δ 168.08, 146.72, 144.98, 139.34, 139.20, 136.52, 136.31, 130.69, 130.60, 129.96, 129.52, 129.42, 129.10, 129.03, 128.88, 128.78, 128.08, 127.93, 123.61, 115.66, 114.88, 112.74, 104.21, 104.11, 18.73, 11.56.

**HRMS** (TOF MS ES+):  $m/z$  calculated for  $C_{92}H_{88}Si_2N_4$  1304.6547. Found 1304.6587.

**Melting point** has not been observed below 300 °C.

**$N^2, N^3, N^7, N^8$ -Tetrakis(diphenylmethylene)amina-5,10-bis-(triisopropylsilylethynyl)anthracene (4-5a)**



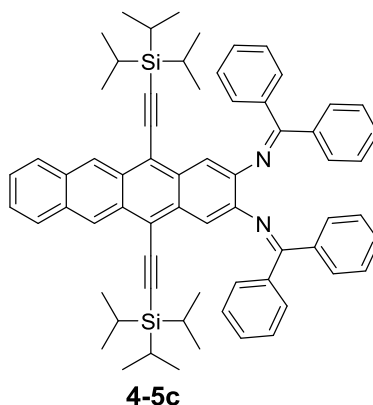
Yield: 60%.

**$^1H$  NMR** (500 MHz,  $CD_2Cl_2$ ):  $\delta$  7.64 (d,  $J = 7.6$  Hz, 8H), 7.35 (t,  $J = 7.3$  Hz, 4H), 7.31 – 7.26 (m, 16H), 7.17 (s, 4H), 7.17 – 7.14 (m, 12H), 1.03 – 1.09 (m, 42H).

**$^{13}C$  NMR** (63 MHz,  $CD_2Cl_2$ ):  $\delta$  168.58, 146.48, 139.65, 136.66, 131.00, 129.92, 129.86, 129.38, 129.22, 128.41, 128.21, 115.49, 113.19, 104.00, 103.04, 19.09, 11.86.

**HRMS** (TOF MS ES+):  $m/z$  calculated for  $C_{88}H_{87}Si_2N_4$  1255.6469. Found 1255.6434.

**Melting point** has not been observed below 300 °C.

***N*<sup>2</sup>,*N*<sup>3</sup>-Tetrakis(diphenylmethylene)amina-5,12-bis-(triisopropylsilylethynyl)tetracene (4-5c)**

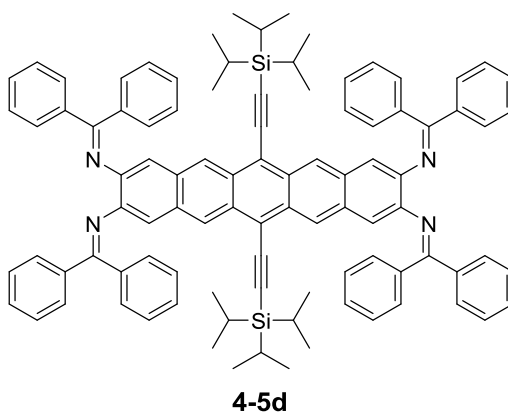
Yield: 55%.

**<sup>1</sup>H-NMR** (700 MHz, CD<sub>2</sub>Cl<sub>2</sub>): δ 9.14 (s, 2H), 7.99 (dd, J = 6.5, 3.3 Hz, 2H), 7.84 (d, J = 7.6 Hz, 4H), 7.52 (s, 8H), 7.46 (dd, J = 6.7, 3.0 Hz, 4H), 7.31 – 7.38 (m, 8H), 1.31 – 1.37 (m, 42H).

**<sup>13</sup>C NMR** (176 MHz, CD<sub>2</sub>Cl<sub>2</sub>): δ 168.42, 147.25, 139.10, 136.28, 131.66, 131.15, 130.80, 129.60, 129.56, 129.02, 128.94, 128.33, 128.11, 127.97, 125.61, 125.47, 116.31, 112.62, 104.83, 103.94, 18.75, 11.59.

**HRMS** (TOF MS ES<sup>+</sup>): m/z calculated for C<sub>66</sub>H<sub>71</sub>Si<sub>2</sub>N<sub>2</sub> 947.5156. Found 947.5139.

**Melting point:** 268.2 – 269.5 °C.

***N*<sup>3</sup>,*N*<sup>4</sup>,*N*<sup>10</sup>,*N*<sup>11</sup>-Tetrakis(diphenylmethylene)amina-7,14-bis-(triisopropylsilylethynyl)pentacene (4-5d)**

Yield: 65%.

**$^1\text{H}$  NMR** (500 MHz,  $\text{CD}_2\text{Cl}_2$ ):  $\delta$  8.80 (s, 4H), 7.82 (d,  $J = 7.6$  Hz, 8H), 7.50 (t,  $J = 7.3$  Hz, 4H), 7.44 (t,  $J = 7.6$  Hz, 8H), 7.39 – 7.30 (m, 20H), 6.90 (s, 4H), 1.29 – 1.38 (m, 42H).

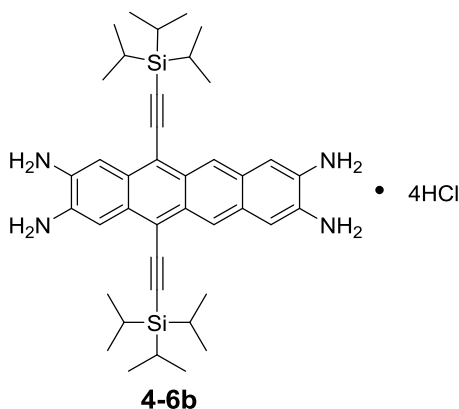
**$^{13}\text{C}$  NMR** (63 MHz,  $\text{CD}_2\text{Cl}_2$ ):  $\delta$  168.62, 145.87, 139.60, 136.88, 131.16, 130.82, 130.15, 129.84, 129.43, 129.24, 128.49, 128.35, 124.31, 116.82, 115.04, 106.52, 105.07, 19.14, 12.01.

**HRMS** (TOF MS ES+):  $m/z$  calculated for  $\text{C}_{96}\text{H}_{91}\text{Si}_2\text{N}_4$  1355.6782. Found 1355.6776.

**Melting point** has not been observed below 300 °C.

**4-6(a-d)** were synthesized using the following general method, taking **4-6b** for example.  $^{13}\text{C}$  NMR spectra have not been obtained due to their bad solubility in commonly used deuterated solvents.

#### 2,3,8,9-Tetraamino-5,12-bis-(triisopropylsilylethynyl)tetracene (**4-6b**)

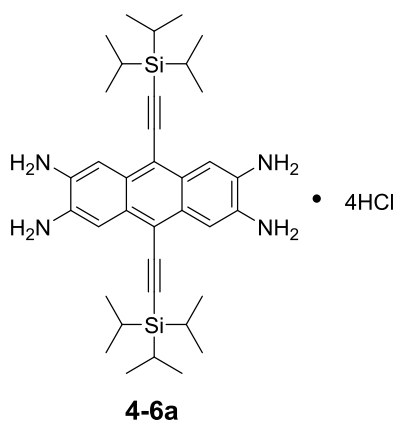


1 mL 37% hydrochloric acid was added to a 10 mL THF solution of **4-5b** (0.13 g, 0.1 mmol). The mixture was stirred for 5 hours at RT. Then the THF was evaporated and residue was dried under freeze drier. The dark purple solid was washed with hexane to give the rough product (**4-6b**) 76 mg with 95% yield. The rough product was used directly as the starting material in the next reaction without further purification. 1 mL 2M HCl works better for yielding compound **4-6d**.

**$^1\text{H}$  NMR** (250 MHz,  $\text{DMSO}-d_6$ ):  $\delta$  8.69 (s, 2H), 7.55 (s, 2H), 7.41 (s, 2H), 1.24 – 1.33 (m, 42H).

**FD-Mass** (8KV): calculated for  $C_{40}H_{56}N_4Si_2$  648.4. Found 648.5.

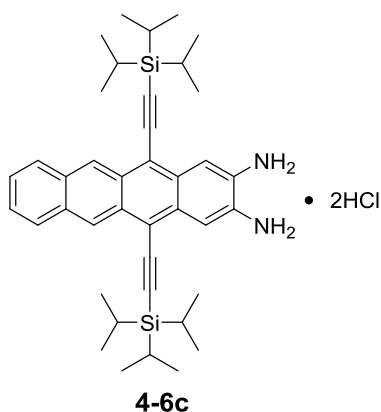
**2,3,6,7-Tetraamino-9,10-bis-(triisopropylsilylethynyl)anthracene (4-6a)**



$^1H$  NMR (250 MHz,  $DMSO-d_6$ ):  $\delta$  7.59 (s, 4H), 1.21 – 1.31 (m, 42H).

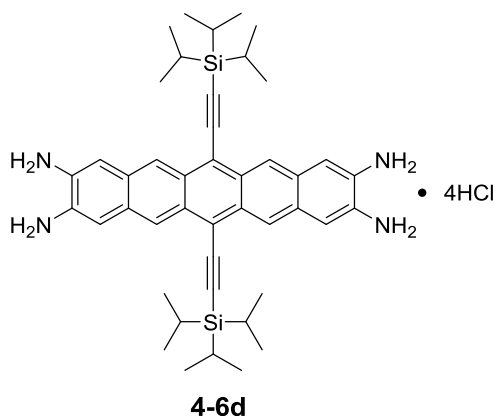
**FD-Mass** (8KV): calculated for  $C_{36}H_{54}N_4Si_2$  598.4. Found 599.0.

**2,3-Diamino-5,12-bis-(triisopropylsilylethynyl)tetracene (4-6c)**



$^1H$  NMR (250 MHz,  $DMSO-d_6$ ):  $\delta$  8.99 (s, 2H), 7.89 (dd,  $J = 6.5, 3.2$  Hz, 2H), 7.50 (s, 2H), 7.47 (dd,  $J = 6.5, 3.2$  Hz, 2H), 1.22 – 1.35 (m, 42H).

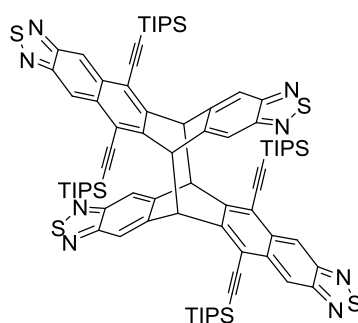
**FD-Mass** (8KV): calculated for  $C_{40}H_{54}N_2Si_2$  618.4. Found 619.1.

**2,3,9,10-Tetraamino-6,13-bis-(triisopropylsilylethynyl)pentacene (4-6d)**

$^1\text{H NMR}$  (300 MHz,  $\text{DMSO-}d_6$ ):  $\delta$  8.65 (s, 2H), 7.15 (s, 2H), 1.27 – 1.40 (m, 42H).

**FD-Mass** (8KV): calculated for  $\text{C}_{44}\text{H}_{58}\text{N}_4\text{Si}_2$  698.4. Found 699.2.

**4-7, 4-8, 4-9, 4-10 and 4-11** were synthesized using the following general method, taking **4-8** for example.

**Trans-tetrakis((triisopropylsilyl)ethynyl)-tetrahydro-bis(epibenzothiadiazolo)cyclooctadinaphtho[1,2,5]thiadiazole (4-8)****4-8**

**4-6b** (30 mg, 0.038mmol) was dissolved in 10 mL pyridine, then N-sulfinylaniline (0.14 mL, 1.28 mmol) and chlorotrimethylsilane (0.18 mL, 1.4 mmol) were added. The mixture was stirred under argon at 80 °C overnight. After the reaction, pyridine was evaporated, and then the residue was subjected to column chromatography on silica gel with hexane/DCM (1:4) as eluent. The material was washed with acetone to give yellow solid product 18 mg in a yield of 66%.

**<sup>1</sup>H-NMR** (250 MHz, CD<sub>2</sub>Cl<sub>2</sub>): δ 9.02 (s, 2H), 7.82(s, 2H), 6.06(s, 2H), 1.37 – 1.52(m, 42H).

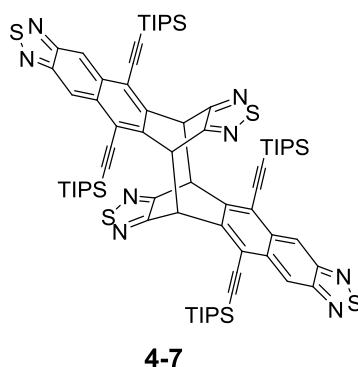
**<sup>13</sup>C NMR** (63 MHz, CD<sub>3</sub>Cl): δ 153.99, 153.04, 141.99, 141.05, 132.32, 119.98, 118.84, 118.71, 105.63, 102.25, 51.50, 19.05, 11.77.

**HRMS** (TOF MS ES+): m/z calculated for C<sub>40</sub>H<sub>48</sub>Si<sub>2</sub>N<sub>4</sub>S<sub>2</sub> 704.2859. Found 704.2850.

**Melting point** has not been observed below 300 °C.

**Crystallographic data** (CCDC deposition number): CCDC 1042600.

**Trans-tetrakis((triisopropylsilyl)ethynyl)-tetrahydro-bis(epithiadiazolo)cyclooctadinaphtho[1,2,5]thiadiazole (4-7)**



Yield: 57%.

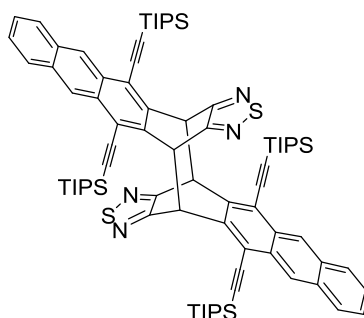
**<sup>1</sup>H NMR** (250 MHz, CD<sub>2</sub>Cl<sub>2</sub>): δ 9.05 (s, 4H), 6.07 (s, 4H) 1.24 – 1.36 (m, 84H).

**<sup>13</sup>C NMR** (63 MHz, CD<sub>2</sub>Cl<sub>2</sub>): δ 162.67, 153.75, 139.20, 132.38, 121.48, 119.40, 107.03, 102.03, 46.72, 19.15, 19.13, 12.15.

**HRMS** (TOF MS ES+): m/z calculated for C<sub>88</sub>H<sub>87</sub>Si<sub>2</sub>N<sub>4</sub> 1309.5483. Found 1309.5487.

**Melting point** has not been observed below 300 °C.

**Crystallographic data** (CCDC deposition number): CCDC 1042599.

**6,9,16,19-Tetrakis((triisopropylsilyl)ethynyl)-7,8,17,18-tetrahydro-7,18:8,17-bis([3,4]epithiadiazolo)cycloocta[1,2-b:5,6-b']dianthracene (4-9)****4-9**

Yield: 77%.

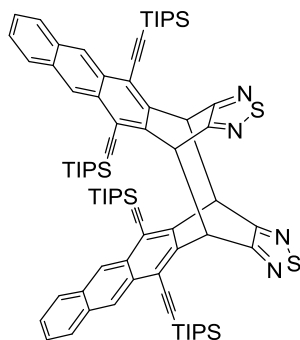
**<sup>1</sup>H NMR** (250 MHz, CD<sub>2</sub>Cl<sub>2</sub>): δ 9.02 (s, 4H), 8.03 (dd, J = 6.4, 3.3 Hz, 4H), 7.58 (dd, J = 6.6, 3.1 Hz, 4H), 6.19 (s, 4H), 1.42 – 1.47 (m, 84H).

**<sup>13</sup>C NMR** (63 MHz, CD<sub>2</sub>Cl<sub>2</sub>): δ 163.43, 138.13, 132.82, 129.80, 128.63, 126.98, 126.70, 120.92, 105.68, 102.70, 46.71, 19.20, 12.17.

**HRMS** (TOF MS ES<sup>+</sup>): m/z calculated for C<sub>80</sub>H<sub>101</sub>Si<sub>4</sub>N<sub>4</sub>S<sub>2</sub> 1293.6545. Found 1293.6586.

**Melting point** has not been observed below 300 °C.

**Crystallographic data** (CCDC deposition number): CCDC 1042601.

**6,9,16,19-Tetrakis((triisopropylsilyl)ethynyl)-7,8,17,18-tetrahydro-7,18:8,17-bis([3,4]epithiadiazolo)cycloocta[1,2-b:5,6-b']dianthracene (4-10)****4-10**

Yield: 15%.

$^1\text{H NMR}$  (250 MHz,  $\text{CD}_2\text{Cl}_2$ )  $\delta$  8.82 (s, 4H), 7.86 (dd,  $J = 6.4, 3.3$  Hz, 4H), 7.43 (dd,  $J = 6.5, 3.2$  Hz, 4H), 6.35 (s, 4H), 1.31 – 1.41 (m, 84H).

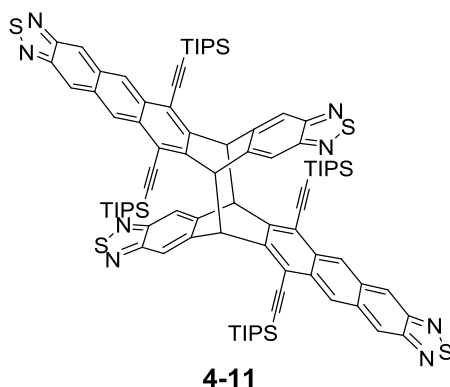
$^{13}\text{C NMR}$  (63 MHz,  $\text{CD}_2\text{Cl}_2$ ):  $\delta$  163.54, 138.85, 132.58, 129.85, 128.44, 126.78, 121.17, 105.27, 103.37, 47.01, 19.24, 12.28.

**HRMS** (TOF MS ES<sup>+</sup>):  $m/z$  calculated for  $\text{C}_{80}\text{H}_{101}\text{Si}_4\text{N}_4\text{S}_2$  1293.6545. Found 1293.6542.

**Melting point** has not been observed below 300 °C.

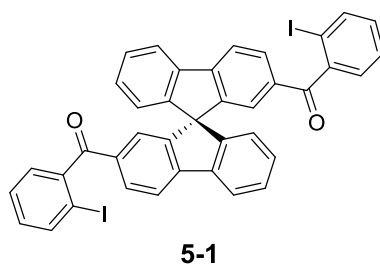
**Crystallographic data** (CCDC deposition number): CCDC 1042602.

**Trans-tetrakis((triisopropylsilyl)ethynyl)-tetrahydro-bis(epibenzothiadiazolo)cyclooctadianthra[1,2,5]thiadiazole (4-11)**



**MALDI-TOF** (MS):  $m/z$  calculated for  $\text{C}_{88}\text{H}_{100}\text{Si}_4\text{N}_8\text{S}_4$  1508.60. Found 1508.26.

**9,9'-Spirobi[fluorene]-2,2'-diylbis((2-iodophenyl)methanone) (5-1)**



A 500-mL round-bottomed flask was charged with 2-iodobenzoyl chloride (10.10 g, 37.97 mmol), dichloromethane (400 mL), and spirofluorene (4.00 g, 12.67 mmol). The reaction mixture was cooled in an ice bath, and aluminum chloride (5.90 g, 44.35 mmol) was added in one portion. The mixture was stirred at room temperature for 24 hours. Water was slowly added to the reaction mixture while cooled with an ice bath. The mixture was extracted with dichloromethane, washed with brine and dried over sodium sulfate, filtered and concentrated. The residue was purified by flash chromatography with 10 – 25% ethyl acetate in hexanes to give the white product in 85% yield.

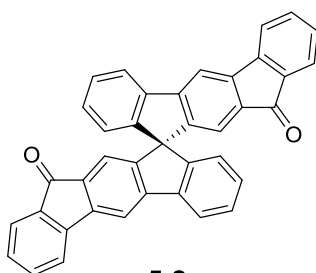
**<sup>1</sup>H NMR** (500 MHz, THF-*d*<sub>8</sub>): δ 6.29 (d, *J* = 7.8 Hz, 2H), 6.27 (d, *J* = 8.0 Hz, 2H), 6.13 (d, *J* = 8.0 Hz, 2H), 5.91 (dd, *J* = 8.1, 1.6 Hz, 2H), 5.68 (dt, *J* = 9.6, 7.6 Hz, 4H), 5.59 (d, *J* = 1.5 Hz, 2H), 5.53 (dd, *J* = 7.6, 1.7 Hz, 2H), 5.46 (t, *J* = 7.5 Hz, 2H), 5.41 (td, *J* = 7.7, 1.7 Hz, 2H), 5.01 (d, *J* = 7.7 Hz, 2H).

**<sup>13</sup>C NMR** (126 MHz, THF-*d*<sub>8</sub>): δ 194.92, 149.29, 148.50, 147.01, 144.77, 140.46, 139.49, 135.48, 131.65, 130.76, 129.21, 128.60, 128.18, 127.60, 124.64, 123.89, 121.29, 119.98, 92.08.

**HRMS** (TOF MS ES<sup>+</sup>): *m/z* calculated for C<sub>39</sub>H<sub>23</sub>O<sub>2</sub>I<sub>2</sub> 776.9788. Found 776.9767.

**Melting point:** 245 °C, decomposed.

### 12H,12'H-10,10'-Spirobi[indeno[2,1-b]fluorene]-12,12'-dione (5-2)



5-2

A mixture of **5-1** (1.40 g, 1.80 mmol) and palladium acetate (0.16 g, 0.72 mmol) in dry dimethylacetamide (100 mL) was heated to 130 °C overnight under argon atmosphere. The mixture was cooled to room temperature and the solvent was evaporated under vacuum. Then, water was added. The mixture was extracted with ethyl acetate, and the organic extracts were washed with 2 M HCl, dried over sodium

sulfate and concentrated. The residue was purified on silica gel with DCM to provide the green product in 65% yield.

**$^1\text{H}$  NMR** (500 MHz,  $\text{C}_2\text{D}_2\text{Cl}_2$ )  $\delta$  7.95 (s, 2H),  $\delta$  7.94 (d,  $J$  = 6.6 Hz, 2H) 7.64 (d,  $J$  = 7.4 Hz, 2H), 7.55 (dd,  $J$  = 7.2, 1.0 Hz, 2H), 7.52 (dd,  $J$  = 7.5, 1.0 Hz, 2H), 7.45 (td,  $J$  = 7.6, 1.1 Hz, 2H), 7.27 (td,  $J$  = 7.4, 1.0 Hz, 2H), 7.21 (td,  $J$  = 7.5, 1.1 Hz, 2H), 6.95 (s, 2H), 6.80 (d,  $J$  = 7.6 Hz, 2H).

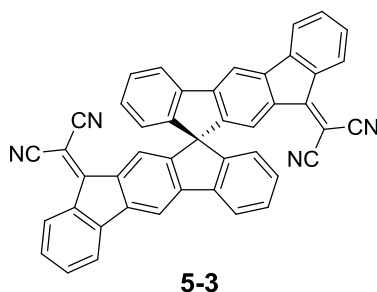
**$^{13}\text{C}$  NMR** (126 MHz,  $\text{C}_2\text{D}_2\text{Cl}_4$ ):  $\delta$  193.15, 148.76, 148.63, 148.47, 145.35, 143.98, 140.48, 134.90, 134.74, 134.09, 129.60, 129.28, 128.58, 124.19, 121.29, 120.50, 120.07, 112.37, 74.18, 65.55.

**HRMS** (TOF MS ES+):  $m/z$  calculated for  $\text{C}_{39}\text{H}_{21}\text{O}_2$  521.1542. Found 521.1552.

**Melting point** has not been observed below 300 °C.

**Crystallographic data** (CCDC deposition number): CCDC 1035931.

### 2,2'-(12H,12'H-10,10'-Spirobi[indeno[2,1-b]fluorene]-12,12'-diylidene)dimalononitrile (5-3)



To a stirred mixture of **5-2** (0.25 g, 0.48 mmol) and malononitrile (1.59 g, 24 mmol) in 100 mL  $\text{CHCl}_3$ , 1mol/L  $\text{TiCl}_4$  (9.60 mL, 9.6 mmol) was slowly added, followed by dried pyridine (1.89 mL, 23.45mmol). The mixture was refluxed for 36 hours under Ar. Every 5 hours, identical amounts of malononitrile,  $\text{TiCl}_4$  and pyridine were added. After cooling down, the mixture was poured into ice/water and extracted with DCM. The combined organic layers were dried with  $\text{Na}_2\text{SO}_4$ . The solvent was removed under vacuum and the residue was purified by column chromatography using DCM as eluent to give **5-3** as red orange solid. Finally the solid was washed with acetone to give the pure product in a 99% yield.

**<sup>1</sup>H NMR** (500 MHz, C<sub>2</sub>D<sub>2</sub>Cl<sub>4</sub>): δ 8.23 (d, J = 7.8 Hz, 2H), 8.01 (s, 2H), 7.96 (d, J = 7.7 Hz, 2H), 7.67 (d, J = 7.5 Hz, 2H), 7.61 (s, 2H), 7.51 (t, J = 7.6 Hz, 2H), 7.47 (t, J = 7.6 Hz, 2H), 7.28 (t, J = 7.8 Hz, 2H), 7.25 (t, J = 7.6 Hz, 2H), 6.81 (d, J = 7.6 Hz, 2H).

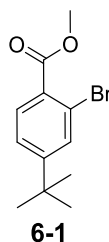
**<sup>13</sup>C NMR** (126 MHz, C<sub>2</sub>D<sub>2</sub>Cl<sub>4</sub>): δ 161.22, 148.89, 148.64, 148.34, 143.66, 141.80, 139.83, 134.86, 134.80, 133.83, 130.22, 129.40, 128.79, 126.61, 124.10, 122.21, 121.64, 120.95, 113.75, 113.50, 112.90, 65.75.

**HRMS** (TOF MS ES<sup>+</sup>): m/z calculated for C<sub>45</sub>H<sub>20</sub>N<sub>4</sub>Na<sub>23</sub> 639.1586. Found 639.1566.

**Melting point** has not been observed below 300 °C.

**Crystallographic data** (CCDC deposition number): CCDC 1035932.

### Methyl 2-bromo-4-(*tert*-butyl)benzoate (6-1)



A solution of NaOH (15.12 g, 0.38 mol) in 140 mL water was cooled in an ice bath 15 min, following by the dropwise of bromine (5 mL, 0.10 mol). After that, a solution of 1-(2-bromo-4-(*tert*-butyl)phenyl)ethan-1-one (6.2g, 0.024 mol) in 120 mL dioxane was slowly added. The reaction took place in room temperature overnight. Around 12 hours later, the reaction flask was put in an ice bath and the mixture was acidified with concentrated hydrochloric acid, which was extracted with 150 mL ethyl acetate three times. The combined extracts were washed with 200 mL water and 200 mL brine separately, dried over Na<sub>2</sub>SO<sub>4</sub>. The solution was concentrated via rotary evaporator, resulting in crude liquid, which was purified by silica column with eluent Hex/EA (4:1) to give the compound 2-bromo-4-(*tert*-butyl)benzoic acid. 2-bromo-4-(*tert*-butyl)benzoic acid in 500 mL methanol was dropwise added a catalytic H<sub>2</sub>SO<sub>4</sub> 2.0 mL. Then, the reaction was refluxed overnight. The resulting mixture was evaporated until around 100 mL solvent left. The residue was poured into 300 mL water and extracted with 200 mL DCM three times. The organic layer was washed

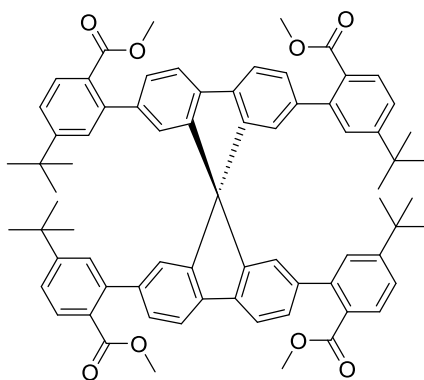
with saturated 50 mL NaHCO<sub>3</sub> two times and dried over Na<sub>2</sub>SO<sub>4</sub>. After evaporating, the pure liquid methyl 2-bromo-4-(*tert*-butyl)benzoate (**6-1**) was obtained in a 90% yield.

<sup>1</sup>H NMR (250 MHz, CD<sub>2</sub>Cl<sub>2</sub>) δ 7.78 (d, *J* = 8.2 Hz, 1H), 7.72 (d, *J* = 1.9 Hz, 1H), 7.44 (dd, *J* = 8.2, 1.9 Hz, 1H), 3.93 (s, 3H), 1.36 (s, 9H).

<sup>13</sup>C NMR (63 MHz, CD<sub>2</sub>Cl<sub>2</sub>): δ 166.66, 157.18, 131.92, 131.50, 129.44, 124.83, 121.87, 52.56, 35.28, 31.05.

HRMS (TOF MS ES<sup>+</sup>): *m/z* calculated for C<sub>12</sub>H<sub>15</sub>O<sub>2</sub>NaBr 293.0153. Found 293.0164.

**Tetramethyl 2,2',2'',2'''-(9,9'-spirobi[fluorene]-2,2',7,7'-tetrayl)tetrakis(4-(tert-butyl)benzoate) (6-2)**



**6-2**

The mixture of 2,2',7,7'-tetrakis(4,4,5,5-tetramethyl-1,3,2-dioxaborolan-2-yl)-9,9'-spirobi[fluorene] (2.31 g, 2.89 mmol), **6-1** (3.6 g, 13.28mmol), tetrakis(triphenylphosphine)palladium(0) (667 mg, 0.58 mmol), 2M aqueous potassium carbonate solution (50 mL) and toluene (200 mL) was heated at 110 °C under argon for two days. Then the resulting mixture was washed 80 mL DCM three times and the organic layer was washed with brine, dried over Na<sub>2</sub>SO<sub>4</sub>. After being concentrated under vacuum to remove the solvent, the crude product was purified by column chromatography using Hex/EA (10:1) as eluent to give the desired compound **6-2** as white solid in a 74% yield.

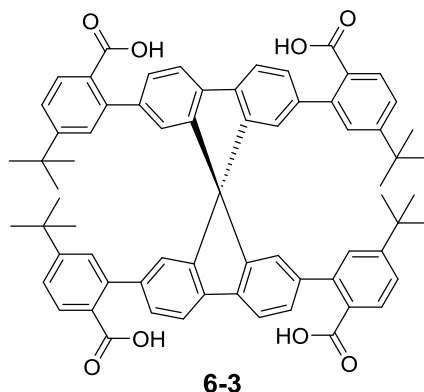
**<sup>1</sup>H NMR** (250 MHz, C<sub>2</sub>D<sub>2</sub>Cl<sub>4</sub>) δ 7.88 (d, *J* = 7.9 Hz, 4H), 7.56 (d, *J* = 8.0 Hz, 4H), 7.38 (dd, *J* = 7.8, 1.7 Hz, 4H), 7.30 (dd, *J* = 8.3, 1.8 Hz, 4H), 7.25 (d, *J* = 1.9 Hz, 4H), 6.65 (s, 4H), 3.06 (s, 12H), 1.25 (s, 36H).

**<sup>13</sup>C NMR** (63 MHz, CD<sub>2</sub>Cl<sub>2</sub>): δ 169.36, 155.13, 149.18, 141.90, 141.85, 141.03, 130.06, 128.70, 128.60, 127.98, 124.82, 124.60, 120.54, 66.28, 51.97, 35.26, 31.31.

**HRMS** (TOF MS ES<sup>+</sup>): *m/z* calculated for C<sub>73</sub>H<sub>73</sub>O<sub>8</sub> 1077.5305. Found 1077.5299.

**Melting point:** 245.4 °C, decomposed.

**2,2',2'',2'''-(9,9'-Spirobi[fluorene]-2,2',7,7'-tetrayl)tetrakis(4-(tert-butyl)benzoic acid) (6-3)**



**6-2** (2.3 g, 2.14 mmol) and 300 mL ethanol were mixed in 500 mL flask, followed by the dropwise of sodium hydroxide solution (12 g in 45 mL water), then the reaction temperature was increased to 90 °C. With the increasing reaction time, the precipitate decreased correspondingly. 12 hours later, the solution became transparent with a little bit of light orange color. Most of the solvent was evaporated, then concentrated HCl was added, resulting in white solid. The mixture was filtrated, and the obtained solid was washed with 1000 mL water, dried in the vacuum oven. 2.18 g pure white solid **6-3** was obtained in a 99% yield.

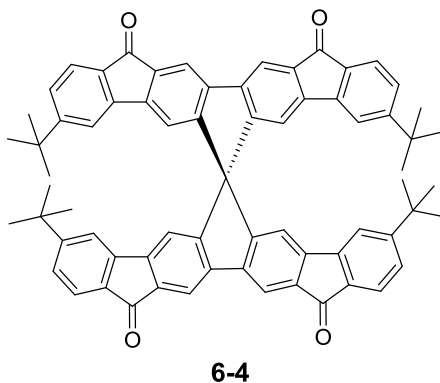
**<sup>1</sup>H NMR** (250 MHz, CD<sub>2</sub>Cl<sub>2</sub>) δ 7.84 (d, *J* = 7.7 Hz, 4H), 7.39 (dd, *J* = 12.9, 8.0 Hz, 8H), 7.29 (d, *J* = 8.5 Hz, 4H), 7.27 (s, 4H), 6.59 (s, 4H), 1.22 (s, 36H).

**<sup>13</sup>C NMR** (63 MHz, CD<sub>2</sub>Cl<sub>2</sub>): δ 176.32, 154.99, 148.70, 141.90, 141.84, 141.13, 129.56, 128.37, 128.23, 127.45, 124.58, 124.53, 120.63, 66.35, 35.26, 31.21.

**HRMS** (TOF MS ES+):  $m/z$  calc. for  $C_{69}H_{65}O_8$  1021.4679, found 1021.4704.

**Melting point** has not been observed below 300 °C.

**3,3',9,9'-Tetra-tert-butyl-6,6'-spirobi[cyclopenta[2,1-b:3,4-b']difluorene]-12,12',15,15'-tetraone (6-4)**



0.07 mL dry DMF was added dropwise to a solution of **6-3** (0.60 g, 0.59 mmol) and 2 mol/L oxalyl chloride (6 mL, 12 mmol) in 120 mL dry DCM. The mixture was stirred for 10 hours at room temperature. The crude tetrachloride was obtained after the evaporation of DCM. Then, the crude tetrachloride in 30 mL dry DCM was added to a suspension of anhydrous  $AlCl_3$  (848 mg, 4.8 mmol) in 100 mL dry DCM at 0 °C. 12 hours later, the reaction mixture was poured into ice water slowly, extracted with DCM, and dried over  $Na_2SO_4$ . The solvent was removed by rotary evaporator. The residue was purified by column chromatography on silica gel with Hex/EA (20:1) as eluent to afford **6-4** as a yellow solid in a yield of 82% (0.46 g).

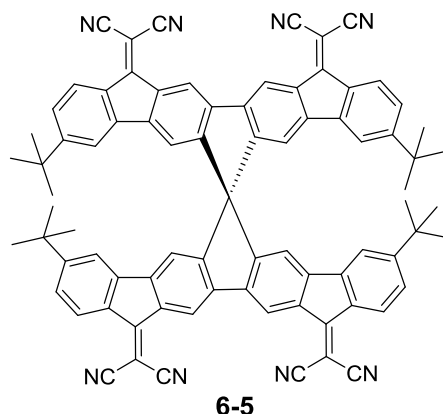
**$^1H$  NMR** (700 MHz,  $C_2D_2Cl_4$ )  $\delta$  8.19 (s, 4H), 7.55 (d,  $J = 7.8$  Hz, 4H), 7.27 (s, 4H), 7.24 (d,  $J = 7.8$  Hz, 4H), 6.93 (s, 4H), 1.19 (s, 36H).

**$^{13}C$  NMR** (63 MHz,  $C_2D_2Cl_4$ ):  $\delta$  192.54, 159.65, 153.64, 145.44, 143.83, 141.74, 135.94, 132.08, 126.64, 124.44, 117.94, 116.37, 116.12, 66.42, 35.55, 31.02.

**HRMS** (TOF MS ES+):  $m/z$  calculated for  $C_{69}H_{57}O_4$  949.4257. Found 949.4249.

**Melting point** has not been observed below 300 °C.

**Crystallographic data** (CCDC deposition number): CCDC 1408336.

**2,2',2'',2'''-(3,3',9,9'-Tetra-tert-butyl-6,6'-spirobi[cyclopenta[2,1-b:3,4-b']difluorene]-12,12',15,15'-tetraylidene)tetramalononitrile (6-5)**

**6-4** (0.20 g, 0.21 mmol) and malononitrile (1.39 g, 21 mmol) were dissolved in dry  $\text{CHCl}_3$  (80 mL) under argon.  $\text{TiCl}_4$  (2.3 mL, 21.0 mmol) and pyridine (2.49 mL) were added dropwise. The mixture was stirred overnight at 80 °C. The solvent was removed by rotary evaporator. The residue was purified by column chromatography on silica gel with pure DCM as eluent to afford crude **6-5**. The crude **6-5** was dissolved in DCM, followed by adding of hexane, the resulting precipitate was filtrated as a grain solid in a yield of 90% (0.22 g).

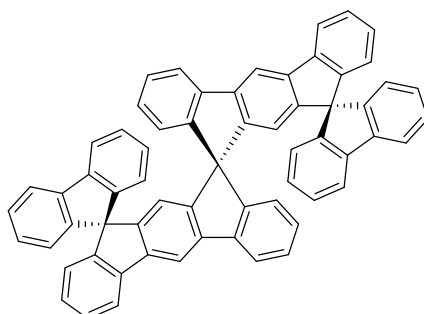
$^1\text{H NMR}$  (250 MHz,  $\text{C}_2\text{D}_2\text{Cl}_4$ )  $\delta$  8.98 (s, 4H), 8.21 (d,  $J = 8.4$  Hz, 4H), 7.30 (s, 6H), 7.27 (s, 2H), 6.97 (s, 4H), 1.20 (s, 36H).

$^{13}\text{C NMR}$  (126 MHz,  $\text{C}_2\text{D}_2\text{Cl}_4$ ):  $\delta$  160.21, 159.95, 153.12, 144.02, 141.63, 141.57, 136.34, 132.35, 126.99, 126.97, 118.81, 118.09, 116.19, 113.54, 113.17, 76.30, 35.60, 30.84.

**HRMS** (TOF MS ES<sup>+</sup>):  $m/z$  calculated for  $\text{C}_{81}\text{H}_{56}\text{N}_8\text{Na}$  1163.4526. Found 1163.4541.

**Melting point** has not been observed below 300 °C.

**Crystallographic data** (CCDC deposition number): CCDC 1408337.

**(S)-12'-(2-(9,9'-Spirobi[fluorene]-3-yl)phenyl)-12'-methyl-12'H-spiro[fluorene-9,10'-indeno[2,1-b]fluorene] (7-1)**

7-1

A solution of 2-bromobiphenyl (1.66 mL, 9.6 mmol) in 30 mL of dry THF was added to a flask in charged with Iodine (10 mg, 0.04 mmol) and magnesium (0.28 g, 11.52 mmol) to initiate the Grignard reaction. After the reaction initiated, the solution was added dropwise, and the reaction mixture was then refluxed for 8 h to complete the reaction. Afterward, a solution of **5-2** (0.5 g, 0.96 mmol) in THF (50 mL) was added all at once to the Grignard solution and the mixture was refluxed overnight. THF was evaporated, followed by the adding of water (100 mL) and 1M HCl (100 mL) to quench the reaction. The mixture was stirring for 3 h and then extracted with DCM (3 × 50 mL). The organic phases were combined, washed with sat. NaCl solution (2 × 100 mL), dried with Na<sub>2</sub>SO<sub>4</sub> and filtered. The solvent was removed by rotary evaporator, resulting in oil intermediate. The oil was then dissolved in acetic acid (40 mL), and the reaction was refluxed at 120 °C overnight. The cooled mixture was poured onto 100 mL of water. The crude product was precipitated and collected by filtration, washed with water and subjected to column chromatography on silica gel with Hex/DCM (5:1) as eluent to afford white solid (700 mg, 92%).

**<sup>1</sup>H NMR** (500 MHz, CD<sub>2</sub>Cl<sub>2</sub>): δ 8.25 (s, 2H), 7.94 (d, *J* = 7.6 Hz, 2H), 7.90 (d, *J* = 7.7 Hz, 2H), 7.77 (t, *J* = 7.0 Hz, 4H), 7.33 – 7.41 (m, 6H), 7.30 (t, *J* = 7.5 Hz, 2H), 7.02 – 7.11 (m, 8H), 6.61 (t, *J* = 6.7 Hz, 4H), 6.53 (d, *J* = 7.5 Hz, 2H), 6.48 (d, *J* = 7.6 Hz, 2H), 6.08 (s, 2H).

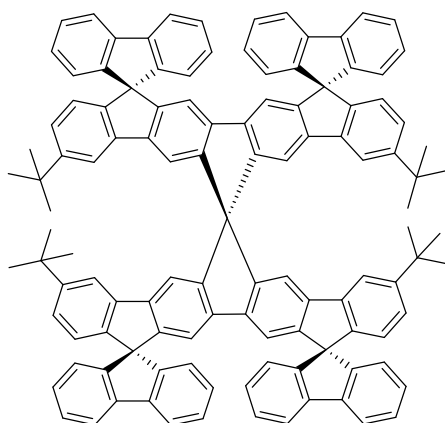
**<sup>13</sup>C NMR** (126 MHz, CD<sub>2</sub>Cl<sub>2</sub>): δ 149.45, 149.08, 148.99, 148.83, 148.59, 148.40, 142.14, 141.87, 141.77, 141.38, 141.31, 141.09, 127.74, 127.73, 127.70, 127.69, 127.67, 127.65, 127.60, 123.53, 123.49, 123.43, 123.32, 119.98, 119.96, 119.89, 119.20, 111.33, 65.71, 65.57.

**HR-MS** (MALDI)  $m/z$  calculated for  $C_{63}H_{36}$  [ $M^+$ ] 792.2818. Found 792.2810.

**Crystallographic data** (CCDC deposition number): CCDC 1408339.

**Melting point** has not been observed below 300 °C.

**3,3',9,9'-Tetra-tert-butyl-6,6'spirobi[cyclopenta[2,1-b:3,4-b']tetrafluorene]-12,12',15,15'-spirotetra[fluorene] (7-2)**



**7-2**

A solution of 2-bromobiphenyl (1.2 mL, 7.1 mmol) in 25 mL of dry THF was added to a flask in charged with Iodine (10 mg, 0.04 mmol) and magnesium (0.18 g, 7.5 mmol) to initiate the Grignard reaction. After the reaction initiated, the solution was added dropwise, and the reaction mixture was then refluxed for 5 h to complete the reaction. Afterward, a solution of **6-4** (0.3 g, 0.32 mmol) in THF (25 mL) was added all at once to the Grignard solution and the mixture was refluxed overnight. THF was evaporated, followed by the adding of water (50 mL) and 1M HCl (50 mL) to quench the reaction. The mixture was stirring for 3 h and then extracted with DCM (3 × 50 mL). The organic phases were combined, washed with NaCl solution (2 × 100 mL) dried with  $Na_2SO_4$  and filtered. The solvent was removed by rotary evaporator, resulting residue was then dissolved in acetic acid (50 mL), and the reaction was refluxed at 120 °C overnight. The cooled mixture was poured onto 100 mL of water. The crude product was precipitated and collected by filtration, washed with water and subjected to column chromatography on silica gel with Hex/DCM (10:1 – 5:1) as eluent to afford white solid (420 mg, 88%).

**<sup>1</sup>H NMR** (500 MHz, C<sub>2</sub>D<sub>2</sub>Cl<sub>4</sub>): δ 7.84 (d, *J* = 7.7 Hz, 8H), 7.59 (d, *J* = 1.9 Hz, 4H), 7.36 (t, *J* = 7.5 Hz, 8H), 7.25 (s, 4H), 7.13 (t, *J* = 7.4 Hz, 8H), 7.04 (dd, *J* = 8.0, 1.9 Hz, 4H), 7.01 (s, 4H), 6.87 (d, *J* = 7.5 Hz, 8H), 6.54 (d, *J* = 8.0 Hz, 4H), 1.30 (s, 36H).

**<sup>13</sup>C NMR** (126 MHz, C<sub>2</sub>D<sub>2</sub>Cl<sub>4</sub>): δ 151.02, 149.78, 149.52, 149.13, 146.54, 142.53, 141.91, 141.70, 141.34, 127.73, 127.54, 125.11, 124.40, 123.20, 119.95, 116.66, 115.76, 115.71, 65.85, 34.75, 31.58, 29.57.

**HR-MS** (MALDI) *m/z* calculated for C<sub>117</sub>H<sub>88</sub> [M<sup>+</sup>] 1492.6881. Found 1492.6874.

**Crystallographic data** (CCDC deposition number): CCDC 1408340.

**Melting point** has not been observed below 300 °C.



## VIII.3 Crystallographic data

### Crystal structure of 2-5b

Cambridge Crystallographic Data Centre deposition number: CCDC 1042607

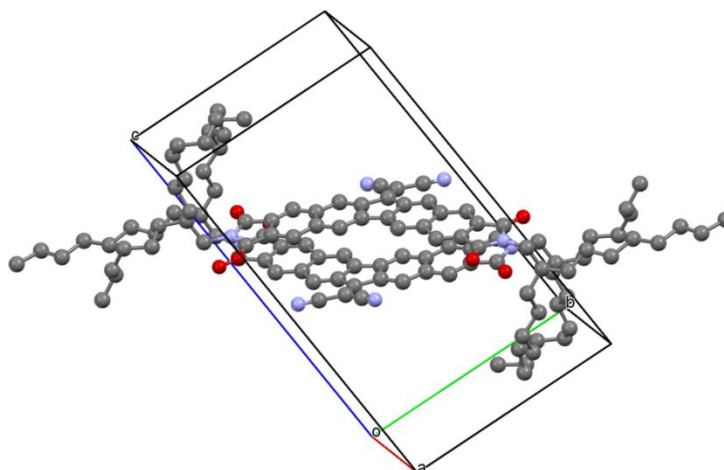


**Table VIII-1.** Crystallographic table.

Compound	<b>2-5b</b>
Molecular formula	$C_{60}H_{74}N_4O_4$
Formula weight	915.23 $\text{g mol}^{-1}$
Absorption coefficient	$\mu = 0.071 \text{ mm}^{-1}$
Crystal size	0.05 x 0.3 x 0.31 $\text{mm}^3$ ; light red plate
Space group	P-1 (triclinic)
Lattice parameters	$a = 11.2497(8) \text{ \AA}$ $\alpha = 95.185(2)^\circ$ $b = 12.3730(9) \text{ \AA}$ $\beta = 106.067(2)^\circ$ $c = 20.0241(15) \text{ \AA}$ $\gamma = 94.622(2)^\circ$
Volume	2651.1(3) $\text{\AA}^3$
Z value	2
F (000)	988
Calculated density	$d_{\text{xray}} = 1.147 \text{ g cm}^{-3}$
Temperature	-100 $^\circ\text{C}$
Scan type	$\omega$ -scans
Theta range for data collection	$2.4^\circ < \theta < 21.0^\circ$
Limiting indices	$-14 \leq h \leq 14$ , $-16 \leq k \leq 16$ , $-25 \leq l \leq 25$
Total number of reflections	39917
Unique number of reflections	12120 ( $R_{\text{int}} = 0.1207$ )
Observed number of reflections	3311 ( $ F /\sigma(F) > 4.0$ )
Structure solution	Program: SIR-97 (Direct methods)
R-values	$wR2 = 0.4299$ ( $R1 = 0.1229$ for observed reflections, 0.3268 for all reflections)
Goodness of fit	$S = 0.994$
Max Shift / Error	0.001 * e.s.d
Largest diff. peak and hole	0.58 and -0.48 $\text{e \AA}^{-3}$

## Crystal structure of 3-6

Cambridge Crystallographic Data Centre deposition number: CCDC 1410009

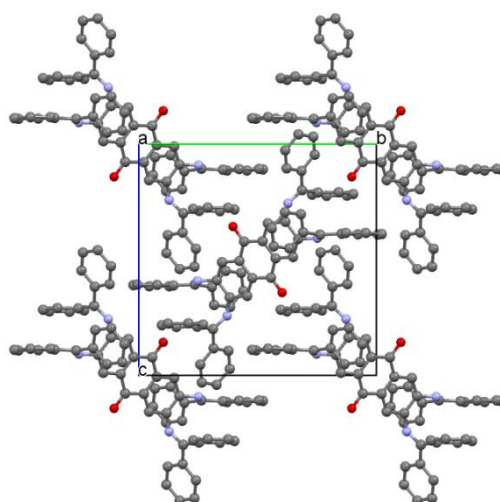


**Table VIII-2.** Crystallographic table.

Compound	<b>3-6</b>
Molecular formula	$C_{66}H_{44}N_4O_2$
Formula weight	$925.05 \text{ g mol}^{-1}$
Absorption coefficient	$\mu = 0.079 \text{ mm}^{-1}$
Crystal size	$0.08 \times 0.19 \times 0.2 \text{ mm}^3$ ; light brown plate
Space group	$P 2_1/n$ (monoclinic)
Lattice parameters	$a = 9.9809(7) \text{ \AA}$ $b = 15.5280(9) \text{ \AA}$ $\beta = 90.154(6)^\circ$ $c = 15.1288(11) \text{ \AA}$
Volume	$2344.7(3) \text{ \AA}^3$
Z value	2
F (000)	968
Calculated density	$d_{\text{xray}} = 1.31 \text{ g cm}^{-3}$
Temperature	$-80 \text{ }^\circ\text{C}$
Scan type	$\omega$ -scans
Theta range for data collection	$2.4^\circ < \theta < 28.3^\circ$
Limiting indices	$-13 \leq h \leq 11, -20 \leq k \leq 20, -20 \leq l \leq 20$
Total number of reflections	14941
Unique number of reflections	5727
Observed number of reflections	3052 ( $ F /\sigma(F) > 4.0$ )
Structure solution	SIR-2004 (Direct methods)
R-values	$wR2 = 0.114$ ( $R1 = 0.0471$ for observed reflections, $0.1092$ for all reflections)
Goodness of fit	$S = 0.918$
Max Shift / Error	$0.001 \text{ * e.s.d}$
Largest diff. peak and hole	$0.22$ and $-0.19 \text{ e \AA}^{-3}$

## Crystal structure of 3-10

Cambridge Crystallographic Data Centre deposition number: CCDC 1400306

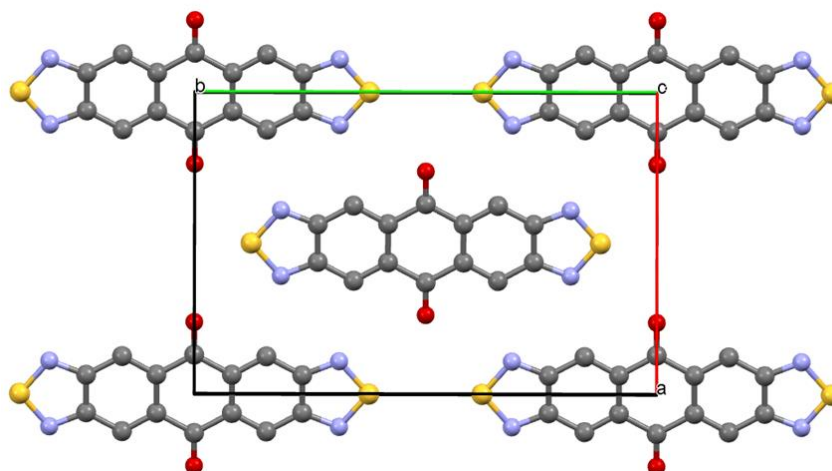
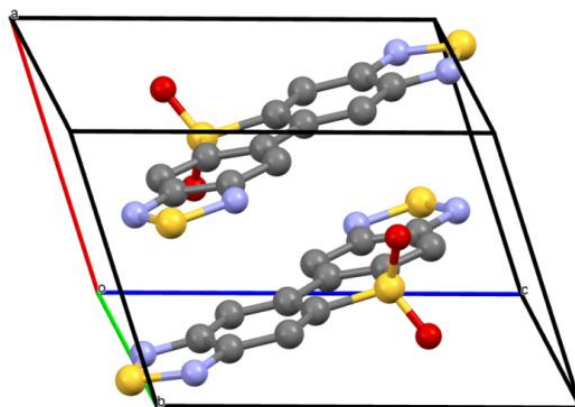


**Table VIII-3.** Crystallographic table.

Compound	<b>3-10</b>
Molecular formula	$C_{14}H_4N_4O_2S_2$
Formula weight	$324.33 \text{ gmol}^{-1}$
Absorption coefficient	$\mu = 4.079 \text{ mm}^{-1}$ corrected with 6 crystal faces
Crystal size	$0.02 \times 0.02 \times 0.2 \text{ mm}^3$ ; light brown needle
Space group	C 2/m (monoclinic)
Lattice parameters	$a = 10.3036(19) \text{ \AA}$ $b = 15.727(2) \text{ \AA}$ $\beta = 96.172(16)^\circ$ $c = 3.8043(8) \text{ \AA}$
Volume	$612.89(19) \text{ \AA}^3$
Z value	2
F (000)	328
Calculated density	$d_{\text{xray}} = 1.757 \text{ gcm}^{-3}$
Temperature	$-50 \text{ }^\circ\text{C}$
Scan type	$\omega$ -scans
Theta range for data collection	$5.15^\circ < \theta < 66.35^\circ$
Limiting indices	$-11 \leq h \leq 12, -18 \leq k \leq 18, -3 \leq l \leq 4$
Total number of reflections	1820
Unique number of reflections	541 ( $R_{\text{int}} = 0.0638$ )
Observed number of reflections	354 ( $ F /\sigma(F) > 4.0$ )
Structure solution	SIR-2004 (Direct methods)
R-values	$wR2 = 0.2617$ ( $R1 = 0.0801$ for observed reflections, $0.1120$ for all reflections)
Goodness of fit	$S = 1.076$
Max Shift / Error	$0.001 \text{ * e.s.d}$
Largest diff. peak and hole	$0.52$ and $-0.47 \text{ e\AA}^{-3}$

## Crystal structure of 3-11

Cambridge Crystallographic Data Centre deposition number: CCDC 1400305

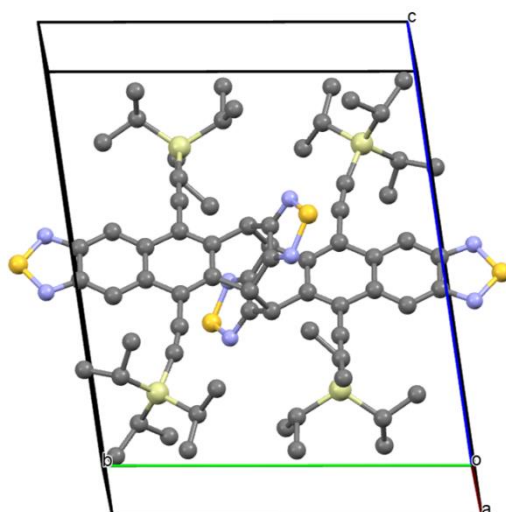


**Table VIII-4.** Crystallographic table.

Compound	3-11
Molecular formula	$C_{12}H_4N_4O_2S_3$
Formula weight	$332.37 \text{ gmol}^{-1}$
Absorption coefficient	$\mu = 0.62 \text{ mm}^{-1}$ correction with 6 faces
Crystal size	$0.04 \times 0.06 \times 0.7 \text{ mm}^3$ ; brown needle
Space group	P-1 (triclinic)
Lattice parameters	$a = 6.7778(7) \text{ \AA}$ $\alpha = 91.812(9)^\circ$ $b = 9.6253(11) \text{ \AA}$ $\beta = 109.511(8)^\circ$ $c = 9.8490(10) \text{ \AA}$ $\gamma = 93.899(9)^\circ$
Volume	$603.22(11) \text{ \AA}^3$
Z value	2
F (000)	336
Calculated density	$d_{\text{xray}} = 1.83 \text{ gcm}^{-3}$
Temperature	$-80 \text{ }^\circ\text{C}$
Scan type	$\omega$ -scans
Theta range for data collection	$3.2^\circ < \theta < 28.3^\circ$
Limiting indices	$-9 \leq h \leq 9, -12 \leq k \leq 12, -13 \leq l \leq 13$
Total number of reflections	14727
Unique number of reflections	11764
Observed number of reflections	8156 ( $ F /\sigma(F) > 4.0$ )
Structure solution	SIR-2004 (Direct methods)
R-values	$wR2 = 0.1537$ ( $R1 = 0.0573$ for observed reflections, $0.0913$ for all reflections)
Goodness of fit	$S = 1.027$
Max Shift / Error	$0.001$ * e.s.d
Largest diff. peak and hole	$0.45$ and $-0.43 \text{ e\AA}^{-3}$

**Crystal structure of 4-7**

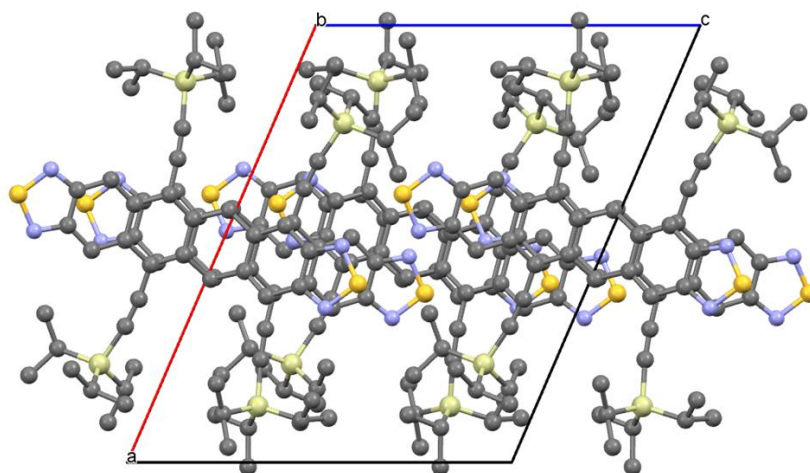
Cambridge Crystallographic Data Centre deposition number: CCDC 1042599

**Table VIII-5.** Crystallographic table.

Compound	<b>4-7</b>
Molecular formula	$C_{72}H_{92}N_8S_4Si_4$
Formula weight	1310.14 $g\text{mol}^{-1}$
Absorption coefficient	$\mu = 0.25\text{ mm}^{-1}$
Crystal size	0.07 x 0.14 x 0.63 $\text{mm}^3$ ; yellow needle
Space group	P-1 (triclinic)
Lattice parameters	$a = 7.769(1)\text{ \AA}$ $\alpha = 78.462(5)^\circ$ $b = 13.928(2)\text{ \AA}$ $\beta = 86.683(5)^\circ$ $c = 17.208(3)\text{ \AA}$ $\gamma = 79.739(5)^\circ$
Volume	1794.8(9) $\text{\AA}^3$
Z value	1
F (000)	700
Calculated density	$d_{\text{xray}} = 1.212\text{ gcm}^{-3}$
Temperature	-100 $^\circ\text{C}$
Scan type	$\omega$ -scans
Theta range for data collection	$2.4^\circ < \theta < 27.0^\circ$
Limiting indices	$-9 \leq h \leq 10$ , $-18 \leq k \leq 18$ , $-22 \leq l \leq 22$
Total number of reflections	19428
Unique number of reflections	8142 ( $R_{\text{int}} = 0.0508$ )
Observed number of reflections	5190 ( $ F /\sigma(F) > 4.0$ )
Structure solution	Program: SIR-97 (Direct methods)
R-values	$wR2 = 0.1264$ ( $R1 = 0.0488$ for observed reflections, 0.0939 for all reflections)
Goodness of fit	$S = 0.996$
Max Shift / Error	0.001 * e.s.d
Largest diff. peak and hole	0.32 and -0.48 $e\text{\AA}^{-3}$

## Crystal structure of 4-8

Cambridge Crystallographic Data Centre deposition number: CCDC 1042600

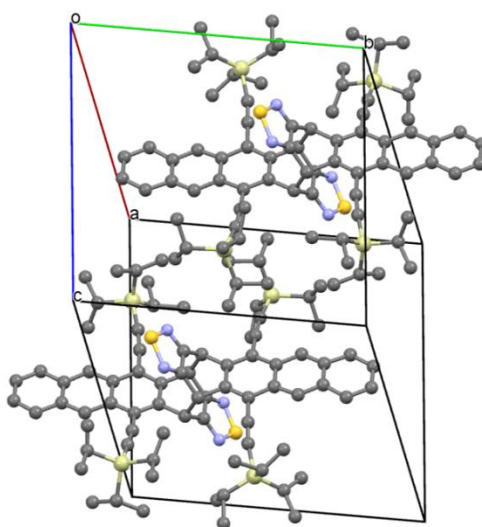


**Table VIII-6.** Crystallographic table.

Compound	4-8
Molecular formula	$C_{80}H_{96}N_8S_4Si_4$
Formula weight	$1410.6 \text{ g mol}^{-1}$
Absorption coefficient	$\mu = 0.23 \text{ mm}^{-1}$
Crystal size	$0.16 \times 0.22 \times 0.24 \text{ mm}^3$ ; yellow block
Space group	$P 2_1/c$ (monoclinic)
Lattice parameters	$a = 18.5577(8) \text{ \AA}$ $b = 15.4895(6) \text{ \AA}$ $\beta = 113.356(4)^\circ$ $c = 15.0011(7) \text{ \AA}$
Volume	$3958.7(3) \text{ \AA}^3$
Z value	2
F (000)	1504
Calculated density	$d_{\text{xray}} = 1.183 \text{ g cm}^{-3}$
Temperature	$-80 \text{ }^\circ\text{C}$
Scan type	$\omega$ -scans
Theta range for data collection	$2.6^\circ < \theta < 28.2^\circ$
Limiting indices	$-24 \leq h \leq 24$ , $-20 \leq k \leq 19$ , $-19 \leq l \leq 19$
Total number of reflections	25804
Unique number of reflections	9483 ( $R_{\text{int}} = 0.0996$ )
Observed number of reflections	4347 ( $ F /\sigma(F) > 4.0$ )
Structure solution	Program: SIR-97 (Direct methods)
R-values	$wR2 = 0.1669$ ( $R1 = 0.0618$ for observed reflections, $0.1560$ for all reflections)
Goodness of fit	$S = 0.943$
Max Shift / Error	$0.001 \text{ * e.s.d}$
Largest diff. peak and hole	$0.46$ and $-0.36 \text{ e\AA}^{-3}$

**Crystal structure of 4-9**

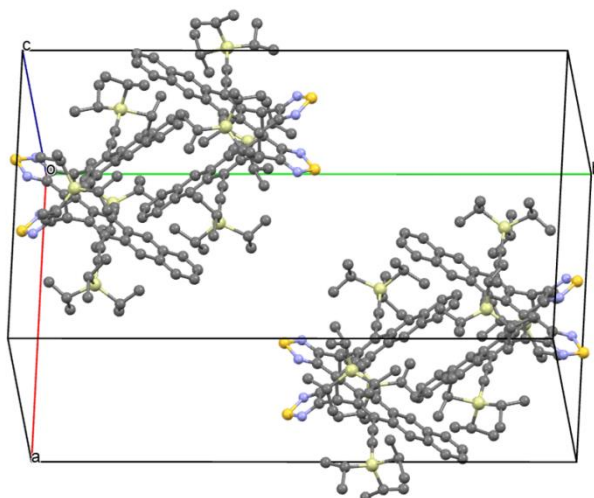
Cambridge Crystallographic Data Centre deposition number: CCDC 1042601

**Table VIII-7.** Crystallographic table.

Compound	<b>4-9</b>
Molecular formula	$C_{80}H_{100}N_4S_2Si_4$
Formula weight	1292.65 $g\text{mol}^{-1}$
Absorption coefficient	$\mu = 1.55\text{ mm}^{-1}$ correction with 6 crystal faces
Crystal size	0.03 x 0.06 x 0.43 $\text{mm}^3$ ; yellow needle
Space group	P-1 (triclinic)
Lattice parameters	$a = 14.5655(10)\text{ \AA}$ $\alpha = 86.867(6)^\circ$ $b = 14.7189(11)\text{ \AA}$ $\beta = 88.326(6)^\circ$ $c = 18.6267(13)\text{ \AA}$ $\gamma = 74.024(6)^\circ$
Volume	3833.0(5) $\text{\AA}^3$
Z value	2
F (000)	1392.0
Calculated density	$d_{\text{xray}} = 1.55\text{ gcm}^{-3}$
Temperature	-80 $^\circ\text{C}$
Scan type	$\omega$ -scans
Theta range for data collection	$2.4^\circ < \theta < 67.2^\circ$
Limiting indices	$-17 \leq h \leq 17$ , $-15 \leq k \leq 15$ , $-22 \leq l \leq 21$
Total number of reflections	36141
Unique number of reflections	12372 ( $R\sigma = 0.1131$ )
Observed number of reflections	14142 ( $ F /\sigma(F) > 4.0$ )
Structure solution	Program: SIR-2004 (Direct methods)
R-values	$wR2 = 0.4318$ ( $R1 = 0.1491$ for observed reflections, 0.02572 for all reflections)
Goodness of fit	$S = 1.178$
Max Shift / Error	0.001 * e.s.d
Largest diff. peak and hole	0.81 and -0.91 $e\text{\AA}^{-3}$

## Crystal structure of 4-10

Cambridge Crystallographic Data Centre deposition number: CCDC 1042602

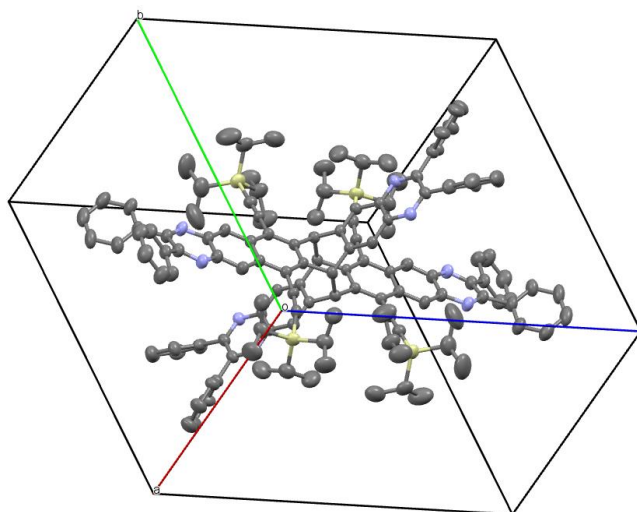


**Table VIII-8.** Crystallographic table.

Compound	<b>4-10</b>
Molecular formula	$C_{80}H_{100}N_4S_2Si_4$
Formula weight	$1292.65 \text{ g mol}^{-1}$
Absorption coefficient	$\mu = 1.54 \text{ mm}^{-1}$ correction with 6 crystal faces
Crystal size	$0.033 \times 0.05 \times 0.14 \text{ mm}^3$ ; yellow needle
Space group	$P 2_1/c$ (monoclinic)
Lattice parameters	$a = 18.7012(10) \text{ \AA}$ $b = 33.6573(13) \text{ \AA}$ $\beta = 106.214(4)^\circ$ $c = 12.8089(7) \text{ \AA}$
Volume	$7741.7(7) \text{ \AA}^3$
Z value	4
F (000)	2784.0
Calculated density	$d_{\text{xray}} = 1.55 \text{ g cm}^{-3}$
Temperature	$-70 \text{ }^\circ\text{C}$
Scan type	$\omega$ -scans
Theta range for data collection	$2.5^\circ < \theta < 63.7^\circ$
Limiting indices	$-22 \leq h \leq 21, -40 \leq k \leq 38, -15 \leq l \leq 15$
Total number of reflections	66070
Unique number of reflections	13745 ( $R_{\text{int}} = 0.2901$ )
Observed number of reflections	3090 ( $ F /\sigma(F) > 4.0$ )
Structure solution	Program: SIR-2014 (Direct methods)
R-values	$wR2 = 0.3294$ ( $R1 = 0.1022$ for observed reflections, $0.2698$ for all reflections)
Goodness of fit	$S = 0.748$
Max Shift / Error	$0.001$ * e.s.d
Largest diff. peak and hole	$0.57$ and $-0.36 \text{ e \AA}^{-3}$

**Crystal structure of 4-12**

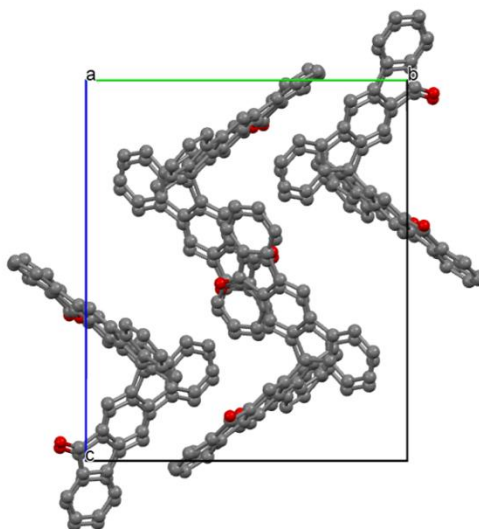
Cambridge Crystallographic Data Centre deposition number: CCDC 1434737

**Table VIII-9.** Crystallographic table.

Compound	<b>4-12</b>
Molecular formula	$C_{136}H_{136}N_8S_4$
Formula weight	2427.50 $\text{g mol}^{-1}$
Absorption coefficient	$\mu = 0.83 \text{ mm}^{-1}$
Crystal size	0.04 x 0.07 x 0.11 $\text{mm}^3$ ; yellow block
Space group	P-1 (triclinic)
Lattice parameters	$a = 12.8535(8) \text{ \AA}$ $\alpha = 109.991(5)^\circ$ $b = 17.9575(11) \text{ \AA}$ $\beta = 109.538(5)^\circ$ $c = 18.3686(9) \text{ \AA}$ $\gamma = 99.052(5)^\circ$
Volume	3573.9(4) $\text{\AA}^3$
Z value	1
F (000)	1304
Calculated density	$d_{\text{xray}} = 1.128 \text{ g cm}^{-3}$
Temperature	-80 $^\circ\text{C}$
Scan type	$\omega$ -scans
Theta range for data collection	$2.0^\circ < \theta < 67.8^\circ$
Limiting indices	$-15 \leq h \leq 15, -21 \leq k \leq 21, -20 \leq l \leq 22$
Total number of reflections	35903
Unique number of reflections	12138 ( $R_{\text{int}} = 0.0566$ )
Observed number of reflections	6133 ( $ F /\sigma(F) > 4.0$ )
Structure solution	Program: SIR-2004 (Direct methods)
R-values	$wR2 = 0.3521$ ( $R1 = 0.1090$ for observed reflections, 0.1727 for all reflections)
Goodness of fit	$S = 1.087$
Max Shift / Error	0.001 * e.s.d
Largest diff. peak and hole	0.75 and -0.53 $\text{e \AA}^{-3}$

## Crystal structure of 5-2

Cambridge Crystallographic Data Centre deposition number: CCDC 1035931

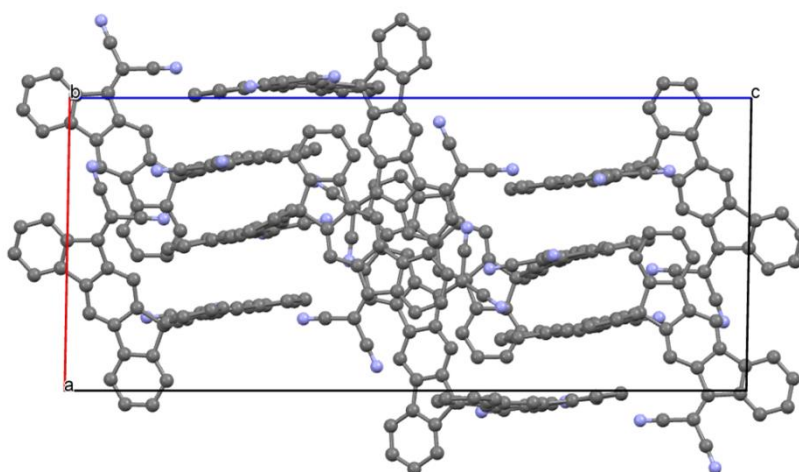


**Table VIII-9.** Crystallographic table.

Compound	5-2
Molecular formula	$C_{39}H_{20}O_2$
Formula weight	520.55 $\text{g mol}^{-1}$
Absorption coefficient	$\mu = 0.08 \text{ mm}^{-1}$
Crystal size	0.26 x 0.27 x 0.3 $\text{mm}^3$ ; yellow block
Space group	$P 2_1/c$ (monoclinic)
Lattice parameters	$a = 17.6736(8) \text{ \AA}$ $b = 15.8144(5) \text{ \AA}$ $\beta = 109.009(3)^\circ$ $c = 19.7873(9) \text{ \AA}$
Volume	5228.9(4) $\text{\AA}^3$
Z value	8
F (000)	2160
Calculated density	$d_{\text{xray}} = 1.322 \text{ g cm}^{-3}$
Temperature	-80 $^\circ\text{C}$
Scan type	$\omega$ -scans
Theta range for data collection	$2.5^\circ < \theta < 28.4^\circ$
Limiting indices	$-18 \leq h \leq 23, -20 \leq k \leq 18, -26 \leq l \leq 26$
Total number of reflections	34000
Unique number of reflections	12573 ( $R_{\text{int}} = 0.0551$ )
Observed number of reflections	7447 ( $ F /\sigma(F) > 4.0$ )
Structure solution	Program: SIR-2004 (Direct methods)
R-values	$wR2 = 0.1168$ ( $R1 = 0.048$ for observed reflections, 0.0975 for all reflections)
Goodness of fit	$S = 1.003$
Max Shift / Error	0.001 * e.s.d
Largest diff. peak and hole	0.27 and -0.17 $\text{e \AA}^{-3}$

**Crystal structure of 5-3**

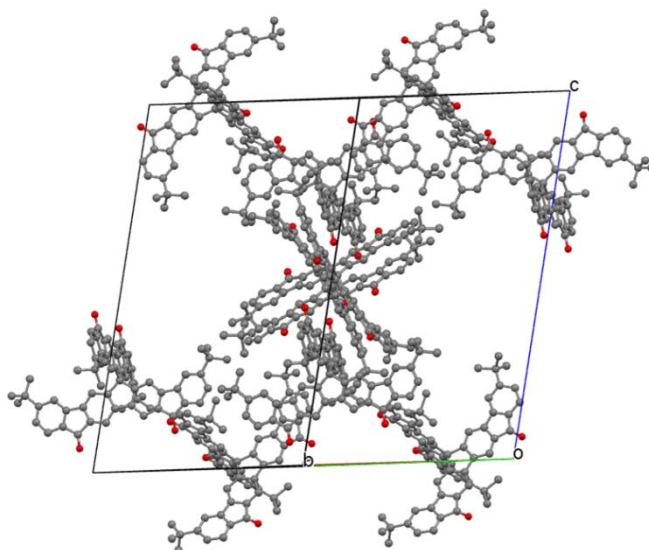
Cambridge Crystallographic Data Centre deposition number: CCDC 1035932

**Table VIII-10.** Crystallographic table.

Compound	<b>5-3</b>
Molecular formula	2(C <sub>45</sub> H <sub>20</sub> N <sub>4</sub> ), CH <sub>2</sub> Cl <sub>2</sub>
Formula weight	1318.23 g mol <sup>-1</sup>
Absorption coefficient	$\mu = 1.273 \text{ mm}^{-1}$ correction with 6 faces
Crystal size	0.01 x 0.01 x 0.2 mm <sup>3</sup> ; brown needle
Space group	P-1 (triclinic)
Lattice parameters	a = 14.0610(12) Å $\alpha = 99.814(7)^\circ$ b = 15.0528(14) Å $\beta = 90.613(7)^\circ$ c = 33.272(3) Å $\gamma = 92.172(7)^\circ$
Volume	6933.3(11) Å <sup>3</sup>
Z value	4
F (000)	2712
Calculated density	$d_{\text{xray}} = 1.263 \text{ g cm}^{-3}$
Temperature	-60 °C
Scan type	$\omega$ -scans
Theta range for data collection	$2.7^\circ < \theta < 51.2^\circ$
Limiting indices	$-15 \leq h \leq 15, -18 \leq k \leq 17, -39 \leq l \leq 39$
Total number of reflections	94677
Unique number of reflections	23561 ( $R_{\text{int}} = 0.3682$ )
Observed number of reflections	3389 ( $ F /\sigma(F) > 4.0$ )
Structure solution	SHELXD-2013
R-values	$wR2 = 0.2318$ ( $R1 = 0.0725$ for observed reflections, 0.3689 for all reflections)
Goodness of fit	S = 0.68
Max Shift / Error	0.001 * e.s.d
Largest diff. peak and hole	0.32 and -0.32 eÅ <sup>-3</sup>

## Crystal structure of 6-4

Cambridge Crystallographic Data Centre deposition number: CCDC 1408336

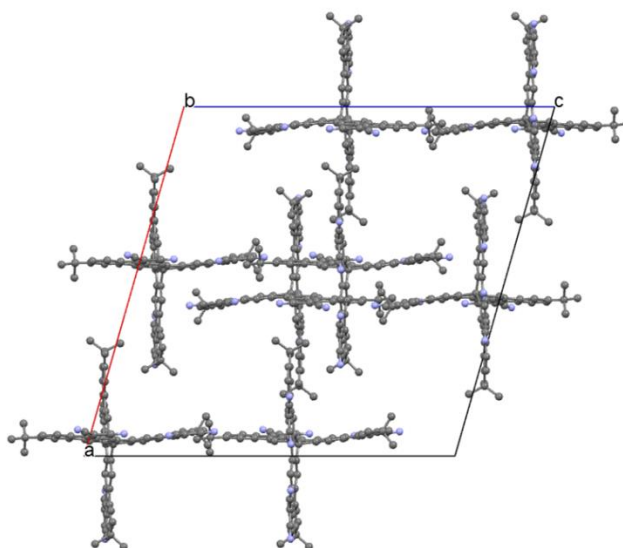


**Table VIII-11.** Crystallographic table.

Compound	6-4
Molecular formula	C <sub>69</sub> H <sub>56</sub> O
Formula weight	949.13 g mol <sup>-1</sup>
Absorption coefficient	$\mu = 0.41 \text{ mm}^{-1}$
Crystal size	0.08 x 0.08 x 0.34 mm <sup>3</sup> ; yellow needle
Space group	C 2/c (monoclinic)
Lattice parameters	a = 34.0876(10) Å b = 20.6528(5) Å $\beta = 110.119(2)^\circ$ c = 32.6782(10) Å
Volume	21604.4(15) Å <sup>3</sup>
Z value	12
F (000)	6024
Calculated density	$d_{\text{xray}} = 0.876 \text{ g cm}^{-3}$
Temperature	-70 °C
Scan type	$\omega$ -scans
Theta range for data collection	$2.6^\circ < \theta < 67.0^\circ$
Limiting indices	$-40 \leq h \leq 40, -20 \leq k \leq 24, -36 \leq l \leq 39$
Total number of reflections	80183
Unique number of reflections	19067 ( $R_{\text{int}} = 0.1063$ )
Observed number of reflections	8614 ( $ F /\sigma(F) > 4.0$ )
Structure solution	SIR-2004 (Direct methods)
R-values	wR2 = 0.2561 (R1 = 0.0820 for observed reflections, 0.1391 for all reflections)
Goodness of fit	S = 0.92
Max Shift / Error	0.001 * e.s.d
Largest diff. peak and hole	0.84 and -0.23 eÅ <sup>-3</sup>

**Crystal structure of 6-5**

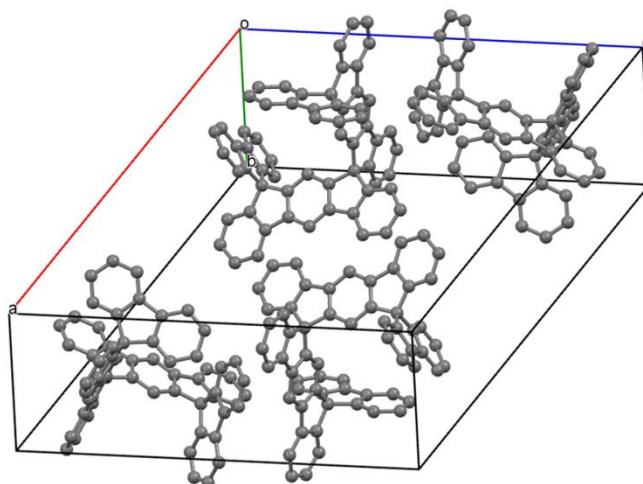
Cambridge Crystallographic Data Centre deposition number: CCDC 1408337

**Table VIII-12.** Crystallographic table.

Compound	<b>6-5</b>
Molecular formula	2(C <sub>81</sub> H <sub>56</sub> N <sub>8</sub> ), CH <sub>2</sub> Cl <sub>2</sub>
Formula weight	2367.59 g mol <sup>-1</sup>
Absorption coefficient	$\mu = 0.72 \text{ mm}^{-1}$ corrected with 6 crystal faces
Crystal size	0.03 x 0.110 x 0.15 mm <sup>3</sup> ; brown plate
Space group	C 2/c (monoclinic)
Lattice parameters	a = 30.9564(13) Å b = 17.6678(5) Å $\beta = 105.930(3)^\circ$ c = 31.5873(12) Å
Volume	16613(1) Å <sup>3</sup>
Z value	4
F (000)	4952
Calculated density	$d_{\text{xray}} = 1.0 \text{ g cm}^{-3}$
Temperature	-60 °C
Scan type	$\omega$ -scans
Theta range for data collection	2.9° < $\theta$ < 66.3°
Limiting indices	-37 ≤ h ≤ 33, -20 ≤ k ≤ 21, -37 ≤ l ≤ 36
Total number of reflections	64811
Unique number of reflections	14760 ( $R_{\text{int}} = 0.1314$ )
Observed number of reflections	3936 ( $ F /\sigma(F) > 4.0$ )
Structure solution	SIR-2004 (Direct methods)
R-values	wR2 = 0.3106 (R1=0.0954 for observed reflections, 0.2334 for all reflections)
Goodness of fit	S = 0.811
Max Shift / Error	0.001 * e.s.d
Largest diff. peak and hole	0.56 and -0.25 eÅ <sup>-3</sup>

## Crystal structure of 7-1

Cambridge Crystallographic Data Centre deposition number: CCDC 1408339

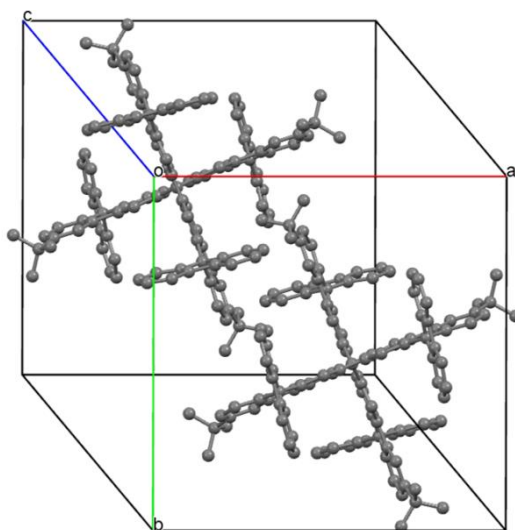


**Table VIII-13.** Crystallographic table.

Compound	7-1
Molecular formula	$C_{63}H_{36}$
Formula weight	$792.9 \text{ g mol}^{-1}$
Absorption coefficient	$\mu = 0.47 \text{ mm}^{-1}$ correction with 6 faces
Crystal size	$0.03 \times 0.08 \times 0.5 \text{ mm}^3$ ; colorless needle
Space group	$P 2_1/c$ (monoclinic)
Lattice parameters	$a = 21.5530(8) \text{ \AA}$ $b = 12.2789(3) \text{ \AA}$ $\beta = 119.414(3)^\circ$ $c = 21.0230(8) \text{ \AA}$
Volume	$4846.5(3) \text{ \AA}^3$
Z value	4
F (000)	1656
Calculated density	$d_{\text{xray}} = 1.263 \text{ g cm}^{-3}$
Temperature	$-80 \text{ }^\circ\text{C}$
Scan type	$\omega$ -scans
Theta range for data collection	$4^\circ < \theta < 68^\circ$
Limiting indices	$-25 \leq h \leq 25$ , $-14 \leq k \leq 13$ , $-25 \leq l \leq 25$
Total number of reflections	34322
Unique number of reflections	8515 ( $R_{\text{int}} = 0.0937$ )
Observed number of reflections	4074 ( $ F /\sigma(F) > 4.0$ )
Structure solution	SIR-2004
R-values	$wR2 = 0.2631$ ( $R1 = 0.0844$ for observed reflections, $0.1398$ for all reflections)
Goodness of fit	$S = 0.91$
Max Shift / Error	$0.001$ * e.s.d
Largest diff. peak and hole	$0.49$ and $-0.37 \text{ e\AA}^{-3}$

**Crystal structure of 7-2**

Cambridge Crystallographic Data Centre deposition number: CCDC 1408340

**Table VIII-14.** Crystallographic table.

Compound	<b>7-2</b>
Molecular formula	$C_{117}H_{88}$
Formula weight	1493.8 $\text{g mol}^{-1}$
Absorption coefficient	$\mu = 0.05 \text{ mm}^{-1}$
Crystal size	0.18 x 0.34 x 0.44 $\text{mm}^3$ colourless block
Space group	P-1 (triclinic)
Lattice parameters	$a = 18.8798(13) \text{ \AA}$ $\alpha = 114.305(5)^\circ$ $b = 18.9690(12) \text{ \AA}$ $\beta = 110.247(5)^\circ$ $c = 20.2269(15) \text{ \AA}$ $\gamma = 90.152(5)^\circ$
Volume	6104.0(7) $\text{\AA}^3$
Z value	2
F (000)	1580.0
Calculated density	$d_{\text{xray}} = 0.813 \text{ g cm}^{-3}$
Temperature	-70 $^\circ\text{C}$
Scan type	$\omega$ -scans
Theta range for data collection	$2.1^\circ < \theta < 28.1^\circ$
Limiting indices	$-24 \leq h \leq 24$ , $-25 \leq k \leq 25$ , $-26 \leq l \leq 26$
Total number of reflections	61356
Unique number of reflections	29346 ( $R_{\text{int}} = 0.1327$ )
Observed number of reflections	8229 ( $ F /\sigma(F) > 4.0$ )
Structure solution	SIR-97 (Direct methods)
R-values	$wR2 = 0.3632$ ( $R1 = 0.1122$ for observed reflections, 0.2521 for all reflections)
Goodness of fit	$S = 0.899$
Max Shift / Error	0.001 * e.s.d
Largest diff. peak and hole	0.39 and -0.27 $\text{e \AA}^{-3}$



# List of Publications

## Papers:

1. **Debin Xia**, B. Wang (co-first), B. Chen, S. Wang, B. Zhang, J. Ding, L. Wang, X. Jing, and F. Wang. Self-host blue-emitting iridium dendrimer with carbazole dendrons: nondoped phosphorescent organic light-emitting diodes. *Angew. Chem. Int. Ed.*, **2014**, 53, 1048-1052.
2. **Debin Xia**, D. Gehrig, X. Guo, M. Baumgarten, F. Laquai, and K. Müllen. A spiro-bifluorene based 3D electron acceptor with dicyanovinylene substitution for solution processed non-fullerene organic solar cells. *J. Mater. Chem. A*, **2015**, 3, 11086-11092.
3. **Debin Xia**, T. Marszalek, M. Li, X. Guo, M. Baumgarten, W. Pisula, K. Müllen. Solution-processable n-type organic semiconductors based on angular-shaped 2-(12 H-dibenzofluoren-12-ylidene) malononitrilediimide. *Org. Lett.*, **2015**, 17, 3074–3077.
4. **Debin Xia**, X. Guo (co-first), L. Chen, M. Baumgarten, A. Keerthi, K. Müllen. Layered electron acceptors via dimerization of acenes end-capped with 1,2,5-thiadiazoles. *Angew. Chem. Int. Ed.*, **2015**, DOI: 10.1002/anie.201508361.
5. X. Guo, H. N. Tsao, P. Gao, **Debin Xia**, C. An, M. K. Nazeeruddin, M. Baumgarten, M. Grätzel, K. Müllen. Dithieno[2,3-d;2',3'-d']benzo[1,2-b;4,5-b']dithiophene based organic sensitizers for dye-sensitized solar cells. *RSC Adv.*, **2014**, 4, 54130-54133.
6. **Debin Xia**, X. Wang, X. Guo, M. Baumgarten, K. Müllen. Fused bis-benzothiadiazoles as electron acceptors. **Submitted** to *Org. Lett.*.

7. **Debin Xia**, X. Guo, M. Baumgarten, H. Xu, K. Müllen. Design, synthesis, and characterization of a novel cruciform electron-deficient molecule. **In preparation.**
8. **Debin Xia**, X. Guo, M. Baumgarten, K. Müllen. Novel cruciform ladder-type phenylene materials: synthesis, physicochemical properties and applications in OLEDs. **In preparation.**
9. **Debin Xia**, A. Keerthi, C. An, X. Guo, M. Baumgarten, K. Müllen. Dithieno[2,3-d;2',3'-d']benzo[1,2-b;3,4-b']dithiophene-based quinoidal small molecule: synthesis, characterization, and radical behavior. **In preparation.**

## Conferences:

1. **Debin Xia**, X. Guo, L. Chen, M. Baumgarten, A. Keerthi, K. Müllen. 16th International Symposium on Novel Aromatic Compounds (ISNA), July, 2015, Madrid, Spain. Poster.
2. **Debin Xia**, X. Guo, L. Chen, M. Baumgarten, A. Keerthi, K. Müllen. 13th European Conference on Molecular Electronics (ECMC), September, 2015, Strasbourg, France. Poster.
3. **Debin Xia**, X. Guo, L. Chen, M. Baumgarten, A. Keerthi, K. Müllen. KOPO 2015 Conjugated Oligomers and Polymers: New Horizons in Functional  $\pi$ -Systems, September, 2015, Würzburg, Germany. Poster.

## Patents:

1. L. Wang, J. Ding, **Debin Xia**, L. Zhao. A series of blue-emitting Iridium (III) complexes for organic light-emitting diodes. CN 102993180 A.
2. L. Wang, J. Ding, **Debin Xia**, L. Zhao. Blue-emitting iridium dendrimer with carbazole dendrons: phosphorescent organic light-emitting diodes. CN 103012492 A.

# Acknowledgments

Eight years ago, I was dreaming to add a doctor title in front of my name. Now, the dream is almost achieved. With utmost sincerity, I would like to thank all the people who have helped me and involved in my life.

First of all, I am deeply grateful to my adviser ..... who gave me the opportunity to work at such world famous group, and the freedom to choose the research topic. I have learned a lot from him in the past years, which will keep guiding me in my future research career. His valuable comments, criticisms, and suggestions on my quarterly reports, manuscripts, and thesis changed my thoughts about how to do decent research. His creativity, enthusiasm, and passion for science and research is keep inspiring me. His unexpected emotions during the numerous meetings also make him so special for me. His encouragement when we first time saw each other in his office always makes me so energetic and ambitious. Thank you, .....

Many thanks must go to ....., who is not only my project leader, but also my close friend (I feel it individually.☺). I can still feel the indescribable moments when I have received his offer three and half years ago. Thank you, .....; Indeed, without your help and support, it could not be so smooth to finish my PhD study. Apart from many discussions and manuscripts polishing, there are also several unforgettable moments: drinking and chatting in the Christmas party, playing table tennis in the midnight, hugging each other while celebrating my first paper acceptance. Also, I would like to acknowledge the support from TR 49.

A special and unique thank you must go to ....., Normally, I call him Brother Guo. Without his recommendation, I could not predict where I would be. When the first time I flew to a foreign country, he picked me up. At the times when chemistry wasn't going so well at the beginning, he raised me up. When the "dimer" research topic confused me for days and nights, he cheered me up. When the future became obscure and uncertain, he lighted me up. My gratitude to him is kept and will be kept in my heart forever.

I would like to thank my former advisors and teachers during my bachelor and master studies. Special thanks to: ....., who isn't here anymore to read this, but who sparked my interests in organic chemistry, and who I miss so much; .....who is my role model and who taught me to prepare my first column chromatography and has supported me over the last eight years; ..... for providing an excellent research platform, individual teaching in the summer of 2010 and also his personal help; ..... for fruitful discussions and organizing nice group meetings, which I have been missing for a long time; ..... for giving me 60 scores, which reminds me "no pain, no gain"; ..... who has given me constant supports no matter in my research career or in my personal life; ..... He for her offering consolation when I was extremely upset; Teacher ..... who made me feel at home in ..... group in Changchun.

Many thanks and hugs to the AK ..... group: .....who was my roommate for three months, helped me a lot when I first came here; ....., ....., and ..... who taught me how to grow single crystals; ..... for fabrication of OFETs; ..... for analysis of molecular organizations; ..... for TGA and DSC measurements; ..... for NMR measurements; ..... for GPC purification assistance; ..... for technical support; ..... for group meeting organization; ..... (who always sent us emails in German 😊) helped me measuring MALDI-TOF; Martin Pfeffermann who always smiles to anybody and gives me five when we see each other; ..... who is my inspiration to behave in an honest, sincere and forthright manner with everyone; ..... and ..... who influence me to deal with work peacefully; .....whom I could see in most evenings either in the lab doing experiment or in the office reading and typing, and with whom we went back to living places with endless interesting chatting topics; ..... who is kind of a perfect-pursuing young scientist impacts me to pursue the perfect; ....., from whom you can always get some positive answers; ..... and ..... for my manuscript polishing; ....., ....., and ..... for their sunshine smiling; ..... and ..... for the together tour in Würzburg; ....., ....., ....., and .....for the memorable meal time.

I would like to express my thanks also to ....., who helped and taught me to analyze 2D NMR spectra, also organized the Every-Thursday soccer playing, "no matter it's raining cats and dogs, we are playing in the rugby field at 4 pm". Thanks also go to my old friend Mr. "Soccer", who enable me harvest so many friendships: ..... who is

my Dad's age, still runs like a young boy; ..... who plays soccer like a super star; ..... and ..... who are awesome defenders; ..... who is girls' team coach and also like guitar playing and photography; ..... who is a young guy and never worries about his graduation and makes a lot of progress of his soccer skills; ..... who is a dangerous striker and any opponent must pay more attention on him..... Anyway, our team (The Last Mülleneration) got the champion cup back. Guys, it's my great honor to be one of teammates.

Thanks to: ..... for fabrication of OPV devices; ..... for the single crystal X-ray measurements; ..... and .....for their kind support with chemicals and also for their donation of postal boxes to me; My German teacher ..... who taught me German more than three years, without whose encouragement and help, I cannot talk with people in German and still have an interest in keeping learning; ..... and ..... for their German teaching; My English teacher ..... whom I met every Monday morning to discuss what's happened around the world.

Finally, I couldn't have done any of this without my family who are always been there for me. Dad and Mum, **THANK YOU** for your endless love; I'm so lucky to be your son. I deeply thank my parents-in-law for their trust, understanding, support, and love. Especially, I acknowledge my lovely wife ....., who is the rock of my family and always waiting for me. We called each other overseas every day in the last three years and three months. Now, *honey*, I'm gonna get back home. I love you.

Debin Xia  
October, Mainz



# Curriculum Vitae

## Personal Details

**Name:** Debin Xia

**Gender:** Male

**Date of Birth:** August 4. 1984

**Place of Birth:** Heilongjiang, China

**Nationality:** China

## Education

**07.2012 – 12.2015** PhD studies, Max Planck Institute for Polymer Research, Mainz  
Germany

Research adviser: .....

**09.2008 – 06.2011** M.Sc. in Organic Chemistry, College of Chemistry and Chemical  
Engineering, Heilongjiang University, Harbin, China

Research advisers: ....., ....., and .....

**09.2004 – 06.2008** B.Sc. in Chemistry, College of Chemistry and Chemical  
Engineering, Heilongjiang University, Harbin, China

Research adviser: .....

## Language skills

Chinese: mother tongue; English: proficiency; German: B1

## Interests

Music, soccer, swimming, travelling and reading

